THE APPLICATION OF SOLID STATE NUCLEAR MAGNETIC RESONANCE TO THE STUDY OF LIGAND PROTEIN INTERACTIONS.

Philip Thomas Franklin Williamson

Thesis submitted to the
Board of the Faculty of Biological Sciences
in partial fulfilment of the requirements for the
Degree of Doctor of Philosophy
at the University of Oxford

St Hugh's College, Oxford
Trinity, 1999

Abstract

Solid state NMR studies have been performed on ligands bound to both the nicotinic acetylcholine receptor and the neurotensin receptor. Isotopically enriched ligands located within the binding sites on their respective receptors have been resolved providing information regarding both the structure and local environment of the ligands whilst bound to their respective receptors.

Magic angle spinning NMR studies of carbon-13 labelled acetylcholine bound to nicotinic acetylcholine receptor ($\alpha_2\beta\gamma\delta$, M_r ~280kDa) enriched membranes (~30-35%) have permitted a full assignment of the ligand. Through the appropriate computer simulations of the perturbation in chemical shifts it has been possible to conclude that the quaternary ammonium group of the agonist acetylcholine is located in a predominantly aromatic binding pocket and from relaxation phenomena, that the agonist acetylcholine remains bound to the receptor for times exceeding 200ms in its desensitised state.

Complimentary deuterium solid state NMR studies of $N^+(CD_3)_3$ bromoacetylcholine covalently bound to the nicotinic acetylcholine receptor show that the quaternary ammonium group of the ligand is relatively well constrained within the binding pocket. Through the development of techniques which enable the orientation of biological membranes under near physiological conditions, the deuterium spectral anisotropy shows that $N^+(CD_3)_3$ bromoacetylcholine has an orientation for the quaternary ammonium group within the agonist binding site of 42° with respect to the membrane normal.

Prior to NMR studies of the neurotensin receptor a previously described heterologous expression system for rat neurotensin receptor (M_r ~100kDa) in *E.coli* was used to produce sufficient (~10 mg) recombinant protein for solid state NMR studies. Neurotensin(8-13), was prepared using ($^{13}C/^{15}N$) labelled amino acids and standard solid phase synthesis protocols. For the longer neurotensin, a suitable expression system has been developed for the production of small recombinant peptides in quantities sufficient for NMR whilst allowing economic labelling of them. Both these ligands have been characterised by a variety of biophysical techniques including mass spectroscopy, solution NMR and reverse phase HPLC.

A variety of homo- and heteronuclear recoupling experiments on neurotensin(8-13) have allowed a partial assignment of neurotensin(8-13) in the solid state and when bound to the neurotensin receptor under solution-like and solid state conditions. Observation of ligand bound to the neurotensin receptor was determined from observed perturbations in chemical shifts. Double quantum filtered spectra were obtained under both solution like and solid state conditions to allow the resolution of sites masked by natural abundance contributions from the spectra arising from the buffer system employed. This has enabled a partial assignment to be made of neurotensin whilst bound to the neurotensin receptor.

Acknowledgements

I would like to thank my supervisor Tony Watts for his support during my time in Oxford, for introducing me to the fields of biomembranes and solid state NMR, and providing the necessary support and infrastructure to carry out this work.

For his constant help over the last five years, I would like to thank Keith Miller, with his supply of fish, his belief in the work, and introducing me to the ideas and people in the field of the nicotinic acetylcholine receptor.

Beat Meier and his group are acknowledged for their valuable discussions on the the application of dipolar recoupling methods.

Thank you to Reinhard Grisshammer for his neurotensin receptor construct and his useful comments on the expression and purification of the neurotensin receptor.

Particular thanks to Gerhard Gröbner for his support during my time in the lab teaching me the basics of solid state NMR, proof reading this thesis, for theoretical discussions on NMR at the Prince of Wales, long walking weekends and for being a great friend.

Many thanks to Boyan Bonev and Paul Spooner for their useful discussions and their practical help fixing and setting up the spectrometers. In addition, I would like to thank Clemens Glaubitz for his work on the rotational resonance, and for some of the simulation software.

I would also like to thank the past and present members of the lab especially Jonathan Boulter, Andy Taylor, Greg Choi, Zareen Ahmed, Jude Watts (particularly for the work during his Part II), James Mason, Tim Hadingham, Vicky Addy, Saffron Rankin, Pete Fisher, Liz Mitchell, Ian Burnett, Jonathan Sharples, Scott Goodall, Richard Kemp Harper and David Middleton.

I am deeply indebted to the people at Glaxo Wellcome for their help during

my time working in their laboratories, especially to my supervisors Rob and Chun-wa. Particular thanks however, should go to Surjit, without whose monumental efforts the expression and purification of neurotensin receptor would neither have been possible nor such fun. I am particularly grateful to Chun-wa for her thorough proof reading and her help with the NMR. Thanks should also go to many others in the lab for their ideas and support in particular Stuart for his hints and tips on purification and Bob for endeavouring to express neurotensin receptor on a large scale.

I would like to acknowledge the financial support of a BBSRC-CASE Glaxo-Wellcome studentship.

A special thought for my friends who have made my life in Oxford so enjoyable, including, Gideon, Pierre, Christelle, Armando, Marie, Andrew, Joost, Conny, Eric and Julie. My thanks goes to Tony and Sheila for being such understanding landlords and friends, from the loud parties to the assistance with car mechanics. I would like to thank Hans and Hannelore for their support and the relaxing times in France.

Finally I would like to thank my family. All my grandparents, aunts and uncles for all the love and support they have shown over the years, my brother Andy, and Cath, for their late night discussions over (perhaps a few too many) bottles of red wine. A special thanks should go to Jeanne for her unfaltering love and support over the last few years, not only putting up with the day to day ups and downs of the lab and keeping me sane, but also for her excellent proof reading and teaching me the more practical aspects of molecular biology. The biggest thanks which has been saved till last has to go to Mum and Dad, whose love, support and belief in me over the last 26 and a bit years has been unfaltering. Thank you Mum and Dad - we did it!

Table of Contents

List of Tables

List of Figures

Abbreviations and symbols

AcCho	Acetylcholine
αBTX	α-bungarotoxin
B_0	Static magnetic field
BAC	bromoacetylcholie bromoide
CHAPS	3-[(chloramidopropyl)dimethylammonio]-1-propanesulfonate
CHS	Cholesterol hemisuccinate
CP	Cross Polarisation
DDCP	Dipolar Dephased Cross Polarisation
DDF	p-(dimethylamino)-benzenediazonium fluoroborate
DFP	Di-isopropylfluorophosphate
EDTA	Ethylenediamine tetraaetic acid
I_{kx},I_{ky}, I_{kz}	Cartesian components of angular momentum spin operators
$\Delta\sigma$	Shielding anisotropy
η	Asymmetry parameter
H_x	Hamiltonian of interaction x
IPTG	isopropyl-β-thiogalactopyranoside
LM/DDM	n-dodecyl-β-D-maltoside
MBP	Maltose Binding Protein
MAS	Magic angle spinning
MBTA	4-(N-maleimido)benzyltrimethylammonium
nAcChoR	nicotinic acetylcholine receptor
NMR	Nuclear magnetic resonance
NT	Neurotensin
NT(8-13)	Neurotensin(8-13)
NTR	Neurotensin Receptor
PMSF	Phenylmethylsulfonylfluoride
RIL-ZQT	Rotating Inverse Laboratory-Zero Quantum Transfer
r.f.	radiofrequency
σ_{11}, σ_{22}, σ_{33}	principle elements of tensor
σ_{iso}	isotropic chemical shift
TOSSY	Total through space correlation spectroscopy
TRIS	Tris-[hydroxymethyl]-aminomethane

Chapter 1

Introduction

1.1 Introduction

Membranes play a vital role in both the structure and function of living cells. Membranes serve not only to compartmentalise the cell, but also regulate the passage of information and material in and out of these compartments. Structurally, biological membranes are formed from a lipid bilayer. However, in addition to the lipids, proteins that are located both within and on the surface of the bilayer (Figure 1.1) allow the structure to perform a wide range of functionally diverse tasks. These proteins serve to regulate both the passage of material and information across the bilayer.

1.1.1 Membrane Proteins

Membrane proteins are loosely classified through the nature of their interaction with the lipid bilayer[13]. Peripheral proteins are characterized by their loose association with the lipid bilayer, allowing their removal with non disruptive techniques such as altering the pH or ionic strength. Structurally, these proteins are functionally important for the maintenance of the cytoskeleton. In addition, this class of protein has been shown to be important in the lateral movement of material across the surface of the membrane. For example, the cytochrome family of proteins is responsible for the shuttling of electrons between the integral membrane complexes of several electron transport pathways[14].

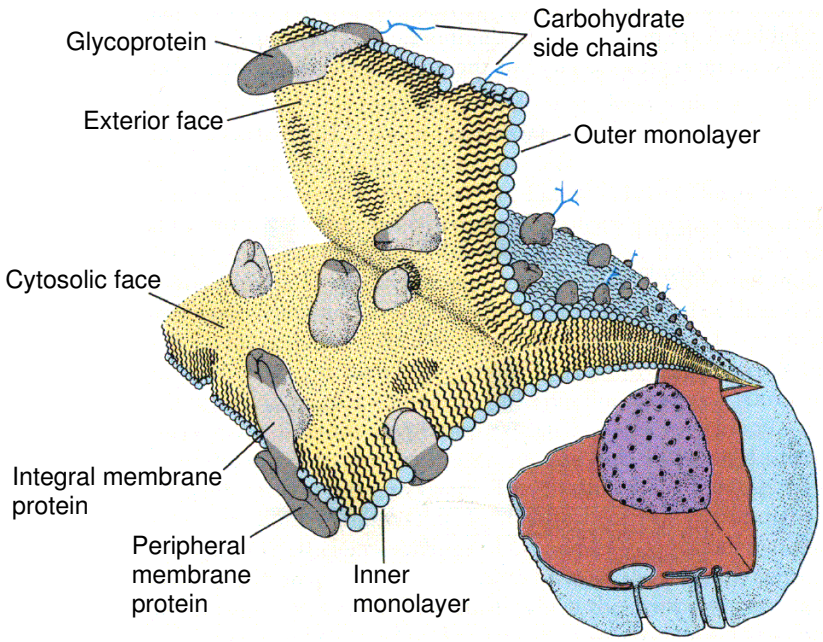

Figure 1.1: Structure of a typical cell membrane. In this schematic view of a membrane, drawn according to the fluid mosaic model of Singer and Nicholson a strip of plasma membrane of a eukaryotic cell has been peeled off to reveal the lipid bilayer and the proteins embedded in it[2].

In contrast, integral membrane proteins are tightly associated with the lipid bilayer and are only released in the presence of membrane disrupting agents such as detergents [13]. This class of protein typically spans the lipid bilayer and as a result many of these proteins are responsible for the transmission of information and material across the lipid bilayer. To date, most of the structural information regarding this class of membrane proteins has been inferred through functional analysis using a variety of techniques such as kinetic studies, chemical labelling and site directed mutagenesis. Very little direct structural information regarding this class of protein has been obtained to date, due to the difficulty in purifying sufficient quantities of protein for structural studies[15]. In addition, the subsequent inaccessibility of such proteins to conventional crystallographic or high resolution NMR techniques limits the ease with which structural information can be obtained [16]. The only medium

to high resolution structures of integral membrane proteins obtained exclusively by the use of X-ray crystallographic or 2D electron diffraction techniques are those shown in Table 1.1.

Protein	Diffraction Method	Resolution	Referece
Bacteriorhodopsin	X-ray	2.5 Å	[17]
Bacteriorhodopsin	Electron	2.8 Å	[18]
Rhodopsin	Electron	6.0 Å	[19]
Cytochrome bc_1	X-ray	1.5 Å	[20]
Cytochrome bc_1	X-ray	2.0 Å	[21]
K^+ channel	X-ray	3.2 Å	[22]
Fe^{2+} transporter	X-ray	2.4 Å	[23]
Ca^{2+} ATPase	Electron	8.0 Å	[24]
Ca^{2+} ATPase	Electron	6.0 Å	[25]
H^+/K^+ ATPase	Electron	8.0 Å	[26]
Light harvesting complex	Electron	3.4 Å	[27]
Light harvesting complex	X-ray	2.5 Å	[28]
Plant PS-II	Electron	8.0 Å	[29]
Bacterial reaction centre	X-ray	2.65 Å	[30]
GAP junction	Electron	7.5 Å	[31]
Maltoporin	X-ray	3.1 Å	[32]
Porins	X-ray	2.4 & 3.0 Å	[33]
Nicotinic acetylcholine receptor	Electron	4.6Å	[4]

Table 1.1: Table of current structures of integral membrane proteins available at medium resolution or better(<10Å).

Although diffraction techniques are proving the only viable method for determining the entire conformation of integral membrane proteins, several alternative methods are being employed to study both the structure and function of these membrane proteins at an atomic level [34]. Of these, solid state NMR is emerging as a suitable method to probe both the structure, function and dynamics of ligands and prosthetic groups of integral membrane proteins [16] [35] [36]. This methodology has been employed to study bacteriorhodopsin, rhodopsin, photoreaction centres, nicotinic acetylcholine receptor, sugar transporters and the family of ATPases (reviewed by Watts *et al.*[16][35]). In addition the backbone conformation of a number

of small membrane spanning peptides have been studied by solid state NMR [37].

1.2 Solid State NMR methodology

Solid state NMR attempts to exploit the anisotropic interactions present in solid state NMR spectrum to provide both structural and dynamic information. This offers the potential to analyse systems that are typically too large (>30 kDa) to be studied by solution state NMR [36]. In a membrane even the smallest peptide (∼2kDa) upon integration into the lipid bilayer has an effective molecular mass of several 100's kDa, thus membrane proteins are ideal targets for the application of such methodology [16] [35].

With the aim of exploiting the anisotropy present in the system, two approaches have been taken to study membrane proteins. Firstly, orientational constraints are obtained by observing spectral parameters in macroscopically orientated bilayers. Secondly, unorientated samples are spun at the magic angle which averages the anisotropic components within the spectra to give well resolved resonances. Through the selective reintroduction of these anisotropic interactions it is possible to deduce structural information from the system.

1.2.1 The NMR Spectrum

This section describes the fundamental properties that govern the interactions responsible for the solid state NMR spectrum, and the methodology that has been used extensively in this work to study these interactions.

The nuclear spin Hamiltonian

In the solid state the nuclear spin Hamiltonian [38] is given as:

$$H = H_Z + H_{CS} + H_J + H_D + H_Q \tag{1.1}$$

The nuclear interactions which the nuclear spin experiences can be split into three categories namely linear, bilinear and quadratic spin operators.

Such nuclear spins observe two types of linear operators. The Zeeman Hamiltonian (H_Z) determines the interaction of the nuclear spin with the static magnetic field ($\boldsymbol{B}_0$) and if $\boldsymbol{B}_0$ is parallel to the z axis we can write it as:

$$H_Z = \gamma\hbar\boldsymbol{B}_0 I_z \tag{1.2}$$

The chemical shift Hamiltonian (H_{CS}) describes the electronic distribution around the nucleus. In the correct axis system, this electronic distribution can be described by a second rank tensor, whose three principal elements are σ_{11}, σ_{22}, σ_{33}. Thus the chemical shift Hamiltonian can be given explicitly as:

$$H_{CS} = -\gamma\hbar(\sigma_{11}\sin^2\theta\cos^2\phi + \sigma_{22}\sin^2\theta\sin^2\phi + \sigma_{33}\cos^2\theta)\boldsymbol{B}_0 I_z \tag{1.3}$$

where θ and ϕ describe the angle formed between the principal axis system and the static field $\boldsymbol{B}_0$. In addition, from these three principle elements we define the shielding anisotropy ($\Delta\sigma$), asymmetry parameter (η) and the isotropic chemical shift (σ_{iso}) as:

$$\begin{aligned} \Delta\sigma &= \sigma_{33} - \frac{1}{2}(\sigma_{11} + \sigma_{22}) \\ \eta &= \frac{\sigma_{22} - \sigma_{11}}{\sigma_{33} - \sigma_{iso}} \\ \sigma_{iso} &= \frac{1}{3}(\sigma_{11} + \sigma_{22} + \sigma_{33}) \end{aligned} \tag{1.4}$$

Interactions that are bilinear with respect to the spin operator, arise due to the interaction between two nuclear spins, and arise from either the electron mediated (H_J) or from direct dipolar (H_D) interactions.

The Hamiltonian arising from indirect, electron mediated interactions (J couplings, H_J) takes the form:

$$H_J = 2\pi \sum_{k<l} \boldsymbol{I_k} \boldsymbol{J_{kl}} \boldsymbol{I_l} \tag{1.5}$$

and is characterised by the indirect spin coupling tensor ($\boldsymbol{J_{kl}}$). This can be split into the isotropic and non isotropic components leading to:

$$\begin{aligned} H_J^{iso} &= 2\pi \textstyle\sum_{k<l} J_{kl} \boldsymbol{I_k} \boldsymbol{I_l} \\ H_J^{aniso} &= 2\pi \textstyle\sum_{k<l} \boldsymbol{I_k} \boldsymbol{J_{kl}} \boldsymbol{I_l} \end{aligned} \tag{1.6}$$

the anisotropic contribution (H_J^{aniso}) cannot be readily distinguished from the dipolar contribution [38].

The second interaction in this category is the direct dipolar interaction (H_D), where the Hamiltonian takes the form:

$$H_D = \sum_{k<l} \boldsymbol{I_k} \boldsymbol{D_{kl}} \boldsymbol{I_l} \tag{1.7}$$

which is more frequently expressed in terms of irreducible tensor operators

$$H_D = \sum_{k<l} \sum_{q=-2}^{q=2} F_{kl}^q A_{kl}^q \tag{1.8}$$

where the function F_{kl}^q describes the spatial dependence of A_{kl}^q, the spin operators. In the high field approximation, it is usually possible to neglect non-secular terms. This truncated form of the dipolar Hamiltonian is now:

$$H_D^{trunc} = \sum_{k<l} b_{kl} \frac{1}{2} (1 - 3\cos^2\theta_{kl})(3I_{kz}I_{lz} - \boldsymbol{I_k}\boldsymbol{I_l}) \tag{1.9}$$

where $b_{kl} = \mu_0 \gamma_k \gamma_l \hbar / (4\pi r_{kl}^3)$ and θ_{kl} represents the angle formed between the internuclear vector and the magnetic field. In the case of heteronuclear spins, further simplification is possible by dropping all terms involving transverse spin operators

$$H_D^{IS} = b_{kl}(1 - 3\cos^2\theta_{kl}) I_{kz} I_{lz} \tag{1.10}$$

The final group of interactions are those which are quadratic in the spin operators, and arise primarily from interactions between the nuclear spin and electric field gradients. The Hamiltonian for this interaction (which vanishes when $I = \frac{1}{2}$) takes the form:

$$H_Q = \sum_{k=1}^{N} \boldsymbol{I_k} \boldsymbol{Q_k} \boldsymbol{I_k} \tag{1.11}$$

where $\boldsymbol{Q_k}$ may be expressed in terms of the electric field gradient at the site of the nucleus:

$$\boldsymbol{Q_k} = \frac{eQ_k}{2I_k(2I_k-1)\hbar}\boldsymbol{V_k} \tag{1.12}$$

and where Q_k is the quadrupolar moment of the nucleus. $\boldsymbol{V_k}$ can be expressed in terms of irreducible tensor operators. Under the high field approximation, it is possible to neglect non-secular terms, such that:

$$\begin{aligned} V^{(2,0)} &= \tfrac{1}{2}(3\cos^2\theta - 1)V_{zz} + \tfrac{1}{2}\sin^2\theta\cos 2\phi(V_{xx} - V_{yy}) \\ V^{(2,0)} &= \tfrac{1}{2}V_{zz}((3\cos^2\theta - 1) + \eta\sin^2\theta\cos 2\phi) \end{aligned} \tag{1.13}$$

Thus for an axially symmetric deuteron (η=0, where η is defined in a manner analogous to that observed for the chemical shielding anisotropy), the quadrupolar contribution to the Hamiltonian can be written as:

$$H_Q = \frac{e^2qQ(3I_z^2 - 2)}{4\hbar}(3\cos^2\theta - 1) \tag{1.14}$$

Cross polarisation.

Cross polarisation was originally introduced by Hartmann and Hahn [39], to facilitate the transfer of magnetization between nuclear spins in the solid state. The use of cross polarisation to transfer magnetization from abundant protons to nuclear spins with low gamma has achieved widespread application. This is primarily due to the significant enhancement in sensitivity that may be achieved when observing such nuclei in the solid state. Practically cross polarization is achieved by two operations:

1. A population of protons are polarized by means of a non selective $\pi/2$ pulse.
2. Magnetisation is then kept locked by means of a strong proton contact pulse. Simultaneously a strong on resonance pulse is applied to the carbon spins. During this time, magnetisation is transferred to the low gamma spins for subsequent observation. The magnitude of this exchange depends greatly on

the magnitude of B_{1S} and B_{1I}, and has been shown to be maximal when the Hartmann Hahn [39] condition:

$$\gamma_I B_{1I} = \gamma_S B_{1S} \tag{1.15}$$

is fulfilled.

This methodology offers important gains, as the sensitivity of the observed nucleus is enhanced by the ratio of the gyromagnetic ratios, offering a 4 and 10 fold theoretical improvement in sensitivity for the observation of carbon-13 and nitrogen-15 respectively [39]. In addition, the generation of magnetization is critically dependent on the relaxation of the proton spin reservoir, which is typically shorter than that of low gamma nuclei in the solid state, thereby increasing the rate at which experiments can be performed. Recently, improvements have been made to reduced the dependence of the cross polarization to the exact match of the two B_1 fields [40] [41] [42] [43]. This becomes of critical importance upon the introduction of magic angle spinning because the Hartmann-Hahn matching profile breaks down into a central condition, with a series of sidebands spaced at intervals of the spinning speed.

Proton Decoupling.

When observing low gamma nuclei in the solid state, the dipolar interaction with adjacent protons usually leads to severe line broadening, even in the presence of magic angle spinning. In order to reduce this line broadening spectra are usually acquired with high power (>80kHz) continuous wave decoupling, which rapidly saturates the proton reservoir. Composite pulse decoupling sequences such as those used in solution (i.e. WALTZ[44] or GARP[44]) fail to offer improvements in the solid state[45], however decoupling schemes based on the rapid phase alternation have lead to significant improvements in the solid state [45] [46]. Homonuclear decoupling sequences offer an alternative strategy for the decoupling of protons. Schemes such as Lee-Goldburg [47], MREV-4 [48] and BLEW-24 [49] effectively remove the homonuclear

dipolar couplings between the protons leaving only a scaled heteronuclear dipolar coupling, which is more readily averaged by magic angle spinning or irradiation of the low gamma nuclei.

Orientated samples.

Preparation of uniaxially aligned samples for NMR simplifies the spectra sufficiently such that the anisotropic interactions associated with the molecular frame can be related to both the macroscopic order in the sample and the laboratory frame providing detailed conformational information about the system. The spectra are further simplified due to the rapid axial rotation that occurs for many transmembrane components, which simplifies many of anisotropic terms, rendering the anisotropic contributions axially symmetric. Due to the axially symmetric nature of these motionally averaged tensors, they can be related to the static magnetic field by a single angle greatly simplifying the spectral interpretation. In order to determine the conformation of molecules using such an approach, it is necessary to understand the relationships between the principal axis system and the molecular axis system. This allows the molecular structure to be fixed in the laboratory frame. The relationship between the principal axis system and the molecular axis system can be obtained from single crystal studies on model compounds or from computer simulations [50]. Recently a technique has been developed which involves spinning orientated samples with their axis aligned along the magic angle in the magnetic field [51]. Such methodology leads to the breakdown of the lineshape into a series of sidebands spaced at intervals of the rotor frequency, analysis of these sideband families allows an accurate determination to be made of the anisotropic interactions being studied.

Magic angle sample spinning.

Inhomogeneous anisotropic interactions can be averaged by rapid rotation about an angle of 54.7° with respect to the static field. This leads to an averaging of all

anisotropic terms containing a $(3\cos^2\theta - 1)$ dependence in the solid state Hamiltonian. If the spinning speed (ω_r) exceeds the magnitude of the interaction, the interactions will be completely averaged leaving only the isotropic contribution[52]. If the the spinning speed fails to completely average the anisotropic interaction, the remaining anisotropic contribution appears as a rotational echo within the free induction decay [52], leading to sidebands spaced at intervals, equaling the rotor period(ω_r) in the frequency domain [52].

Although incomplete averaging of the anisotropic interactions leads to a reduction in sensitivity, the presence of the sideband families associated with the isotropic resonance provides information necessary to determine the nature of the second order tensor that describes the anisotropic interaction which would otherwise be lost. This feature can then be exploited to yield information relating to the chemical nature of the nucleus, molecular motion and relative orientation of anisotropic interactions. However, in these powder samples it is not possible to relate the orientation of these interactions to the laboratory frame due to macroscopic disorder.

1.2.2 Solid state NMR studies of biological membranes.

Orientational approaches.

Static NMR of uniaxially aligned samples benefits from the anisotropic interactions that contain considerable structural information and can be readily related to a known coordinate system. Although the application of this method requires macroscopically orientated systems, for many smaller peptides, a variety of orientation protocols have been devised (See Chapter 3 for description) whilst for large integral membrane proteins isopotential spin dry ultracentrifugation (ISDU) has proved invaluable [53].

Initial studies on such orientated peptides relied on the incorporation of NMR sensitive isotopic labels at specific sites of interest [54]. Anisotropic interactions such

as the quadrupolar interaction and chemical shielding anisotropy were subsequently exploited to orientate groups within the peptide with respect to the magnetic field. Such methods have allowed the conformation of the entire conformation of peptides such as gramacidin to be determined [54]. These techniques have been applied to the larger membrane proteins rhodopsin and bacteriorhodopsin where methyl groups within the retinal have been selectively deuterated and used to provide angular constraints along the length of the ligand. This has allowed the entire conformation of the retinal in both the dark and light adapted forms of both photoreceptors to be determined [55] [56].

Orientational studies of uniaxially aligned proteins have been extended to the study of uniformly nitrogen-15 labelled systems. Here multidimensional solid state NMR experiments such as PISEMA have been performed with separate anisotropic interactions in each dimension *e.g.* the orientation of the nitrogen chemical shielding tensor, the nitrogen-proton dipolar coupling tensor and the proton chemical shift[57]. To date such methodologies have allowed the resolution of amide nitrogens in membrane proteins containing up to 160 residues including the transmembrane protein colicin [58] and the M2 fragment of the nicotinic acetylcholine receptor [59]. However, as with MAS spectra, assignment of these residues proves problematic. To overcome these problems assignment protocols have been proposed on the basis of spin diffusion [59]. More recent techniques exploited both carbon and nitrogen labelling and offer the potential to facilitate sequential assignment of uniaxially aligned peptides [60] [61].

High resolution magic angle spinning approaches.

Magic angle spinning NMR has been demonstrated to produce high resolution spectra of biological membranes under near physiological conditions [16]. This methodology leads to the removal of many interactions containing structural information, such as the orientation and the magnitude of dipolar and chemical shielding tensors.

To overcome this loss of information many experiments have been designed to selectively reintroduce these interactions and allow the determination of the magnitude and relative orientation of the tensors [62].

Early structural studies using MAS NMR focused on small transmembrane peptides with labels specifically introduced in the peptide backbone. This allowed the measurement of dipolar couplings between homonuclear [63] and heteronuclear spin pairs [64]. The backbone conformation of several peptides have been determined including β-amyloid fibrils [65], glyophorin A [66] and magainin [67]. The methodology has subsequently been adapted to study the conformation of the transmembrane section of the dimeric bacterial chemotactic receptor [68] and to monitor the changes upon ligand binding [68]. More recent investigations of peptide structure have centred on the direct determination of the torsion angles that define the protein secondary structure, although to date, these have only been employed in model peptide systems [69] [70].

In addition to these studies of protein and peptide backbone conformations, solid state MAS methodology has been widely employed to study the conformation and dynamics of ligands at their binding sites both in lyophilysed soluble proteins and membrane bound receptors. Early work on the photoreceptors, rhodopsin and bacteriorhodopsin have demonstrated the applicability of homonuclear recoupling methods to determine internuclear distances between labelled sites in the covalently attached ligand retinal [71] [72]. Subsequent studies have determined directly the torsion angles within the polyene chain of the retinal [73]. Although these have been performed on ligands covalently attached to the protein, other work on the sugar transporters, H^+/K^+ ATPase and the nicotinic acetylcholine receptor have demonstrated the feasibility of selectively detecting bound ligand in the presence of excess ligand in bulk solution [74] [75] [76]. Together with selective recoupling by rotational resonance these experiments have provided detailed structural information at near physiological conditions [76].

Attempts to extend solid state NMR past the determination of single structural constraints have been frustrated with two problems, assignment and suitable methods by which to obtain long range structural data. Currently methods are being developed to circumvent these problems.

Early attempts to study uniformly labelled systems were performed on the relatively rigid prosthetic group bacteriochlorophyll as aggregates and whilst located in their binding site in the light harvesting complex. Due to the rigid nature of these molecules broadband dipolar recoupled exchange experiments based on the radiofrequency driven recoupling (RFDR) scheme were performed [77]. Optimization of conditions such that only strongly coupled carbon-13 correlations between adjacent carbon atoms were observed provided the basis of a full resonance assignment of the bacteriochlorophyll molecules. More recently methods have been developed for peptidic systems in which sequential assignment can be performed in a manner analogous to that used in the solution state [78][79]. Advances towards generating information on multispin systems will prove invaluable for the future of solid state NMR.

Multispin systems have so far been limited to the study of the relatively rigid bacteriochlorophyll. Information from the broadband recoupling experiments RFDR optimized to observe weaker dipolar couplings have yielded information relating to the stacking of the bacteriochlorophyll molecules in both aggregates and bound to the light harvesting complex [77]. However, to date the application of such broadband dipolar recoupling methods to the structural elucidation of more flexible molecules has been limited due to the motional averaging of the dipolar interactions.

1.3 The Acetylcholine Receptor.

The nicotinic acetylcholine receptor (nAcChoR) is a non selective ligand gated cation channel, which is activated by the binding of the agonist, acetylcholine. Nicotinic acetylcholine receptors can be found in the peripheral nervous system where they

are present at the neuromuscular junction, autonomic neurons and adrenal chromaffin cells. In addition the nicotinic acetylcholine receptor is found in many types of neurons in the central nervous system. The role of the nicotinic acetylcholine receptor at the neuromuscular junction, where it is concentrated on the endplate, is to sense the presence of the agonist acetylcholine, within the synapse. When agonist is present it mediates excitatory transmission in the form of the action potential. Nicotinic acetylcholine receptors located in the nervous system are thought to be involved in the control of electrical stimulation and the release of neurotransmitters, where acetylcholine is thought to act as a neuromodulator.

1.3.1 The structure of the nicotinic acetylcholine receptor.

The nicotinic acetylcholine receptor is possibly one of the best characterized members of the pentmeric ligand gated ion channel family of membrane proteins, which includes the γ-aminobutyric acid, glycine and 5-hydroxytryptamine (5-HT_3) receptors. The glutamate receptors are more distantly related members of this family. The five subunits of the nicotinic acetylcholine receptor show between 35 and 50% identity with each other, sharing a similar arrangement of both synaptic, transmembrane and cytoplasmic domains (See Figure 1.2). This homology extends from the nicotinic acetylcholine receptor to other members of the pentameric ligand gated ion channel family of receptors [80]. The five subunits that make up this pentamer with pseudo-five fold symmetry ($\alpha_2\beta\gamma\delta$) have molecular masses 38-44 kDa (α), 48-53kDa (β), 57-60kDa (γ) and 64-67 kDa (δ) as determine by SDS-PAGE [81]. Each subunit is clearly split into three domains, a large 200 amino acid N-terminal synaptic domain, four hydrophobic transmembrane domain(M1-4), and a small intracellular domain located between M3 and M4 [80] (Figure 1.2) [3].

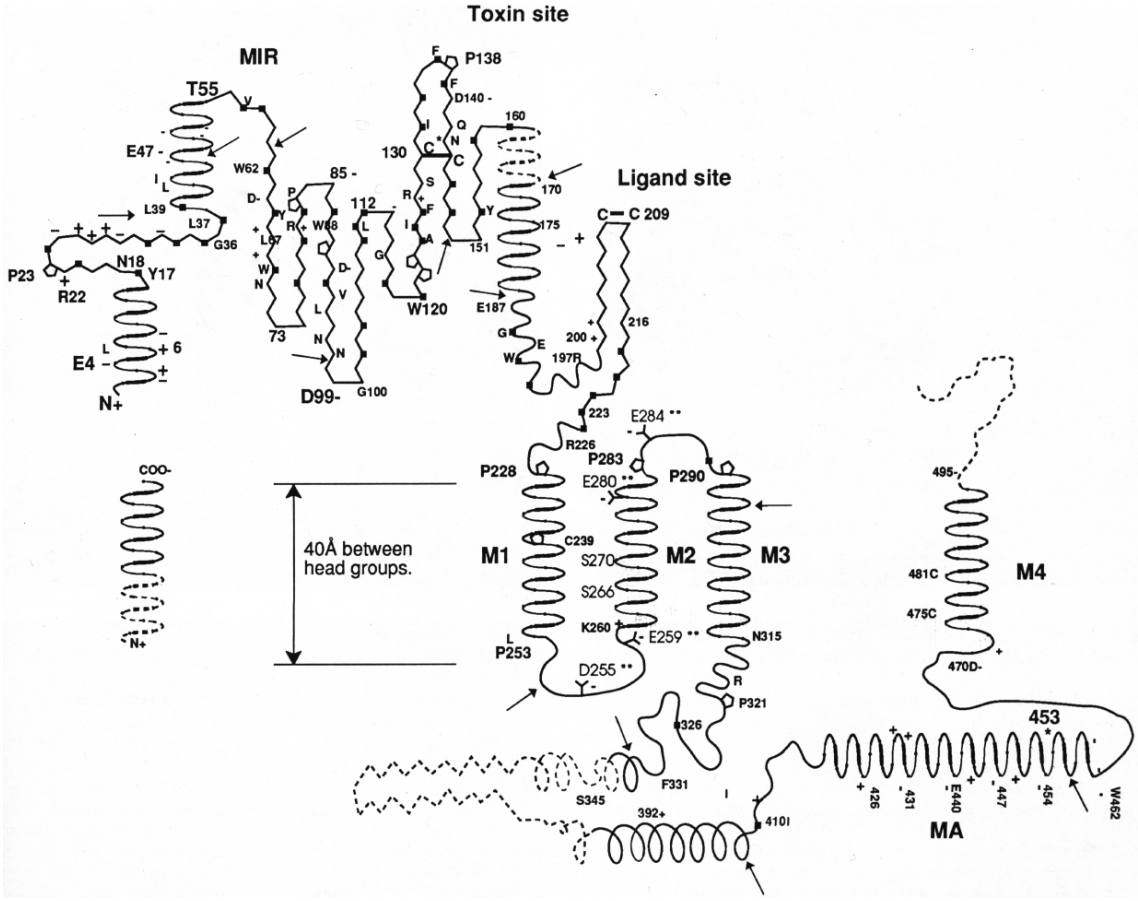

Figure 1.2: Schematic diagram indicating the proposed secondary structure and layout of a single subunit of the nicotinic acetylcholine receptor. Sites indicated include the main immunogenic region (MIR), toxin and ligand binding sites as well as the four transmembrane domains(M1-M4). Diagram taken from Stroud, 1990[3].

Overall morphology.

The best structural insight of the nicotinic acetylcholine receptor so far obtained has been from cryoelectron microscopy studies performed by Unwin [4] [82] [83] [84] yielding structures between 4.6Å and 9Å in resolution for the closed, open and desensitized structures. These studies describe a barrel like structure 110-125Å long and 65-80Å wide with a 25 Å wide depression in the centre thought to be an ion conducting pathway [84] (Figure 1.3A). This structure displays a five fold symmetry along the long axis. The structure protrudes 55Å into the the synaptic cleft and

15-20Å into the the cytoplasm with about 25% of the protein in the membrane. The entry to the channel is bordered by a wall of protein 25Å thick. The central cavity formed by this wall of protein extends about 54Å into the centre of the protein. At this point, the channel has narrowed to 7-8Å as it passes through the bilayer. The structure at 9Å although able to distinguish the five subunits, does not facilitate the identification or positioning of the subunits with respect to each other. Electron microscopy studies of nicotinic acetylcholine receptor subunits labelled with toxins or antibodies specific to the subunits have enabled the positioning of the subunits with respect to one another (Figure 1.3B) [80]. More recent studies of the nicotinic acetylcholine receptor at 4.6 Å have provided a more detailed view of the synaptic domain as well as the ligand binding site. Electron density can now be attributed to the β sheet structures originally located in the synaptic domain and shown in Figure 1.2 [3]. These appear to line a channel about 10-15 Å long that leads from the extracellular vestibule to the binding site which is proposed to be the major route for the binding of acetylcholine. This is analogous with that of the acetylcholinesterase which shows a similar channel for the targeting of acetylcholine to the binding site [85].

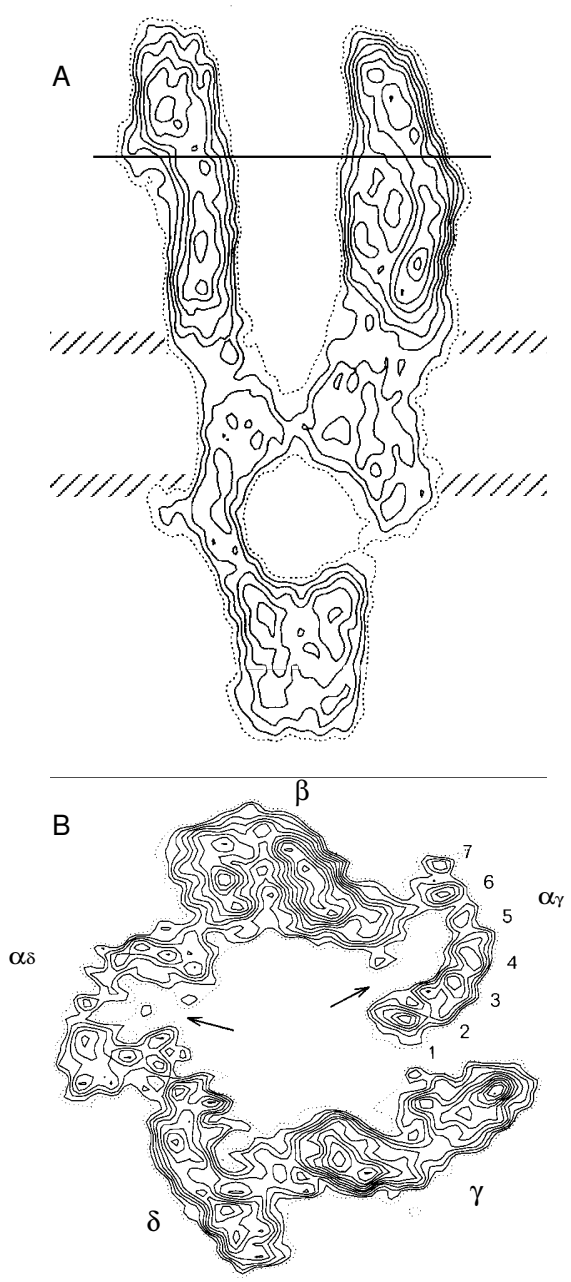

Figure 1.3: 3D reconstruction of the nicotinic acetylcholine receptor obtained from electron diffraction studies of tubular arrays of receptor [4]. Cross section through the receptor viewed perpendicular to the membrane normal (A). Cross section of the receptor taken along the line indicated in (A) viewed along the membrane normal (B). Subunits assigned as indicated, with arrows indicating the acetylcholine binding sites. Numbers 1 to 7 indicate the beta-sheet structure that has been proposed to line the entrance to the ligand binding site [4].

Residue(s)	Subunit	Label	Reference
Cys192/193	α	bromoacetylcholine bromide (BAC)	[92]
Cys192/193	α	4-(N-maleimido)benzyltrimethylammonium (MBTA)	[93]
Tyr190	α	lyophotoxin	[93]
Tyr190	α	p-(dimethylamino)-benzenediazonium fluoroborate	[93]
Tyr93/149	α	p-(dimethylamino)-benzenediazonium fluoroborate	[93]
Tyr93/198	α	acetylcholine mustard	[94]
Tyr93/198	α	nicotine photoaffibity analogue	[95]
Trp86	α	lyophotoxin	[96]
Tyr151	α	lyophotoxin	[97]

Table 1.2: Sites of labelling using reactive analogues of acetylcholine to identify residues contributing to the ligand binding site.

Ligand Binding Sites.

Two distinct ligand binding sites have been identified on the nicotinic acetylcholine receptor. They were first localised to the α subunits by western blot analysis of the subunits with ^{125}I α-bungarotoxin as a probe [86] [87] [88]. After these initial experiments, a wide variety of chemical labelling studies have been performed using analogues of acetylcholine which have the potential to react irreversibly with the receptor, these are summarized in Table 1.2. In addition to chemical labelling studies, site directed mutagenesis and unnatural amino acid incoorporation experiments have been performed [89] which implicate Tyr92 and Tyr190 in the ligand binding site. Although this data does not allow a high resolution structure to be proposed, a consistent picture is appearing where the ligand binding site is lined with aromatic residues. These have been proposed by Dougherty and co workers to be involved in the interaction with the quaternary ammonium group of the acetylcholine molecule [90], in a manner analogous to the interaction between acetylcholine and its binding site on the acetylcholinesterase[85]. Such data has enabled a consensus picture of the ligand binding site to be built and is shown in Figure 1.4. In addition structures of the synaptic domain have been proposed on the basis of homology modelling in agreement with the above chemical and site directed mutagenesis data [91].

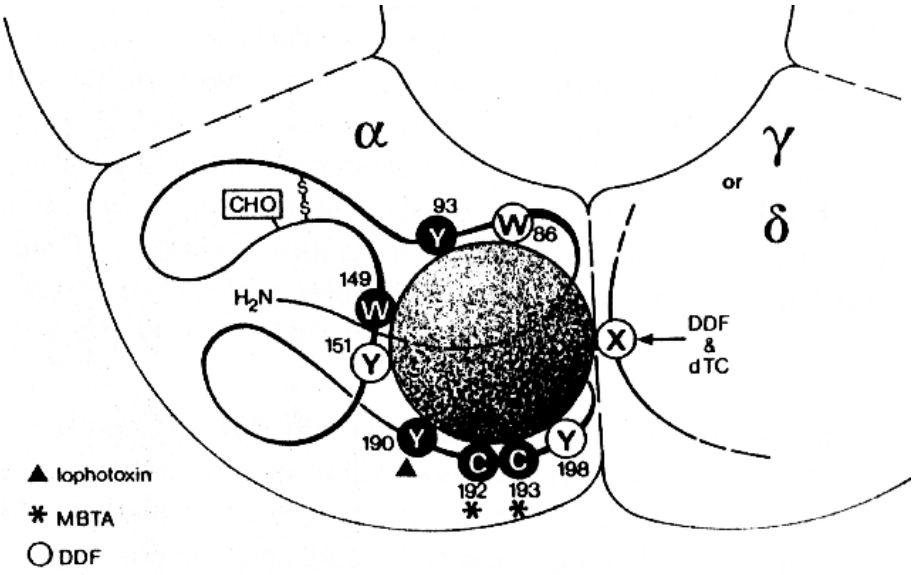

Figure 1.4: Proposed agonist binding site on the nicotinic acetylcholine receptor based on chemical labelling studies using lophotoxin, MBTA and DDF. The alpha chain has been folded such that all sites that have been labelled lie on the surface of a sphere defined by the volume that would be occupied by DDF if it was positioned in any possible orientation [5].

Synaptic domain.

The N-termini of the subunits form the bulk of the nicotinic acetylcholine receptor found in the synapse. The N-terminal domain contains 46 to 56% of the total volume of the protein as determined from electron diffraction studies [98]. The position of the N-terminus has been determined to be on the synaptic face of the membrane as it contains the main immunogenic region (MIR) which is a target for plasma antibodies [99][3] and sites for N-linked glycosylation [100]. Residues involved in the acetylcholine binding site have been mapped by covalent labelling of adjacent residues using agonist analogues [101], photoaffinity labels [102] and snake α toxins [103][104]. Although labelling studies demonstrate that the ligand binding site is at the subunit interface [102], the electron diffraction studies of Unwin [82] show three rod shaped densities, presumably helical regions within the structure. Within these three rod shaped densities there is a pocket with a channel to the

synaptic vestibule [4]. At lower resolution these pockets appear to disappear upon the addition of acetylcholine [82]. This has been proposed by Unwin [82] to represent the ligand binding pocket. Due to the non-equivalence of the two ligand binding sites, it is thought that the neighbouring subunits must influence the shape of the ligand binding site. Such studies of the N-terminal domain have helped in the determination of the topology of the receptor, however very little high resolution structural information is available. In an attempt to rationalise all the labelling data, Tsigny and co-workers [91] have proposed a model of the N-terminal domain based on sequence homology between the five subunits and the known crystal structure of the copper binding proteins plastocyanin and pseudoazurin. The structure proposed rationalises the positioning of the MIR, the glycosylation sites and the chemically labelled residues [5][105] within the binding site. Some regions, where chemical labelling data is scarce are still rather undefined.

Transmembrane Domain.

It has been proposed on the basis of hydropathy plots that the nicotinic acetylcholine receptor contains four transmembrane domains (M1-M4) [106][107]. Although the position and secondary structure of these four transmembrane domains remains unclear, in the absence of any high resolution structural data labelling studies and structural studies on fragments of the receptor channel are leading to a clearer understanding of the transmembrane domain of the nicotinic acetylcholine receptor. Several methods have been employed to look at the overall secondary structure of the transmembrane domain of the nicotinic acetylcholine receptor. Electron diffraction studies [82] have shown five distinct rods that run along the lining of the channel, these have been suggested to be helical domains which correspond to the transmembrane domain M2 on the basis of additional chemical labelling. Surrounding these five clear helical domains is a ring of protein, which at the available resolution does not appear to be helical. This observation has led to the proposal that the additional

transmembrane domains may adopt a β sheet conformation somewhat analogous to that found in the porins [33]. However Fourier transform infra-red spectroscopy(FT-IR) [108][109][110] and circular dichroism(CD) [110] studies of both intact receptor and the transmembrane domains indicate that the transmembrane domain is composed primarily of helical secondary structures in good agreement with the chemical labelling studies of the M1, M3 and M4 transmembrane domains.

The best characterised and most highly conserved of the transmembrane domains is M2 transmembrane domain [3]. Due to its relatively hydrophilic nature this transmembrane domain is implicated in the ion conducting channel across the membrane. Site directed mutagenesis of nicotinic acetylcholine receptor transiently expressed in Oocytes has correlated the presence of charged residues on the putative amphipathic M2 helix, to interactions with a non competitive channel blocker, which is thought to bind within the channel [111] and to the nature of the channel conductance [112]. These studies have been supported by chemical labelling studies using photoreactive non competitive channel blockers such as chlorpromazine that react with charged residues within the M2 TMD that are thought to line the channel [113] [114]. Through the use of photoreactive non-competitive channel blocker 3-(trifluoromethyl)-3-(m-[^{125}I]iodophenyl)diazerine (TID) in the presence and absence of the the agonist carbomylcholine, differential labelling supports the model of a M2 α helical TMD which is involved in channel gating [115]. In addition to M2 lining the channel, chemical labelling with open channel blockers such as quinacrine has resulted in the labelling of the M1 transmembrane domain [100]. This labelling has supported the hypothesis that the M1 transmembrane domain is helical, and is in close proximity to the channel, in the clefts left between the M2 transmembrane domains [100] [106].

In contrast to M1 and M2, labelling of M3 and M4 is scarce, and thus it is thought that these transmembrane domains are predominantly involved in the interaction of the receptor with the lipids. This is reflected in the relative hydrophobicity

of these two transmembrane domains. Labelling studies using both hydrophobic lipids [116] and the hydrophobic probe TID [117] indicate that the M3 and M4 transmembrane domains are all relatively exposed to the lipid and their labelling patterns are consistent with them adopting a α-helical structure [116].

Intracellular Domain.

The intracellular domain of the nicotinic acetylcholine receptor is thought to be composed mainly of the M3-M4 loop [118]. By comparison of this loop between members of the pentameric ligand gated ion channel family of receptors it has been proposed that this loop is involved in discriminating between ions of different charges [118][4], suggesting that this region, in part, is responsible for determining ion selectivity for this class of proteins [4]. This has been further supported by the most recent electron diffraction structure which shows the presence of small pores (< 10Å) that could potentially serve as filters to prevent the bulk of cytoplasmic anions approaching the channel entrance [4]. The most proximal part of the synaptic domain of the nicotinic acetylcholine receptor has been identified as the 43kDa protein raspin. This protein is associated with the nicotinic acetylcholine receptor as a complex at stoichiometry of 1:1 [119][120] and has beeen shown to interact with the β-subunit of the nioctinic acetylcholine receptor and actin [121]. This suggests that the raspin/actin complex localizes the nioctinic acetylcholine receptor to the subsynaptic region in muscle cells [122][123].

1.3.2 Nicotinic Acetylcholine Receptor Kinetics.

In the absence of agonist the nicotinic acetylcholine receptor is thought to exist in a equilibrium between the resting (R_r) and the slow desensitized states (R_{sd}) (Figure 1.5), under such conditions 80% of the receptors are thought to exist in the resting state.

The formation of the open state (L_2R_{open}) occurs within 10 μs of the addition

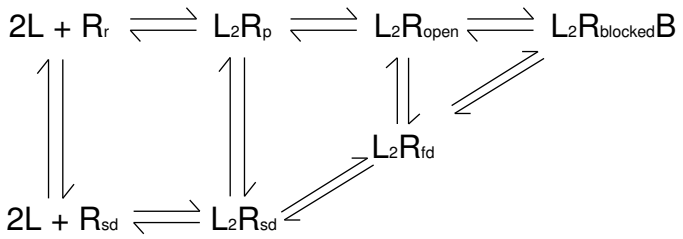

Figure 1.5: Summary of receptor states and the pathways between them, where L is the agonist and R the receptor. The sub-scripts indicate the various states of the receptor: R_r resting, R_{sd} slow desensitized, R_{fd} fastdesensitized, R_{open} open channel, R_P pre-open and $R_{blocked}$ blocked channel and B is a non competitive inhibitor.

of acetylcholine(L). Dose response curves from a preparation from *Torpedo nobiliana* have Hill coefficients of 2, indicating that 2 molecules of acetylcholine are required for channel opening [124]. The channel remains open on the order of milliseconds [125], during which time there is an unhindered flow of Na^+ ions through the ion channel (10^4 $msec^{-1}nAcChoR^{-1}$). This causes the postsynaptic membrane to depolarize from -50 to -5 mV [125]. Ion channel conductances have been reported to be anywhere between 78 and 18 pS [126][127], although these values have been shown not to vary with agonist [128]. Therefore, the observed efficacy differences between agonists are due to a difference in the equilibrium between the open and closed states rather than a variation in channel conductance.

In continued presence of agonist, the receptor has been observed to flicker open and closed until after several hundreds of milliseconds they convert into the non conducting desensitized state. The slow desensitized state (R_{sd} - also present in the absence of agonist) has a high affinity for agonist (K_D=3nM for the slow desensitized state compared to 1mM for the resting state) and most antagonists. It is possible to identify the R_{sd} using ligand binding assays [129]. At lower concentrations of agonist that do not trigger channel opening, the receptor adopts a high affinity slow desensitized form [130]. Neubig and Cohen originally suggested the existence of a non conductive state [124]. This was subsequently confirmed by stopped flow

fluoresence measurements and rapid quench flow techniques [131] [132] [133] [134] [135] and classified as a fast desensitized state (R_{fd}).

The physiological role of desensitisation is not clear, as the residency time of acetylcholine in the synapse is short due to the presence of acetylcholinesterase. Acetylcholine is effectively removed prior to the onset of desensitisation. The rate of formation of this desensitised state has been shown to be modulated by the selective phosphorylation of serine and tyrosine residues in the nicotinic acetylcholine receptor [136][137][138].

The flux of ions through the channel has been found to be inhibited by high concentrations of agonist (the $L_2R_{blocked}$) [139][140]. Analogous channel block occurs in the presence of non-competitive inhibitors(NCI) [141] [142] and studies have shown that some of the NCIs bind to the self inhibition site which is thought to be located within the ion conducting channel [143].

1.4 The Neurotensin Receptor.

The neurotensin receptor is a member of the G protein coupled receptor (GPCR) family of transmembrane proteins, and is activated upon binding of the agonist, a basic tridecapeptide, neurotensin (Glu-Leu-Tyr-Glu-Asn-Lys-Pro-Arg-Arg-Pro-Tyr-Ile-Leu)(for structure see Figure 1.9). The neurotensin receptor is found both in the central nervous system and in the periphery. In the periphery, neurotensin stimulates smooth muscle contraction [144] [145]. In the central nervous system, neurotensin induces a variety of effects including antinociception, hypothermia, and increased locomotor activity [146] [147] [148]. These effects are probably mediated through the regulation of the nigrostriatal and mesolimbic dopamine pathways [149]. As a result the pharmacological activity of neurotensin is similar to that of dopamine, where compounds function as antipsychotics [150] [151] [152] and intervention might provide useful insights for the development of treatments for conditions such as schizophrenia [149] and Parkinsons disease[149].

1.4.1 Overview of G-protein coupled receptors.

The superfamily of G protein coupled receptors are a family of structurally similar integral membrane proteins that all contain 7 hydrophobic transmembrane domains. The role of this family of receptors is to potentiate the transfer of information across the cell membrane. A schematic representation of the transfer of this information across the membrane and into the cell is outlined in Figure 1.6. This model for the mode of action for G-protein coupled receptors has been determined primarily from work on the β-adrenergic receptor and rhodopsin. Briefly, upon agonist binding the receptor associates with a trimeric GDP bound G-protein. The complex formation facilitates the exchange of GDP for GTP, resulting in the release of ligand and trimeric G-protein/GTP complex from the receptor. Subsequent signalling is dependent on the G-protein complex which dissociates into its component parts α and $\beta\gamma$. These proteins activate a wide range of effector systems including a variety of channels and enzymes depending on the particular isoform of the α, β and γ chains in the G-protein complex. Hydrolysis of the GTP to GDP, results in the re-association of the trimeric complex and the attenuation of signalling to the effector systems. The GPCR superfamily respond to a structurally diverse set of ligands, including light, odour, amino acids, small peptides, proteins, lipid analogues and biogenic amines. The wide range of receptors coupled to such a variety of isoforms of the trimeric G-protein complex, leads to a complex interaction between the different stimulatory pathways, allowing tight yet subtle control over many cellular processes.

The superfamily of GPCRs have been shown to be structurally homologous, each containing 7 hydrophobic transmembrane domains, which have been proposed, or in the case of rhodopsin shown [8][19], to be helical in nature. Although medium resolution structural information is only available for rhodopsin [19] this data has been used as the basis for much homology modelling[7]. Electron diffraction studies of these systems have provided much information regarding the structure of the

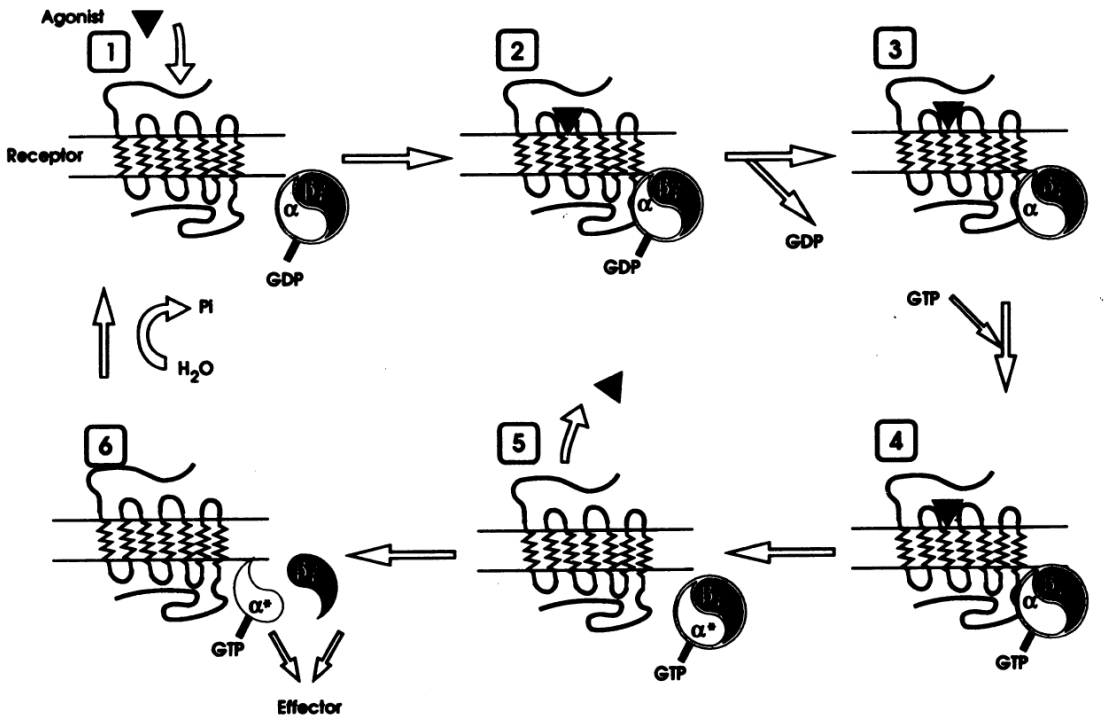

Figure 1.6: Schematic diagram showing how the binding of a ligand to a GPCR initiates a signal tranduction cascade within the cell. See text for description. Diagrams modified from the G-protein coupled receptor facts book[6].

transmembrane domain of such receptors, however the structure of the extracellular domains has remained intractable to such approaches. Solution NMR studies of these extracellular loops cleaved from the intact rhodopsin, have been shown to adopt a tertiary structure in solution [153] [154] [155] and are being used in conjunction with electron diffraction data and other biophysical studies [156] to predict a global structure of the protein [155] [157].

The structure-function relationship of regions of G protein coupled receptors has been studied primarily through the analysis of chimeric receptors. These studies were first carried out on the adrenergic receptors where a high degree of homology between the α_2 and the β_2 adrenergic receptors favoured the correct folding of the protein. Additionally, pharmacological specificity and coupling to two differing

G-proteins ($G_{\alpha i}$ and $G_{\alpha s}$) allowed the assignment of functional activity to several regions of the proteins [158]. These concluded that all but the 6th transmembrane domain are involved in the binding of the agonist epinephrine[159], with the 7th transmembrane domain being critical in antagonist specificity. This system exploiting the adrenergic receptor was also used to probe the interaction of the intracellular loops with various G-proteins. These studies concluded that the third intracellular loop and the loop formed through the anchoring of the C-terminus to the membrane by palmitoylation were key domains in for G-protein specificity [159]. These results appear to be consistent with data obtained for other G-protein coupled receptors including rhodopsin [158] and the muscarinic acetylcholine receptor [160]. Although the above studies appear to converge towards a consensus agonist binding site other members of the G-protein coupled receptor family show a greater diversity in the location of the agonist binding site. The agonist binding sites have been localised to three distinct regions which reflect the nature of the ligand. The ligand binding site for the retinal in rhodopsin has been localize to the central region of the bilayer through a series of both site-directed mutagenesis studies [161] and biophysical studies [161]. Such organisation is conserved in many of the receptors which bind relatively small ligands with putative transmembrane binding sites such as the dopamine receptors [162] [163] and adrenoreceptors [163][162]. In contrast, GPCRs that bind large peptidic ligands are proposed to have binding sites located on the extracellular surface of the protein as is the case for the neurotensin and substance P receptors[164]. There are numerous exceptions to these cases, in particular the odorant receptor family, where the ligand binding sites are proposed to be structurally diverse, probably reflecting the rather diverse nature of compounds they bind [165].

Following prolonged exposure to ligand, G-protein receptors undergo desensitisation. Desensitisation of G-protein coupled receptors can be broken down temporally into long and short term desensitisation. Two distinct mechanisms have been found to underlie short term desensitization in the β-adrenergic and opsin receptors. The

first of these, homologous desensitisation, leads to a reduced responsiveness to the original stimulus, the second, heterologous desensitization, leads to a decrease in responsiveness as a result of the activation of other receptors.

In the case of the β-adrenergic receptor heterologous desensitization is believed to occur due to receptor phosphoryation by the cAMP dependent protein kinase, protein kinase A [166] [167] [168] [169]. Thus, any receptor enhancing intracellular levels of cAMP might result in a desensitization of the β-adrenergic receptor. The resulting phosphorylation mediates its action by reducing the coupling between the G-protein coupled receptor and the G-protein (G_S), by reducing the affinity of the G-protein coupled receptor for the G-protein.

Homologous desensitization of the β-adrenergic receptor occurs only at high levels of agonist. Upon exposure to agonist the receptor undergoes cAMP independent phosphorylation by the β-adrenergic receptor kinase (βARK) [170]. Phosphorylation by βARK is dependent upon agonist binding [170]. Receptor phosphorylation is not sufficient to trigger desensitisation, as it is dependent on the binding of β-arrestin to the phosphorylated receptor [171]. β-arrestin shares a sequence similarity to the G-protein α-subunit and is thought to mediate its action by sterically blocking the G-protein binding site [171]. This mode of desensitisation is conserved amongst the G-protein coupled receptor family of proteins with similar processes occurring for the visual receptor rhodopsin[158].

Long term desensitization occurs over a period of 60 minutes [172] and is characterized by a decrease in the overall number of receptors on the cell surface, and a requirement for *de novo* protein synthesis for receptor recovery. The reduction in receptor number appears to be mediated by an endocytotic process which sequesters the receptors from the cell surface [172]. It has been suggested that, in the case of the β-adrenergic receptor, the binding of β-arrestin to the phosphorylated receptor mediates not only homologous desensitisation, but also acts as a signal for the sequestration of the receptor from the cell surface [173].

1.4.2 Structural studies of the neurotensin receptor.

No high resolution structures are currently available for the neurotensin receptor as attempts to produce 2D and 3D crystals for diffraction experiments have proved largely unsuccessful (R. Grisshamer *pers. comm.*). Size constraints have also limited the application of solution NMR to the study of this protein. Circular dichroism studies of the neurotensin receptor have indicated that in detergent micelles the receptor is predominantly α-helical in nature. No extensive modelling of the overall structure has been performed on the neurotensin receptor. To date the only model for the arrangement of the transmembrane domains of the neurotensin receptor has been generated by largely automated methods [7] on the basis of the helical arrangements found in either bacteriorhodopsin[7] or rhodopsin[7](Figure 1.7). Models of the neurotensin receptor generated in this way have been used by several groups as the basis for producing models of the agonist and antagonist binding site (See below).

The proposed structure for the agonist binding domain of the neurotensin receptor has focused on the third extracellular loop (E3) of the neurotensin receptor [9] following analysis of chimeric proteins [174](Figure 1.8). After identication of the putative binding domain as E3, extensive homology modelling and site directed mutagenesis studies were performed to identify the likely structure of the ligand binding site [9], subsequent docking of the ligand to this structure gave rise to the proposed model of the ligand in its binding site on the extracellular face of the neurotensin receptor [9](Figure 1.8). These studies of rat neurotensin receptor have implicated the residues Phe331, Ile334, Trp329, Phe342, Phe344, Phe346, Tyr347, Tyr349 to be critical for the binding of the agonist neurotensin and its analogue NT(8-13). On the basis of this modelling the ligand NT(8-13) is proposed to form a Type-I β-turn with Arg^{9} folding back to form an intramolecular hydrogen bond with Tyr^{11} of the neurotensin. The abundance of aromatic residues in the ligand binding pocket also suggests that the binding of neurotensin is mediated primarily

through cation-π interactions and base stacking [9].

Additional modelling studies performed for the neurotensin antagonist SR48692, suggest that a separate antagonist binding site exists with residues from the extracellular face and the 4th, 6th and 7th transmembrane domains involved with antagonist binding [175].

Few studies have been performed to date on the structural requirements for G-protein activation by the neurotensin receptor. Deletion analysis of the third intracellular loop, attenuates the receptors ability to stimulate the formation of either phosphatidylinositol or cAMP [176]. This is consistent with studies on other members of the GPCR family of proteins where the third intracellular loop and C-terminal tail are important in G-protein binding. Deletion of this loop, does not attenuate the rate at which the receptor is sequestered from the bilayer [176] suggesting that upon receptor activation, other sequences within the protein signal its sequestration from the cell surface.

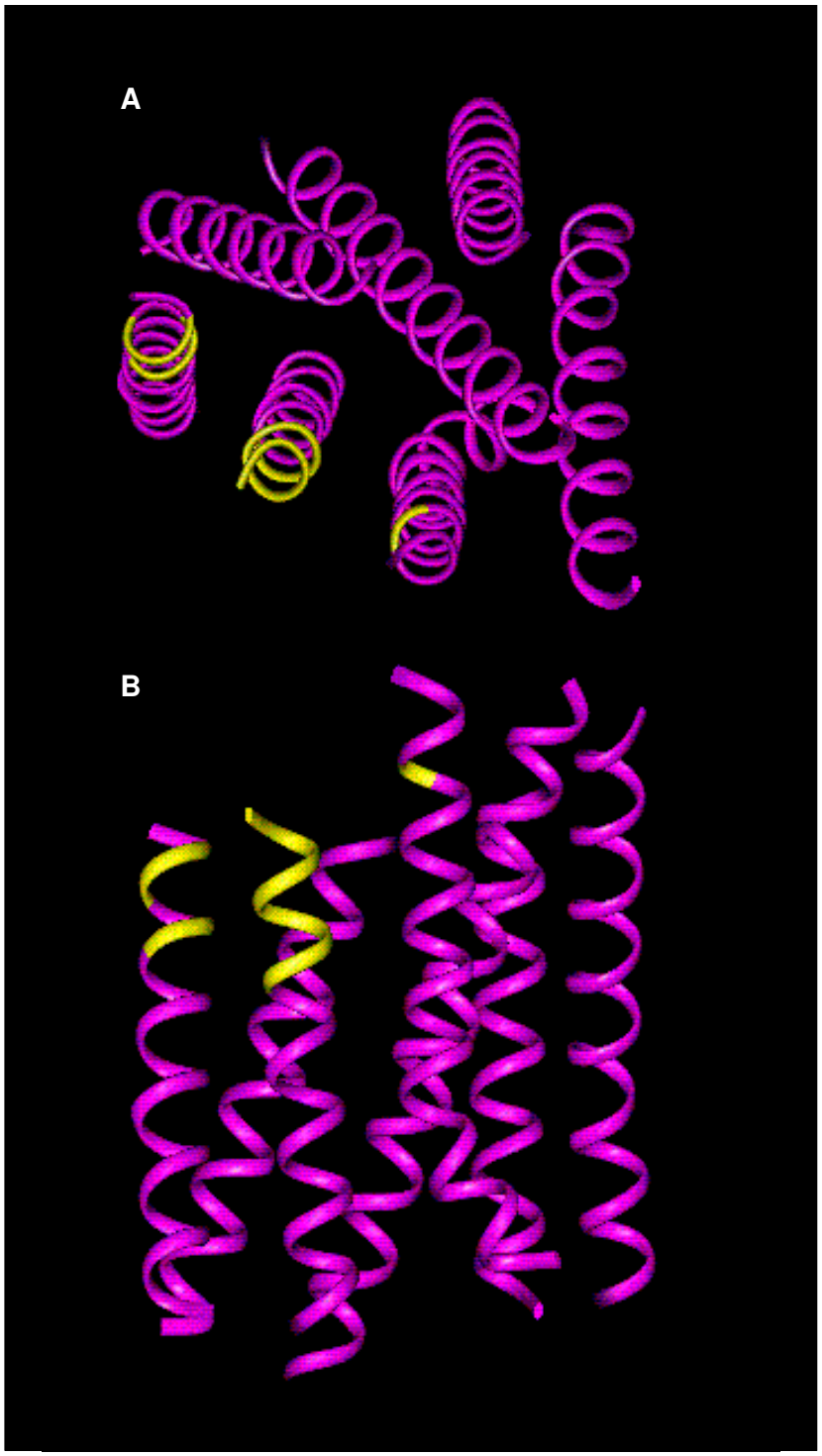

Figure 1.7: Model of the neurotensin receptor transmembrane domain, based on the model of rhodopsin [7] constructed from low resolution electron diffraction structures, sequence alignment and biochemical data [8]. The yellow region defines a 10Å region around the proposed neurotensin binding site (Figure 1.8) based on site directed mutagenesis data. View along the membrane normal towards the extracellular face (A), and perpendicular to the membrane normal (B).

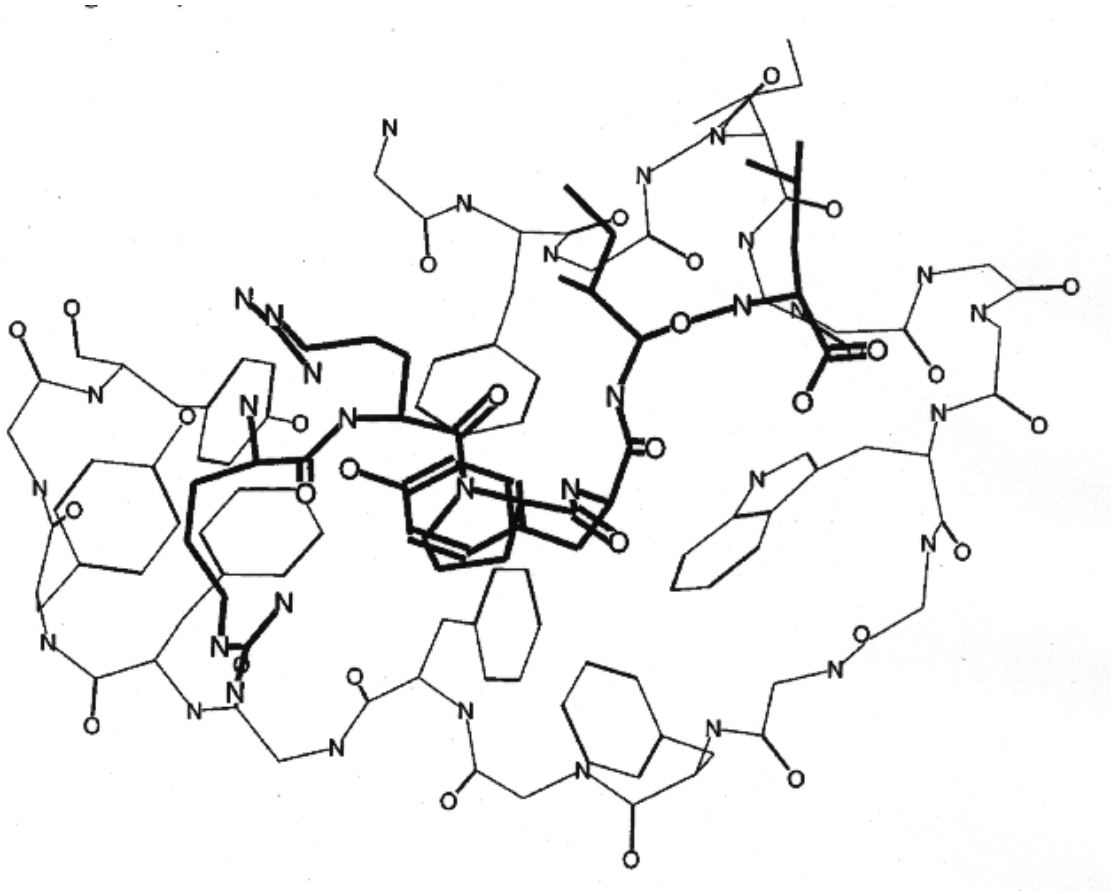

Figure 1.8: Structure of NT(8-13) bound to the agonist binding site located on the third extracellular loop of the rat neurotensin receptor. Bold lines NT(8-13), thin third extracellular loop [9]

1.4.3 Neurotensin receptor activation, heterotrimeric G-protein coupling.

Upon binding of the agonist, neurotensin, to the neurotensin receptor, a conformational change is presumed to occur that facilitates binding of the heterotrimeric G-protein and passage of information into the cell. The nature of the heterotrimeric G-protein that is coupled to the neurotensin receptor has been shown to be tissue specific. In dopaminergic neurons in the substantia nigra, for example, the neurotensin receptor is coupled to a pertussis toxin insensitive pathway[177] and is involved in the modulation of cation and potassium channels. These effects are probably mediated by the $G_{\alpha q}$ and $G_{\alpha 11}$ which have been shown to be expressed in a wide variety of tissues, and are largely insensitive to pertussis toxin [177]. In contrast, neurotensin receptors expressed in mast cells are responsible for the mobilization of the intracellular calcium through the activation of the inositol triphosphate pathway by phospholipase C. Stimulation via this pathway is thought to be mediated through the interaction of the $\beta\gamma$ subunits with phospholipase C [178]. This pertussis sensitive pathway occurs through a separate pertussis sensitive heterotrimeric G-protein[177].

Following activation, the neurotensin receptor undergoes desensitization. This process is thought to occur via activation of protein kinase C [179], which leads to both homologous desensitization and heterologous desensitization of other receptors [173]. Following prolonged activation of the neurotensin receptor, β-arrestin is found to be localised to intracellular vesicles, suggesting that receptor phosphorylation and subsequent binding of β-arrestin are involved in the sequestration of material from the cell surface [173]. Whether this sequestration results from the binding of β-arrestin to the heterologously desensitized β-adrenergic receptor or homologously desensitized neurotensin receptor is unclear. To date, no homologue of β-arrestin has been found for neurotensin. Recovery from desensitization has been shown to require gene transcription, suggesting that receptors sequestered from the cell

surface, cannot readily be recycled for fresh signalling events [180].

1.4.4 Neurotensin receptor pharmacology.

The native ligand of the neurotensin receptor is the 13 residue peptide neurotensin (K_D=2nM)(Figure 1.9)[181]. Truncated forms of neurotensin have been shown to function as an agonist [181], with the minimal sequence showing similar efficacy being neurotensin(8-13)(K_D=13nM). Studies of these truncated peptides and mutated peptides have indicated that the 6 C-terminal residues and the 2 arginines are critical for the binding of neurotensin [181][182]. Studies of cyclic peptide derived from the 6 C terminal residues (Figure 1.9) have demonstrated that if the peptide backbone is constrained with a bridge formed between the sidechains of Arg^8 and Glu^{12} an increase in efficacy is observed [183](K_D=16nM). This further supports the proposed β-turn structure for bound neurotensin(8-13) by modelling studies [9]. In addition, a free N-terminus was found to be critical for agonist binding [183].

The only non-peptidic ligands with similar binding affinities as the agonist discovered to date are a family of structurally related compounds based on the generic drug SR48692 [184]. These have been shown to act as neurotensin antagonists [184] (K_i=11.4nM). It has been suggested that this drug has a distinct binding site based on binding studies of expressed receptor containing deleted region [184]. This binding site has subsequently been modelled on the basis of site directed mutagenesis data [175], which located the binding site in the transmembrane domains and the third intracellular loop.

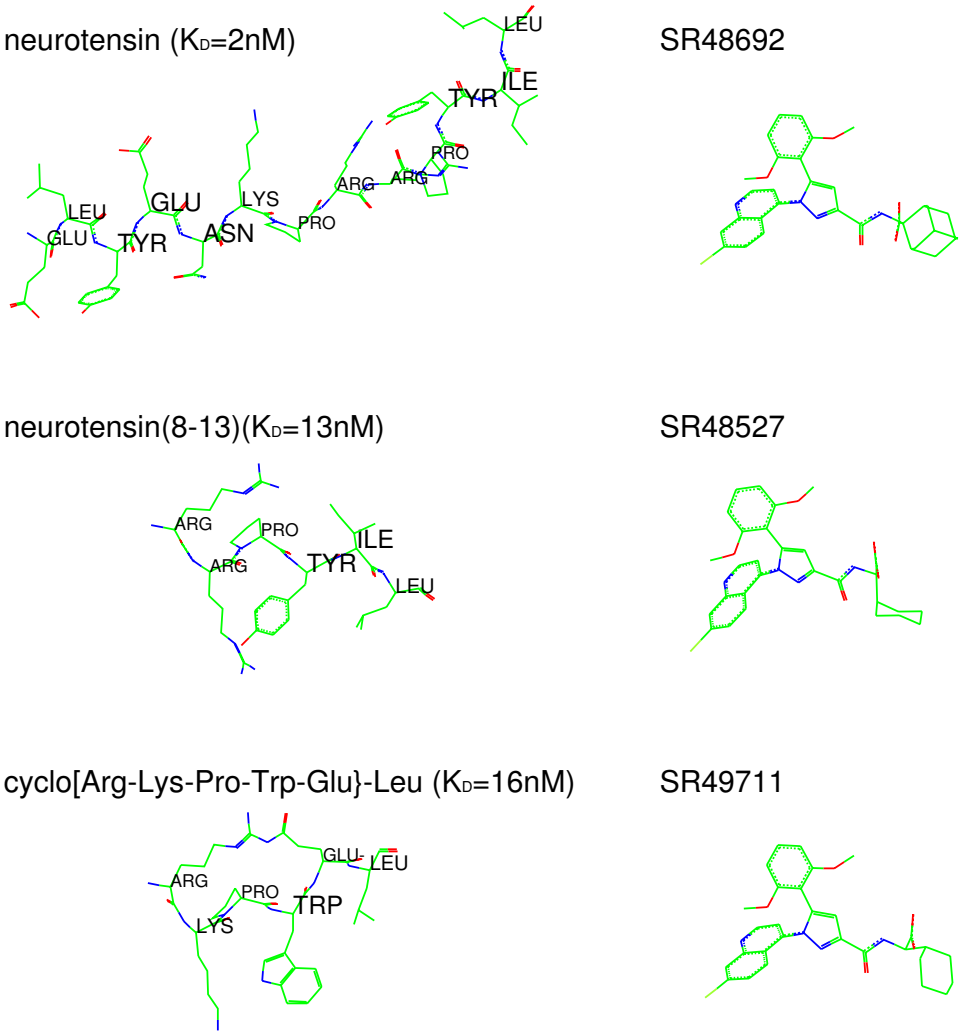

Figure 1.9: Structures of known agonists and antagonists which bind to the neurotensin receptor.

1.5 Aims of thesis.

The overall goal of this thesis was to develop the application of solid state NMR to the study of ligand protein interactions for membrane bound receptors. This has been achieved through solid state NMR studies of two large integral membrane proteins (M_r ~100kDa-280kDa), namely the nicotinic acetylcholine receptor and the neurotensin receptor. The choice of these two systems has enabled us to compare the applicability of such methodologies to two of the most important classes of integral membrane proteins, the pentameric ligand gated ions channels and the G-protein coupled receptors. The information obtained during these studies has contributed to the understanding of events surrounding ligand binding to transmembrane receptors. The specific aims of each of the experimental chapters is given below.

- In Chapter 2 the application of MAS-NMR to the study of the nicotinic acetylcholine receptor was developed. Data arising from the perturbations in chemical shift for bound labelled agonist have been interpreted in terms of the local environment occupied by the ligand whilst bound to the receptor.
- Chapter 3 describes how the anisotropy present in the deuterium NMR spectrum in the solid state provides information regarding the dynamics and orientation of the $N^+(CD_3)_3$ in bromoacetylcholine, an analogue of acetylcholine, whilst bound to the nicotinic acetylcholine receptor.
- Chapter 4 describes the preparation of the ligands neurotensin and neurotensin(8-13) with both carbon-13 and nitrogen-15. Both of these ligands have been characterised by mass spectroscopy, solution state NMR and reverse phase HPLC.
- The final experimental chapter, Chapter 5, shows MAS-NMR studies of uniformly labelled neurotensin(8-13) bound to detergent solubilised neurotensin receptor. Ligand binding was observed, and binding specificity demonstrated

through the observed perturbation of chemical shifts. Subsequent experiments were aimed at resolving labelled peptide against the background of natural abundance signals.

The general conclusions that can be drawn from this work are then presented in Chapter 6.

Chapter 2

Assignment of acetylcholine bound to the nicotinic acetylcholine receptor.

2.1 Introduction

Although structural information regarding the nicotinic acetylcholine receptor is now available to a resolution of 4.6 Å [4] from electron diffraction studies and ligand binding sites have been identified, a detailed understanding is still missing about the molecular events associated with the binding of acetylcholine to the agonist binding site. In this chapter using a variety of carbon-13 labelling schemes and MAS NMR methods a full assignment was carried out of the agonist acetylcholine bound to the nicotinic acetylcholine receptor. Through the comparison of chemical shifts of free and bound acetylcholine it has been possible to determine the nature of the agonist binding site. In addition, the assignments obtained here will act as a suitable reference for subsequent structural studies of the agonist bound to the nicotinic acetylcholine receptor under MAS conditions.

The use of CP-MAS NMR has allowed the study of isotopically enriched ligands bound to membrane proteins in a wide variety of systems [16][35]. Introduction of carbon-13 labels at the N-methyl position in the acetylcholine, has enabled the detection of bound acetylcholine under MAS conditions at near physiological conditions. The specificity of this observation has been demonstrated through the use of the specific inhibitor α-bungarotoxin, which displaces acetylcholine from its binding site. In addition, through the use of relaxation phenomena and a dipolar dephased cross polarization sequence, it is possible to give an estimate for the residency time of the ligand whilst bound to the nicotinic acetylcholine receptor.

Studies with acetylcholine labelled at both the N-methyl and C-methyl positions has enabled detailed geometries to be obtained for the crystalline ligand acetylcholine perchlorate as a crystalline salt. Structural investigations using established methodologies such as rotational resonance [76] were hindered by an inability to assign the labelled sites against the natural abundance carbon-13 arising from the receptor membranes. Subsequent studies centred on obtaining a full assignment of uniformly labelled acetylcholine which provides information about the local electrostatic environment within the agonist binding site, and act as a suitable starting point for further structural investigations.

Initial attempts to obtain both assignments and structural information were focused on the application of broadband dipolar recoupled exchange MAS NMR. These were chosen in preference over other techniques, as they facilitated both assignment and structural information from one experiment. During the course of these experiments we have been able to obtain pure absorption 2D exchange spectra of uniformly labelled acetylcholine perchlorate. Qualitatively these can be interpreted as in agreement with the known structure of the acetylcholine perchlorate obtained by X-ray diffraction methods [185]. Application of this methodology to biological membranes was hindered due to the presence of molecular motion in the system thereby interfering with the recoupling schemes used and enhancing the rate of relaxation. Together, these effects limited the quality of data obtainable under conditions where long range structural constraints may be observed.

With the advent of efficient double quantum excitation schemes under MAS, 1D double quantum filtered CP-MAS experiments were performed in order to effectively supress natural abundance signal from the membrane whilst allowing the selective observation of uniformly carbon-13 labelled agonist, acetylcholine. These were demonstrated to give reasonable double quantum excitation for a multiply labelled compounds, as many previous experiments had centred on the study of double labelled material [69]. Subsequent investigations of the ligand bound to the

nicotinic acetylcholine receptor were initially hindered by residual motions, even at -60°C. However, at -120°C these had been sufficiently suppressed to allow efficient double quantum excitation and the assignment of all sites within the acetylcholine, whilst bound to the nicotinic acetylcholine receptor.

In this chapter we therefore present the work necessary for a complete assignment of labelled acetylcholine bound to the nicotinic acetylcholine receptor, and for the detection of chemical shift perturbations upon binding to the presence of particular functional groups within the binding site.

2.1.1 Rotational Resonance Studies

Rotational resonance has seen widespread application in the study of structure elucidation in biological sciences (for review see Section 1.2.2), due to the exact relationship between the dipolar coupling and the internuclear distance. In this work rotational resonance studies were perfomed on crystalline acetylcholine perchlorate labelled strategically at both the N and C methyl positions. These studies have provided detailed structural information regarding the crystalline ligand. If sufficient resolution was available structural studies of acetylcholine bound to its binding site in the nicotinic acetylcholine receptor would be possible.

The extent to which magic angle spinning averages the dipolar interaction between homonuclear spin pairs depends strongly on both the magnitude of the interaction and the rate of sample spinning. In addition, if the isotropic chemical shift difference ($\Delta\omega_{iso}/2\pi$) greatly exceeds the magnitude of the dipolar coupling strength then the energy mis-match between the two states will limit magnetization exchange between the two spins. An exception to these conditions occurs when the rate of sample rotation is equal to a multiple of the chemical shift difference the rotational resonance condition is met ($\Delta\omega_{iso} = n\omega_r$)[186][63]. The relevant Hamiltonian for

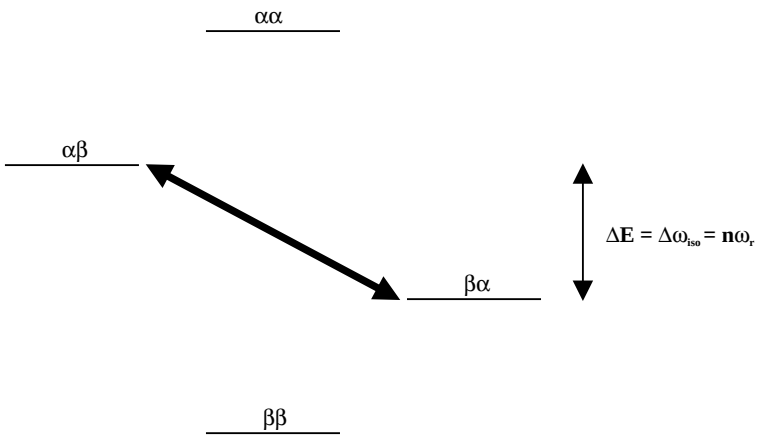

Figure 2.10: Energy level diagram for a chemically shifted homonuclear spin pair, demonstrating how rotation of the sample at the rotational resonance condition provides the necessary quanta of energy to stimulate exchange via a flip flop mechanism.

two chemically shifted spins is given by:

$$H(t) = \omega_k(t)S_{kz} + \omega_l(t)S_{lz} + \omega_A(t)2S_{kz}S_{lz} + \omega_B(t)\frac{1}{2}(S_k^+S_l^- + S_k^-S_l^+) \qquad (2.16)$$

Under MAS conditions each spin has a time independent isotropic contribution to the chemical shift along with a anisotropic oscillatory component, whilst the dipolar terms average to zero over the rotor cycle [186][187]. Under normal conditions where $\Delta\omega_{iso} \gg H_D$ then exchange via the dipolar flip flop term $\omega_B(t)\frac{1}{2}(S_k^+S_l^- + S_k^-S_l^+)$ is usually insignificant. However, if the rotational resonance condition is met $\Delta\omega_{iso} = n\omega_r$, then energy associated with the macroscopic reorientation of the sample occur at the right energy to reintroduce the flip flop process between the two spins and both dipolar terms become significant (Figure 2.10) [186][63].

Reintroduction of dipolar coupling can have a pronounced effect on lineshapes when the dipolar coupling is strong [63][186] and can be used to estimate the size of the dipolar coupling. However it is more conventional to measure the dipolar coupling as a magnetization exchange experiment, which allows dipolar couplings as small as 200 Hz to be measured accurately. Magnetisation at one of the labelled sites is selectively inverted and then the exchange between the two sites monitored as a function of mixing time [63][186]. The evolution of this magnetization can be

simulated [186][188] in order to accurately determine the strength of the dipolar interaction. The magnetization exchange trajectories obtained do not depend solely on the dipolar coupling, additional contributions are made from T_{2ZQ}, the chemical shift anisotropy and relative orientation of the chemical shift tensors [186][188][189]. At the n=1 rotational resonance condition, many of these terms can be neglected, with the exchange curves being dominated primarily by the dipolar coupling and the T_{2ZQ} [188][189]. The T_{2ZQ} contribution can be estimated experimentally from the linewidths of the two labelled sites [189]

$$T_{2ZQ} = \frac{1}{\Delta v_{1/2}^{S_k} + \Delta v_{1/2}^{S_l}} \tag{2.17}$$

This only provides an estimate of the T_{2ZQ}, however a suitable fit of the exchange curves enables an accurate determination of both the dipolar coupling and the T_{2ZQ} contributions [188].

2.1.2 Broadband Dipolar Recoupled Exchange MAS-NMR Spectroscopy.

For structure elucidation in the solution state, both through space and through bond correlations spectra are required to provide information for both resonance assignment and structure elucidation. In the solution state through space information is obtained from nuclear Overhauser experiments, where the dipolar interactions are observed in the form of cross relaxation effects. In the solid state the dipolar couplings can be observed directly, however this is frequently impossible as spectral resolution is also compromised through the presence of the chemical shift anisotropy. This is typically overcome through the application of MAS, unfortunately this also efficiently averages the homonuclear dipolar coupling required to provide through space information. In order to obtain structural information in the solid state one would ideally want to obtain total through space correlation spectra (TOSSY) [190] where cross peaks arise solely from the presence of dipolar coupling between two

nuclei and are insensitive to experimental conditions employed such as spinning speed, frequency offset, radiofrequency amplitude and the relative orientation of the chemical shielding and dipolar tensors. To this end a variety of experimental techniques have been developed aimed at reintroducing the dipolar interaction under the presence of MAS.

Rotating inverse laboratory frame zero quantum transfer(RIL-ZQT) broadband dipolar recoupling under MAS.

The initial goal in the implementation of broadband recoupling techniques to uniformly carbon-13 labelled acetylcholine bound to the nicotinic acetylcholine receptor was to facilitate the assignment of the ligand against a background arising from natural abundance carbon-13 present in the membrane. In addition the technique would ideally allow multiple structural constraints to be obtained from the uniformly labelled ligand.

As outlined above, total through space correlation spectroscopy under MAS conditions (TOSSY) [190], demands the reintroduction of only the dipolar term of the Hamiltonian during the mixing period of a 2D exchange experiment. Several techniques have been proposed to reintroduce the dipolar term in such experiments ranging from flipping of the rotor axis away from the magic angle during the mixing period, whilst others lead to the exchange of magnetization solely through zero ($S_k^+ S_l^- + S_k^- S_l^+$) or double ($S_k^+ S_l^+ + S_k^- S_l^-$) quantum terms. The primary difference between these two types of transfer arises from the evolution of these two operators, as double quantum transfer conserves the difference polarization whilst allowing the sum of the polarization to evolve. In contrast zero quantum transfer retains the sum of the magnetization and allows the evolution of the difference polarization. For the purpose of studying multispin systems a zero quantum transfer technique was preferred as the total magnetization remains constant and thus the exchange of magnetisation between labelled sites can be discussed in terms of a kinetic matrix,

where the redistribution of magnetization occurs whilst retaining the sum of the magnetization. The terms of such a kinetic matrix allows the determination of relative constraints between labelled sites within the molecule.

The zero quantum transfer scheme used (Figure 2.11) is similar to that proposed by Baldus & Meier [190][191][192] which is based on the rotating frame/laboratory frame transfer principle originally exploited by Fujiwara *et al.*[193]. The sequence exploits the change in sign of the dipolar Hamiltonian in the laboratory and rotating frames, and when applied synchronously with sample rotation can lead to a recovery of the dipolar Hamiltonian under MAS conditions.

If one assumes that the applied r.f. field is sufficiently high to effectively spin lock all nuclear spins and all pulses occur at the delta limit then the dipolar Hamiltonian over the R (rotating frame) component of the pulse sequence is given as:

$$\langle H_{S,D}\rangle_L = \sum_{(k<l)} \frac{-b^{(k,l)}}{\sqrt{2\pi}} \sin(2\theta^{kl}) \sin(\varphi^{kl}) \times [2S_{kz}S_{lz} - \frac{1}{2}(S_k^+ S_l^- + S_k^- S_l^+)] \quad (2.18)$$

and over the L (laboratory frame) component is given as:

$$\langle H_{S,D}\rangle_L = \sum_{(k<l)} \frac{-2b^{(k,l)}}{\sqrt{2\pi}} \sin(2\theta^{kl}) \sin(\varphi^{kl}) \times [2S_{kz}S_{lz} - \frac{1}{2}(S_k^+ S_l^- + S_k^- S_l^+)] \quad (2.19)$$

where b_{kl} is $-\mu_0\gamma_l\gamma_k\hbar/4\pi r_{kl}^3$. Thus the average Hamiltonian over the entire sequence is given as:

$$H^0_{(S,D)} = \langle H_{S,D}\rangle_L + \langle H_{S,D}\rangle_R = \sum_{(k<l)} \frac{-3b^{(k,l)}}{\pi\sqrt{2}} \sin(2\theta^{kl}) \sin(\varphi^{kl}) \times [2S_{kz}S_{lz} - \frac{1}{2}(S_k^+ S_l^- + S_k^- S_l^+)] \quad (2.20)$$

Thus under the strong r.f. limit where all but the homonuclear dipolar Hamiltonian disappear, the average Hamiltonian over the sequence leads to a pure zero

quantum polarization transfer by a flip-flop process. For a 2 spin system this zero quantum term evolves as:

$$\langle I_{kz} - I_{lz}\rangle t = \langle I_{kz} - I_{lz}\rangle(0) \times \{1 + S\cos((\frac{-3b^{(k,l)}}{2\pi\sqrt{2}}\sin(2\theta^{kl})\sin(\varphi^{kl}))t) - 1)\} \quad (2.21)$$

Where the strong r.f. approximation does not hold, then other terms contribute to the Hamiltonian. However the modifications of the original rotating/laboratory frame recoupling method [193] suggested by Baldus and Meier [191] effectively compensate for such effects leading to an effective Hamiltonian during the mixing sequence arising solely from zero quantum transfer.

Pure phase exchange spectroscopy under MAS.

Two dimensional exchange spectroscopy, has long been used to study exchange processes occurring on timescales too slow to have any effect on lineshapes such as cross-relaxation, nuclear Overhauser effects, spin diffusion, cross polarization effects and molecular reorientation. Here 2D exchange spectroscopy is being used to observe the exchange of magnetization being driven by rotating inverse laboratory frame zero quantum transfer.

In order to obtain optimal resolution adsorptive lineshapes are required for both diagonal and cross peaks. In 1D NMR adsorptive lineshapes are obtained through quadrature detection and subsequent phase correction of the Fourier transformed spectra. In 2D NMR adsorptive lineshapes can be obtained through the use of the Time Proportional Phase Incremented (TPPI) acquisition[38] which results in both the real and imaginary components being retained allowing pure phase lineshapes ($S(\omega_1, \omega_2)$) to take the form $a_i(\omega_1)a_j(\omega_2)$. However, when TPPI acquisition is applied to a sample rotating at the magic angle the experiment does not consist only of these simple pure phase peaks. In addition auto cross peaks between sidebands appear due to insufficient averaging of the chemical shift anisotropy as well as non

pure lineshapes. Both these effects have a detrimental effect on the quality of data obtained lowering both sensitivity and resolution[194].

To eliminate the auto correlated cross peaks in 2D exchange MAS NMR, De Jong *et al.* suggested synchronising the mixing time with the rotor synchronisation [195]. To obtain pure adsorptive lines, Hagemeyer *et al.* combined the 2D spectra measured with rotor synchronisation with the 2D spectra using a time reversal scheme [194][196][197]. During the course of this work a similar scheme using time proportional phase incremented (TPPI) acquisition was proposed by Boender [198] which is similar to that outlined below.

Here we have employed the scheme outlined by Luz [194] with TPPI, however through the correct choice of coherence transfer during t_1 it is possible to collect both normal and time reversed signals in one experiment, alleviating the need for subsequent data manipulation after Fourier Transformation in the frequency domain. This scheme is outlined in Figure 2.11. Briefly, transverse magnetization is generated by a preparatory cross polarization pulse with a two step phase cycle on the carbon-13 mixing pulse for axial peak suppression. This initial cross polarisation pulse sequence is also phase cycled according to the TPPI protocol. The magnetization is then allowed to evolve for a period (t_1) with continuous wave proton decoupling. At the end of this evolution period magnetization is stored along the longitudinal axis by a carbon $\pi/2$ pulse which serves to select both the p=$\pm$1 coherence pathway. The following delay selects for either normal or time reversed acquisition in t_1. Magnetization is returned to the transverse plane by a non selective carbon $\pi/2$ pulse. Magnetization is exchanged using the rotating inverse laboratory zero quantum transfer scheme described above, and subsequently observed. Thus for each increment under the TPPI scheme both normal and time reversed acquisitions must be performed. Previously these two datasets had been acquired and processed independently, after which one dataset was reflected about ω_1=0 prior to their addition. This resulted in pure phase lineshapes in both ω_1 and ω_2. We have

allieviated the necessity to acquire two independent datasets by affecting the reflection about the ω_1 axis in the time domain. This has been achieved by selecting the p=+1 coherence pathway during t_1 for the non-time reversed acquisition and the p=-1 pathway for the time reversed acquisition. Following the appropriate Fourier Transform pure lineshapes are obtained in both ω_1 and ω_2.

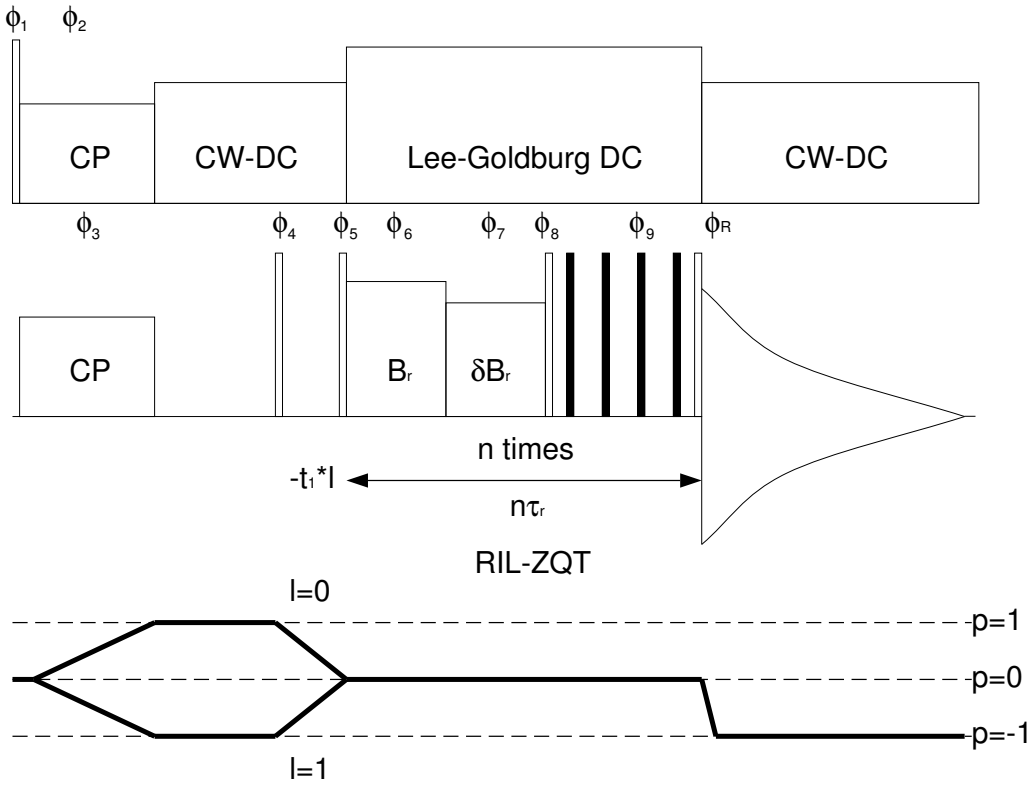

Figure 2.11: Diagram of RIL-ZQT transfer sequence used to acquire pure adsorption broadband dipolar recoupled exchange spectra. Initially magnetization is generated using a conventional cross polarization sequence, subsequently the magnetization is allowed to evolve during t_1 under continuous wave proton decoupling. After the initial evolution period magnetization is stored longnitudinally by a non selective $\pi/2$ pulse. The magnetization is then either stored longitudinally until the start of the next rotor cycle ($l = 1$) and then retuned to the transverse plane by a second $\pi/2$ pulse or returned there directly. During the following RIL-ZQT mixing sequence zero quantum transfer is allowed to proceed for a fixed number of rotor periods. The magnetization is then sampled. Pulses are phase cycled according to ϕ_1= 0; ϕ_2= 90; ϕ_3= 0,180; ϕ_4= 0, 0, 90, 90, 180, 180, 270, 270; ϕ_5=0 ; ϕ_6= 270; ϕ_7= 90; ϕ_8= 180; ϕ_9= 0;ϕ_R= 0, 180, 270, 90, 180, 0, 90, 270, 0, 180, 90, 270, 180, 0, 270, 90; l= 0, 0, 0, 0, 0, 0, 0, 0, 1, 1, 1, 1, 1, 1, 1, 1. The phases of the initial cross polarization are phase cycled according to a TPPI scheme.

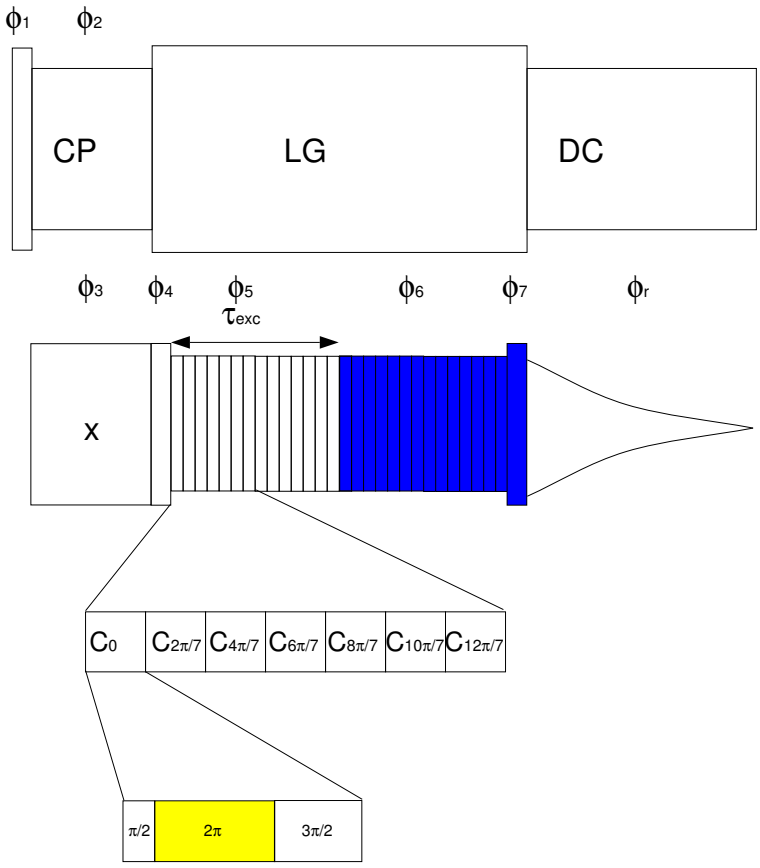

Figure 2.12: Diagram outlining the POST-C7 pulse sequence used to acquire double quantum filtered spectra under MAS conditions. C7 elements during the reconversion sequence (blue) are phase cycled together with the receiver to selectively observe double quantum coherence. The $\pi/2 - 2\pi - 3\pi/2$ C element is incremented by $2\pi/7$ for each C element, whilst the central 2π pulse (yellow) has opposite phase with respect to with both the $\pi/2$ and $3\pi/2$ pulse. Phases cycles according to ϕ_1=0; ϕ_2=90; ϕ_3=0; ϕ_4=0; ϕ_5=0; ϕ_6=0,90,180,270; ϕ_7=0,90,180,270; ϕ_r=0,270,180,90.

2.1.3 Double quantum filtered MAS NMR

Broadband dipolar recoupled exchange MAS spectroscopy offers the potential to both assign and provide structural information about ligands bound to large membrane associated complexes, allowing labelled sites to be identified via cross peaks

in the exchange spectra. An alternative approach allowing us to distinguish labelled molecules against a background of unlabelled material was made by the use of double quantum filtered spectra. In double quantum filtered spectra, the nuclear magnetisation of coupled spin pairs is passed through double quantum coherence, a quantum state of correlated transverse spin polarization. This is readily selected for by the appropriate phase cycle. Such double quantum filtered spectra distinquish between molecules containing multiple spins and those from isolated spins which are unable to support double quantum coherence. Thus in the case for carbon-13 spectroscopy, the probability of finding two neighbouring carbon atoms that are both labelled is 0.01% (ie 1% of 1%). Such techniques offer an excellent approach for the suppression of background signals.

Although several methods have been proposed for double quantum filtered spectra under MAS condition [199][200], to date the sequence that offers both high levels of double quantum excitation, whilst tolerating rf inhomogeneities, large isotropic and anisotropic shifts is C7 and its derivatives[201][202]. In addition, the relatively short double quantum excitation times (<1ms) reduces losses arising from relaxation and inefficient decoupling, which may hinder the implementation of other techniques offering higher double quantum excitation efficiencies [203] but required extended excitation times.

The C7 double quantum filtered experiment used is shown in Figure 2.12. Initially transverse magnetization is created through the use of a conventional cross polarization sequence. Subsequently longitudinal magnetization is generated by means of a non selective $\pi/2$ pulse. Following this a C7 double quantum excitation sequence is employed as shown in Figure 2.12 for a period of τ_{exc}. A second period of C7 excitation of duration τ_{exc} is then used to reconvert double quantum coherence into longitudinal magnetization. Observable transverse magnetization is subsequently selected by means of a non selective $\pi/2$ pulse. Double quantum coherence is generated by means of the appropriate phase cycling of both the C7

reconversion sequence, final $\pi/2$ pulse and the receiver.

During the C7 excitation and reconversion sequence, dipolar averaging under MAS conditions is avoided through the use of a N fold symmetric sequence composed of N sequential Cφ elements. Each of these elements has a duration of $2\tau_{\mathrm{r}}/N$ where $\tau_{\mathrm{r}} = 2\pi/\omega_{\mathrm{r}}$ and the phase of consecutive elements incremented by $\varphi = 2\pi/N$. This recoupling scheme has been shown to give rise to an average Hamiltonian of the form[201][202]:

$$H_D = -\frac{1}{2}\frac{\mu_0\gamma_I^2\hbar}{4\pi r_A^3 B}\sin(2\beta_{CR})(\kappa_N \exp\{i(\omega_r t_0 - \gamma + CR)\}I_A^+ I_B^+ + \kappa_N^* \exp\{-i(\omega_r t_0 - \gamma_C R)\}I_A^- I_B^-)\} \tag{2.22}$$

The scaling factor κ_N depends on the exact nature of the C_φ elements used but for both C7 and POST C7, where the C elements are composed of $2\pi_x 2\pi_{\bar{x}}$ and $\pi/2_x 2\pi_{\bar{x}} 3\pi/2_x$ respectively, κ_N is given as:

$$\kappa_N = \frac{3iN(1 - \exp\{4i\pi/N\})}{8\sqrt{2}(4N^2 - 1)} \tag{2.23}$$

For all the studies performed here, POST-C7 has been chosen. Although the dipolar scaling factor is identical to that of C7, it offers greater compensation for off resonance effects, chemical shift anisotropy and r.f. inhomogeneity[202].

The application of this technique for the filtering of background, isolated spins from multiply labelled samples, is demonstrated in Figure 2.13. Here a sample has been created containing a 1:1 mix of 1-^{13}C leucine(174ppm) and 2,3-^{13}C sodium propionate(26.8/8.9ppm). The conventional CP spectra are shown in Figure 2.13A where all three labelled sites are clearly resolved. The POST-C7 double quantum filtered spectra of the same sample are shown in Figure 2.13B, The carbonyl from the 1-^{13}C leucine has been totally suppressed (not visible above noise) whilst the adjacent labels in the sodium propionate able to support double quantum coherence, are selected for. Similar experiments applied to ligands bound to membrane receptors offer a valuable route to the assignment of labelled ligands against a background of natural abundance arising from protein and lipid within the system. This

has been used in this chapter to partially assign uniformly carbon-13/nitrogen-15 labelled acetylcholine bound to the nicotinic acetylcholine receptor.

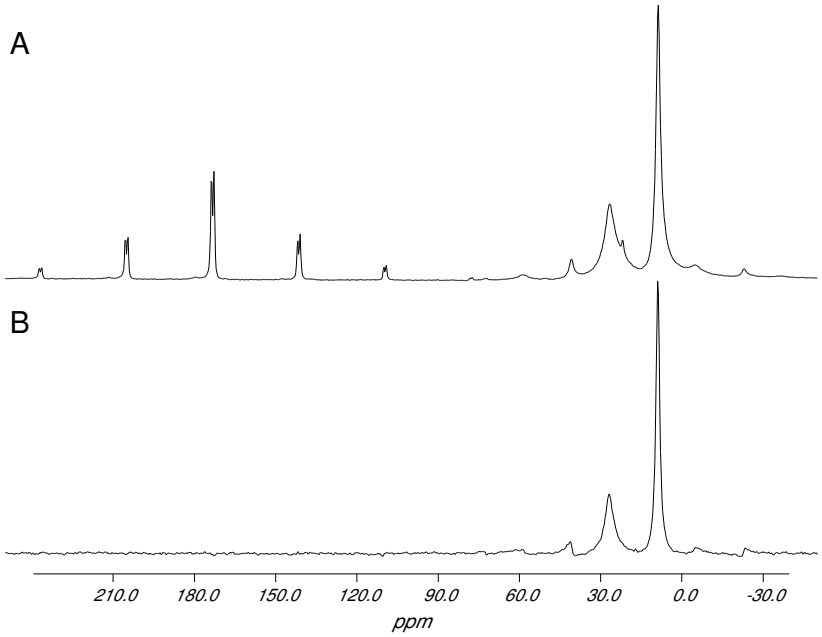

Figure 2.13: Demonstration of the effective suppression of uncoupled/natural abundance spins under CP-MAS conditions using the POST-C7 seqeunce. 1ms cross polarization spectrum (A) double quantum filtered cross polarization experiment(B). Both spectra acquired at 4kHz spinning, and the result of 64 acquisitions.

2.2 Materials & Methods

2.2.1 Synthesis of isotopically enriched acetylcholine.

Choline labelled at the N-methyl position was synthesized from ethanolamine and ^{13}C methyliodide (Sigma). The product was subsequently acetylated using 2,2' acetic anhydride (Cambridge Isotope Ltd) to give acetylcholine iodide. Recrystallization from a hot saturated solution of ammonium perchlorate in ethanol gave acetylcholine perchlorate. Identity and purity were monitored by ^{1}H NMR and electrospray mass spectroscopy. Acetylcholine perchlorate was added to the membrane preparation in small aliquots (no more than 25μl of liquid were added to the pellet

during any experiment) from a concentrated stock solution in 10 mM phosphate buffer (pH 7.0), until the concentration of agonist was equivalent to the number of receptor binding sites.

For the rotational resonance studies acetylcholine perchlorate was singly labelled at the N-methyl group and the C-methyl group to aid the interpretation of the data. This was achieved by the methylation of dimethylaminoethanol (Sigma) with ^{13}C methyliodide (Sigma). The product of this reaction was subsequently purified by crystallization. The choline formed was subsequently acetylated, purified and characterized as described above and shown to be doubly labelled acetylcholine perchlorate. Prior to solid state NMR studies the sample was recrystalised at a ratio of 1:6 with unlabelled acetylcholine perchlorate from hot ethanol.

2.2.2 Synthesis of uniformly labelled acetylcholine perchlorate

Uniformly carbon-13 labelled acetylcholine was synthesized by methylation of 250 mg of 1,2-^{13}C ethanolamine (Isotec Inc., MA) with 5g ^{13}C iodomethane (Sigma, UK) in 5ml of ethanol. The product choline iodide was subsequently purified by recrystallization from hot ethanol. The choline iodide was then acetylated with 1,2-^{13}C acetic anhydride (Isotec Inc.) in 5ml pyridine using trace dimethylaminopyridine as a catalyst. The product, acetylcholine iodide, was collected by filtration and subsequently purified by recrystallisation from a saturated ammonium perchlorate ethanol solution, yielding acetylcholine perchlorate (160mg).

The product was characterised by electrospray mass spectrometry. A single molecular ion peak at 153 was observed, indicating over 99% enrichment. ^{1}H NMR on the U-^{13}C labelled acetylcholine gave the expected proton spectra, with the appropriate splitting for carbon-13 labelled material.

2.2.3 Purification of nicotinic acetylcholine receptor enriched membranes.

Membranes rich in the nicotinic acetylcholine receptor were purified according to the method of Sobel [204] from *Torpedo nobiliana*. Membranes were resuspended in 20 mM phosphate buffer (pH 7.0) to a protein concentration of 1mg ml^{-1} and treated with 10 mM diispropylfluorophosphate (DFP) to inhibit the action of acetylcholine esterase. Specific inhibition of the nicotinic acetylcholine receptor was achieved by incubating membranes (4°C/ 24h) with α-bungarotoxin at a stoichiometry of between 5 and 10 times the agonist binding sites prior to the treatment with DFP. Membrane pellets were prepared by ultracentrifugation (4°C; 80000g; 1h) of membrane suspension and contained typically 0.8 nmoles binding site per mg of protein, as determined using a dansyl-choline displacement fluoresence assay [124]. About 50mg of pellet was subsequently loaded into a 7mm MAS-NMR rotor and sealed using Kel-F caps for subsequent NMR studies.

2.2.4 NMR experiments.

Carbon-13 natural abundance CP-MAS spectra of acetylcholine perchlorate were acquired on a Bruker MSL-400, at 100.63 MHz for carbon-13 (400.13MHz for protons). A spinning speed of 2500±2 Hz was used for all samples and the temperature maintained at 283 K using the bearing air. A proton field strength of 50kHz was applied for cross polarization and decoupling.

Dipolar dephased cross polarization studies used to determine the rates of ligand exchange is similar to those used for spectral editing in crystalline samples. Initially magnetisation is converted to transverse magnetisation by a non selective $\pi/2$ pulse. Half way through the initial rotor period a π pulse with opposite phase, refocuses any chemical shift and accounts for any error in pulse length. After this initial rotor period, magnetisation is restored along the longitudinal axis by means of a non selective $\pi/2$ pulse. During this initial rotor period, transverse magnetisation

associated with the immobile membrane bound components, including receptor and bound ligand, have sufficient time to dephase due to their short T_2 whilst ligand in free solution retain their coherent magnetisation. The subsequent mixing time allows the ligand to exchange with that in free solution. The subsequent observation by conventional cross polarisation allows the selective detection of newly bound ligand provided that the rate of exchange is faster than the recovery of magnetisation due to T_{1z} relaxation. Therefore, a lower limit can be placed on the residency time for the carbon-13 enriched acetylcholine which is bound to the receptor.

Rotational resonance studies of $N^{13}CH_3(CH_3)_2,^{13}CH_3$ acetylcholine perchlorate were recorded at 100.63 MHz for ^{13}C and 400.13 MHz for ^1H using a Bruker MSL 400 and a double resonance 4mm probe (Bruker, Germany). Typical pulse lengths were 4μs. Rotational resonance experiments were performed using a DANTE pulse sequence and RAMP cross polarization. The spinning speed was controlled within a range of $\pm$ 1 Hz using a home built spinning speed controller.

Magnetisation exchange curves were simulated using the program RR-FIT, developed in our group by Dr C. Glaubitz and is based on an analytical expression for the magnetization exchange curve [188]. This was combined with the non-linear fitting package MINUIT(CERN) [205] which facilitated the fitting of any combination of spin parameters within a reasonable time. All simulations were performed on a SGI-INDY 4600 workstation.

Rotating Inverse Laboratory Frame Zero Quantum Transfer (RIL-ZQT) experiments were acquired on a Chemagnetics CMX-500 at 125.7 MHz carbon-13 (500 MHz proton) equipped with either a 6mm double or triple resonance probe head. Spinning was maintained at 4000$\pm$2 Hz using a Chemagnetics spinning speed controller. The temperature was set to that defined for the particular experiment and maintained with $\pm$1°C using a Chemagnetics temperature controller. Total through space correlation spectra were acquired with the RIL-ZQT mixing scheme and time reversal for pure phase lineshapes as described in the introduction and

shown in Figure 2.11. A proton field strength of 50 kHz was employed for cross polarization. During both t_1 and t_2 evolution periods broadband decoupling was performed at 75 kHz. Although TPPM decoupling has been applied in similar situations, no improvements over broadband decoupling were observed for acetylcholine perchlorate under the conditions described, although at higher spinning speeds and B_1 fields it offered some advantage. During mixing a variety of decoupling sequences were tried to ascertain which performed optimally for homonuclear recoupling using the RIL-ZQT scheme. No improvement was found on the original frequency offset Lee Goldberg decoupling, thus during mixing a proton B_1 field of 75 kHz was applied offset from the carrier frequency by 53 kHz. During the RIL-ZQT mixing sequence, magnetization was locked during the first quarter of the rotor period using a carbon field of 50 kHz, and scaled during the second quarter of the rotor period by (δ) 0.92 as described in earlier work [190]. During the second half of the rotor cycle π and $\pi/2$ pulses were performed at 3.5 and 7.0 μs respectively. Pure phases data was acquired with the time reversal scheme described previously and the phase cycling as shown. Unless stated, data was acquired with 2048 points in t_2 and 128 points in t_1 with 128 acquisitions per t_1 increment. A complex Fourier Transformation was applied in t_2. Data was linear predicted in t_1 from 128 points to 512 and processed with a sinebell function (512 points, 90° offset). The data was subsequently zero filled to 2048 points and processed with a real Fourier Transform.

Cross polarization double quantum filtered spectra were acquired on a Chemagnetics CMX-500 at 125.7MHz carbon (500 MHz proton frequency) equipped with either 6mm double to triple resonance probehead. Spinning was maintained at 4000±2Hz using a Chemagnetics spinning speed controller. The temperature was set to that defined for the particular experiment and maintained with ±1° using a Chemagnetics temperature controller. A proton field of 50kHz was used for cross polarization. Double quantum filtered CP-MAS spectra were acquired with the POST-C7 sequence as described before. The B_1 field was matched to 7 times the

spinning speed, 28kHz, and 13 C7 cycles were performed for both excitation and reconversion, giving a total excitation time of 0.598 ms. Double quantum coherence was selected for by the phase cycles given in Figure 2.12. Data was zero filled to 4096 points and processed with 50 Hz linebroadening prior to Fourier Transformation.

2.2.5 Computer predictions of ring current contributions to chemical shifts.

The expected perturbation in carbon-13 chemical shift due to the presence of aromatic systems was calculated on a SGI-Indy workstation, using simulations available from Dr M.P. Williamson [206][207] based on the Haugh-Mallion model [208]. The predictions were based on the position of aromatic resonances within the crystal structure of acetylcholine bound to the acetylcholinesterase [209] (Protein databank accession number 2ACE)

2.3 Solid state NMR studies on solid acetylcholine perchlorate.

2.3.1 Assignment of resonances in acetylcholine perchlorate.

CP-MAS spectra of unlabelled acetylcholine perchlorate gave five resonances which could be assigned to the five magnetically inequivalent sites (Figure 2.14). The resonances have been assigned on the basis of those from solution, and shielding considerations; CO(172.1ppm, a), NCH_2(64.5ppm, b), OCH_2 (59.2ppm, c), $N(CH_3)_3$ (53.9ppm, d) and CH_3 (20ppm, e).

2.3.2 Rotational resonance studies of crystalline $N(^{13}CH_3)$,$C^{13}CH_3$ acetylcholine perchlorate.

Rotational resonance studies of $N(^{13}CH_3CH_3CH_3$,$C^{13}CH_3)$ acetylcholine perchlorate were performed in order to obtain detailed structural information relating to the

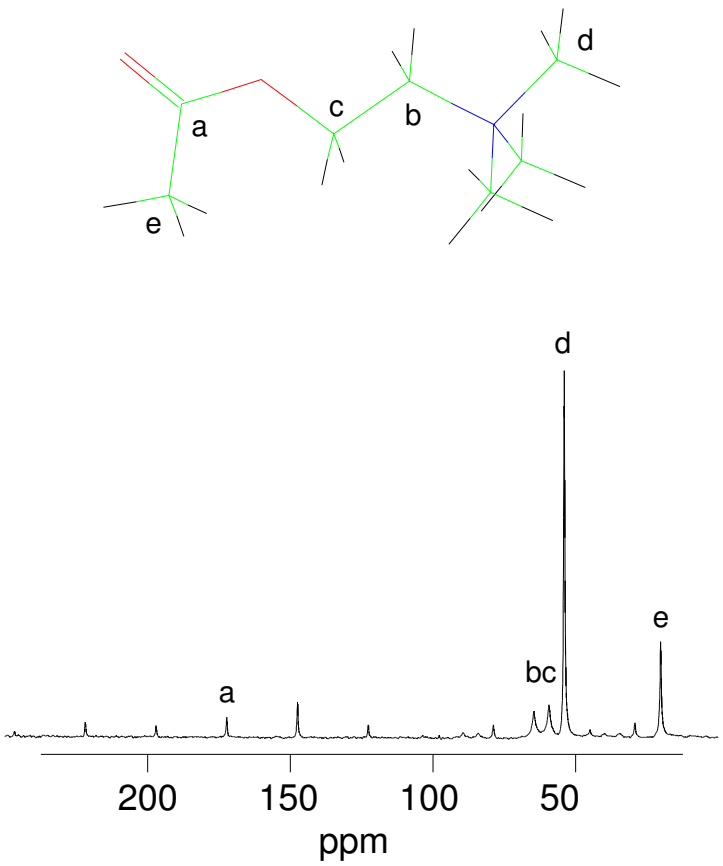

Figure 2.14: Structure of acetylcholine perchlorate (A) with CP-MAS spectrum of acetylcholine perchlorate obtained with 64 acquisitions using a 1ms contact time and a spinning speed of 2500Hz at room temperature (B) showing the assignments of the resonances apparent in the carbon-13 spectrum.

acetylcholine in the acetylcholine perchlorate. In order to facilitate detailed simulations of the magnetisation exchange trajectories, the chemical shift anisotropy of the two labelled groups was ascertained from the study of static and low speed CP-MAS spectra (Figure 2.15). The resulting spectra were analyzed using the Hertzfeld-Berger algorithim [210] and the software SPEEDYFIT [210]. The results of these studies are shown in Table 2.3. Importantly for the analysis of the rotational resonance data, the CSA values of the two labelled sites do not overlap, but are of a similar magnitude to the chemical shift difference.

The magnetization exhange curve for the n=1 condition (ω_r=3416Hz) measured for the above sample is shown in Figure 2.16. The data has been corrected for intensity arising from natural abundance carbon-13 and the data normalized to an average of the first five points of the exchange curve. The best fit (sum of squares of errors=0.9*10^{-4}) obtained from optimising the T_{2ZQ} and the b_{IS} is plotted over the experimentally determined points. The observed dipolar coupling of $b_{IS}/2\pi$ is -85±7Hz (0.447±0.012nm) corresponds well with that observed in the crystal structure of the acetylcholine perchlorate (0.44nm). The T_{2ZQ} of 10.5±4ms is also in good agreement with the value estimated from the off resonance linewidths measured from the two labelled sites (8.0ms), based on $T_{2ZQ} \geq 1/(\pi(\Delta v^I_{1/2} + \Delta v^S_{1/2}))$

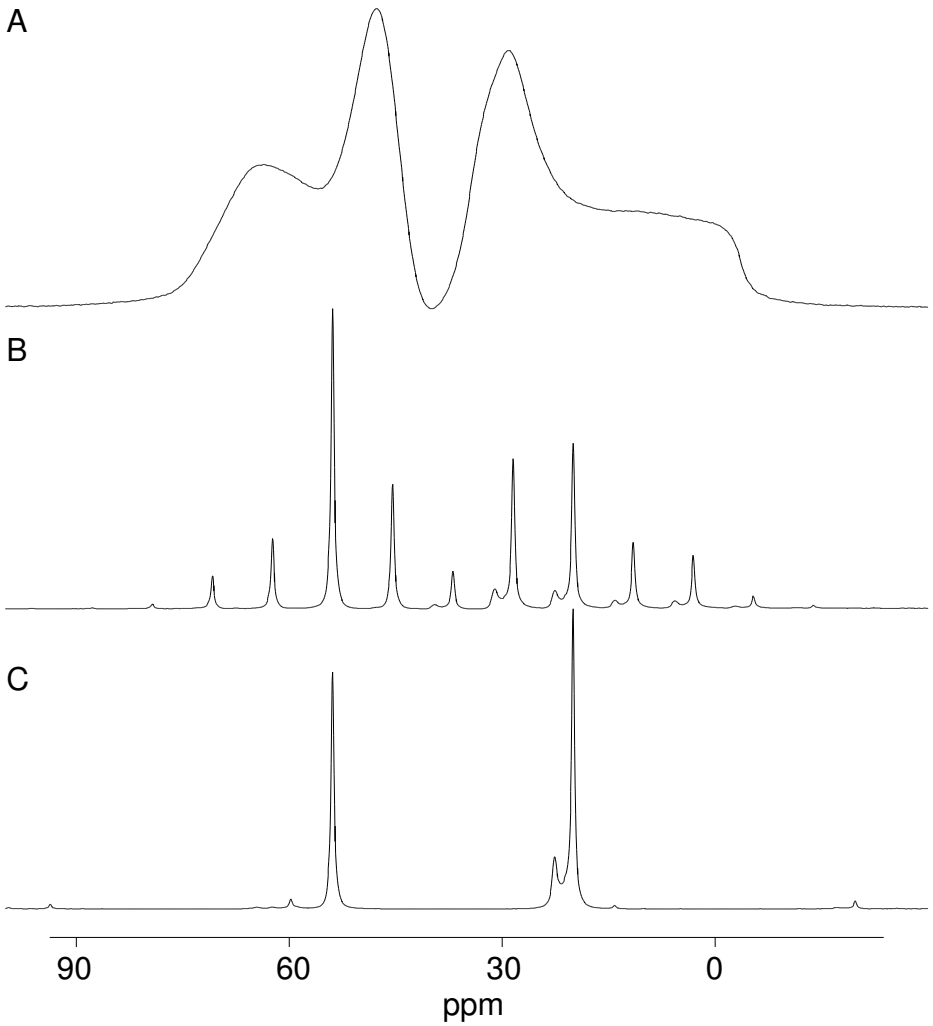

Figure 2.15: ^{13}C CP-MAS Spectra of double labelled acetylcholine perchlorate. Static (A), 1000Hz (B) and 7000 Hz (C) spinning speed.

Parameter	N-Methyl	C-Methyl
σ_{iso}	53.77	19.82
$\sigma_{zz} - \sigma_{iso}$	-23.96	14.10
η	0.44	0.99
$\Delta\sigma_{iso}$	3416 Hz	
T_2^{ZQ}	0.085s	

Table 2.3: Data obtained through the analysis of CP-MAS spectra of acetylcholine perchlorate using the SPEEDYFIT algorithim. Data was used in subsequent simulations of magnetization exchange curves.

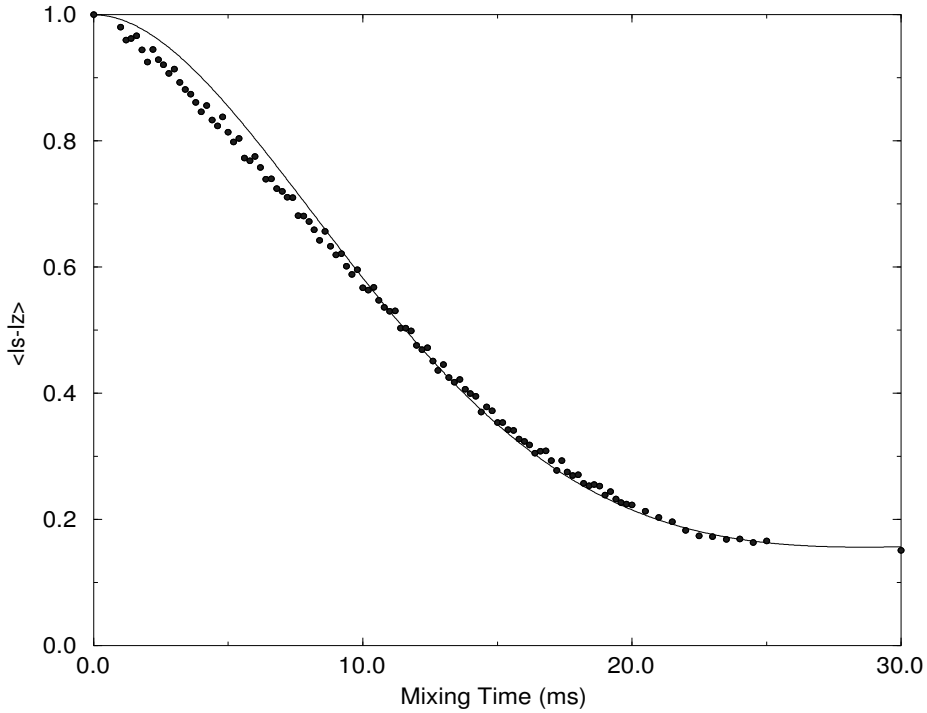

Figure 2.16: Magnetisation exchange data for crystalline acetylcholine perchlorate labelled at the N-methyl and C-methyl positions. Experimental data acquired at the n=1 condition, with a 1ms contact time, followed by selective DANTE inversion of the C-methyl resonance. Magnetisation exchange was monitored over the course of 30ms. The experimentally determined values (•) together with the best simulated fit obtained (-) are shown.

2.3.3 Broadband dipolar recoupling studies of U-^{13}C acetylcholine perchlorate

TOSSY spectra of uniformly carbon-13 and nitrogen-15 labelled acetylcholine perchlorate utilizing the RIL-ZQT mixing sequence for the reintroduction of dipolar couplings are shown in Figure 2.17 and Figure 2.18. The major observable difference between uniformly labelled carbon-13 and nitrogen-15 acetylcholine and the unlabelled material is the apparent increase in linewidth observed in the CP-MAS spectra (data not shown, but apparent in the TOSSY spectra). These increased linewidths have been attributed to unresolvable scalar couplings that are present between labelled carbon-13 nuclei and are largely unaffected by MAS. However, it is still possible to identify the five magnetically inequivalent sites within the acetylcholine perchlorate previously described both in solution and CP-MAS studies of unlabelled material.

At short mixing times (Figure 2.17) magnetisation exchange is observable between the adjacent carbon atoms of the acetyl group (21 ppm and 173 ppm) and the ethyl groups (59 ppm and 64.5 ppm). Such exchange is expected as the degree of magnetization exchange is meant to mirror the relative intensities of the dipolar couplings. Interestingly, autocorrelated sidebands of the carbonyl group which have previously been suppressed by the rotor synchronized time reversal scheme are beginning to become apparent. This could be caused by both proton and carbon spin diffusion between adjacent molecules or molecular reorientation. The presence of both efficient proton homonuclear docoupling and the dilution of the labelled material with unlabelled acetylcholine perchlorate suggests that spin diffusion is probably not occurring. This allows us to conclude that motion is probably occurring about the carbonyl group in the acetylcholine perchlorate on the timescale of exchange (<4ms).

The TOSSY spectra using a long mixing time of acetylcholine perchlorate are shown in Figure 2.18. In addition to the connectivities between the ethyl groups

(59ppm and 64.5ppm) and the adjacent atoms of the acetyl group (21ppm and 173ppm) we now see longer range interaction including those between the OCH_2 and the CMe (59ppm and 21ppm), the N-methyl and the NCH_2 (53.9ppm and 64.5ppm). These data are consistent with the structure of acetylcholine with the newly resolved coupling arising from connectivities occurring over two bonds. In addition although not apparent in Figure 2.18 intensity is also appearing between the C-methyl and the N-CH_2 and the $N(CH_3)_3$ indicating that long range couplings are beginning to be resolved.

Monitoring the longer range couplings with these sequences is problematic at these higher fields. These difficulties are primarily associated with the unfavourable relaxation of the acetycholine perchlorate under the RIL-ZQT scheme. These effects are demonstrated in Figure 2.19 where the intensity arising for each resonance in the first free induction decay of a 2D dataset is plotted as a function of rotor (RIL) cycles. The most apparent feature of these decay curves is the rapid fall in signal intensity with respect to the number of RIL cycles with all sites losing 50% of their intensity within the first 10 rotor cycles. This causes an inherent problem with the level of sensitivity possible under such conditions. These difficulties are compounded by the unfavourable rates of relaxations from the OCH_2 and NCH_2 groups in contrast to the methyl groups present in the sample. This leads to a number of problems associated with the acquisition of the TOSSY datasets, with low sensitivity sites such as the OCH_2 and NCH_2 being acquired against a background of high intensity signals such as the N-methyl and C-methyl. Experimentally the signal decay rate appeared to be sensitive to the efficiency of decoupling. A variety of homo- and heteronuclear decoupling schemes were employed during the RIL-ZQT transfer sequence including broadbanded decoupling, BLEW, MREV and Lee-Goldburg. Of these the original Lee-Goldburg homonuclear decoupling proposed by Baldus & Meier [190] was observed experimentally to perform the best in our hands, in addition to being experimentally robust. The unfavourable relaxation observed

in these samples under the RIL-ZQT scheme probably arises because of an inability to efficiently mis-match the proton and carbon B_1 fields due to the limited power levels available on these probes.

This data demonstrates the feasibility of using broadband dipolar recoupled exchange spectroscopy for the assignment of labelled sites in a uniformly carbon-13 labelled sample. In addition the couplings resolved appear to be (at least qualitatively) in agreement with those expected from the crystalline acetylcholine perchlorate. The methodology employed here, should also allow the resolution of labelled ligand against a background of unlabelled membranes, with labelled sites appearing off the diagonal.

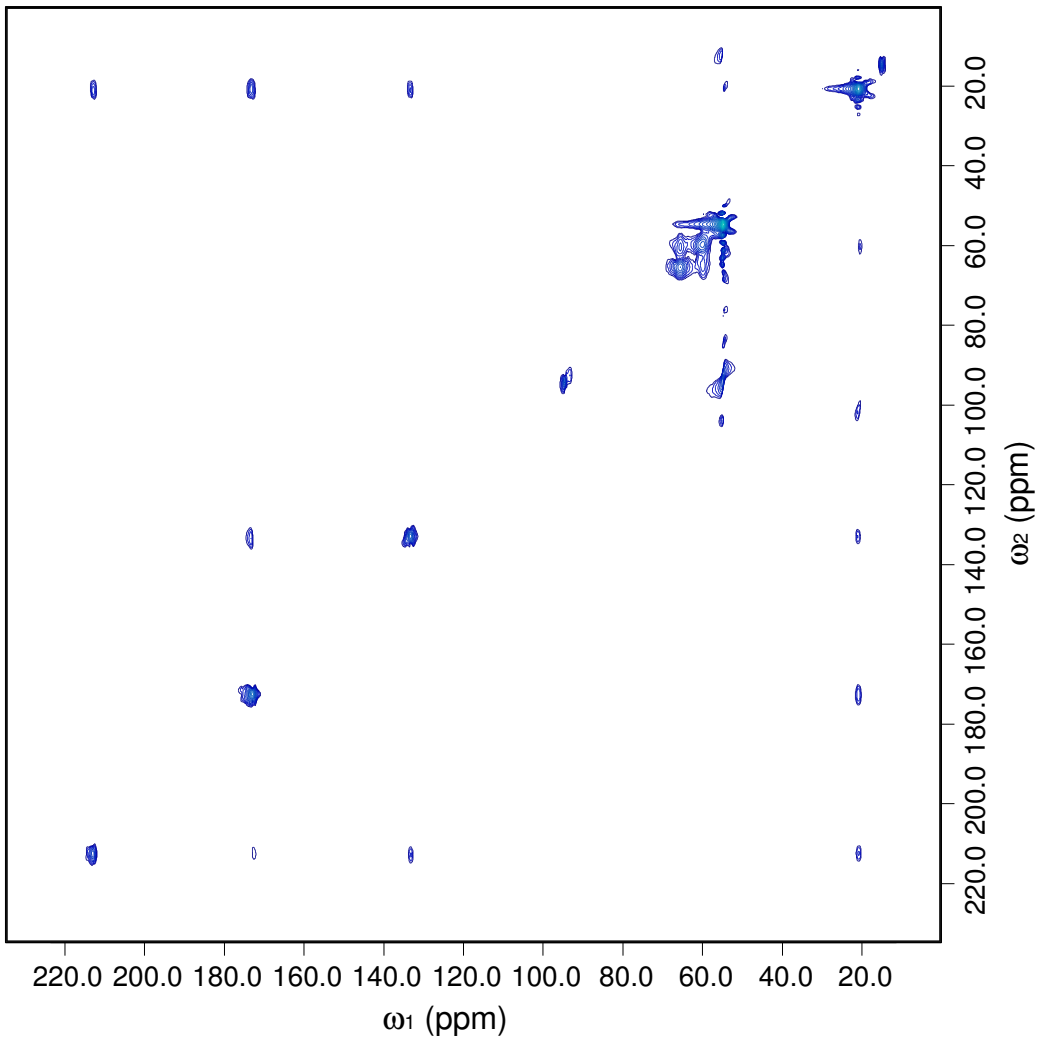

Figure 2.17: TOSSY spectra of crystalline acetylcholine perchlorate with 4ms exchange time, at 5kHz spinning speed at room temperature. Data acquired with 128 t_1 points, of 128 acquisition each. Data processed with 50 Hz linebroadening in t_2 prior to Fourier Transformation. Data was then linear predicted from 128 to 512 points in t_1 prior to the application of a sinebell apodization function. Data were then processed using a real Fourier Transform.

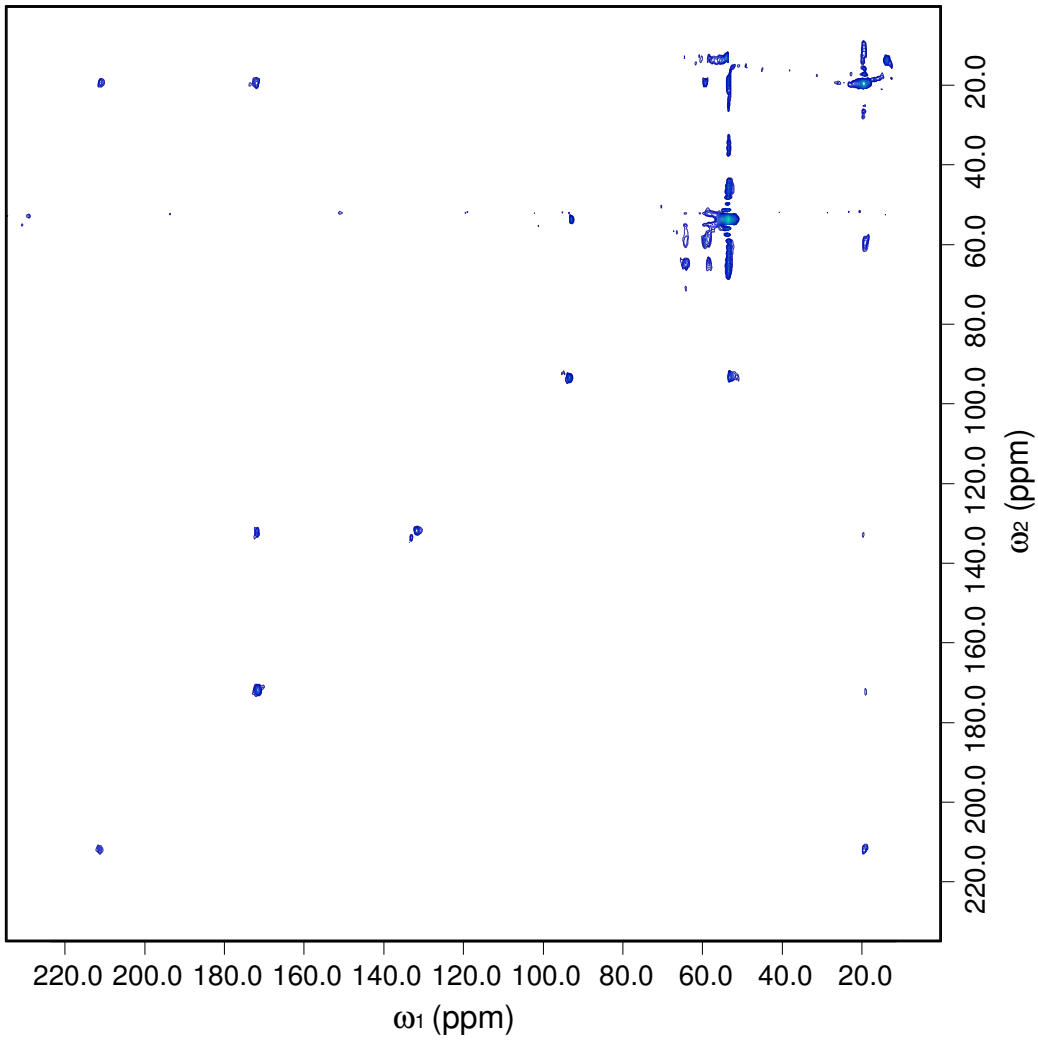

Figure 2.18: TOSSY spectra of crystalline acetylcholine perchlorate with 16ms exchange time, at 5kHz spinning speed. Data acquired with 128 t_1 points, of 128 acquisition each. Data processed with 50 Hz linebroadening in t_2 prior to Fourier Transform. Data was then linear predicted from 128 to 512 points in t_1 prior to the application of a sinebell abodization function. Data was then processed using a real Fourier Transform.

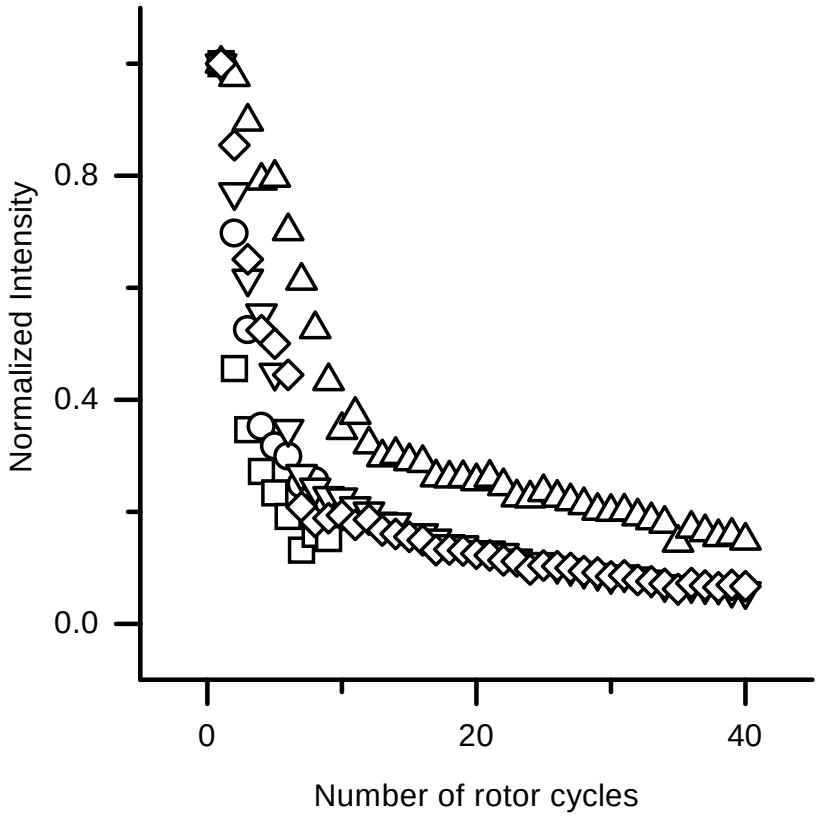

Figure 2.19: Decay of magnetization observed under the RIL mixing scheme as a function of the length of the mixing time. Data for each resonance normalized to the intensity observed after one rotor cycle (Carbonyl, $\diamond$), (OCH_2, $\square$), (NCH_2, $\circ$), (N-methyl, $\triangle$), (C-methyl, $\triangledown$).

2.3.4 Double quantum filter CP-MAS studies of uniformly labelled ^{13}C acetylcholine perchlorate.

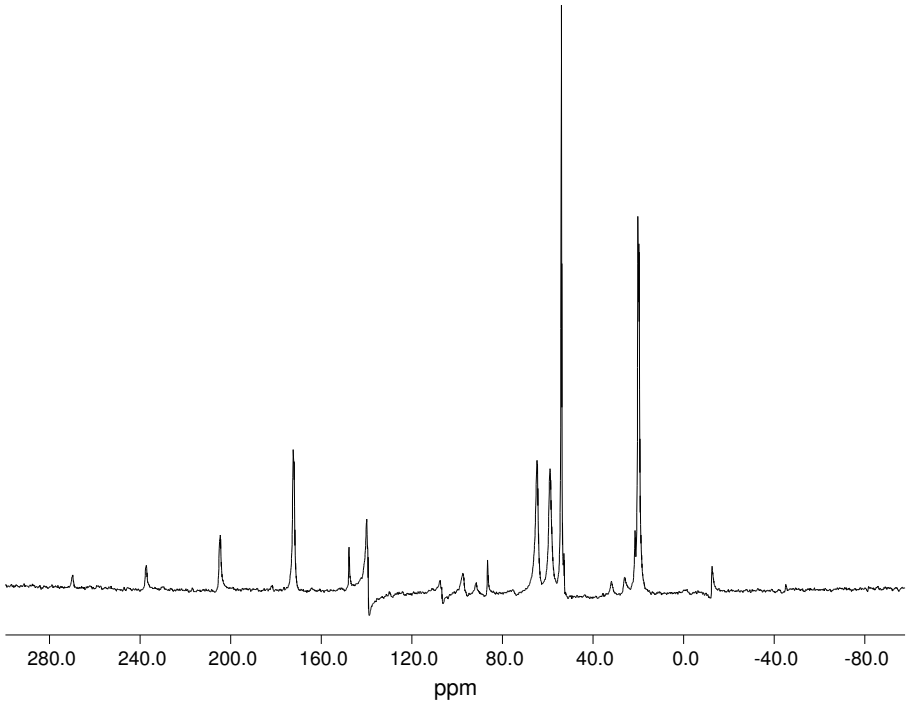

Figure 2.20: C7 Double quantum filtered spectra of uniformly labelled acetylcholine perchlorate. Data acquired at 4 kHz spinning speed with 1ms contact time, 512μs double quantum excitation time and averaged over 16 acquisitions at room temperature. Data processed with 30 Hz linebroadening and zero filled to 4096 points prior to Fourier Transformation.

The C7 double quantum filtered CP-MAS spectrum of uniformly carbon-13 labelled acetylcholine perchlorate is shown in Figure 2.20. The characteristic CP-MAS spectrum of acetylcholine perchlorate is observed displaying resonances at 172.1ppm (carbonyl), 64.5ppm (NCH_2), 59.2ppm (OCH_2), 53.9 ppm ($N(CH_3)_3$) and CCH_3 (20ppm). Other peaks are spaced at intervals of the spinning speed from these isotropic lines, and arise from incomplete averaging of the chemical shift anisotropy. The phase distortions associated with these sidebands arise from the inefficient excitation during the C7 mixing sequence as the B_1 field is limited to 28 kHz due

the $B_1 = n\omega_r$ criterion which has to be met for efficient recoupling under the C7 pulse scheme. In addition the linewidths observed for the double quantum filtered spectrum of acetylcholine are typically less than that observed for uniformly labelled acetylcholine perchlorate (*e.g.* a reduction in linewidth from 226Hz to 156Hz for the OCH_2 resonance). This probably reflects the selection of particular orientational components by the double quantum filter, reducing inhomogeneous broadening of the normal spectrum induced by off resonance homonuclear dipole-dipole couplings [201].

2.4 Solid state NMR studies of ^{13}C enriched acetylcholine bound to the nicotinic acetylcholine receptor.

2.4.1 Binding Studies of $N(^{13}CH_3)_3$ acetylcholine to the nicotinic acetylcholine receptor.

Work extensively described in Biochemistry 1998 [74]

To samples of nicotinic acetylcholine receptor containing 40nmoles of binding site 20 nmoles of $N^+(^{13}CH_3)_3$ acetylcholine was added. Upon the addition of acetylcholine the receptor adopts its desensitized state, with a K_D for acetylcholine of 10^{-9}M. Under such conditions the bulk of the acetylcholine is bound to the receptor.

The cross polarization spectrum of the nicotinic acetylcholine receptor membranes is shown in Figure 2.21. The spectrum is dominated by the natural abundance carbon-13 from phospholipid acyl chains between 10 and 40ppm. The short cross polarization employed here (1ms) enables the immobile protein, with its efficient cross polarization characteristics to be observed between 45 and 70ppm. Upon the envelope, resonances which can be attributed to the lipid headgroups are resolved with linewidths approaching the homogeneity of the magnet ($\Delta\nu_{\frac{1}{2}}$=15Hz).

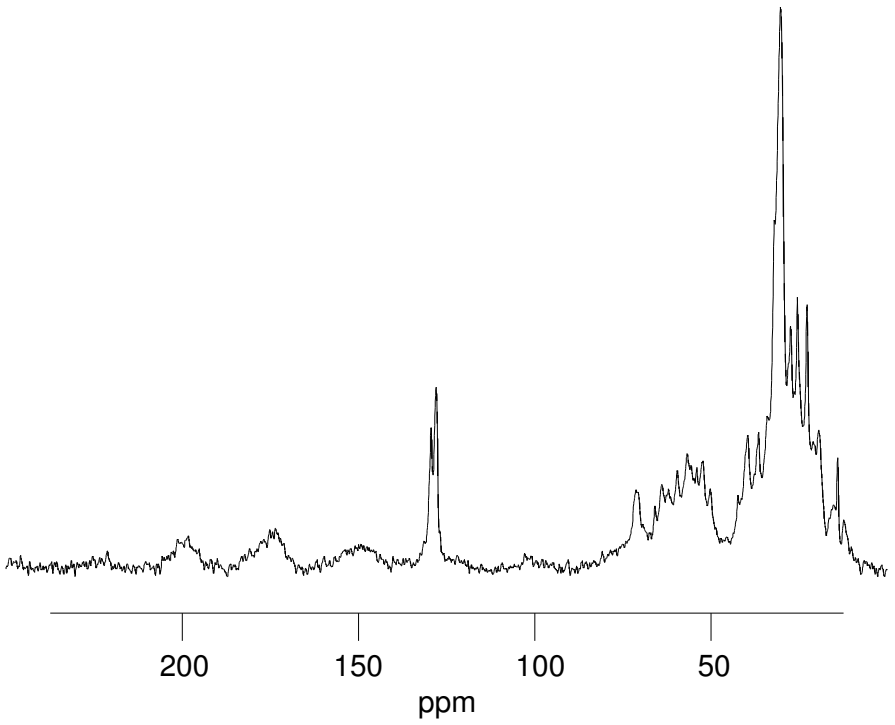

Figure 2.21: ^{13}C CP-MAS NMR spectrum of nicotinic acetylcholine receptor membranes containing 40nmoles of receptor binding site to which 20 nmoles of $N^{+}(^{13}CH_3)_3$ acetylcholine have been added. Recorded with a 1ms cross polarization and averaged over 8600 acquisitions at 283 K. Data processed with 20Hz linebroadening.

The glycerol backbone of the phospholipids gives rise to an envelope appearing between 70 and 80ppm. Resonances arising between 125 and 130ppm are attributable to the unsaturated groups within the phospholipid acyl chains. Carbonyl group arising from the protein backbone and the lipid are observed between 170 and 180ppm, and due to their highly anisotropic nature give rise to sidebands spaced 2500 Hz from the isotropic envelope.

The resonance from $N^{+}(^{13}CH_3)_3$ acetylcholine in solution observed in a conventional solution experiment, and in the solid observed by cross polarization magic angle spinning, gives rise to a resonance at 53.90ppm with reference to adamantane. When added to receptor rich membranes (50 mg of total protein), at a 100

fold excess over the number of binding sites for acetylcholine, a narrow resonance ($\Delta v_{\frac{1}{2}}$=25Hz) at 53.90ppm dominates the spectrum acquired using proton decoupled carbon-13 NMR (Figure 2.22A).

In the absence of $N^+(^{13}CH_3)_3$ acetylcholine, using CP methods, the broad envelope (48-64ppm) of protein resonances are observed (Figure 2.22B) a signal from $N^+(^{13}CH_3)_3$ acetylcholine is apparent when an equimolar concentration of agonist is added (40 nmoles in the membrane sample used)(Figure 2.22C). A difference spectrum generated from the subtraction of Figure 2.22B from 2.22C shows a single spectral line (Figure 2.22D) with a larger width ($\Delta v_{\frac{1}{2}}$=100Hz) than for acetylcholine in free solution ($\Delta v_{\frac{1}{2}}$=25Hz) or in the solid (Figure 2.14). The width of this line may reflect heterogeneity in the local environment of the bound substrate, attributable to the two kinetically distinguishable binding sites in the α-subunits of the receptor, or the presence of three distinct sites for each of the labelled methyls, as a result of the hindered rotation of the quaternary trimethylammonium group within the binding site.

To demonstrate the selectivity of the binding of acetylcholine to the receptor agonist binding site observed in Figure 2.22C, the agonist has been competitively prevented from accessing the binding site through the use of the specific inhibitor of acetylcholine binding, α-bungarotoxin. The CP-MAS spectum of receptor rich membranes treated with α-bungarotoxin in the absence of $N^+(^{13}CH_3)_3$ acetylcholine is shown in Figure 2.23A. When $N^+(^{13}CH_3)_3$ acetylcholine is added to the membrane at a concentration equivalent to the number of binding sites, no resonance appears in the region between 52 and 54 ppm (Figure 2.23B); the region where the resonance from the $N^+(^{13}CH_3)_3$ acetylcholine should be observed.

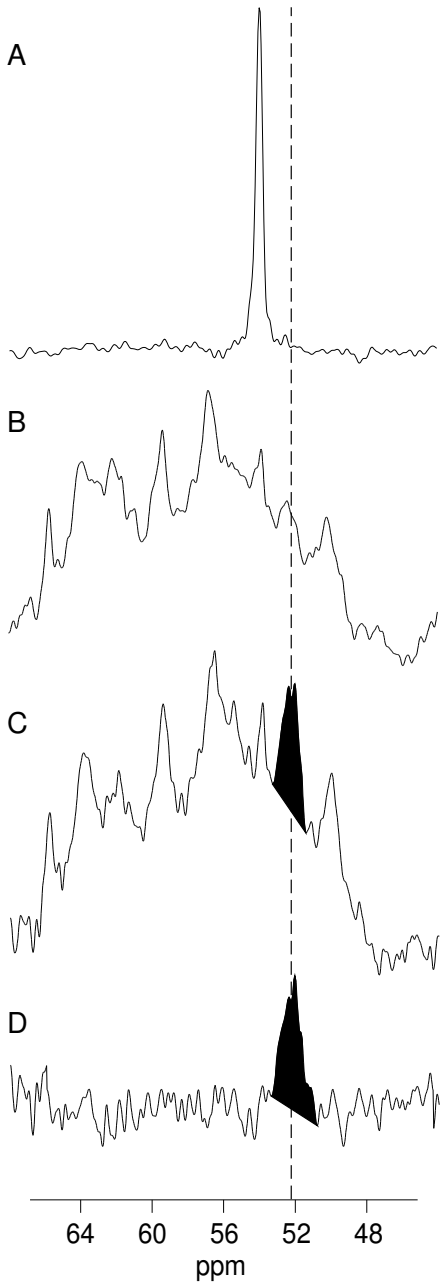

Figure 2.22: Carbon-13 MAS Spectra (68-44ppm) of acetylcholine receptor rich membranes containing 40nmoles of receptor binding sites. Proton decoupled spectrum acquired with an excess of $N^+(^{13}CH_3)_3$ acetylcholine added and averaged over 4000 acquisitions at 283 K. Data processed woth 40Hz linebroadening (A). As in (A) but recorded using CP-MAS in the absence of $N^+(^{13}CH_3)_3$ acetylcholine (B), upon the addition of 40 nmoles of $N^+(^{13}CH_3)_3$ acetylcholine (C). Difference spectrum resulting from the subtraction of B from C (D). Spectra acquired with 1ms cross polarization and averaged over 8600 acquisitions at 283 K, data processed with 20Hz linebroadening. Shaded area represents intensity due to bound $N^+(^{13}CH_3)_3$ acetylcholine, and dotted line indicates the position for the bound acetylcholine.

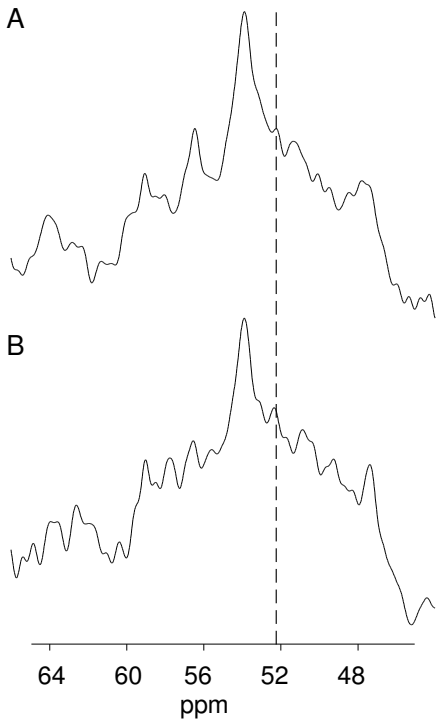

Figure 2.23: CP-MAS NMR carbon-13 spectra (68-44ppm) of nicotinic acetylcholine receptor membranes containing 40 nmoles of binding siteas in Figure 2 but with added α-bungarotoxin in the absence of $N^+(^{13}CH_3)_3$ (A) and in the presence of $N^+(^{13}CH_3)_3$ acetylcholine (B). Spectra recorded with 1ms cross polarization and averaged over 8600 acquisitions at 283 K. Data processed with 20 Hz linebroadening. Dotted line located at same position as Figure 2.22.

The significant upfield shift of 1.6±0.2 ppm for the resonance assigned to $N^+(^{13}CH_3)_3$ acetylcholine bound to the nicotinic acetylcholine receptor demonstrates the $N^+(^{13}CH_3)_3$ group experiences a different electronic environment when bound compared to that in free solution and crystalline solid. Carbon-13 chemical shifts are sensitive to molecular conformation, local electronic environment and ring currents created by local aromatic groups. Through the use of appropriate computer simulation (See Materials and Methods) it has been possible to accurately predict the contribution of these effects to the observed chemical shifts [206][207]. These simulations have

currently been used to predict the chemical shifts within proteins and their prosthetic groups [206][207]. Here we extrapolate these observations in an attempt to determine the nature of the acetylcholine receptor binding site.

Carbon-13 chemical shifts show greatest sensitivity to rearrangements of molecular conformation. However, due to the location of the observed nucleus at the periphery of the molecule, changes in the chemical shift due to conformational distortions are thought to be unlikely.

In the presence of charged residues, the perturbation of the local electron shell has the potential to perturb the observed carbon-13 chemical shift. Such perturbations are thought to have a limited effect (<1.0ppm) on carbon-13 chemical shifts due to the high dielectric of the surrounding environment. The remaining contribution to carbon-13 chemical shifts arises due to the presence of ring currents from local aromatic systems. Simulations of carbon-13 chemical shifts for $N^+(^{13}CH_3)_3$ quaternary ammonium groups have been carried out on the structure of acetylcholine bound to the known crystal structure of acetylcholine esterase, to predict the likely perturbations due to local aromatic groups upon binding. This has been done because the binding site of the acetylcholinesterase is rich in aromatic residues, and is proposed to have an acetylcholine binding site homologous to the nicotinic acetylcholine receptor. These simulations have yielded a perturbation of -1.6ppm in carbon-13 chemical shift of the $N^+(^{13}CH_3)_3$ group, in agreement with that observed for acetylcholine bound to the nicotinic acetylcholine receptor.

On the basis of this agreement, and the unplausible nature of the other possible contributions to the $N^+(^{13}CH_3)_3$ chemical shifts, we propose that the acetylcholine binding site on the nicotinic acetylcholine receptor is lined with aromatic residues, as previously suggested on the basis of the homology with the esterase. Such an observation supports the work of I. Tsigelny and co-workers[91], who propose a model of the extracellular domains of the nicotinic acetylcholine receptor containg an acetylcholine binding site rich in aromatics. This lends further support to the

hypothesis that the interaction between acetylcholine and the nicotinic acetylcholine receptor is mediated primarily through the positively charged quaternary ammonium group interacting with delocalized π systems in the aromatic sidechains.

2.4.2 Residency time for acetylcholine bound to the nicotinic acetylcholine receptor.

The DDCP experiments, carried out on receptor samples not inhibited in agonist binding by α-bungarotoxin, were analysed to give the recovery curves shown in Figure 2.24. All resonances studied (protein backbone, acyl chains, unsaturated groups) as well as those from the bound acetylcholine, show a similar exponential increase in spectral intensity as a function of mixing time. Non-linear least square fitting of these curves to the simplified Bloch equation [38] for T_{1z} relaxation, assuming the absence of agonist exchange, is given as:

$$M_Z = M_0(1 - e^{\frac{-t}{T_{1z}}}) \tag{2.24}$$

Where T_{1z} is the longitudinal relaxation time for the individual spectral components of the membrane (Table 2.4).

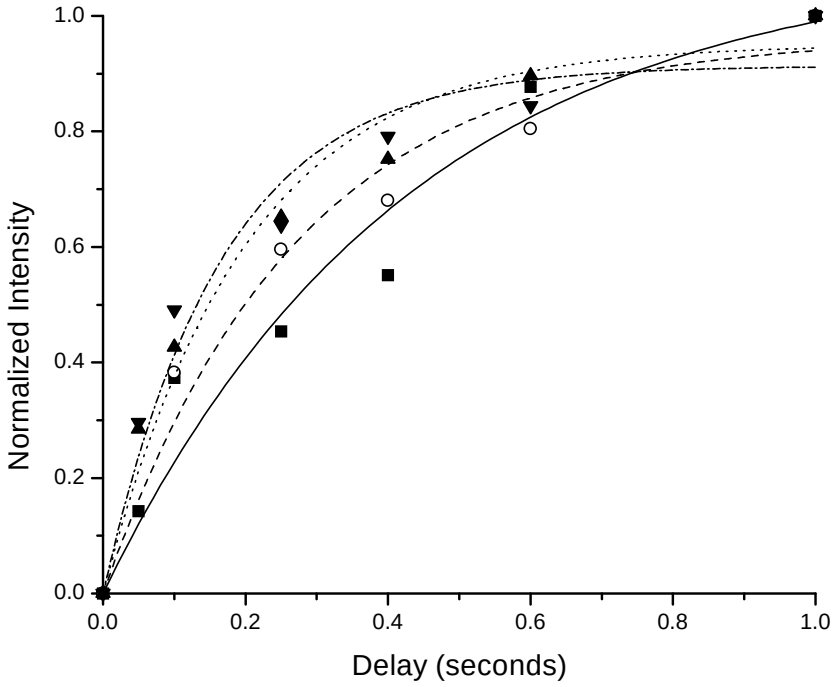

Figure 2.24: Recovery of magnetisation for 20 nmoles of $N^+(^{13}CH_3)_3$ acetylcholine added to a sample of receptor membranes (40nmoles of binding site) with respect to the delay time (τ) during a DDCP experiment. Intensities (I) are plotted with respect to the maximum observed intensity. Protein envelope (■, – – –, 45-70ppm), unsaturated resonances (▼, - ● -, 128ppm), $N^+(^{13}CH_3)_3$ (◯, - - -, 52.34ppm), aliphatic resonances (▲, ● ● ●, 29.00ppm). Data obtained from DDCP experiments with 1ms cross polarisation, 1.5s recycle time and averaged over 4000 acquisitions. Data processed with 30Hz linebroadening.

The appearance of $N^+(^{13}CH_3)_3$ acetylcholine to give a value of T_{1Z} of 0.27s, shows a similar rate of appearance to the protein (T_{1z}=0.43s) resonances in the spectrum. These similar relaxation rates would suggest that the appearance of magnetization from the bound $N^+(^{13}CH_3)_3$ acetylcholine arises primarily from the T_{1z} relaxation whilst in the protein binding site, rather than from exchange of the bound ligand possessing dephased magnetisation with ligand in free solution, and which would have therefore retained its magnetization during the initial dephasing period. This result shows that the rate of ligand exchange is long on the T_{1z} timescale (>200ms).

Assignment	T_{1z}(s)	χ_2 [1]
Protein backbone	0.430	0.007
$N^+(^{13}CH_3)_3$ acetylcholine	0.270	0.004
Acyl chains	0.190	0.003
Unsaturated chains	0.160	0.005

Table 2.4: Relaxation data obtained for acetylcholine bound to the nicotinic acetylcholine receptor membranes. T_{1Z} obtained through the fitting of equation to the DDCP curves shown in Figure 2.24 ([1] $\chi_2 = \frac{1}{n}\sum_1^n(x_{obs} - x_{calc})$)

This is consistent with the previously observed kinetics for agonist binding to the desensitized nicotinic acetylcholine receptor having a K_D of 10^{-9}M and a diffusion limited on rate of 10^8 $M^{-1}s^{-1}$.

Comparison of the T_{1z} for bound ligand with that of other membrane components (Table 2.4), indicates that both bound ligand and protein are undergoing a limited set of motions on the nanosecond timescale, which affects T_{1z} relaxation compared to the lipid resonances where such motions lead to efficient T_{1z} relaxation. However, the similarity of the T_{1z} for $N^+(^{13}CH_3)_3$ acetylcholine with other membrane protein components, when compared to the T_{1z} measured for such a small molecule when free in solution where T_{1z} is relaxation is in the order of seconds, further confirms that the $N^+(^{13}CH_3)_3$ acetylcholine is bound to the membrane environment.

2.4.3 Assignment of resonances from carbon-13 enriched acetylcholine bound to the nicotinic acetylcholine receptor.

Broadband Dipolar Recoupled Exchange Spectra of acetylcholine bound to the nicotinic acetylcholine receptor.

Broadband dipolar coupled spectra were obtained for uniformly labelled acetylcholine bound to the nicotinic acetylcholine receptor. At short mixing times (<1ms) sufficient signal was available to obtain 'reasonable' homonuclear correlation spectra at temperatures of -120°C. At such short mixing times insufficient time had elapsed for the transfer of magnetization between even adjacent atoms within the acetylcholine whilst bound to the receptor. Further extension of the mixing time led to an overall drop in signal intensity (as described for the crystalline solid). This drop in signal intensity and the low temperatures required limited the overall acquisition time. This resulted in the inability to obtain good quality datasets for assignment purposes. Data obtained at -60°C again suffered from severe attenuation of the signal at longer mixing times, however the extended acquisition times available at this temperature allowed longer acquisitions. At these temperatures, no exchange was observed suggesting that motions occurring in the membrane are sufficient to interfere with the recoupling under the RIL-ZQT scheme. The major problem associated with the application of these techniques to this system appears to be the rapid decay of signal intensity with respect to the mixing time, as exemplified by studies of the crystalline solids. This effect appeared to be sensitive to decoupling. A variety of decoupling schemes including broadband decoupling, MREV and BLEW-48 were tried in order to ascertain if any offered improvements in decoupling efficiency during recoupling under the RIL-ZQT scheme. Applying these schemes to membranes offered no improvement over frequency offset Lee-Goldburg for the study of membrane systems in our hands, although many showed greater sensitivity to exact experimental setup.

DQF Spectra of uniformly labelled acetylcholine bound to the nicotinic acetylcholine receptor.

A POST-C7 double quantum filtered spectrum of carbon-13 uniformly labelled acetylcholine bound to the nicotinic acetylcholine receptor is shown in Figure 2.25. The spectrum is dominated by two intense resonances at 56.3 and 67.2 ppm. The peak at 67.2 ppm reflects the NCH_2 group of the choline backbone. The larger of the peaks at 56.3 ppm probably results from intensities arising from both the N-methyl(53ppm) and the OCH_2(59ppm). The bulk of the intensity probably arises from the OCH_2 which is observed with a higher efficiency due to the strong dipolar interaction with a directly bonded carbon. The shoulder on the side of this resonance may be due to intensity from the N-methyl, which will be poorly excited due to the relatively weak coupling present between spins in this site and other carbon atoms. The relatively intense nature of these resonances reflects the bias with which these spectra were acquired with the carrier frequency located close to N-methyl, OCH_2 and NCH_2 groups.

An intensity arises at 173.7ppm with sidebands spaced at intervals of 4 kHz. These are assignable to the carbonyl group of the acetylcholine, and indicates that no hydrolysis of the sample has occurred (signal from free acid arising at 183ppm). A weak resonance also appears at 26 ppm, this does not seem to arise from sidebands of the N-methyl, OCH_2 or NCH_2 groups and thus might come from the C-methyl group of the acetylcholine. This resonance appears downfield some 6.1ppm from the C-methyl group in free solution or crystalline acetylcholine perchlorate.

The data shown were collected at -120°, at higher temperatures we were unable to perform broadband dipolar recoupling experiments, presumably due to the presence of motions occurring in the bilayer interfering with the efficiency of recoupling. At these low temperatures the lineshapes have been disturbed due to inhomogeneous broadening and the low sensitivity afforded by both the sample and

experiment. As a result any determination of chemical shift values will be less accurate than those determined at 5°C. The assigned values are given in Table 2.5. In addition to the perturbation observed for the N-methyl group many of the other resonances appear to change upon binding. Amongst these the only perturbation that is significant with respect to the linewidth (∼500Hz) is that of the C-methyl group which is shifted 6.4 ppm downfield. Previous perturbations in chemical shift have been explained on the basis of aromatic sidechains in close proximity of the labelled ligand. Simulations performed as described in materials and methods indicate that for the C-methyl position of the acetylcholine receptor, the contribution of aromatic residues to the perturbation of chemical shift should be -0.57 ppm. This suggests that the perturbations observed in this instance cannot be attributed to ring current effects. Ruling out possible contributions to the chemical shift based on both the magnitude and sign of the perturbation from both ring currents and charge effects, this leads us to conclude that the perturbation observed arises from a change in the molecular geometry.

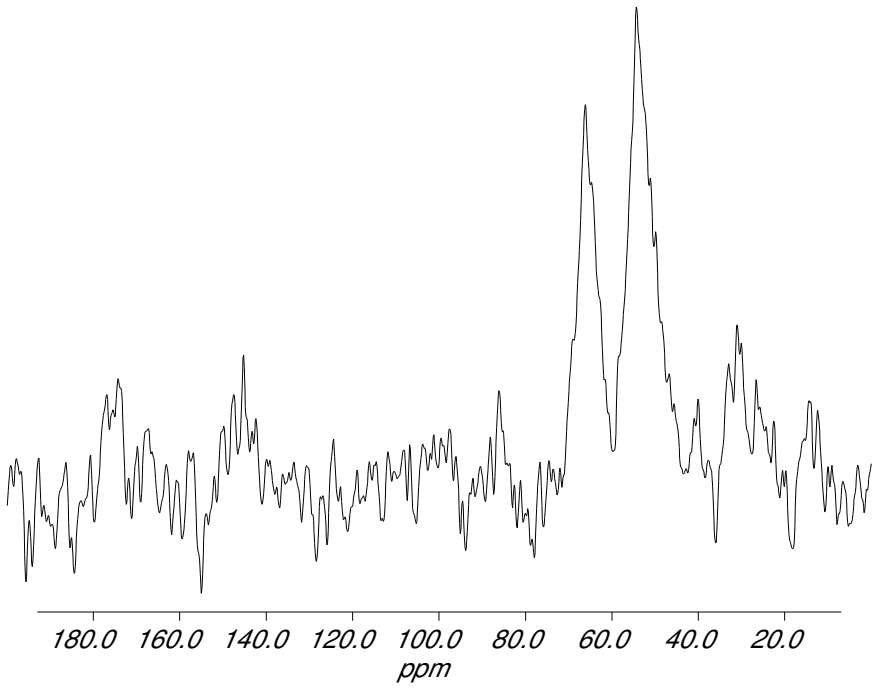

Figure 2.25: Double quantum spectra of U-^{13}C labelled acetylcholine bound to the nicotinic acetylcholine receptor. Results of 8192 acquisitions at -120°C.

Assignment	δ(ppm)	T(°C)
CMe	26.4	-120
$N^+(^{13}CH_3)_3$	52.3	5
$N(CH_2)$	~56.3	-120
$O(CH_2)$	67.2	-120
C=O	173.7	-120

Table 2.5: Assignments for acetylcholine bound to the nicotinic acetylcholine receptor.

2.5 Conclusion

2.5.1 $N^+(CH_3)_3$ acetylcholine bound to the nicotinic acetylcholine receptor.

It has been demonstrated that ^{13}C CP-MAS NMR can be successfully applied to the study of $N^+(CH_3)_3$ acetylcholine bound to the nicotinic acetylcholine receptor. Through the use of the specific inhibitor α-bungarotoxin, it has been possible to assign a resonance that appears at 52.3ppm to the $N^+(CH_3)_3$ acetylcholine that is bound in a pharmacologically specific manner. The observed 1.6ppm upfield perturbation in chemical shift for receptor bound agonist compared with the excess that remains in free solution or the crystalline solid has been assigned to the presence of aromatic residues in the agonist binding site. This provides further evidence that interactions between acetylcholine and the receptor are mediated primarily through cation-π bond interactions. Exploiting the differing relaxation phenomena between ligands in free solution and those bound to the receptor we have been able to demonstrate that the exchange of $N^+(CH_3)_3$ acetylcholine is slow on the timescale of longitudinal relaxation (T_{1z}) in excess of 200ms.

2.5.2 Uniformly labelled acetylcholine bound to the nicotinic acetylcholine receptor.

Studies on uniformly carbon-13 labelled acetylcholine bound to the nicotinic acetylcholine receptor have made use of a variety of broadband dipolar recoupling techniques. All of these techniques have been compromised by the presence of extensive motions in the sample which are not totally suppressed even at low temperatures. Broadband dipolar recoupled exchange MAS-NMR spectroscopy on crystalline acetylcholine provided correlation spectra which were in qualitative agreement with the crystal structure of the acetylcholine perchlorate. Application of these techniques to membrane systems was compromised by rapid relaxation due

to inefficient decoupling. Although the application of double quantum filtered CP-MAS NMR to uniformly labelled acetylcholine bound to the nicotinic acetylcholine receptor was unsuccessful at -60 °C on lowering the temperature to -120°C it was possible to obtain spectra of bound acetylcholine. However, the presence of inhomogeneous broadening limited the analysis of chemical shifts. The observation suggests that significant motions are still present at low temperature, these appear to interfere with the dipolar recoupling schemes applied and limit the potential to obtain structural and assignment information from some membrane systems.

Chapter 3

Orientation of bromoacetylcholine in the nicotinic acetylcholine receptor.

3.1 Introduction

The gross morphology of the nicotinic acetylcholine receptor has been probed to a medium resolution(4.6Å) using electron diffraction methods [4](Figure 1.3). Although these studies have suggested putative binding sites, the resolution is still insufficient to enable the location, structure and orientation of the ligand to be determined with respect to the overall structure of the receptor. In this chapter, an *ab initio* deuterium NMR study has been used to probe the orientation of the quaternary ammonium group of the agonist analogue, bromoacetylcholine with respect to the membrane normal. Simultaneously the dynamics of the quaternary ammonium group of bromoacetylcholine bromide have been probed through the qualitative analysis of the temperature dependence of deuterium lineshapes through a comparison with the dynamics determined for deuterated crystalline ligands and other similar compounds described in the literature. Such an approach has enabled the definition of both the orientation and dynamics of the ligand in its binding site.

The dynamics of ligands present in their binding site has been shown to give detailed information relating to the nature of binding and the local protein environment [211][212][213][214][215]. Although several forms of spectroscopy offer the potential to provide dynamic information, NMR spectroscopy confers many advantages over other methods due to its sensitivity to motions occurring over a wide range of time scales whilst exploiting non perturbing probes. Solid state NMR in

particular has demonstrated its applicability to the study of various dynamic processes occurring within the protein backbone, sidechains and ligands bound to them [216]. Furthermore deuterium NMR has found wide spread application to the study of protein dynamics both for soluble proteins in the solid state [212][211] and for membrane proteins in their native environment [213][214][215]. The well characterized lineshapes of compounds containing a deuterated quaternary ammonium group [217][218][219] has facilitated a qualitative analysis of the lineshapes allowing the nature of the dynamics of the ligand bound to the receptor to be determined in a non-perturbing manner.

The application of deuterium NMR to macroscopically aligned systems to obtain orientational constraints from membrane systems is well established for both lipids [220] and small peptides in bilayer structures[37]. A prerequisite for such studies is the macroscopic orientation of the bilayer structure. For lipids and small peptides this has been achieved using a variety of techniques including pressure annealing [221], rehydrating and temperature annealing [222][223], smearing of membrane suspension onto glass plates with partial rehydration [222][223], magnetic orientation [224][225] or natively aligned membranes [226]. In contrast, for studies of larger membrane embedded proteins such as the nicotinic acetylcholine receptor, these techniques are largely unsuitable due to the harsh physical conditions which would lead to rapid denaturation of the sample. To overcome these problems, during the course of this work we have developed the isopotential spin dry ultracentrifugation technique[53] based on the early work of Clark and Rothschild [227][228], and later modified by Freed [221]. This approach enables the orientation of the biological membranes at near physiological conditions. ^{31}P NMR spectra of membrane lipids were used to measure the degree of orientation within the samples prepared by isopotential ultracentrifugation.

Angular constraints for the quaternary ammonium group have been obtained by analysis of the ^{2}H spectra of orientated nicotinic acetylcholine receptor membranes

labelled with deuterated bromoacetylcholine bromide using the theory outlined by Seelig [229] and subsequently used by Ulrich [55][10] and Groebner [56] to study the orientational distribution of C-CD_3 bond vectors in orientated systems. Such analysis provided an accurate determination of the angle formed between the cone axis of the quaternary ammonium group and the magnetic field, thereby allowing the orientation of the bound ligand to be fixed with respect to the bilayer normal.

3.1.1 Analysis of ^{2}H NMR spectra.

Deuterium NMR spectra are dominated by the orientationally dependent anisotropic quadrupolar interaction of the nuclear spin (I=1) with the external magnetic field. For a single crystal in the absence of molecular motion, the resonance position $v_{\pm}$ of the $\Delta m = \pm 1$ transitions is directly related to the angle between the deuterium bond vector and the magnetic field, giving rise to a quadrupolar splitting $\Delta v_Q(\theta)$ of:

$$\Delta v_Q(\theta) = v_+ - v_- = \frac{3e^2qQ}{2h}.\frac{(3\cos^2\theta - 1)}{2} \tag{3.25}$$

The static quadrupolar coupling constant is defined as e^2qQ/h where eQ is the nuclear quadrupolar moment, eq is the electric field gradient and h is Planck's constant. This typically gives rise to a quadrupolar coupling constant of approximately 170kHz for a static aliphatic deuteron.

Motion of the C-D bond occurring on the same timescale as the quadrupolar interaction (10^{-6}s) leads to its partial averaging. Rapid molecular reorientation (k>10^{-6}s) about a given axis results in a reduction of the quadrupolar splitting (Δv_Q) by a factor of $(3\cos^2\rho - 1)$ where ρ is the angle formed between the deuterium bond and the axis of motional averaging [217]. The deuterons introduced into the quaternary ammonium group of the bromoacetylcholine have been shown in many compounds to undergo rapid rotation about the C_3 and C_3' axis. Thus the quadrupolar coupling constant is scaled by both rotations and the Δv_Q is given as

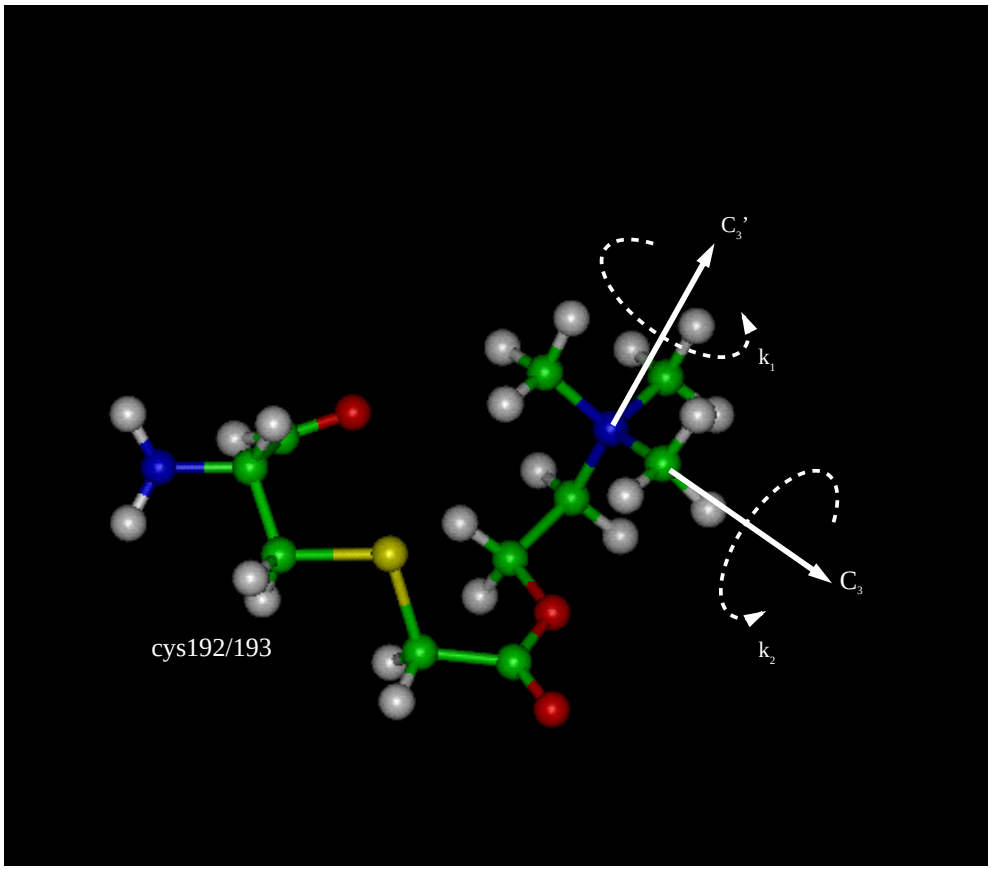

Figure 3.26: Diagram showing the axis under which motional averaging occurs, in addition the linkage between the cys(192/193) and the bromoacetylcholine is shown.

[217]:-

$$\Delta v_Q = \frac{3e^2qQ}{16h}(\overline{3\cos^2\theta_{CD} - 1})(\overline{3\cos^2\theta_{NC} - 1}) \tag{3.26}$$

where ρ has been substituted with the time averaged angles between the C-D bond (θ_{CD}) and the N-C bond (θ_{NC}).

When the motions fall into the intermediate timescale of the deuterium NMR experiment (10^{-4}s$< \tau_c < 10^{-7}$s) then the time dependent averaging between several environments leads to non axially symmetric lineshapes. Although these are more complex in origin, the lineshapes can still be simulated providing the geometry of the molecule and the rates of the individual motional processes are known [230].

Motions in this range offer the potential to provide detailed information about the energetics of many dynamic processes [213].

The deuterium lineshapes measured thus reflects the weighted distribution of bond vectors within the sample. Mathematically this can be described as a probability density function $p(\zeta)$, which is a function of the reduced resonance frequency ζ and the spectral offset v_0, where:

$$\zeta = \frac{(v_{\pm} - v_0)}{\Delta v_Q^{powder}} = \pm\frac{(3\cos^2\theta - 1)}{2} \tag{3.27}$$

In the case of the deuterated bromoacetylcholine bound to a uniaxially orientated sample of the nicotinic acetylcholine receptor where the proteins show rotational disorder due to slow rotational diffusion [132], the averaged deuterium bond vectors trace out the rim of a cone (of angle γ), whose axis is orientated at an angle α with respect to the magnetic field. The probability density function for such a distribution is described by Ulrich and Watts [10], and can be calculated as:-

$$p(\zeta_{\pm}) = \left\{\sqrt{\frac{\pm 2\zeta + 1}{3}}.\sqrt{\sqrt{\frac{\pm 2\zeta + 1}{3}} - \cos(\alpha + \gamma)}.\sqrt{\cos(|\alpha - \gamma|) - \sqrt{\frac{\pm 2\zeta + 1}{3}}}\right\}^{-1} \tag{3.28}$$

When the membrane normal coincides with the magnetic field ($\alpha = 0$), then θ is defined by the cone angle (γ), upon which the above equation reduces to:-

$$\Delta v_Q(\gamma) = \Delta v_Q^{powder}(3\cos^2\gamma - 1) \tag{3.29}$$

For values of γ between 35° and 90° (where -0.5 < ζ < +0.5) only the magnitude of the quadrupolar splitting for the single angle α=0 can be determined. However, the sign of $\Delta v_Q(\gamma)$ is readily obtained by measuring the spectral dependence of the lineshape with respect to the angle α. This can be achieved by altering the angle of the sample with respect to the magnetic field (See Figure 3.27).

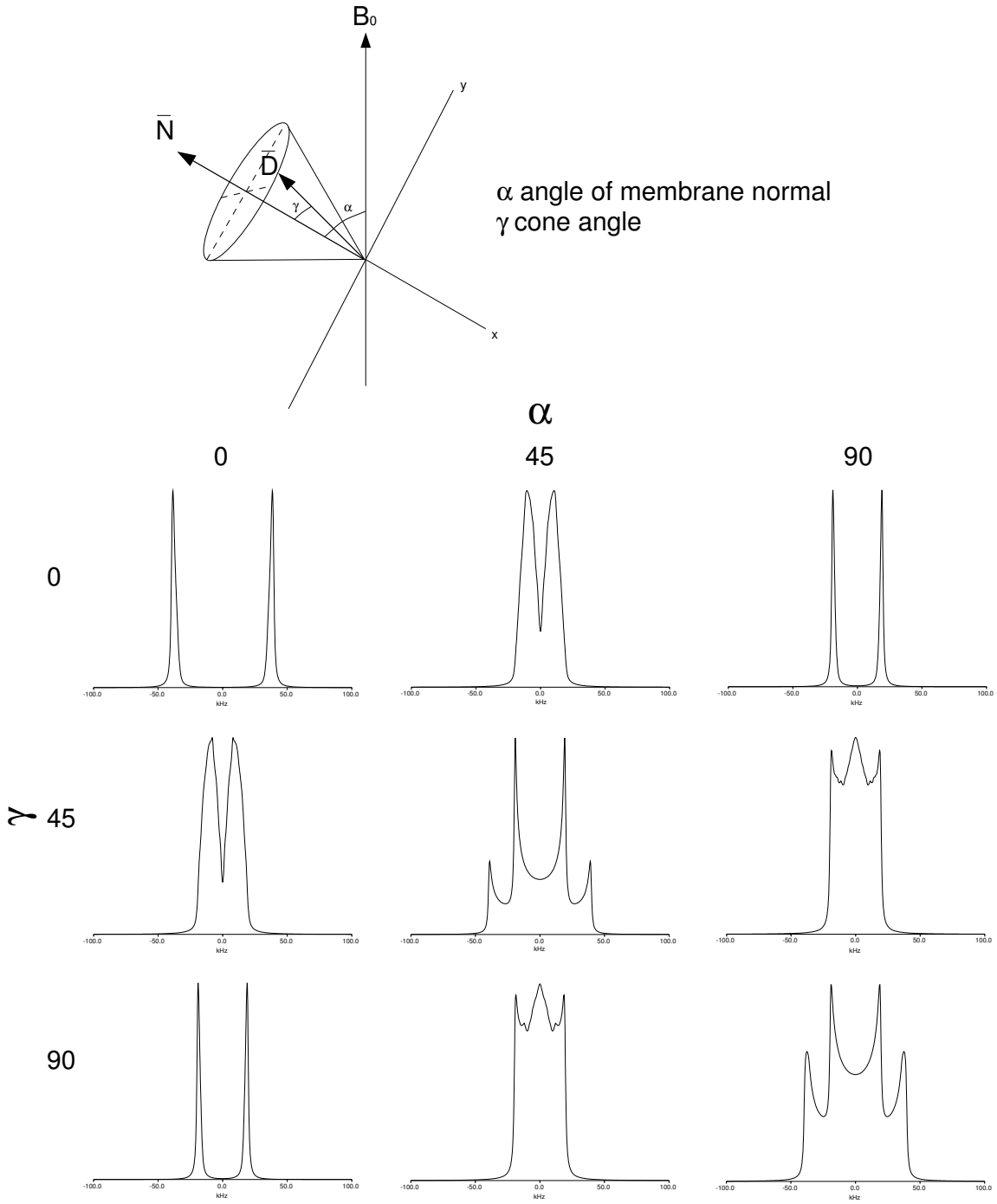

Figure 3.27: Explanation of the spectral parameters required for accurate lineshape simulation of macroscopically orientated samples. Diagram showing geometric relationships used to calculate the lineshapes (top)[10], and the relative effects of these parameters on the observed lineshapes (bottom).

3.1.2 ^{31}P NMR of macroscopically orientated samples.

The static ^{31}P NMR spectra of lipids are governed by the asymmetric electronic distribution around the phosphate group within the lipid. This asymmetric electronic environment is reflected in the chemical shift anisotropy observed in the phosphate group which is described by the three principal components σ_{11}, σ_{22} and σ_{33}. These three terms describe the interaction of the chemical shift anistropy with the applied magnetic field. Considering a spherical distribution of all possible angles of the phosphorous nucleus the powder spectrum can be calculated(Figure 3.28) [231] and the three principal components can be readily observed. In a biological membrane where the lipids are in their L_α phase, rapid rotation about the membrane normal leads to averaging of the chemical shift anisotropy such that the resulting shielding of the phosphorous can be described by the two components of a uniaxially averaged system $\sigma_{||}$ and $\sigma_\perp$ [231]. These terms are readily evaluated from the powder spectrum of a lipid dispersion in the L_α phase as shown in Figure 3.28. The two extremes in the spectrum represent the anistropic component of the chemical shift anisotropy ($\Delta\sigma$) which is defined as $\sigma_{||} - \sigma_\perp$.

For a macroscopically orientated lipid multilayers the angular dependence of the interaction of the chemical shift anisotropy can be calculated as[231]:-

$$\Delta v(\text{ppm}) = -\frac{2}{3}\Delta\sigma\left(\frac{3\cos^2\theta - 1}{2}\right) \tag{3.30}$$

When the lipid bilayers are orientated at 0° with respect to the magnetic field then the observed resonance appears at $\sigma_{||}$ whilst at 90° the resonances appear at $\sigma_\perp$. Coupled with the intrinsic sensitivity of phosphorous NMR due to both its high natural abundance and relative receptivity, the orientational dependence offers an excellent method by which the macroscopic order of the lipid bilayers can be estimated.

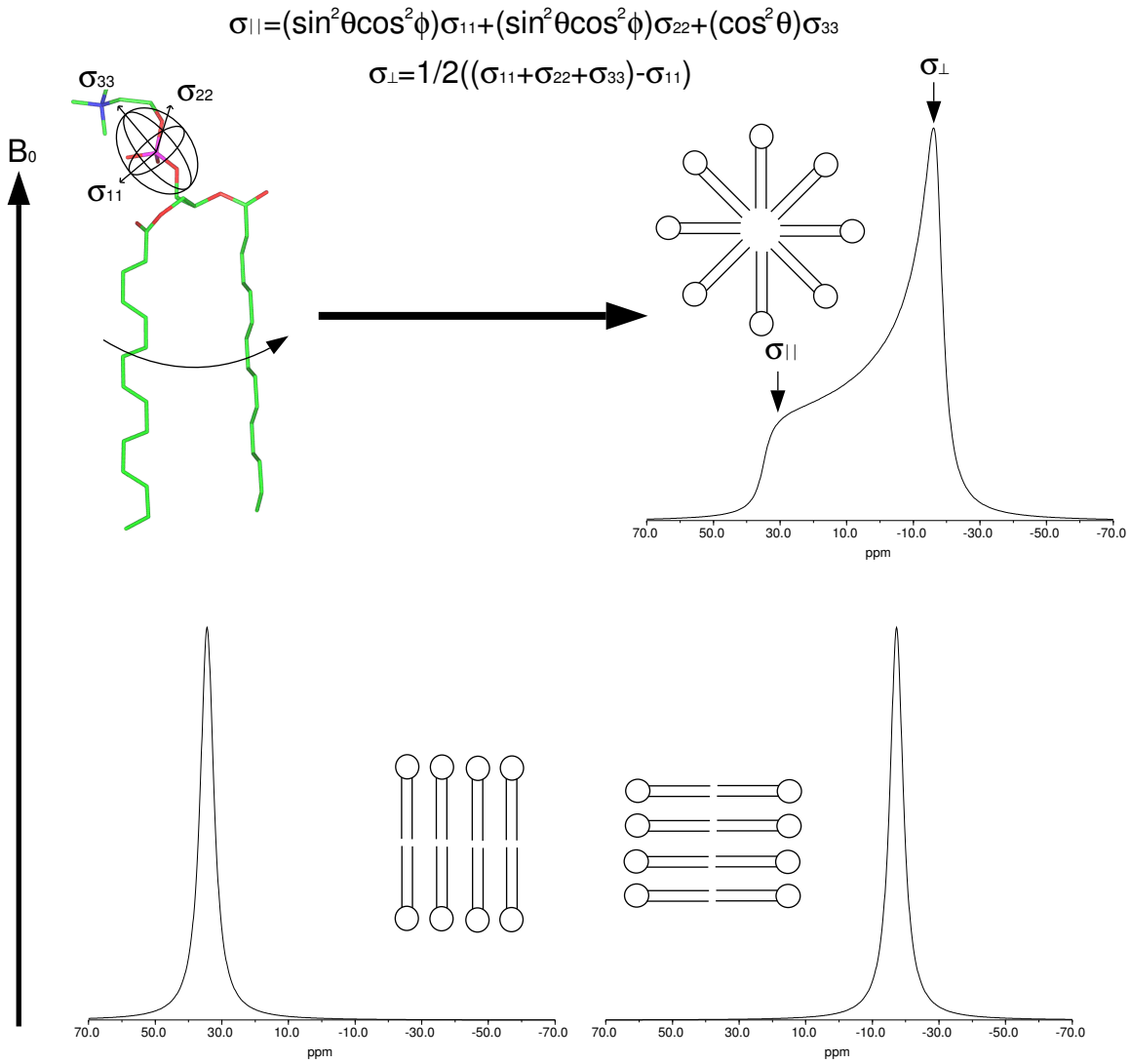

Figure 3.28: Explanation of the spectral parameters obtainable from ^{31}P spectra of powder and orientated systems of lipid bilayer systems. In lipid bilayers rotation about the lipid long axis leads to an averaging of the principle components of the chemical shielding tensor, leading to an axially symmetric powder pattern(top right). Macroscopic orientation of the lipid bilayers allows the $\sigma_{||}$ and $\sigma_{\perp}$ to be observed (bottom, left and right respectively).

3.2 Materials & Methods

3.2.1 Synthesis of $N^+(CD_3)_3$ bromoacetylcholine.

$N(CD_3)_3$ Bromoacetylcholine was synthesized according to Chiou[232], through the addition of bromoacetyl bromide to $N^+(CD_3)_3$ choline bromide. $N(CD_3)_3$ Bromoacetylcholine bromide was subsequently purified by recrystallisation out of isopropanol. The purity was confirmed by ^{1}H NMR (δ= 3.0, 3.6, 3.9, 4.5 ppm) and electrospray mass spectrometry (Fw=233/235).

3.2.2 Synthesis of $N^+(CD_3)_3$ acetylcholine perchlorate.

$N^+(CD_3)_3$ acetylcholine perchlorate was synthesised through the methylation of ethanolamine with a slight excess of deuterated methyliodide in ethanol. The crystalline product, $N^+(CD_3)_3$ choline iodide, was collected by filtration and purified by recrystallization from hot ethanol. Subsequent acetylation using acetic anhydride in pyridine in the presence of the catalyst dimethylaminopyridine, led to the formation of $N^+(CD_3)_3$ acetylcholine iodide. This was subsequently purified by recrystallization from hot ethanol. Acetylcholine perchlorate was produced through the recrystallization of acetylcholine iodide in an ethanol solution saturated with ammonium perchlorate. The purity of the compounds was checked by ^{1}H NMR (δ=1.92, 3.00, 3.52, 4.32, 3.60 ppm) and electrospray mass spectrometry (Fw=164). The nature of the counterion, was checked by CP-MAS NMR and paper chromatography.

3.2.3 Synthesis of $N^+(CD_3)_3$ acetylcholine chloride.

$N^+(CD_3)_3$ acetylcholine chloride was purchased from MSD Isotopes, this was subsequently recrystallised out of a hot ethanol solution. The purity was confirmed by ^{1}H NMR (δ=1.92, 3.00, 3.52, 4.32, 3.60 ppm) and electrospray mass spectrometry (Fw=164).

3.2.4 Purification and labelling of enriched nicotinic acetylcholine receptor membranes.

Membranes were prepared according to the method of Sobel [204] from *Torpedo nobilana* and resuspended in 20 mM TRIS buffer (pH 7.0) to a protein concentration of 1mg ml^{-1} and treated with 10mM DFP to inhibit esterase action and prevent non-specific binding of the bromoacetylcholine to the acetylcholine esterase [232]. The membranes were then treated with N-ethyl maleimide (3mM, 24h, 4°C) to mask free cysteine within the membrane suspension. The receptor membranes were then washed and subsequently reduced by incubation with dithiothreitol (9μM) for 1h to reduce the vicinal disulphide bond. Following extensive washing, the membranes were incubated with 0.1mM bromoacetylcholine (1h room temperature). The membranes were then washed thoroughly with TRIS buffer to prepare them for orientation. Membranes labelled in such a manner have been shown to be exclusively labelled at the two agonist binding sites of the nicotinic acetylcholine receptor [233][234]. Binding studies of a variety of ligands to membranes prepared in such a way have suggested that under these conditions the nicotinic acetylcholine receptor has adopted its desensitised conformation [233][234].

3.2.5 Orientation of enriched nicotinic acetylcholine receptor membranes.

Work described extensively in Analytical Biochemistry, 1997 [53]

Nicotinic acetylcholine receptor membranes were orientated using an isopotential spinning technique (For details of apparatus see Figure 3.29). Alignment was achieved through pelleting 1ml of nicotinic acetylcholine receptor membranes (1mg ml^{-1}) onto a Mellanex sheet (Agar Scientific, UK) by centrifigation (90000g for 15h at 4°C) without drying. The samples were then removed from the apparatus, dried and subsequently rehydrated (85% humidity at 20°C for 3 hours).

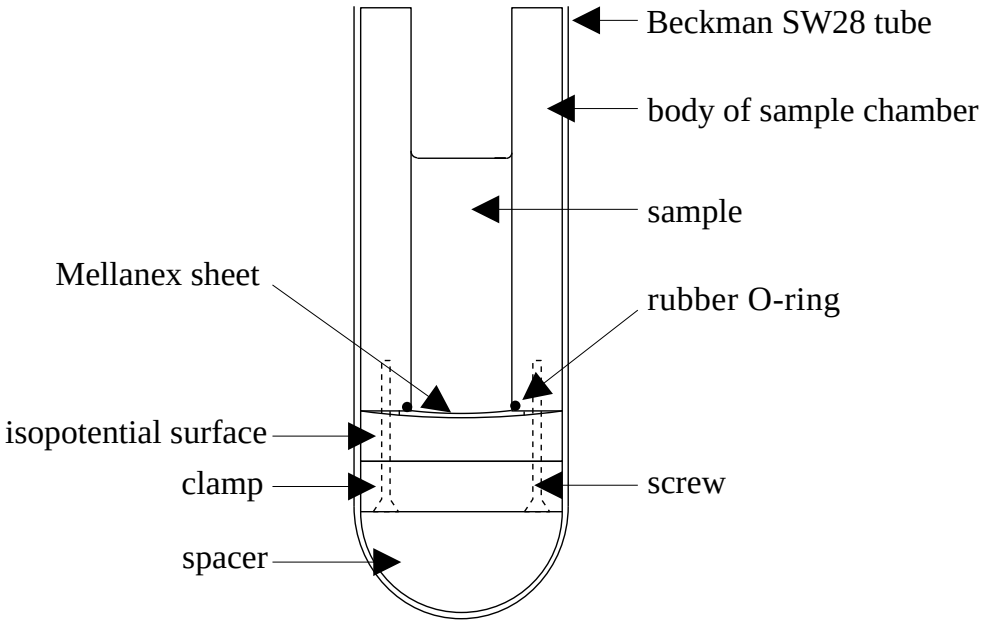

Figure 3.29: Diagram describing the apparatus used for the alignment of nicotinic acetylcholine receptor bilayers onto Mellanex sheets. A membrane suspension is placed in the sample chamber and the assembly placed in a bucket of an SW 28 rotor (Beckmann). Membranes are deposited by centrifugation onto an isopotential surface created as the Mellanex sheet is forced onto the isopotential steel surface. All other components fabricated from polycarbonate.

3.2.6 NMR Measurements.

^{31}P NMR measurements were performed on a Bruker MSL 400 spectrometer at 161.98 MHz with a 8mm double resonance CP probe. Data was acquired using a standard Hahn-echo pulse sequence with broadband proton decoupling during acquisition. 90° pulse lengths were typically 5μs with an interpulse delay of 30 μs; and a recycle delay of 3.5 s. Powder deuterium spectra of crystalline solids were acquired on a Bruker MSL 400 at 61 MHz using a 10mm single resonance static probe. Temperature was regulated to within $\pm$1°K with a Bruker VT1000 temperature control unit. Both powder and orientated samples of nicotinic acetylcholine receptor membranes labelled with N$(CD_3)_3$-bromoacetylcholine bromide were acquired on a CMX 500 Infinity machine at 75 MHz using a 10mm single resonance static probe.

Deuterium spectra were acquired using a standard quadrupolar echo pulse sequence with a 5 μs 90° pulse, 30 μs interpulse delay and a 0.5 s recycle time.

3.2.7 Lineshape Simulations.

To obtain values for both the mosaic spread and the angular dependence of the aligned membranes computer simulations were performed, for both orientated phosphorous and deuterium spectra. The lineshape simulation algorithm was based on that of Ulrich and Watts[10] as described earlier and subsequently modified by Dr C. Glaubitz in our laboratory [10][229][231]. The computer program was written in C++ using GAMMA [235] and simulations typically took less than 30 seconds on a SGI Octane workstation. These simulations allowed a detailed determination of the mosaic spread to be performed, as well as the angular dependence of the $N(CD_3)_3$ group of the bromoacetylcholine bound to the receptor to be extracted from the experimental spectra.

3.3 Results and discussion.

3.3.1 Dynamics of bromoacetylcholine bound in the nicotinic acetylcholine receptor.

$N^+(CD_3)_3$ Bromoacetylcholine bromide.

The temperature dependence of the deuterium spectra of $N(CD_3)_3$ bromoacetylcholine bromide between 170°K and 293°K is shown in Figure 3.30. At 293°K, a narrow central resonance appears upon a powder pattern with a inner splitting of 13kHz. The narrow resonance superimposed on the powder pattern probably results from the residual solvent trapped in the crystal lattice. The powder pattern although not a characteristic Pake doublet, still retains significant intensity in the inner wings ($\Delta\nu_Q$=13kHz). However, the rather rounded characteristics suggests that one of the motions about either the C_3 or C_3' axis of rotation is entering the

intermediate regime [216][219][218]. Reducing the temperature to 270°K leads to a coalesence of the inner wings giving rise to an intense central component indicative of either the C_3 or C_3' motion occurring on an intermediate timescale. As the temperature is decreased the central intensity disappears into a single sharp resonance superimposed on a broad low intensity component. At 230 and 210°K intensity develops of the broad component increases, giving rise to a powder pattern with a characteristic splitting of 40kHz. These lineshapes are characteristic of a quaternary ammonium group undergoing free rotation about either the C_3 or C_3' axis, leading to an averaging of the coupling constant by $1/2(3\cos^2\theta - 1)$[216][219][218]. At 210°K the lineshape starts to regain central intensity at the expense of the inner wings suggesting the motions about the remaining axis of averaging are entering the intermediate regime[216][219][218].

$N(CD_3)_3$ acetylcholine chloride.

The temperature dependence in the deuterium spectra of crystalline $N(CD_3)_3$ acetylcholine chloride between 170°K and 293°K is shown in Figure 3.31. At 293°K the spectrum is dominated by a narrow central resonance $\Delta\nu_Q$ = 1kHz, this is superimposed upon a broad feature of 20kHz width, resembling the outer wings of a deuterium spectrum of a quaternary ammonium group undergoing averaging about the C_3 and C_3' axis. Lowering the temperature to 273°K further reduces the intensity in the wings and the spectrum is predominantly characterized by a central narrow resonance. At 250°K a low intensity broad component appears with $\Delta\nu_Q$ of 40kHz. The intensity of the broad component continues to increase at 230°K consistent with the quaternary ammonium group undergoing free rotation about either the C_3 or C_3' axis. This suggests that the quadrupolar coupling constant is averaged by only one axis of rotation, resulting in the observed $\Delta\nu_Q$ of 40kHz. As the temperature is lowered to 210°K, a characteristic Pake doublet appears consistent with rotation about either the C_3 or C_3' axis[216][219][218]. Already intensity

from a broad central component is apparent. This is consistent with the absence of motion about the either the C_3 or C_3' axis of rotation, whilst the remaining axis of rotation is entering the intermediate regime [216][219][218]. At 170°K there is no intensity left in the inner spectral wings leaving only the broad central resonance consistent with the remaining motion occurring on an intermediate regime [216][219][218]. The relative ease with which these motions are restricted correlates with the known crystal structure of acetylcholine chloride [236] where rotation of the quaternary ammonium group would be sterically hindered by several short range intramolecular contacts. These hindered interactions occur primarily between the quaternary ammonium group and the ester oxygen (3.17 Å, r_{vdw}=3.40Å), the second between the OCH_2 group and the quaternary ammonium (3.2 Å, r_{vdw}=4.00Å). In addition the chloride counterion is located proximal to the quaternary ammonium group resulting in further steric hinderance about the C_3' axis.

$N(CD_3)_3$ acetylcholine perchlorate.

The temperature dependence of the deuterium spectra of $N(CD_3)_3$-acetylcholine perchlorate between 170°K and 293°K is shown in Figure 3.32. At 293°K the spectrum represents the characteristic Pake doublet with a $\Delta\nu_Q$ of 13kHz. This is consistent with fast rotation about both the C_3 and C_3' axis. As the temperature is lowered through 273°K to 250°K no change in the lineshape is observed suggesting that even at 250°K the quaternary ammonium group is free to undergo rotation about the C_3 and C_3' axis. As the temperature is lowered through 230°K to 210°K, intensity is lost in the outer wings, to be replaced by additional intensity in the centre of the spectra, consistent with a slowing of motions about one of the axes, either C_3 or C_3', entering the intermediate motional regime. As the temperature is lowered through 190°K to 170°K, the intensity is further pushed into a central region 9kHz wide, typical of the motion about one of the axis of rotation being in the intermediate regime [216][219][218]. Our inability to freeze out the motion about the C_3 and C_3' axes

can be rationalized with the crystal structure [185] where the quaternary ammonium group has few intramolecular contacts from the backbone of the acetylcholine molecule, with only limited intermolecular contacts between the crystal planes.

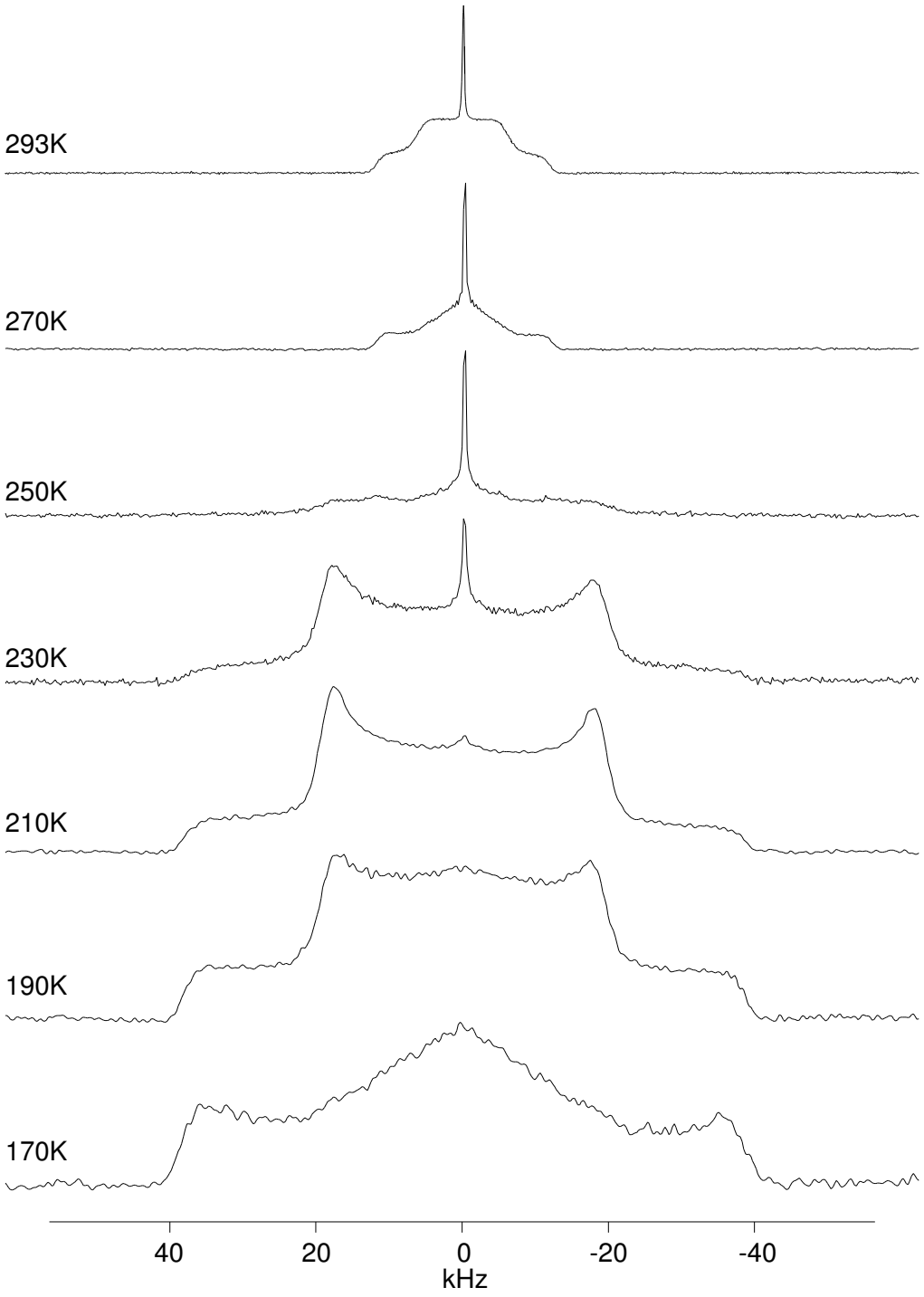

Figure 3.30: Variable temperature deuterium NMR spectra of crystalline bromoacetylcholine bromide. Spectra acquired as described in the text (1024 acquisitions).

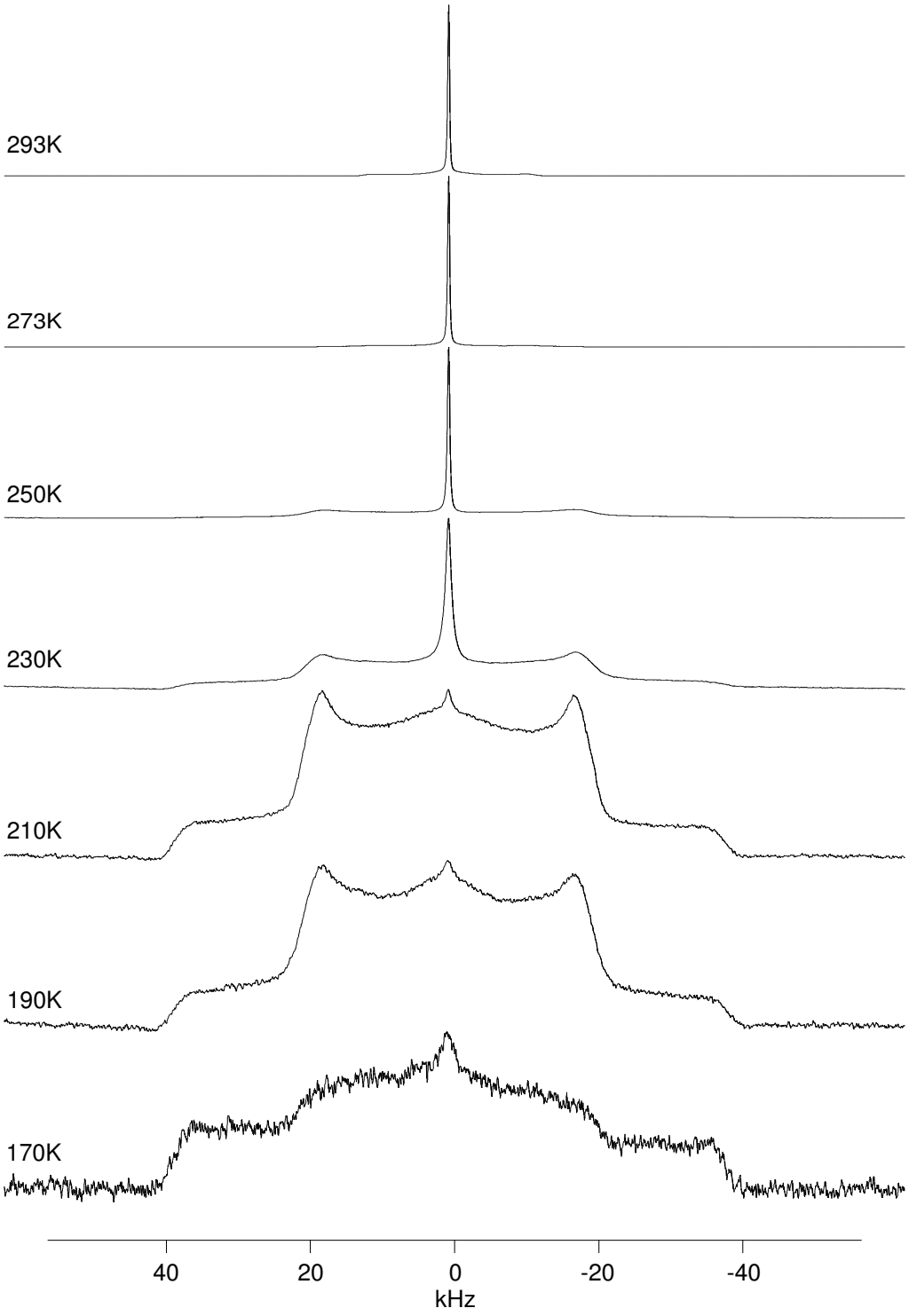

Figure 3.31: Variable temperature deuterium NMR spectra of crystalline acetylcholine chloride. Spectra acquired as described in the text (1024 acquisitions).

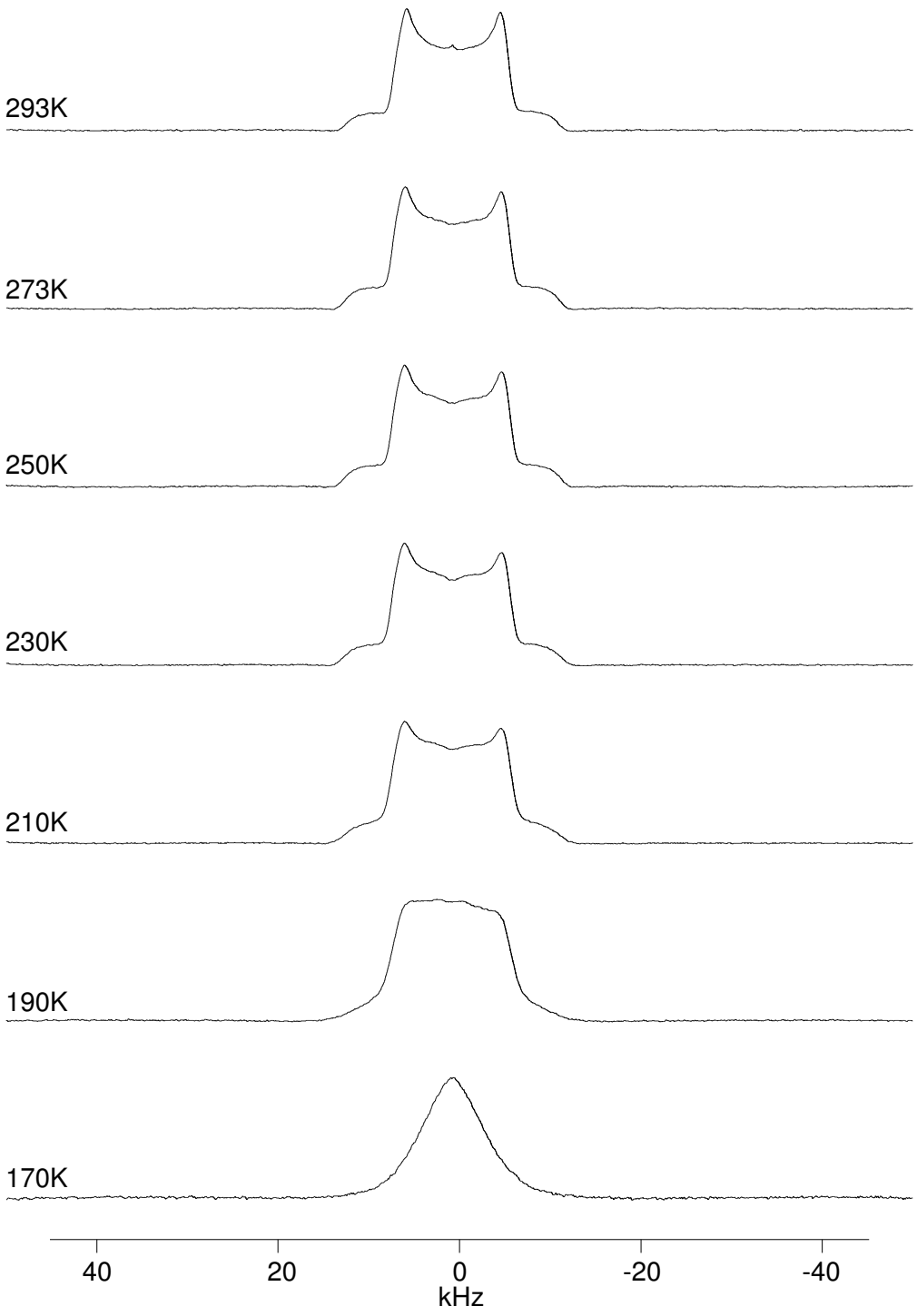

Figure 3.32: Variable temperature deuterium NMR spectra of crystalline acetylcholine perchlorate. Spectra acquired as described in the text (1024 acquisitions).

Nicotinic acetylcholine receptor membrane labelled with $N(CD_3)_3$ bromoacetylcholine

Deuterium NMR spectra of nicotinic acetylcholine receptor membranes labelled with $N(CD_3)_3$ bromoacetylcholine were acquired between 278°K and 153°K and are shown in Figure 3.33. At 278°K the lineshape is dominated by a narrow resonance whose width approaches the homogeneity of the magnet. On lowering the temperature to 253°K the resonance broadens, adopting a Lorentzian characteristic with a line width of 500Hz suggesting that the labelled species is becoming more motionally restricted. At 233°K the lineshape continues to broaden with wings appearing with a splitting of 36kHz. At 213°K these wings gain in intensity at the expense of the central resonance. In addition a broad component appears covering 160kHz. At 193°K the bulk of the central intensity no longer dominates the lineshape but both inner and outer wings at 36 and 160 kHz splitting gain in intensity. On lowering the temperature through 173 to 153°K the intensity continues to be lost from the central resonance leaving well defined wings with splittings at 36 and 160 kHz. In addition, although not as well defined, wings are also visible with an apparent splitting of 78 kHz.

The temperature dependence of the deuterium lineshape mirrors that observed for similar compounds containing deuterated quaternary ammonium group [217], suggesting that the lineshapes are governed primarily by motions occurring about the C_3 and C_3' axis of rotation. However, it should be noted that although this similarity provides a basis for an analysis of the dynamics, it is plausible that additional motions can be propagated from the protein backbone, and more general motions associated with the bilayer may also occur on a timescale suitable to perturb the lineshapes. At high temperatures (>233°K), the deuterium spectrum exhibits a narrow resonance adopting a 'pseudo-isotropic' lineshape [219]. This probably as a result of motion about both the C_3 and C_3' axis of rotation in addition to motions being propogated from the protein backbone, and slower processes attributable to

the reorientation of the protein and bilayer within the sample. As the temperature is lowered to 213°K the central isotropic line acquires wings with a characteristic 38 kHz splitting, similar to those observed for a non motionally averaged methyl group [56]. As the temperature is lowered to 153°K a broad feature appears underneath this 38 kHz wide intensity. Although the spectral quality does not allow detailed analysis of the broad component due to inefficient excitation caused by the limited pulse power attainable, there is evidence that two components, one with a splitting of 76 kHz and a second more pronounced with a 160 kHz splitting. These lineshapes mirror those observed for the inorganic salt trimethylammonium iodide [219] although some of the spectral features are not so pronounced due to the finite power levels used and residual motions being propagated from the protein which may have not been totally suppressed even at these temperatures.

Although the spectra still show some degree of motional averaging at 153°K in comparison with the crystalline solids studied before, a far greater degree of motional constriction has been observed. In the case of the $N(CD_3)_3$ bromoacetylcholine bromide at 170°K there is still sufficient motional averaging occurring about either the C_3 or C_3' axis to render the spectrum no broader than 80 kHz. This suggests that within the binding site the quaternary ammonium group observes a more restricted environment than in the crystalline solid. Through the use of both variable temperature deuterium NMR studies and CP-MAS studies (F. Riddell *pers comm.*) it has been demonstrated that in this class of compounds, the motional restriction can be caused through intramolecular steric contacts or intermolecular contacts between the quaternary ammonium group and its counter ion. Thus it would suggest that within the binding site the ligand is somehow sterically constrained to a greater degree than observed in the crystalline solid. However it is not possible to ascertain whether this is a result of the conformation the ligand adopts in the binding site or due to the nature of the interaction of the quaternary ammonium group of the ligand with residues within the binding site.

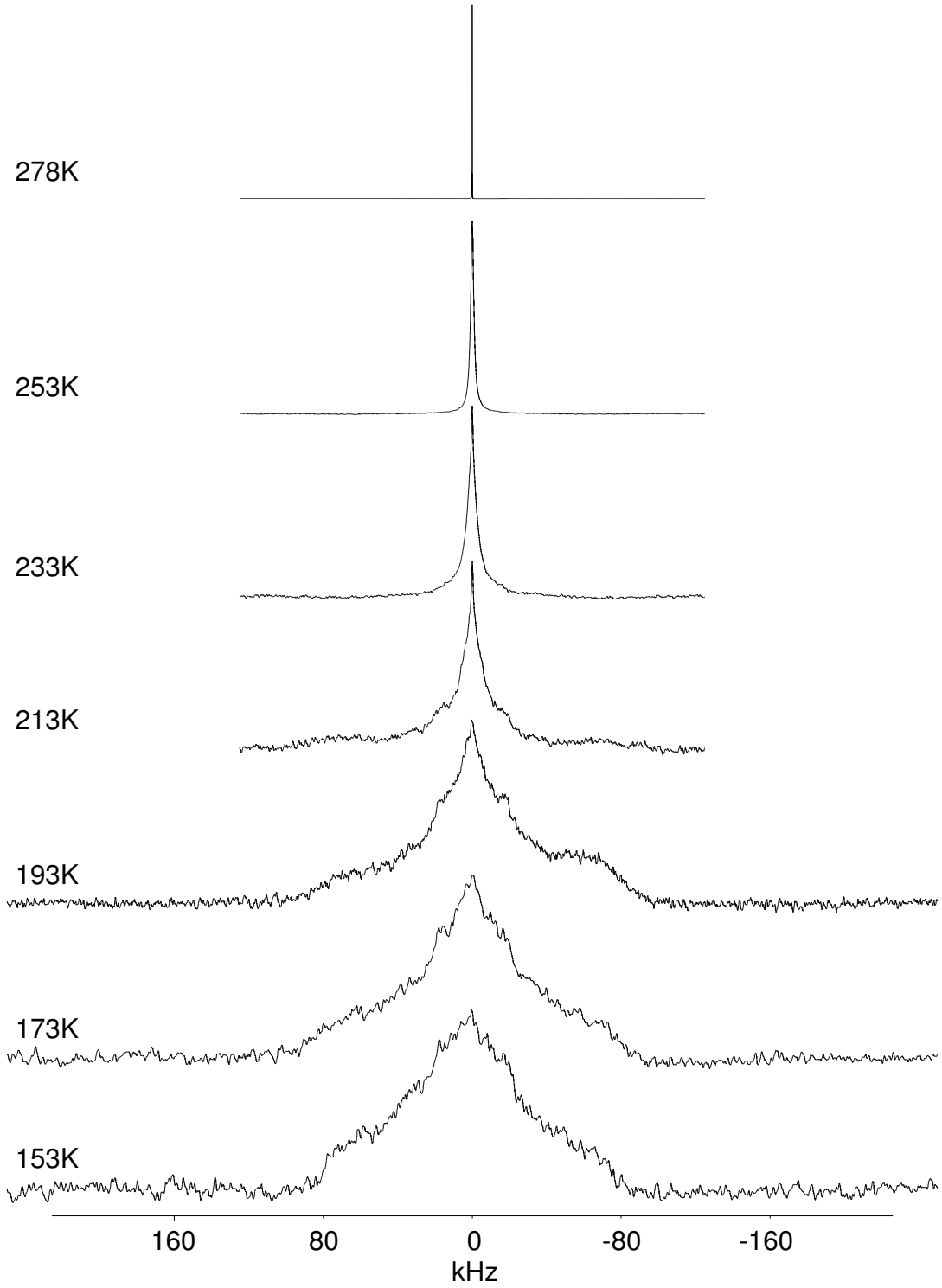

Figure 3.33: Variable temperature deuterium NMR spectra of 50mg of nicotinic acetylcholine receptor membranes labelled with $N(CD_3)_3$ bromoacetylcholine bromide. Spectra acquired as described in materials and methods and result from averaging 60000 acquisitions. Spectra acquired at the temperatures indicated.

3.3.2 Orientation of enriched nicotinic acetylcholine receptor membranes.

^{31}P NMR spectra of orientated nicotinic acetylcholine receptor membranes at 0° and 90° with respect to the applied magnetic field are shown in Figure 3.34. At 0° a broad resonance covering 40ppm to 10ppm is observed with a main peak at 25ppm (Figure 3.34A). Changing the tilt angle to 90° results in a shift in the resonance to -15ppm (Figure 3.34B) as expected for macroscopically aligned lamellar membranes. The observed chemical shift anisotropy is typical for a mixed phosphatidylcholine/phosphatidylethanolamine lipid system in its L_α phase. The broad nature of the 0° and the 90° spectrum can be attributed to the distribution of different lipid types (phosphatidylcholine, phosphatidylethanolamine and phosphatidylserine) within the sample, each of which exhibits a slightly different chemical shift anisotropy. Although this may partially account for the broad distribution, there is also a significant contribution from the mosaic spread around the principle axis. Simulations of the lineshapes observed at both 0° and 90° indicates that the mosaic spread approaches 20-25° from the membrane normal.

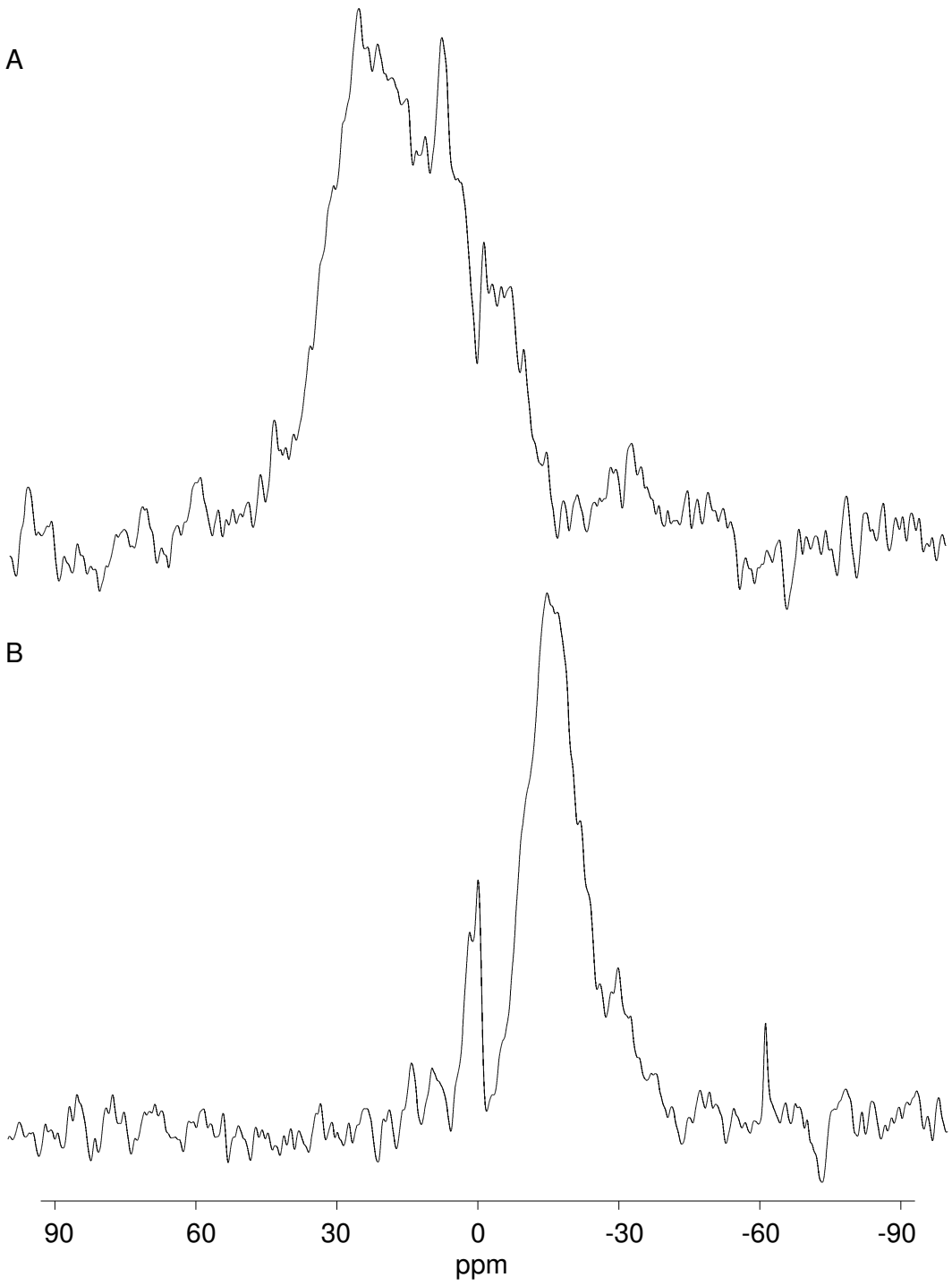

Figure 3.34: Static ^{31}P NMR Spectra of oriented nicotinic acetylcholine receptor rich membranes labelled with deuterated bromoacetylcholine. Spectra recorded using two plates containing 2mg of protein each. Spectra were the result of 4000 acquisitions and acquired under the conditions described in materials and methods. Membrane normal orientated a 0° to the magnetic field (A). Membrane normal orientated at 90° to the magnetic field (B).

3.3.3 Deuterium NMR of $N(CD_3)_3$-bromoacetylcholine labelled orientated enriched nicotinic acetylcholine receptor membranes.

The spectra of oriented nicotinic acetylcholine receptor membranes labelled with $N(CD_3)_3$ bromoacetylcholine bromide are shown in Figure 3.35 (Black line). The 0° orientation is characterized by a central intensity with a splitting of 30 kHz, beneath a 100 kHz wide broad component (Figure 3.35D). In contrast, the 90° spectra adopts a rather featureless peak, whose base is 50 kHz wide (Figure 3.35A). Notably though, edges appear on this line with an apparent splitting of 30 kHz. Even though the powder spectra at this temperature does not show a static lineshape, it is already apparent that the $N(CD_3)_3$ group of the bromoacetylcholine shows an angular dependence with respect to the membrane normal, indicating that the ligands located in both sites are well constrained within the agonist binding site.

Using the simulations outlined in the Materials and Methods, the lineshapes for the 0° and the 90° orientations have been simulated (Figures 3.35A and 3.35D respectively. For the sample with the membrane normal oriented at 0° the best fit with the experimental data was otained using an angle of 42° with a mosaic spread of 40° and a linebroadening of 50Hz (Figure 3.35A). The major discrepancies between the experimental and simulated data arise at the wings of the spectrum at ±50kHz and have been attributed to the finite power levels used during these experiments which leads to inefficient excitation of the wings of wider spectra. An optimal fit for the sample with the membrane normal oriented at 90° with respect to the magnetic field was obtained using an angle of 42° with a mosaic spread of 7.5° and a linebroadening of 50Hz (Figure 3.35D). Variations of γ by +5° (Green) and -5° (Blue) for the both the 0° and 90° orientations (Figure 3.35B and E respectively) indicate very little deviation from this angle can be tolerated before the quality of the fit is reduced.

Although the angle formed between the magnetic field and the cone axis remains constant, the mosaic spread used to simulate the lineshapes obtained at 0° and 90°

do not correlate with each other or that determined by ^{31}P NMR ($\sim$30°). Such descrepancies between mosaic spread of the lipid environment and the embedded protein have been observed previously in such studies[53], however it is not expected that the mosaic spead should change significantly as the angle of the membrane normal is altered with respect to the magnetic field.

In making these simulations several assumptions have been made wich may contribute to these observations, Firstly, we assume that the bromoacetylcholine molecules located at each agonist binding site are similarly orientated with respect to the bilayer normal and secondly, that the deuterium lineshapes are not domainated by intermediate motions.

In principle this technique should allow us to distinguish the orientation of the quaternary ammonium group located within each of the agonist binding pockets as the resulting spectral intensity will arise from the superimposition of two uniaxially symmetric distributions. However, our ability to resolve this situation would be rapidly compromised due to the poor signal to noise obtained in these spectra, which would hinder any attempt at spectral deconvolution. Biochemical data [5] and medium resolution electron diffractioon data [4] suggests that the binding sites share significant structural homology, with any perturbations arising through the interaction of the α subunit with its neighbours. This would suggest that the ligand would adopt and similar orinetation with respect to the membrane normal with any descrepancies being small compared to the resolution of the experiment.

In contrast the deuterium spectra of the same sample prior to orientation acquired at a similar temperature indicated that significant motions were still present on the intermediate timescale even at these low temperatures (-120°C). Lineshape simulations which incorporate such dynamic processed have been developed [230] however these are highly model dependent and to date have not been used to study such systems as either powder or uniaxially oriented samples. However, in an attempt to ascertain whether this angular dependence of mosaic spread significantly

effects the interpretation of the data we have systematically varied the mosaic spread for both the 0° and 90° spectra by both +5° (Green) and -5° (Blue) and are shown in Figure 3.35C and 3.35F respectively. These suggest that although the overall lineshape shows a significant dependence the inner and outer wings of the 0° lineshape and the overall width of the 90° spectrum show very little dependence. This would indicate that the estimate of the angle formed between the quaternary ammoium group and the membrane normal is not significantly compromised by the simulations employed. However, work is underway to allow the accurate simulation of deuterium spectra of both powder and uniaxially oriented motionally averaged samples.

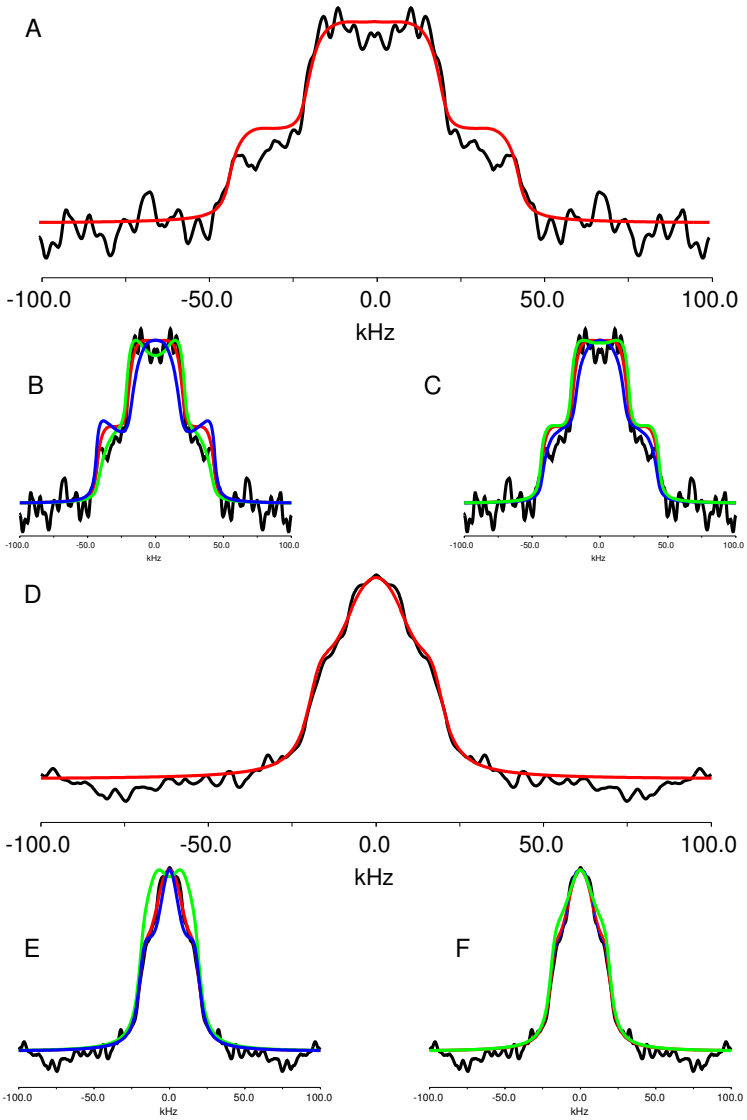

Figure 3.35: Deuterium spectra of 40mg of orientated nicotinic acetylcholine receptor membranes labelled with $N(CD_3)_3$-bromoacetylcholine oriented with the membrane normal parallel (A) and perpendicular (C) to the magnetic field (data shown in black). Spectra acquired with 80000 acqusitions, using a standard quadrupolar echo sequence ($\tau = 30us$). Optimal simulated lineshapes shown in red (A-F). Effect on simulated spectra of small changes in γ for both the parallel and perpendicular cases are shown in B and E repectively (black, experimental; red, best fit as shown in A and D; green, +5° from best fit; blue, -5° degrees from best fit). Effect on simulated spectra of small changes in the mosaic spread for the parallel and perpendicular cases are shown in C and F respectively (black, experimental; red, best fit as shown in A and D; green, +5° from best fit; blue, -5° degrees from best fit).

3.4 Conclusion.

The deuterium NMR studies of unoriented sample of nicotinic acetylcholine receptor labelled with $N(CD_3)_3$-bromoacetylcholine bromide have revealed that at near physiological conditions sufficient overall mobility exists within the system such that the anisotropy present in the deuterium spectrum is almost completely averaged. This almost certaintly results from both intramolecular rearrangements and overall rearrangement of the complex on the timescale of the NMR experiment (10^{-6}s). At temperatures where reorientation of the overall assembly is suppressed we begin to observe lineshapes characteristic of those obtained from both the quaternary ammonium salts studies here and previously [218]. A qualitative comparison of the various data suggests that the quaternary ammonium group of the bromoacetylcholine bromide bound to the receptor is sterically more hindered than in the crystalline salts of acetylcholine and bromoacetylcholine. Detailed simulations that would have enabled a quantitative analysis of the activation energies associated with the reorientation of the methyl and trimethyl rotation have not been performed due to the presence of additional motions that could not be accurately modelled and spectral distortions arising due to the finite power levels used.

Qualitatively this data supports the hypothesis that the quaternary ammonium group is relatively constrained within the binding site based on the observations from structure activity relationship studies[237]. The studies also suggest that minor modifications of the quaternary ammonium group lead to a dramatic drop in affinity suggesting a high degree of complimentarity between the ligand and the receptor[237]. However in the absence of the structure of bromoacetylcholine in the binding site we cannot exclude the possibility that a conformational rearrangement of the ligand has not brought about the change in dynamics observed.

The orientational constraints obtained from the deuterium NMR spectra of aligned nicotinic acetylcholine receptor membranes labelled with bromoacetylcholine

bromide have allowed us to fix the orientation of the quaternary ammonium group at 42±5° with respect to the membrane normal in the desensitized state, however from this study we are unable to distinguish whether the quaternary ammonium group makes this angle with respect to the synaptic or cellular face. From this data we would also propose that this moiety would adopt a similar orientation for the native ligand acetylcholine, as it appears that the quaternary ammonium group is vital to both the pharmacology [237] and the binding kinetics [233] of these ligands to the nicotinic acetylcholine receptor. As the conditions used here for labelling permit the binding of acetylcholine to both agonist sites [233][234], the value obtained for this angular constraint represents the spatial average of the two quaternary ammonium groups.

Correlating these constraints with data obtained from electron diffraction studies [82] and fluoresence resonance energy transfer measurements [11][12] we can now orientate the ligand within its widely accepted binding site some 30Å above the membrane surface (Figure 3.36).

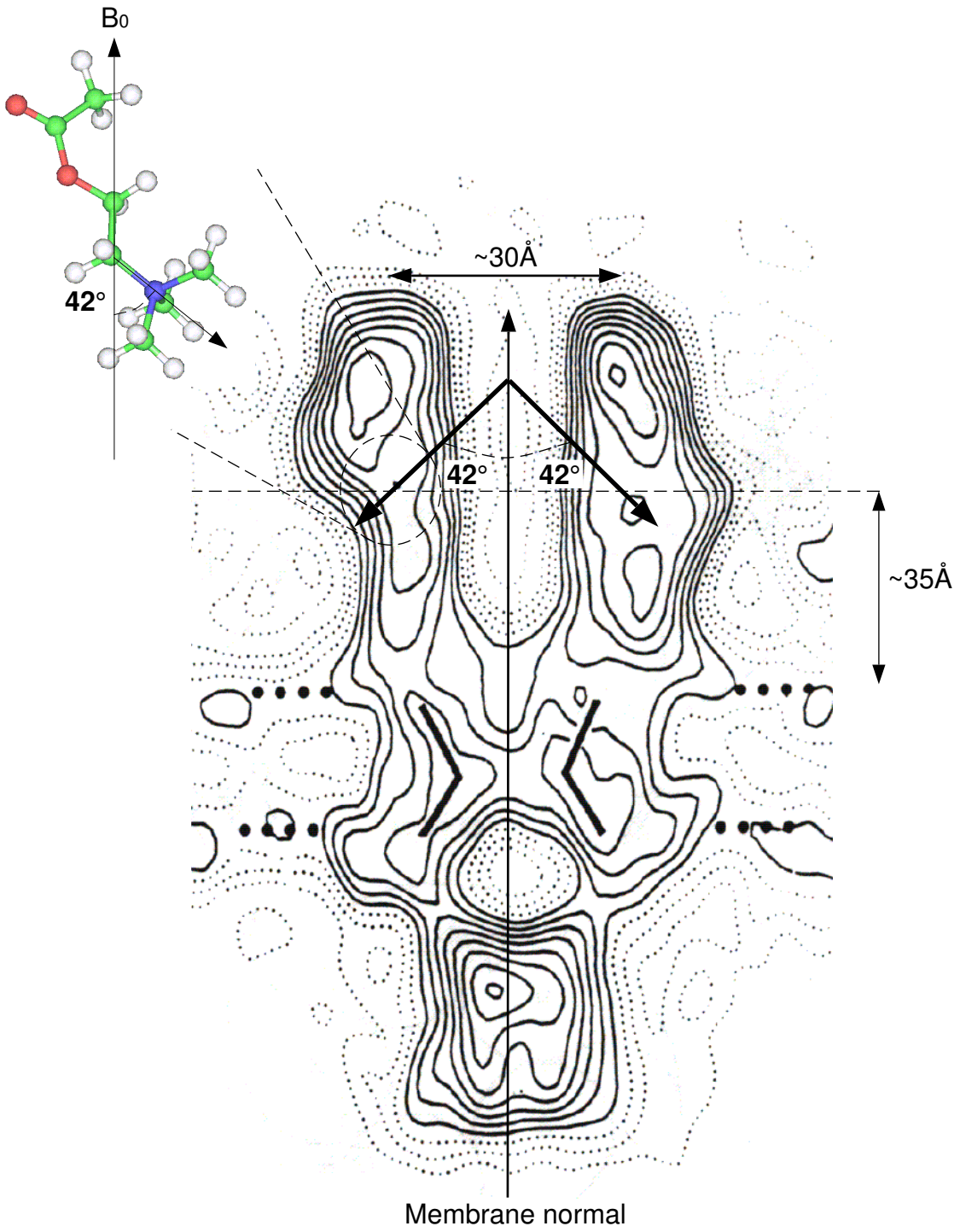

Figure 3.36: Diagram showing the orientation of the quaternary ammonium of the bromoacetylcholine bound in the nicotinic acetylcholine receptor binding site. The ligand has been positioned within the receptor on the basis of fluoresence energy transfer measurements [11] [12] and electron diffraction data.[4]

Chapter 4

Expression, purification and characterisation of neurotensin.

4.1 Introduction.

A prequisite to solid state NMR measurement of ligands bound to their receptors is the introduction of NMR sensitive isotopes into the molecule of interest. In this chapter we aim to produce and characterise carbon-13 and nitrogen-15 labelled neurotensin and neurotensin(8-13) for subsequent solid state NMR studies. In many systems, the only possible approach is the introduction of labels by synthetic chemistry. A potential alternative which can be used for complex peptidic ligands is the recombinant expression of both the labelled ligand and the receptor. Previous solid state NMR-MAS studies of either transmembrane proteins, or their ligands, have relied on the introduction of dilute spin pairs to allow the accurate determination of dipolar coupling from which internuclear distances can be calculated [65] [69] [76].

As outlined such approaches provide an excellent method by which to test a structural model. Although systematic approaches have been developed to ascertain the backbone conformation of peptides [65], mapping the entire conformation would require the synthesis of numerous labelled peptides, providing that labels can be introduced at the relevant sites. An alternative approach to this systematic determination of the backbone structure relies on strategic positioning of spin pairs to allow testing of several proposed models where specific constraints may be diagnostic of entire conformation. However, for studies of the neurotensin receptor little, structural information is available on which to base such a labelling strategy.

In order to circumvent these problems, an approach based on obtaining structural information from multiple sites within the ligand was adopted. For assignment

purposes many have advocated the use of dilute spin systems thereby minimizing linebroadening observed as a result of incomplete averaging of residual dipolar couplings and the presence of J-couplings [79]. However, such an approach would reduce the potential to obtain multiple structural restraints, as partial labelling rapidly reduces the number of internuclear distances that could potentially be probed using dipolar recoupling methodologies.

In this chapter two ligands, neurotensin and neurotensin(8-13), have been produced uniformly labelled with carbon-13 and nitrogen-15. The shorter of these two ligands, neurotensin(8-13), has been synthesised using a classical solid phase synthetic approach using uniformly labelled 9-fluorenylmethoxycarbonyl (FMOC) protected amino acids as the building blocks for the synthesis. For the longer ligand, neurotensin, an expression system that allows the production of peptide in sufficient quantity for solid state NMR studies has been developed, as well as allowing rapid manipulation of labelled sites and economic isotopic labelling.

4.1.1 Expression of full length neurotensin.

In order to achieve satisfactory recombinant expression of small peptides several points need to be addressed:

1. Ease of manipulation and scalability of host system;
2. Inducibility of the expression system;
3. Stability and solubility of the protein; and,
4. Speed and yield of purification.

In an attempt to satisfy these criteria, the glutathione S-transferase fusion protein system was used(pGEX-5X-2)[238] to express the neurotensin as a glutathione S-transferase neurotensin fusion protein in *E.coli*.

The use of *E.coli* was preferred over other hosts due to its ease of use, scalability of fermentation and the ability to allow labelling during cell growth. This is achieved

using either minimal media with inorganic salts as the sole nitrogen or carbon source or proprietary, commercially available labelled media. For protein expression experiments, *E.coli* strain BL21 was chosen. This strain is protease deficient reducing the likelyhood of cleavage of the fusion protein [239] [240].

The pGEX-5X-2 glutathione S-transferase expression vector, offered several advantages over other expression vectors including:

1. expression controlled by the strong *tac* inducible promoter[238];
2. ease of purification with a single glutathione affinity column [238][241]; and,
3. stabilisation of the peptide by synthesis as a fusion protein [242].

The vector has been designed in order to obtain both protease and chemical cleavage sites at the N-terminus of the neurotensin, allowing the removal of the peptide from the glutathione S-transferase protein. Subsequent removal of either the glutathione S-transferase or other peptides after chemical hydrolysis would be facilitated by either a second glutathione affinity column purification to remove the carrier protein or reversed phase HPLC of the peptide mixture.

4.1.2 Solid phase synthesis of neurotensin(8-13).

In contrast to the expression system employed for the full length neurotensin, the shorter analogue neurotensin(8-13) was synthesised using conventional solid phase synthesis. In the absence of information allowing the rational design of a specific labelling strategy a uniform labelling approach was used.

Solid phase synthesis of neurotensin(8-13) was performed in collaboration with Dr M Pitkeathly at the Oxford Centre for Molecular Sciences. All amino acids were FMOC protected prior to synthesis of the labelled ligand as outlined in Materials and Methods.

4.1.3 Characterisation of neurotensin and neurotensin(8-13).

Prior to solid state NMR studies, preliminary studies were performed on the peptide in the solution state to provide an accurate set of chemical shifts and allow subsequent comparisons with the chemical shifts obtained when the ligand was bound to the receptor. Information regarding the perturbations of chemical shifts have been used to provide information regarding the electrostatics within the binding site [243]. In addition assignments of backbone resonances in proteins, have been used to predict the nature of the secondary structure adopted by the peptide [244]. Thus, an accurate set of resonance assignments might aid subsequent structural studies by providing evidence for any preferred conformation.

4.2 Materials & Methods.

4.2.1 Synthesis of 8-13 neurotensin by solid phase synthesis.

Neurotensin(8-13) was synthesized using FMOC protection chemistry at the Oxford Centre for Molecular Sciences. Prior to peptide synthesis, the uniformly labelled amino acids were purchased from Promochem (Glossop, UK). Amino acids were protected using standard amino acid protection protocols [245] with the modifications shown below.

FMOC-Arginine. To a mixture of 2.14ml 10% $NaCO_3$ and 5ml dioxane chilled on ice was added 100 mg of arginine. To this 160mg of FMOC-succinimide ester was added over the course of 5 minutes. The reaction was stirred on ice for 4 hours and then left stirring overnight at room temperature. The reaction mixture was acidified to pH 2.0 before being extracted into ethyl acetate. The ethyl acetate layer was rotary evaporated until a dry solid formed. Subsequently, this was recrystallised from an ethyl acetate petroleum ether mix. The product was subsequently collected as a white solid. The product was analysed by thin layer chromatograhy using a chloroform:methanol:ammonia (65:15:1/v:v:v) solvent system.

FMOC-Leucine: To a mixture of 2.14ml 10% $NaCO_3$ and 5ml dioxane chilled on ice was added 100 mg of leucine. To this 160 mg of FMOC-succinimide ester was added over the course of 5 minutes. The reaction was then stirred on ice for 4 hours and then stirred overnight at room temperature. The reaction mixture was acidified to pH 2.0 before being extracted into ethyl acetate. The ethyl acetate layer was rotary evaporated until a dry solid formed. Subsequently, this was recrystallised from an ethyl acetate. The product was analysed by thin layer chromatography using a chloroform:methanol:ammonia (65:15:1/v:v:v) solvent system.

FMOC-Isoleucine: To a mixture of 2.14ml 10% $NaCO_3$ and 5ml dioxane chilled on ice was added 100 mg of isoleucine. To this 160 mg of FMOC-succinimide ester was added over the course of 5 minutes. The reaction was stirred on ice for 4 hours before being left stirring overnight at room temperature. The reaction mixture was acidified to pH 2.0 before being extracted into ethyl acetate. The ethyl acetate layer was rotary evaporated until a dry solid formed. Subsequently, this was recrystallized from ethyl acetate. The product was analysed using thin layer chromatography using a chloroform:methanol:ammonia (65:15:1/v:v:v) solvent system.

FMOC-Tyrosine: To a mixture of 2.14ml 10% $NaCO_3$ and 5ml acetone chilled on ice was added 100 mg of tyrosine. To this 160 mg of FMOC-succinimide ester was added over the course of 5 minutes. The reaction was stirred on ice for 4 hours before being left stirring overnight at room temperature. The reaction mixture was acidified to pH 2.0 before being extracted into ethyl acetate. The ethyl acetate layer was rotary evaporated until a dry solid formed. Subsequently, this was recrystallized from an ethyl acetate petroleum ether mix. The product was analysed by thin layer chromatography using a chloroform:methanol:ammonia (65:15:1/v:v:v) solvent system.

FMOC-Proline: To a mixture of 2.14ml 10% $NaCO_3$ and 5ml dioxane chilled on ice was added 100 mg of proline. To this 160 mg of FMOC-succinimide ester was added over the course of 5 minutes. The reaction was stirred on ice for 4

hours before being left stirring overnight at room temperature. The reaction mixture was acidified to pH 2.0 before being extracted into ethyl acetate. The ethyl acetate layer was rotary evaporated until a dry solid formed. This was recrystallised from an ethyl acetate petroleum ether mix. The product was collected as a white solid. The product was analysed using thin layer chromatography using a chloroform:methanol:ammonia (65:15:1/v:v:v) solvent system.

4.2.2 Design rationale for the expression vector.

A codon optimized synthetic gene encoding the native neurotensin was designed according to the codon preference in *E.coli*. The neurotensin gene was cloned into the glutathione S-transferase gene fusion vector pGEX-5X-2 (Pharmacia, Sweden). In the pGEX-5X-2 plasmid the glutathione S-transferase expression is regulated by the *tac* promoter. The desired peptide or protein is then expressed as a C terminal fusion with the glutathione S-transferase protein. In order to clone the desired synthetic gene, two complementary oligonucleotides of 60 bases were synthesised (Figure 4.37). These oligonucleotides also contained a linker region between the 3' end of the glutathione S-transferase gene and the 5' end of the neurotensin gene. This linker region encodes a methionine codon at the 5' of the neurotensin sequence. Following expression, the presence of this methionine allows the cleavage of the neurotensin peptide from the glutathione S-transferase by a conventional cyanogen bromide cleavage protocol (See below). In addition a *Hind*III restriction site was also included in the oligonucleotides to facilitate the identification of recombinant plasmids.

The pGEX-5X-2 plasmid (Pharmacia, Sweden) plasmid was digested with *Bam*HI and *Not*I (New England Biolabs, UK) according to the manufacturers instructions. The cleaved vector was then treated with alkaline phosphatase to prevent subsequent self-religation. The cleaved plasmid was then purified with a Wizard Cleanup Kit (Promega, UK) following the manufacturers recomendations. The cleavage process

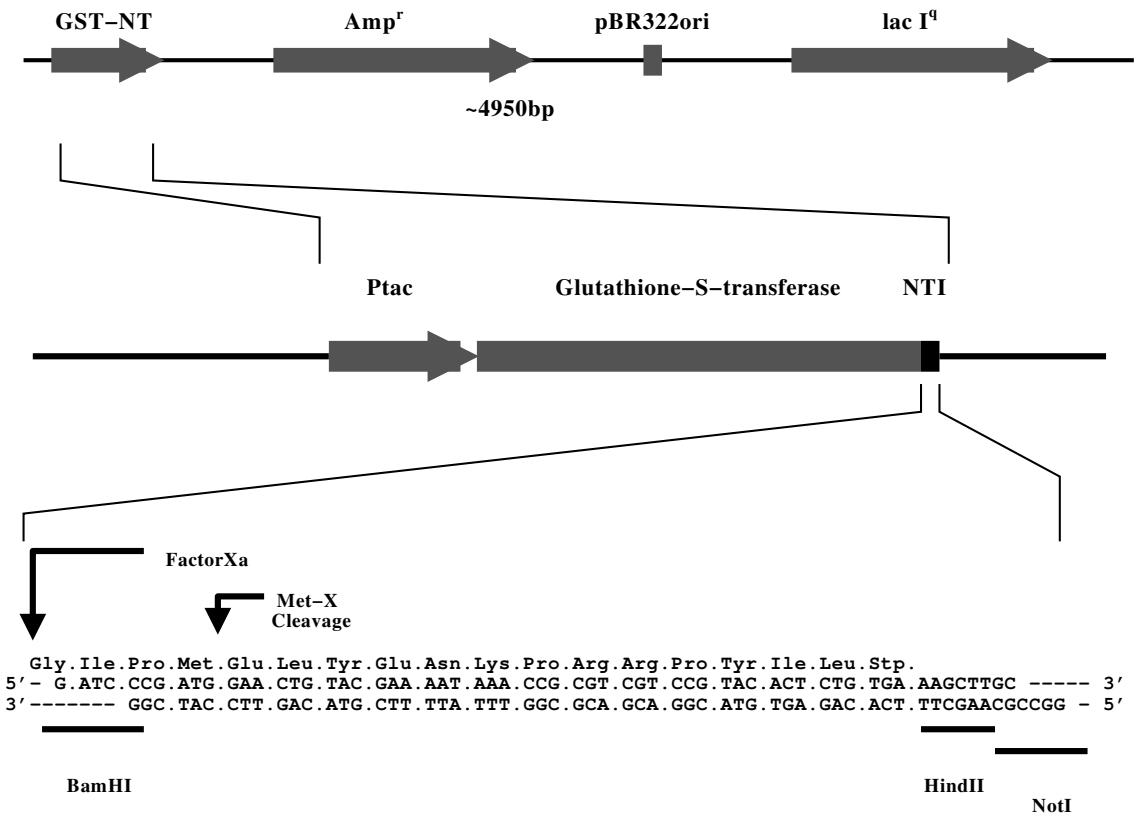

Figure 4.37: Structure of synthetic gene for GST-NT plasmid.

was then checked on a 1% agarose gel electrophoresis and stained with 1% ethidium bromide. The single band observed was consistent with the linearization of the plasmid, in contrast to the undigested plasmid.

The oligonucleotides were prepared for ligation by treatment with polynucleotide kinase (New England Biolabs, UK) following the manufacturers recommendations. The mixture was subsequently heat inactivated by heating at 65 °C for 5 minutes. The two oligonucleotides were then mixed and annealed by reducing the temperature from 65° to 30° over the course of 1 hour. The oligonucleotides were then ligated into the pretreated plasmid at a molar ratio of 1:3 with 1U of T4 DNA ligase (New England Biolabs, UK) in 20 μl for 4 hours. XL-1 blue (*recA1 endA1 gyrA96 thi-1 hsdR17 supE44 relA1 lac [F' proAB lacI^{q}ZΔM15 Tn10 (Tet^R)]*) competent cells were prepared using the rubidium chloride method [246] and then transformed with

the ligation mix using a heat shock protocol [246]. The cells were then plated out onto a Luria Broth agar plates supplemented with 50μg ml^{-1} ampicillin and grown overnight at 37°C. Colonies were innoculated in 2ml of Luria Broth supplemented with 50μg ml^{-1} ampicillin and grown overnight with shaking (200 rpm). These overnight cultures were used to prepare plasmid DNA using the Quiagen miniprep kit (Quiagen, UK). To check the correct formation of the construct, a sample of the plasmid treated with *Hind*III and *Eco*RV. The digests were the analysed on a 1% agarose gel stained with 1% eithidium bromide. The presence of two fragments of 1.7 kb and 3.2kb indicated that recombinant plasmids were obtained. This plasmid was called pGEX-NT. A large scale preparation of pGEX-NT was obtained from a 500ml overnight culture of XL-1 blue transformed with the pGEX-NT vector and grown in the presence of 50μg ml^{-1} ampicillin. The plasmid was subsequently purified using a Quiagen Maxiprep kit (Quiagen, UK) following the manufactures instructions and the resulting plasmid DNA used for all subsequent protein expression experiments.

4.2.3 Fusion protein expression.

Competent BL21(DE3) (F$^-$, ompT, hsd, S($r_B^- m_B^-$), gal) cells were prepared using the rubidium chloride method [246], transformed by a heat shock method [246] plated out onto a Luria Broth agar plates supplemented with 50μg ml^{-1} ampicillin and grown overnight at 37°C. Transformants were used to inoculate in 10ml of Luria Broth supplemented with 50μg ml^{-1} ampicillin and grown overnight at 37°C with shaking (200 rpm). The overnight culture was used as a 0.1% innoculum for 1l of Luria Broth supplemented with 50μg ml^{-1} ampicillin. The cells were grown at 37°C with shaking (200 rpm) to late exponential phase (OD_{660}=0.7). Expression of the recombinant protein was then induced with 0.1mM isopropyl-β-thiogalactoside for 4 hours. The cells were then harvested in a Beckmann JA-10 rotor at 4,000 rpm and washed in cold PBS (150mM NaCl, 20mM $NaPO_4$, pH 7.2).

4.2.4 Purification of fusion protein GST-NT

The cells expressing the GST-NT fusion protein were broken in B-Per extraction reagent (Pierce, UK) with mild sonication (6, 10 second bursts) and adequate cooling. The cell lysate was subsequently clarified by ultracentrifugaion in a Beckmann JA-20 rotor at 20,000 rpm for 30 minutes. The GST-NT fusion protein was purified from the clarified cell lysate by glutathione affinity chromatography. A 2ml Pharmacia glutathione Sepharose 4B affinity column was equilibrated in PBS. The clarified cell lysate was subsequently loaded onto the column at 0.5 ml min^{-1}. The column was then washed with 10 bed volumes of PBS. The bound protein was subsequently eluted with 10mM reduced glutathione in 50mM TRIS buffer (pH 8.0).

4.2.5 Cleavage of GST-NT

The neurotensin was cleaved from the fusion protein GST-NT following a cyanogen bromide protocol[247]. Briefly, to a protein solution of 1 to 5 mg ml^{-1} GST-NT was added an equal volume of 0.4M ammonium bicarbonate solution together with 5% 2-mercaptoethanol. The sample was sealed under a nitrogen atmosphere and incubated at room temperature overnight. The sample was then lyophilised with a little heating to remove any remaining bicarbonate. The sample was then dissolved in trifluoroacetic acid (TFA) at a concentration of between 1 and 5 mg ml^{-1}, to which water is then added to make the acid (50% v/v). White crystalline cyanogen bromide was subsequently added to the sample in 100 fold excess (typically a mass equal to that of the protein). The reaction was subsequently incubated at room temperature for 24h. The reaction was terminated by lyophilisation.

4.2.6 Purification of NT

Separation of products following the cyanogen bromide cleavage was performed by reverse phase HPLC, using a C18 Dynamax 83-213-C column. The column was

equilibrated with 0.1% TFA in water until a stable base line was obtained, and then loaded with 100μl of 1mg ml^{-1}. The products were eluted with a linear gradient of acetonitrile from 0 to 40% over 25 minutes.

4.2.7 Preparation of neurotensin(8-13) and neurotensin for solution NMR.

Solution NMR experiments were performed on 5mg of lyophilised neurotensin dissolved in 650 μl of a 5% solution of D_2O in H_2O and loaded in a 5mm NMR tube. Solution NMR experiments were performed on 2.2mg of lyophilized neurotensin(8-13) dissolved in 650μl of a 5% solution of D_2O in H_2O and loaded into a 5mm NMR tube.

4.2.8 Resonance Assignments for neurotensin(8-13) in solution.

Resonance assignments for neurotensin(8-13) were performed on a Varian Inova at 750MHz. Proton assignments where performed by sequential assignment. All spectra were acquired with 1.5 seconds water presaturation. All spectra were processed with solvent suppression using a time domain convolution solvent suppression algorithim developed by Dominique Marion and implemented in Felix 97.0 (MSI Inc., CA)

A DQF-COSY dataset was acquired with 128 t_1 increments using States-TPPI phase cycling. Data in t_1 was linear predicted to 512 points. Both dimensions were zero filled to 2048 and 1Hz linebroadening applied before Fourier transform.

TOCSY data was acquired with a MLEV-16 clean, 80ms mixing sequence, using a B_1 field of 11kHz. 128 t_1 increments were acquired with States-TPPI phase cycling. Data in t1 was linear predicted to 512 points. Both dimensions were zero filled to 2048 and 1Hz linebroadening applied prior to Fourier transform.

NOESY data was acquired with 300ms mixing time. 128 t_1 points were acquired with States-TPPI phase cycling and the data was subsequently linear predicted to

512 points. Both dimensions were zero filled to 2048 data points and 1Hz linebroadening applied prior to Fourier transformation.

ROESY data was acquired with a 300ms mixing time using a B_1 field of 8.4kHz. 128 t_1 increments were acquired with States-TPPI phase cycling, data was subsequently linear predicted to 512 data points. Both dimensions were zero filled to 2048 data points and 1Hz linebroadening applied prior to Fourier transformation.

4.3 Results

4.3.1 Synthesis of FMOC-amino acids.

The synthesis of the FMOC-amino acids was performed as described above. Following the synthesis, the nature and purity of the product was determined by thin layer chromatography and electrospray mass spectroscopy through comparison with standard unlabelled compounds. The results are given in Table 4.6. The r.f. values and electrospray mass spectroscopy fragmentation patterns shown in Table 4.6 were identical to those obtained from standard FMOC-amino acids (Bachem, Germany) allowing for uniform isotopic enrichment with carbon-13 and nitrogen-15.

Amino Acid	Yield(%)	r.f. value	Major Species (Da/e)
Arginine	84	0.28	113.9, 131.9, 173.0, 193.0, 341.1
Leucine	95	0.71	129.9, 155.9,352.0
Isoleucine	89	0.46	130.0, 156.0, 352.2
Tyrosine	83	0.40	106.9, 118.9, 163.0, 160.0, 206.1
Proline	95	0.33	130.0, 158.1, 177.1

Table 4.6: Summary of results obtained from the synthesis and characterization of FMOC amino acids used in the synthesis of neurotensin(8-13).

4.3.2 Solid Phase Synthesis of Neurotensin(8-13)

The protected amino acids were supplied to the Oxford Center for Molecular Science where 54mg of labelled neurotensin were synthesised using conventional solid

phase FMOC chemistry. The peptide was purified by reverse phase HPLC and eluted at an acetonitrile concentration of 27%. The neurotensin(8-13) co-eluted with standard neurotensin(8-13) (Sigma, UK). Electrospray mass spectroscopy of the purified peptide gave rise to a single molecular species with a molecular weight of 868 Da consistent with uniform labelling of neurotensin(8-13) with both carbon-13 and nitrogen-15. This product was subsequently used in all solution and solid state NMR experiments without further treatment.

4.3.3 Bacterial Expression Construct.

The expression of neurotensin was undertaken in *E.coli* fused to the C-terminus of glutathione S-transferase. The fusion of small peptides to carrier proteins such as glutathione S-transferase has been shown to improve the stability of expressed proteins in vivo and during purification and enhance their solubility[242]. The fusion of the peptide with glutathionine S-transferase also enables the rapid purification of the fusion protein, by using a single glutathione affinity column. The presence of both a Factor Xa and a chemical cleavage site to the N-terminus of the neurotensin, offers two possibilities for the cleavage of the peptide from the fusion protein.

4.3.4 Production of Recombinant GST-NT fusion protein.

From a 1l culture, 35mg of GST-NT protein were typically purified after affinity chromatography. This was 95% pure as shown by densitometry of a 12% Tris SDS-PAGE gel loaded with 10 μg of protein (Figure 4.38B). Due to the small discrepancy between the molecular weight of glutathione S-transferase and the glutathione S-transferase-neurotensin fusion protein, the molecular weight of these proteins was confirmed by matrix assisted laser disorption ionisation-time of flight mass spectroscopy (MALDI-TOF MS) which gives a higher resolution analysis of the molecular weight compared to conventional SDS-PAGE. Early mass spectroscopic analyses

indicated a range of molecular species with a higher molecular mass than that expected by multiples of 317 Da. This is consistent with the presence of several glutathione adducts. Treatment of the GST-NT with 100mM dithiothreitol, gave rise to a single molecular species of 28395±20 Da which is consistent with that predicted from the amino acid sequence. This analysis indicates that the fusion protein GST-NT is the primary product formed with little or no C-terminal truncations.

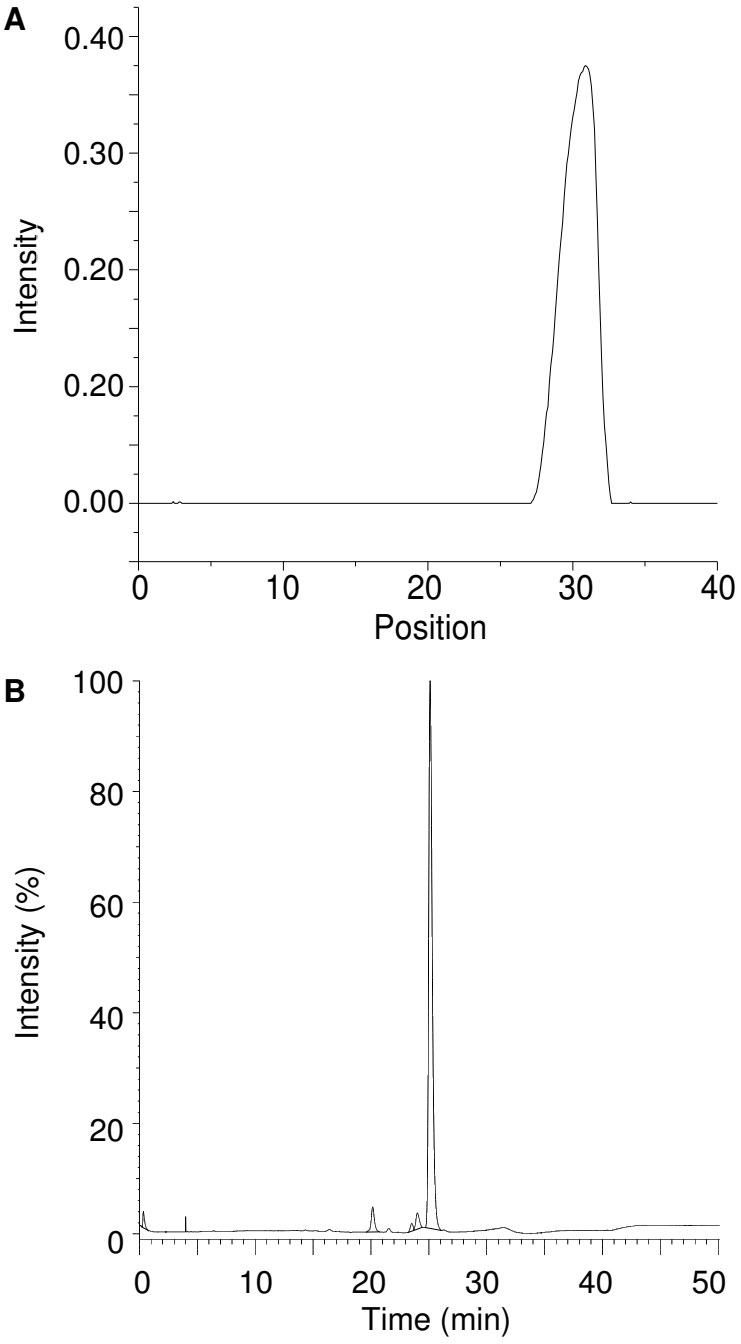

Figure 4.38: 10 μg of GST-NT purified by affinity chromatography were run on a 12% Tris SDS-PAGE and stained with Comassie Blue. The densitometry scan of the resulting lane is given (A). HPLC trace (254nm) of purified neurotensin, following cleavage and purification by reverse phase HPLC (B).

4.3.5 Cleavage and Purification of NT.

Following cyanogen bromide cleavage, the fragments were purified by reverse phase HPLC using native neurotensin (Sigma, UK) as a standard; a typical trace is shown in Figure 4.38B. The standard neurotensin eluted at an acetonitrile concentration of 27%, the corresponding peak from the cyanogen bromide cleavage was collected. The fractions were pooled, lyopholyse and resuspended in 200μl of water.

A portion of this sample was mixed with standard neurotensin, the resulting mixture co-eluted under the same HPLC conditions. The fraction collected, corresponding to the neurotensin was analysed by MALDI-TOF MS. The resulting spectrum consisted of a single molecular ion peak, in addition to neurotensin as the monosodium, disodium and monopotassium salt; no other fractions were apparent. The peptide was further characterised by N-terminal sequencing by Dr Tony Willis and MALDI-TOF fragmentation analysis by Dr D. Neville at the Oxford Centre for Molecular Sciences. These experiments confirmed both the sequence and purity of the peptide to be full length neurotensin. The final yield of peptide from 35mg of pure GST-NT was 1.8mg as determined by UV spectrscopy at ($E_{280}^{1\text{mg ml}^{-1}}$=1.37) giving an 83% recovery with respect to the theoretical yield.

4.3.6 Resonance Assignments for neurotensin in solution.

In order to determine the subsequent effects of binding of the neurotensin to the neurotensin receptor, a proton and carbon-13 chemical assignment of neurotensin was performed in collaboration with Dr C.Chung (Glaxo-Wellcome, UK). The results of these studies are summarised in Table 4.7 and Table 4.8. These data are based on the assignment of unlabelled peptide using a conventional sequential homonuclear assignment protocol. These assignments correlate with those previously obtained [248]. Carbon-13 chemical shifts were subsequently assigned using a ^{1}H-^{13}C HSQC experiment.

Residue	NH	H_α(ppm)	H_β(ppm)	H_γ(ppm)	H_δ(ppm)	Other
Glu	7.865	4.314	1.898/2.485	1.898		
Leu	8.281	4.317	1.414/1.535	1.400	0.838/0.891	
Tyr	8.295	4.600	2.930/3.070			6.839/7.122
Glu	8.335	4.252	1.896/1.995	2.194		
Asn	8.497	4.655	2.739/2.818		6.930/7.611	
Lys	8.155	4.620	1.705/1.816	1.438	1.690	2.988
Pro		4.370	1.811/2.217	1.979	3.617/3.768	
Arg	8.560	4.294	1.758/1.813	1.660	3.200	
Arg	8.356	4.615	1.615/1.798	1.439	2.983	
Pro		4.413	1.849/2.291	2.001	3.616/3.792	
Tyr	8.071	4.585	2.994/3.040			6.801/7.147
Ile	7.696	4.142	1.818	0.894/1.116/1.416	0.838	
Leu	7.801	4.175	1.576	1.590	0.883/0.929	

Table 4.7: Proton resonance assignments for neurotensin in solution (pH 3.5, 10% D_2O)

Residue	C_α(ppm)	C_β(ppm)	C_γ(ppm)	C_δ	C_ϵ
Glu	51.0	24.5	29.0		
Leu	53.0	39.0	21.0	24.0	
Tyr	54.0	36.0	129.2	114.53	
Glu	52.5	27.0	32.5		
Asn	51.0	26.0			
Lys	49.0	26.0	21.5	38.5	39.0
Pro	60.0	29.0		47	
Arg	52.5	28.5			
Arg	51.0	29.0	39		
Pro	60.0	29.0		47	
Tyr	54.0	36.0			
Ile	53.0		24	10	
Leu	53.5	24.0	41.0		

Table 4.8: Partial carbon-13 resonance assignments for neurotensin in solution (pH 3.5, 10% D_2O)

Residue	NH	H_α(ppm)	H_β(ppm)	H_γ(ppm)	H_δ(ppm)	Other
Arg		4.50	2.02/2.26	1.84	3.60/3.73	
Arg	8.88	4.39	2.02/2.31	1.85	3.83/3.65	
Pro		4.07	1.61/1.92	1.72	3.15/3.23	
Tyr	8.01					7.14/6.84
Ile	7.97	4.14	1.80	1.142/1.12/0.93	0.85	
Leu	8.15	4.27	1.63	1.62	0.90/0.95	

Table 4.9: Partial proton resonance assignments for neurotensin(8-13) in solution (pH 3.5, 10% D_2O),

Residue	NH(ppm)	C_α(ppm)	C_β(ppm)	CO(ppm)
Ile	130.8	61.5	39.5	174.9
Tyr	122.6	58.0	39.0	175.3
Leu	119.4	63.5	32.0	176.2
Arg	124.8	56.0	31.0	172.2

Table 4.10: Partial nitrogen-15 and carbon-13 assignments of NT(8-13) in solution; spectra acquired in DMSO.

4.3.7 Assignment of neurotensin(8-13)

The proton resonance assignments for NT(8-13) is given in Table 4.9 and were sequentially assigned on the basis of the datasets described above. The carbon and nitrogen chemical shifts were assigned on the basis of several 3D heteronuclear experiments which were acquired and processed in collaboration with Dr C. Chung (Glaxo Wellcome) Table 4.10. These spectra allowed a carbon-13 and nitrogen-15 assignment by correlating all carbon and nitrogen resonances to the amide proton of each amino acid residue. The absence of an amide proton on the secondary nitrogen of the proline limited any assignments. In addition, rapid exchange of the N-terminal protons limited assignment of the N terminal arginine.

4.4 Conclusion.

4.4.1 Production of neurotensin and neurotensin(8-13)

The synthesis and expression of neurotensin described in this chapter was required for subsequent solid state NMR studies to determine the assignment and the structure of neurotensin bound to the neurotensin receptor. Preliminary experiments based on the analogue neurotensin(8-13) both as a lyophilyized solid and bound to the receptor will be described in Chapters 5. The expression system developed for the production of uniformly labelled neurotensin, allows the production of sufficient quantities of neurotensin (∼mg's) from 1 to 2l of culture for solid state NMR studies.

With regard to the criteria laid out in the introduction of this chapter, the system has allowed the efficient expression and purification of a small peptide without significant proteolysis of the desired sequence (See Section 4.1.1). It has become apparent that the limiting factor associated with the expression system employed here is neither the expression nor the purification. The major consideration is the quantity of carrier protein (glutathione S-transferase) produced in contrast to the desired product (only 6% of the mass of all protein expressed is required in the final neurotensin). One alternative proposed in the literature, is the expression of tandem peptide as fusion proteins [249]. In this case, the yeast α mating factor has been expressed in *E.coli* from a vector containing a *tac* promoter and a large array of tandem repeated coding units separated by a single methionine codon and a C-termininal $(His)_8$ tag allowing purification. In such an expression system the protein synthesis is focused into the production of the sequence of interest [249].

Despite possible alternative strategies, the system described above has allowed the production of sufficient quantities of labelled peptide for our solid state NMR studies. In addition, the simplicity of the system has facilitated its application to the expression of β-amyloid protein and the M4 transmembrane domain from the nicotinic acetylcholine receptor (P.T.F. Williamson & T. Haddingham, unpublished

results).

4.4.2 Resonance assignment.

Proton resonance assignments for neurotensin in solution have been published previously and indicate that no preferred structure exists in solution [248]. However, to date no carbon-13 or nitrogen-15 assignments have been published for either the neurotensin or neurotensin(8-13). Such an assignment in the solution state would allow a detailed comparison to be made with carbon-13 and nitrogen-15 assignments of ligand bound to the neurotensin receptor obtained by solid state NMR. Such comparison may allow us to indicate any preferred conformation adopted by the ligand upon binding and give information regarding the electrostatic nature of the ligand binding site [243].

Chapter 5

Assignment of neurotensin(8-13) upon binding to the neurotensin receptor.

5.1 Introduction.

Studies relating to the structure and function of the neurotensin receptor have so far relied on a combination of both site directed mutagenesis and homology modelling studies (for review see Section 1.4.2). These studies have centred on producing a satisfactory model of the neurotensin binding site from which further pharmaceutical strategies may be developed. Here we have undertaken preliminary solid state NMR studies of the ligand neurotensin(8-13) as both a lyophilized solid and whilst bound to the neurotensin receptor. It is hoped ultimately that these studies will allow a detailed dynamic and structural model for the ligand neurotensin within its binding site on the neurotensin receptor. Such information will be the key in providing further information for the detailed modelling studies underway on this system [9], and the rational development of pharmaceuticals to interact with this receptor. Such pharmaceuticals may have a significant contribution in the treatment of schizophrenia [149] and Parkinsons disease [149].

Successful NMR studies relied on the purification of suitable quantities of neurotensin receptor. The low density of neurotensin receptor in most tissues [250] precluded the purification of sufficient quantities from natural tissue, and thus a suitable expression system was sought. A recently developed *E.coli* heterologous expression system for rat neurotensin receptor was kindly donated by Dr R. Grisshammer (LMB, Cambridge). This system had been shown to express about 800 copies of active neurotensin receptor per cell [251]. This expression level coupled

with the efficient purfications developed by Dr R. Grisshammer (LMB, Cambridge) [252] allowed the purification of sufficient material for subsequent NMR studies.

Using uniformly carbon-13 and nitrogen-15 labelled neurotensin(8-13) prepared as described in Chapter 4, we have carried out a series of solid state NMR experiments. These experiments centred on the application of broadband recoupling techniques to extensively labelled neurotensin(8-13) and served two goals. Firstly, through the implementation of both homo- and heteronuclear correlation spectroscopy attempts were made to assign the majority of resonances within the neurotensin(8-13) in the solid state. The chemical shifts obtained from these experiments would act as a suitable reference for data obtained from ligand bound to detergent solubilised receptor. Secondly, through the reintroduction of dipolar couplings, we aim to selectively observe labelled neurotensin(8-13) whilst suppressing the strong signals arising from natural abundance carbon-13 present in the buffer system. This should enable the resolution of resonances previously masked from neurotensin(8-13) bound to the neurotensin receptor.

NMR experiments were then performed upon the uniform carbon-13 and nitrogen-15 labelled neurotensin(8-13) bound to the detergent solubilised neurotensin receptor. Initial experiments demonstrated that it was possible to acquire data under MAS conditions at both 5°C under near 'solution like' conditions or at -120°C where solid state CP-MAS NMR methodology became more applicable. The specificity of the binding of neurotensin(8-13) to the neurotensin receptor was monitored on the basis of the observed perturbation in chemical shift which appears to mirror activity previously established by radioligand binding assays.

Studies were hindered by our inability to resolve resonance from labelled sites within the neurotensin(8-13) against the strong background of natural abundance signals arising from the components within the buffer system employed. Through the use of double quantum filtered NMR experiments utilizing both J-couplings and dipolar couplings we have been able to suppress these signals and resolve many of

the sites within the labelled ligand under 'solution like' and solid state conditions.

The work below outlines the NMR experiments necessary to resolve many of the resonances within the ligand neurotensin(8-13) whilst bound to the detergent solubilised receptor. Additionally a partial assignment of neurotensin(8-13) was performed on the lyophilised solid. These studies offer some of the information and methodology required to perform a full structural and dynamic analysis of the ligand neurotensin(8-13) whilst bound to the neurotensin receptor.

5.1.1 Expression of G-protein coupled receptors.

Overexpression of integral membrane proteins has proved notoriously difficult, with only a few expression systems able to produce sufficient quantities of materials for biophysical studies [15][253]. To date the successful over-expression of G-protein coupled receptors has been limited to the visual G-protein coupled receptor rhodopsin. Expression systems have been established for rhodopsin both in a baculovirus\Sf 9 cell expression system [254] and in stably in HEK293S cells [255]. These have permited sufficient quantities of materials for biophysical studies including solid state NMR and electron spin resonance studies [256][257][258].

Of the other G-protein coupled receptors, few others have been readily expressed [15] in either homo- or heterologous expression systems. The expression system we used to produce neurotensin receptor for solid state NMR studies, involves the heterologous expression of a cDNA clone of rat neurotensin receptor [259]. The neurotensin receptor is expressed in a N terminal truncated form as a fusion protein in *E.coli* [251]. Although this system does not lead to the levels of expression that have been obtained for other bacterial proteins in *E.coli* [253], the levels do permit the purification of 1 mg of pure protein from 10 l of culture.

Expression in *E.coli* has several advantages over other expression systems due to its simplicity of use, the high levels of expression which have been shown possible, and the large variety of well characterised strains and plasmids in which expression

is possible. In addition expression in *E.coli* offers significant advantages in the early stages of development of an expression system, with only a short delay from cloning steps to protein expression and purification trials. This enables a wide variety of constructs to be tested with a range of differing affinity tags, in order to ascertain which confers the best stability and purification strategy for the protein.

Several drawbacks are associated with the heterologous expression of membrane proteins in *E.coli*, most of these centre on the absence of the complex post translational processing machinery that is either absent or different from that found in higher eukaryotic organisms [15]. This is thought to have a particular impact on the expression of membrane proteins into the *E.coli* inner membrane, where the signal sequences required for the correct insertion of the recombinant protein into the membrane are frequently absent or inappropriate [15]. Following expression of the protein other environmental factors need to be taken into consideration, these include the stability of the protein against proteases that may be present during purification as well as the suitable choice of detergent with which to extract the protein from the membrane without disrupting the tertiary structure [15].

The expression system and subsequent purification strategy kindly provided by Dr R. Grisshammer (LMB, Cambridge) has evolved to overcome many of these problems. A schematic diagram of the vector used is shown in Figure 5.39. Briefly, the vector is derived from pBR322 and the protein is expressed as a fusion protein under the control of a wild type *lac* promoter, with other plasmid maintenance systems as described in Material and Methods.

The choice of this promoter and plasmid for protein expression leads to low rates of protein expression, due to the low copy number of the plasmid [246] and the relatively weak nature of the wild type *lac* promoter [15]. Although stronger promoters are available, these appear to offer little advantage for the expression of membrane proteins where it appears that the rate determining step is not that of transcription and translation but the insertion and folding into the membrane

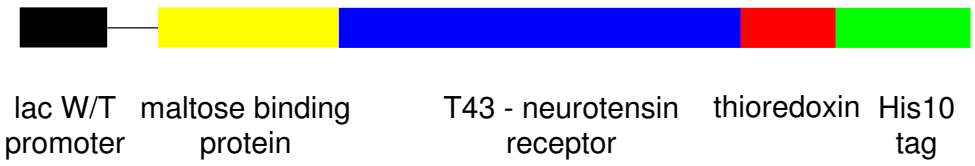

Figure 5.39: . Schematic diagram representing the plasmid used to express functional neurotensin receptor.

[15]. Alternative strategies based on the coexpression of the membrane targetting and insertion machinary have worked with limited success [15]. In the absence of such systems, the buildup of unprocessed translation products has been shown to be toxic to the cell leading to reduced growth rates and plasmid loss [15]. An additional concern for the expression of membrane proteins arises from the regulation of expression. Strong promoter systems such as T7 are frequently 'leaky' allowing a basal level of expression prior to induction. Frequently expression of membrane proteins has been shown to be toxic to cells and this level of basal expression can lead to a reduction in growth rates, plasmid loss and the concurrent drop in the levels of protein expression upon induction.

The neurotensin receptor is expressed as a fusion protein, with a maltose binding protein (MBP) linked to its N terminus and the thioredoxin-His_{10} attached to its C terminus. The presence of the MBP and its associated signal sequence at the N-terminus of the protein targets the protein to the periplasm and the subsequent insertion of the truncated neurotensin receptor into the membrane [251]. The truncation of the region between the N-terminus and T43 and the presence of the thioredoxin domain between the C-terminus and the His_{10} was shown to improve the stability of the fusion protein to proteases both during expression and purification[251]. The His_{10} tag attached to the C-terminus of the fusion protein was present to aid the purification of the protein following detergent solubilisation of the *E.coli* inner membranes. The His_{10} tag was shown to be preferable to other

methods of affinity purification including the shorter His_6 tag due to is higher specificity for the column. This allows more stringent washing of the column facilitating higher levels of enrichment. The Ni affinity column was shown to be more suitable for the large scale purification of material from 10's l of culture [252].

Ni affinity chromatography serves to remove the bulk of contaminating protein leaving only well characterised Ni affinity contaminants and both active and inactive neurotensin receptor [252]. A neurotensin affinity column subsequently allowed the purification of only those receptors which show ligand binding activity [251]. Cleavage of the MBP and thioredoxin from the fusion protein was not attempted due to the absence of suitable specific protease cleavage sites, however previous binding studies have demonstrated that the pharmacology of this recombinant fusion protein is similar to that of the wild type receptor[251]. On the basis of this observation we believe that studies of the ligand binding events using this fusion protein will not be unduly perturbed by the presence of these extra domains. No attempts were made to reconstitute the protein into lipid bilayers due to the limited amount of material available and the absence of an established reconstitution protocol for this system. Establishing such a protocol would demand significant quantitites of protein which would have limited possible NMR studies.

5.1.2 Solid State Dipolar Recoupling Experiments.

Many of the experiments employed in this chapter rely on the reintroduction of dipolar couplings between homonuclear spins, for the purpose of either broadband dipolar exchange MAS-NMR spectroscopy or double quantum filtered MAS spectroscopy. The theoretical basis of these experiments has been detailed in Chapter 2 and will not be repeated, although exact experimental conditions used for studies on neurotensin(8-13) are given in the following Material and Methods section (Section 5.2). The theoretical basis of the additional experiments employed in this chapter for heteronuclear correlation spectroscopy and double quantum filtered J coupled

spectroscopy (1D-INADEQUATE) are given in sections 5.1.3 and 5.1.4 respectively.

5.1.3 Heteronuclear Correlation Spectroscopy.

Heteronuclear solid state NMR techniques have been applied in a wide range of studies of biological systems with both single and multiple distance constraints obtained for ligands/substrates in their binding site (for review see Section 1.2.2). These techniques based on the rotational echo double resonance (REDOR) methodology, are useful when distances are to be measured between singly labelled sites and heteronuclear spins [64] where dephasing curves can be simulated. However, to aid the assignment of uniformly labelled molecules, it is useful to be able to correlate carbon-13 to nitrogen-15 labels. Such techniques should allow the correlation of adjacent labelled sites irrespective of the exact experimental conditions, relating the presence or absence of correlation to the presence or absence of adjacent labels. Several techniques have been proposed to correlate carbon-13 and nitrogen-15 chemical shifts under MAS conditions, including Hartmann-Hahn cross polarization (HHCP)[39] and transferred echo double resonance (TEDOR) [260]. These techniques suffer from several drawbacks including a maximal transfer efficiency of 73% and 53% respectively. In addition the optimal transfer depends critically on the experimental setup, as exemplified by the HHCP, where extreme caution must be taken to ensure that the match is maintained on one of the sidebands of the Hartmann-Hahn match.

In order to aid in the assignment of the uniformly labelled neurotensin(8-13), we have adopted a modified form of the HHCP, refered to as the adiabatic pass through the Hartmann-Hahn condition (APHH-CP)[261](Figure 5.40). In contrast to conventional HHCP, the theoretical limit for transfer of magnetisation by this technique is 100%. In addition, the sensitivity to experimental conditions is reduced. Such an adiabatic transfer can be described thermodynamically by an adiabatic demagnetisation of the I spins followed by a adiabatic repolarization of the S

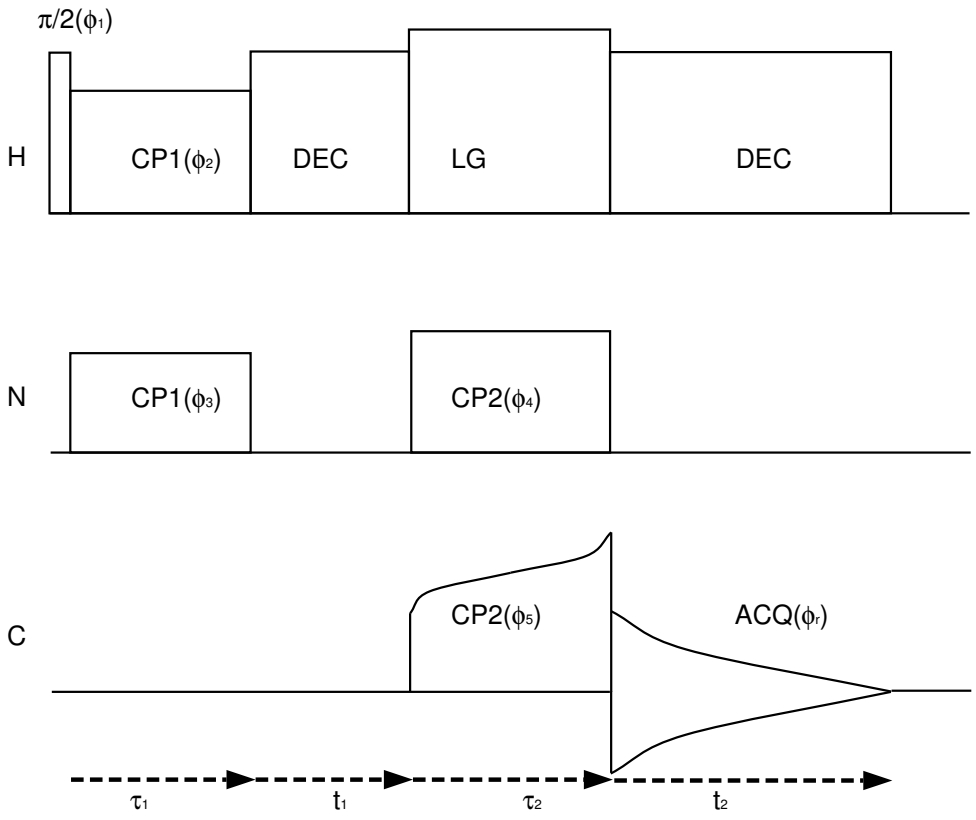

Figure 5.40: Pulse sequence used to obtain ^{13}C-^{15}N correlation spectra, of neurotensin(8-13) in the solid state. Pases cycles according to ϕ_1=0; ϕ_2=90; ϕ_3=0, 180; ϕ_4=0; ϕ_5=0, 180, 180, 0, 90, 270, 270, 90; ϕ_r=0,180,180,0,90,270,270,90.

spins. During the initial adiabatic demagnetisation, the r.f. amplitude is brought to the Hartmann-Hahn condition. This reduces the heat capacity associated with the Zeeman interaction ($C_I B_{1I}^2$) to zero whilst keeping the heat capacity of the dipolar reservoir constant ($(C_I + C_S)B_L^2$). Thus, the entire spin entropy is transferred to dipolar order. During the final adiabatic remagnetisation the r.f. field is increased above the local field (B_L) creating magnetisation on the S-spin by concentrating all the entropy in the S-spin Zeeman interaction ($C_S B_{1S}^2$). Such an adiabatic transfer should allow the theoretical improvements offered by cross polarization to be attained. In contrast, the efficiency of conventional HHCP is limited to 73% due to the 'hole' in the powder dipolar spectrum arising from the scaling of the dipolar

coupling by $1/2(3\cos^2\theta - 1)$ as the dipolar vector becomes colinear with the magic angle. In addition to theoretical improvements in efficiency, the APHH-CP is experimentally more robust as the requirement for the exact matching of the field with the Hartmann-Hahn sideband is reduced due to the presence of the adiabatic sweep in r.f. field.

In the context of the triple resonance experiment performed to facilitate the carbon-13 and nitrogen-15 assignments, where polarization transfer is between two low gamma nuclei other considerations become important: the low gamma nuclei have a chemical shift range, which is significant with respect to the dipolar coupling frequencies, and during the APHH-CP both low gamma nuclei experience the local field of the protons. The effect of the large chemical shift range with respect to the dipolar decoupling frequency is largely removed as the APHH-CP is not directly influenced by large chemical shift offsets. To cope with a wider distribution of chemical shifts the amplitude modulation of the adiabatic sweep must be extended, resulting in prolonged contact times in order to maintain the adiabatic nature of the sweep [261]. The removal of the dipolar couplings between the high abundance protons and the two low gamma nuclei have been largely suppressed through the use of high power Lee-Goldburg decoupling [261]. This removes the homonuclear dipolar interactions between the abundant protons leaving only a scaled heteronuclear interaction which is readily averaged by the MAS and r.f. irradiation of the two low gamma nuclei.

The only potential drawback associated with the use of an adiabatic sweep for cross polarization between low gamma nuclei arises from the requirement to sweep the r.f. amplitude slowly to maintain the adiabatic nature of the transfer. Thus, the major efficiency losses are likely to be incurred due to the relaxation of the magnetisation in the rotating frame($T_{1\rho}$).

5.1.4 Double Quantum filtered J-coupled spectra.

In the solid state, double quantum excitation sequences such as C7 (for description see Chapter 2) offer the potential to provide both structural information and filter signals from labelled biomolecules against a background of unlabelled material. For these methodologies to be successful, the double quantum excitation sequence has to reintroduce the dipolar couplings, previously averaged by MAS, across the entire frequency range. This allows the selective observation of the coupled nuclei through the application of the appropriate phase cycle. In contrast, J-couplings arising from indirect electron mediated interactions remain largely unaltered by magic angle spinning. These couplings also offer the potential to filter signal from labelled biomolecules against a background of natural abundance signal. Although these interactions are always present in the solid state, they are usually masked in the spectra by large linewidths due to the presence of inhomogeneous broadening, chemical shift anisotropy and the much larger dipolar couplings.

Many of the dipolar recoupling techniques developed for solid state NMR fail when the mobility within the sample is high, necessitating the use of low (-120°C) temperatures for the study of biological membranes, as demonstrated in Chapter 2. This requirement was also necessary for the experiments that follow on the neurotensin receptor. In contrast, J-couplings remain largely unaffected by the presence of molecular motion and thus offer great potential to aid in the assignment of resonances in the semi fluid state present in biological membranes at near physiological conditions. Although some experiments have been proposed to utilize J-couplings in the solid state [262], this area has received little attention as many of the solution NMR techniques require clear resolution of the J-coupling in order to function with high efficiency[263].

When clear resolution of the J-couplings is observed many of these experiments can be exploited. In the work presented below, we have used a 1D INADEQUATE experiment to selectively observe resonances arising from the labelled ligand bound

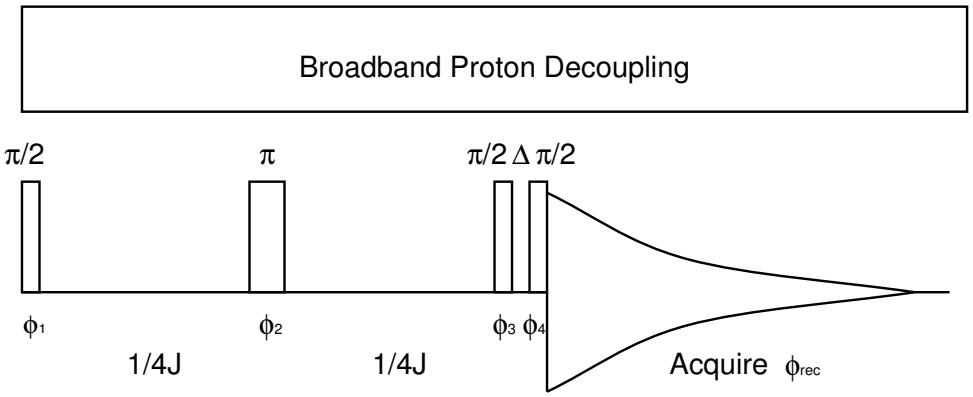

Figure 5.41: INADEQUATE pulse sequence used to selectively acquire DQF spectra of uniformly carbon-13 labelled ligands against a background of natural abundance carbon-13. Phases are cycled according to ϕ_1=0, 0, 0, 0, 90, 90, 90, 90, 180, 180, 180, 180, 270, 270, 270, 270; ϕ_2=90, 90, 90, 90, 180, 180, 180, 180, 270, 270, 270, 270, 0, 0, 0, 0; ϕ_3=ϕ_1; ϕ_4=0, 90, 180, 270, 90, 180, 270, 0, 180, 270, 0, 90, 270, 0, 90, 180; ϕ_R=0, 270, 180, 90, 90, 0, 270, 180, 180, 90, 0, 270, 270, 180, 90, 0.

to the neurotensin receptor solubilised in detergent under slow MAS conditions. The sequence for this experiment is shown in Figure 5.41 [263]. In the two 1/4J delays, carbon-13 magnetisation evolves under the homonuclear J coupling whilst the chemical shifts evolution is suppressed by the presence of a spin-echo. At the end of this 1/2J period anti-phase carbon-13 magnetisation is transformed into homonuclear double quantum coherence by the second $\pi/2$ pulse. After a short delay (Δ), the last pulse produces detectable single quantum coherence. The phase cycling given in Figure 5.41 selects only magnetisation which has passed through the p=$\pm$2 coherence pathway. This has been shown to offer a background suppression in the order of 1:1000 [263].

5.2 Materials and Methods.

Strains

Expression of neurotensin receptor was performed in E.coli DH5α (*supE*44 *hsdR*17 *recA*1 *endA*1 *gyrA*96 *thi*-1 *rel A*1). Cells were transformed using a standard heat

shock protocol [246] with the expression plasmid kept as a glycerol stock.

Neurotensin receptor expression vector

The construct used for the expression of the neurotensin fusion protein was kindly provided by Dr R. Grisshammer (LMB, Cambridge). The plasmid is a pBR322 derivative encoding a truncated form of the neurotensin receptor starting at Thr-43. At its N terminus a maltose binding protein is fused together with its signal peptide, and fused to its C-terminus to thioredoxin (TrxA) followed by a deca histidine tag. Expression is under the control of a wild type lac promoter. Plasmid loss [252] was prevented through selection by ampicillin and the *hok/sok* plasmid maintenance system [264][265][266].

5.2.1 Expression & purification of neurotensin receptor.

Growth conditions.

Transformed *E.coli* DH5α were grown in 10ml of 2*TY broth (16g bactotryptone(Difco, UK), 10g yeast extract(Difco, UK), 5g NaCl, pH 7.4 (NaOH)) supplemented wih 0.1ml of 20% glucose and 0.1mg ml^{-1} ampicillin overnight (37°C, 200rpm). 2ml of overnight culture were used to innoculate 1l of 2*TY broth supplemented as before. The cultures were grown until an OD_{600} reached 0.4-0.6 and subsequently recombinant protein expression was induced by the addition of 0.5ml of 1M IPTG. The temperature was then dropped to 22°C and the culture grown for a further 44h. The cells were then harvested by flow through centrifugation at 4800 rpm in a Sorvall TZ-28/GK rotor. The cells were then flash frozen in liquid nitrogen for storage prior to purification.

Purification of neurotensin receptor

The neurotensin receptor was solubilised as follows, 200g of *E.coli* cell paste was resuspended in 1.2 l of neurotensin buffer (50 mM Tris, 0.2 M NaCl, 30% glycerol, 0.5% CHAPS, 0.1% CHS, 0.1% LM). To prevent proteolytic degradation pepstatin A, leupeptin A, and PMSF were added, in addition 120mg of lysosyme and 3mg of DNase were added to aid cell lysis and material handelling. The cells were subsequently broken open, by 3 passes through a flow-through sonicator. This mixture was stirred at 4°C for 30 minutes. The mixture was then clarified by ultracentrifugation in a Sorvall SA-300 for 2h at 16000 rpm. The supernatant was subsequently loaded onto a 150 ml Nickel affinity column (Quiagen, UK) in 1mM imadazole at a flow rate of 10 ml min^{-1}. The flow through was monitored at OD_{280} until the baseline returned to zero. The column was washed with neurotensin buffer containing 50 mM imidazole at a flow rate of 20 ml min^{-1} until the baseline returned to zero. The neurotensin receptor was then eluted in neurotensin buffer containing 350 mM imidazole at 10 ml min^{-1}. The protein eluant containing the neurotensin receptor was concentrated using an Amicon with YM-30 filter until the sample had been reduced to 30 ml.

The fraction containing neurotensin receptor was desalted using a Sephadex G25 column. The 150 ml column was equilibrated with 3 column volumes of desalting buffer (50 mM Tris, 20 mM NaCl, 1mM EDTA, 30% glycerol, 0.5% CHAPS, 0.1% CHS, 0.1% LM). The sample was loaded onto the column from a superloop at 3 ml min^{-1}. The protein was then eluted with desalting buffer at 5 ml min^{-1}.

The desalted fraction was subsequently purified using a neurotensin affinity column to remove non-functional receptors. The affinity column was pre-equilibrated with desalting buffer, and the fraction containing neurotensin receptor loaded at a flow rate of 0.5 ml min^{-1}. The column was then washed with desalting buffer until the baseline returned. The affinity column was further washed with a KCl buffer (50 mM Tris, 200 mM KCl, 1mM EDTA, 30% glycerol, 0.5% CHAPS, 0.1% CHS,

0.1% LM) until the baseline returned. Finally, the neurotensin was eluted from the affinity column with a neurotensin high salt buffer (50 mM Tris, 1 M NaCl, 1mM EDTA, 30% glycerol, 0.5% CHAPS, 0.1% CHS, 0.1% LM). The sample was subsequently concentrated to 1.5ml using an Amicon with YM-30 membrane. The NT affinity column was prepared as follows: 2ml of tetrameric avidin suspension was succinylated in 50mM borate buffer, pH 9.0. The buffer was extensively washed with 50mM Tris, 1mM EDTA, pH7.4 and incubated with 240 nmol (2 fold excess) of biotinylated NT (biotin-βAla-βAla-Gln-Leu-Tyr-Glu-Asn-Lys-Pro-Arg-Arg-Pro-Tyr-Ile-Leu-OH) in the above buffer for 1h at room temperature. After washing the resin in water, unoccupied biotin binding sites were blocked with 5mM biotin in the above buffer. The NT resin was extensively washed with 50mM Tris, 500mM NaCl, 1mM EDTA, pH 7.4. The resin was washed with water and stored in 50mM Tris, 1mM EDTA, pH 7.4, 0.02% sodium azide buffer at 4°C.

The receptor was finally prepared for NMR studies by desalting the sample into a low salt buffer using a 150ml Sephadex G-25 column, preequilibrated with low salt NT buffer. This low salt sample was concentrated using a Amicon with YM30 membrane to a volume of 4-5ml. Finally the neurotensin receptor was concentrated to a volume of 250 μl using a Centricon(Eppendorf, UK), prior to being used to fill a 6mm Chemagnetics rotor.

5.2.2 Proton decoupled carbon-13 experiments of soluble ligand and protein.

Carbon-13 proton decoupled spectra of neurotensin(8-13) both in solution and bound to the solubilised neurotensin were acquired on a Chemagnetics CMX-500, at 125.1 MHz for carbon-13 (500 MHz for proton) equipped with a 6mm triple resonance probe head. Samples were spun at 500 Hz about the magic angle to eliminate residual anisotropy and average inhomogeneities present within the B_0 field. Data were

acquired with a simple pulse acquire experiment with proton decoupling during acquisition. Carbon pulse lengths were typically 3.5 μs with proton decoupling fields of 70 kHz. A 50 kHz spectral width was used with 6144 points acquired within a total acquisition time of 122 ms. The data was zero filled to 32k points to give a final resolution of 1.52Hz/point in the final spectrum.

5.2.3 CP-MAS Experiments.

Carbon-13 CP-MAS spectra of neurotensin(8-13) were acquired on a Chemagnetics CMX-500, at 125.1MHz for carbon-13, 50 Mhz for nitrogen-15 and 500.5 MHz for protons. A spinning speed of 4000$\pm$2 Hz was used for all samples and the temperature was maintained at 25°C. A proton field strength of 70 kHz was applied for cross polarization and decoupling.

5.2.4 Nitrogen-15, Carbon-13 Correlation Spectra.

Nitrogen-15, carbon-13 correlation spectra were acquired on a Chemagnetics CMX-500, at 125.5 MHz carbon-13, 50.5 MHz nitrogen-15 and 500.5 MHz for protons using a Chemagnetics triple resonance 6mm probe. A spinning speed of 6000 Hz was used to obtain spectra of lyophilised neurotensin(8-13). The pulse sequence in Figure 5.40 was used to provide nitrogen, carbon correlation spectra. Transverse magnetisation is initially generated by a proton $\pi/2$ pulse. During the subsequent mixing period (τ_{m1}) nitrogen magnetisation is generated by cross polarization, and subsequently evolved during t_1 under is chemical shift. During this period, heteronuclear interactions are eliminated by either rapid magic angle spinning or high power proton decoupling. Subsequently magnetisation is transferred from nitrogen to carbon by an adiabatic sweep through the Hartmann Hahn condition(τ_{m2}) covering the $\pm$2 sidebands. The transverse magnetisation is then observed during t_2. Phase sensitive nitrogen-15/carbon-13 correlation spectra were acquired through the use of TPPI phase cycling of the initial proton/nitrogen cross polarization sequence.

Efficient transfer of magnetisation between nuclei was achieved by matching of the B_1 field of each nuclei to 45.5kHz during either τ_{m1} or τ_{m2}. Proton decoupling during t_1 and t_2 was performed at 71.5kHz, whilst Lee-Goldburg decoupling was applied during mixing with a B_1 field of 75 kHz and a frequency offset of 53 kHz.

5.2.5 Cross polarization - C7 double quantum filtered NMR.

Cross polarization - C7 double quantum filtered NMR spectra were acquired on a Chemagnetics CMX-500 at 125.7 MHz carbon-13 (500MHz proton frequency) equipped with a 6mm triple resonance probehead. Spinning speeds were maintained at 5000 Hz using a Chemagnetics spinning speed controller to within ±2Hz. The temperature was set to -120±1°C using a Chemagnetics temperature control unit. A proton field strength of 50 kHz was used for cross polarisation. Double quantum filtered CP-MAS spectra were acquired with the POST-C7 sequence described in Chapter 2. The B_1 field was matched to 7 times the spinning speed, 35 kHz, and 10 C7 cycles were performed for both excitation and reconversion, a total excitation time of 0.598ms. Double quantum coherence was selected as decribed in Chapter 2. Data were zero filled to 4096 points and processed with 100 Hz linebroadening prior to Fourier Transform.

5.2.6 Rotating Inverse Laboratory Frame Zero Quantum Transfer (RIL-ZQT) experiments.

Rotating Inverse Laboratory Frame Zero Quantum Transfer (RIL-ZQT) experiments were acquired on a Chemagnetics CMX-500 at 125.7 MHz carbon (500Mhz proton) equipped with a 6mm triple resonance probe head. Spinning speed was maintained at 5000±5 Hz using a Chemagnetics spinning speed controller to within ±5Hz. The temperature was set to that defined for the particular experiment and maintained within ±1° using a Chemagnetics temperature controller. Total through space correlation spectra (TOSSY) were acquired with the RIL-ZQT mixing scheme and time

reversal for pure phase lineshapes as described in Section 2.1.2 and shown in Figure 2.11[190]. A proton field strength of 50 kHz was employed for cross polarization, during both t_1 and t_2 evolution broadband decoupling was performed at 75 kHz. Although TPPM decoupling has been applied in similar situations previously, no improvements over broadband decoupling were observed. During the RIL-ZQT sequence Lee Goldberg decoupling was applied with a proton B_1 field of 75 kHz applied offset from the carrier frequency by 53 kHz. During the RIL-ZQT mixing sequence, magnetisation was locked during the first quarter of the rotor period using a carbon field of 50 kHz, and scaled during the second quarter of the rotor period by (δ) 0.90 as described in earlier work [190]. During the second half of the rotor cycle $\pi/2$ and π pulses were performed at 3.5 and 7.0 μs respectively. Unless stated data was acquired with 2048 points in t_2 and 128 points in t_1 with 128 acquisitions per t_1 increment. Data in t_2 was processed with a complex Fourier Transform. Data were linear predicted in t_1 from 128 points to 512 and processed with a sinebell function. The data were subsequently zero filled to 2048 points and processed with a real Fourier Transform.

5.2.7 INADEQUATE NMR.

INADEQUATE spectra were acquired on a Chemagnetic CMX-500 at 125.7 MHz for carbon-13 (500MHz for protons) equipped with a 6mm triple resonance MAS probehead. The samples were spun at 500 Hz to remove residual anisotropy and average the residual inhomogeneities present in the B_0 field. Data were acquired with the pulse sequence described in Figure 5.41 with a interpulse delay optimised at 5ms consistent with a carbon-carbon J coupling of 50 Hz. Carbon-13 $\pi/2$ pulses were typically 3.5 μs with a proton decoupling field of 50 kHz. Data were acquired with a 50 kHz spectral width with 6144 points giving a total acquisition time of 122 ms. Data was processed with 32 k points giving a digital resolution of 1.52 Hz/point.

5.3 Results

5.3.1 Purification of neurotensin receptor.

The expression of neurotensin receptor was performed as described in Materials and Methods. The details of 7 purifications are shown in Table 5.11 which resulted in a total of 38.8 nmoles of binding site as determined by a radioligand binding assay. These results appear to mirror those published with this system [252][251]. Both the expression and purification of neurotensin receptor in this system proved highly variable, however attempts were made to improve both the yield and reproducibility of the expression and purification of the neurotensin receptor, in both shaker flasks and fermentors.

Scaling of the growth conditions to both larger shaker flasks and fermentors frequently led to a lower quality of material to that obtained in 500ml shaker flask (typically 1-2 pmoles mg^{-1} as opposed to 4-6 pmoles mg^{-1}). The subsequent purification of this material typically gave lower yields. Attempts to improve the reliability of the purification also proved problematic with any modifications having little or no effect.

Source	crude lysate (pmoles mg^{-1})	Ni affinity (pmoles mg^{-1})	NT affinity (pmoles mg^{-1})	Total (nmoles)
200g, shaker flask	3.04	306.29	N/A	7.4
200g, shaker flask	3.01	305.1	N/A	6.9
200g, 50l ferment	3.60	950.0	2200	3.4
118g, shaker flask	4.51	910.2	2878	6.22
108g, shaker flask	2.93	610.5	2167	5.14
165g, shaker flask	2.07	240.0	3461	5.66
200g, shaker flask	3.60	753.1	2845	4.24
170g, shaker flask	2.14	801.2	Used after Ni affinity	
325g, shaker flask	1.56	311.2	Used after Ni affinity	

Table 5.11: Yields obtained from the purifications used to produce solubilized neurotensin receptor for study by solid state NMR. Final yield measured in nmoles of binding site. (N/A - data not available)

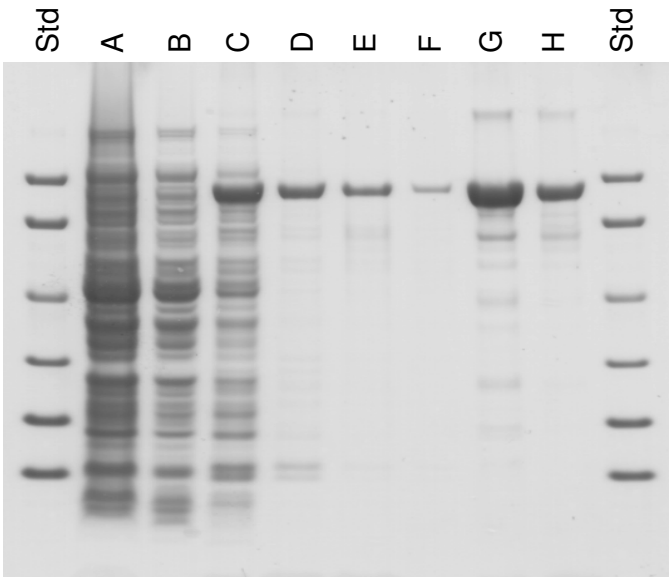

Figure 5.42: 4-12% Comassie stained MES SDS polyacrylamide gradient gel of samples obtained from the purification of the neurotensin receptor, lanes, Standards (Std), Clarified sample (A), Quiagen-NTA-Flow through (B), 500mM imidazole elution (C), Desalted sample (D), neurotensin column flow through(E), 200mM KCl neurotensin column wash (F), 1M NaCl elution from neurotensin column(G), concentrated sample of neurotensin receptor(H).

After initial solubilization, the sample was clarified by ultracentrifugation, the resulting supernatant was then initially purified by a Ni affinity column step. This removed the bulk of the contaminating protein resulting in a $\sim$ 200 fold enrichment (Table 5.11). The remaining contaminating proteins after this step are non-functional NTR and contaminating E.coli proteins that have been previously shown to bind to Ni affinity columns [252]. Subsequently the neurotensin column selects for a population of receptors which is functionally active. This results in another $\sim$4.5 fold enrichment, and a average specific activity of 2710 pmoles mg^{-1} as opposed to the theoretical value of 10000 pmoles mg^{-1}. In part this has been shown to be due to the presence of sodium chloride in the binding assays which prevents the theoretical yield being obtained. Comassie blue staining of the polyacrylamide gel confirmed the relative purity of the preparation (Figure 5.42 lane H).

5.3.2 CP-MAS Experiments.

A carbon-13 CP-MAS spectrum of NT(8-13) is shown in Figure 5.43A. Individual sites are not resolved in the spectra of the lyophilized solid, probably due to the inhomogeneous linebroadening present in such systems where the peptide is structurally heterogeneous [188]. These broad resonances can be assigned to the individual functional groups which constitute the NT(8-13). A broad resonance between 170 and 180ppm is assignable to the carbonyl group, with sidebands spaced 4.0 kHz either side due to the high degree of chemical shielding anisotropy. The resonance between 150 and 165ppm was assigned to the side chain of the arginine residue, again sidebands are spaced at intervals of 4.0kHz. Between 50 and 70 ppm a broad resonance is apparent assignable to the α carbon based on values taken from solution assignments [1]. Resonances between 30 and 50 ppm and 10 and 30 ppm have also been assigned primarily to the β and γ carbons respectively on the basis of the solution assignments[1].

The nitrogen-15 spectrum of NT(8-13) is shown in Figure 5.43B and is dominated by the amide resonances centred around 120 ppm, with the sidebands arising due to the highly anisotropic nature of the chemical shielding anistropy. The other two main signals appear at 20 and 70 ppm and were assigned to the arginine guanidium group on the basis of assignments of similar peptides in solution.

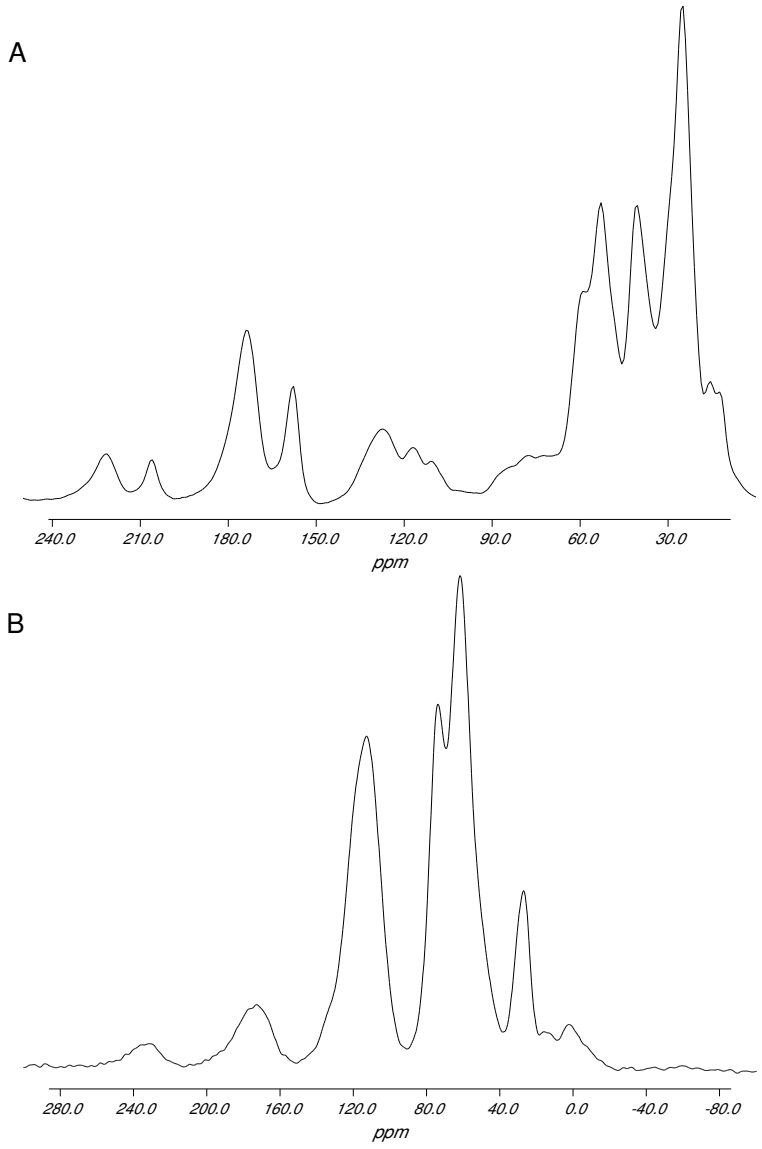

Figure 5.43: Cross polarization magic angle spinning NMR spectra of neurotensin(8-13) uniformly labelled with carbon-13 and nitrogen-15. Carbon-13 CP-MAS spectrum(A) was acquired with 128 acquisitions, 1 ms contact time and 4.0 kHz spinning speed. Nitrogen-15 CP-MAS spectrum(B) was acquired with 256 acquisitions, 1ms contact time and 4.0 kHz spinning speed. Both data sets were processed with 50 Hz linebroadening.

Residue	CO(ppm)	C_α(ppm)	C_β(ppm)	Others
Arg	172.82-169.15	60.00-45.00	30.00-40.00	156.46 (C_ζ)
Arg	172.82-169.15	60.00-45.00	30.00-40.00	156.46 (C_ζ)
Pro	172.82-169.15	60.00-45.00	30.00-40.00	47.46 (C_δ)
Tyr	172.82-169.15	60.00-45.00	30.00-40.00	115.06 (C3,5)
				127.24 (C1)
				130.11 (C2,6)
				154.26 (C4)
Ile	172.82-169.15	60.00-45.00	35.89	14.35 (C_γ)
				9.73 (C_δ)
Leu	178.153	60.00-45.00	40.23	22.06 (C_δ)
				20.83 (C_δ)

Table 5.12: Partial carbon-13 assignment of neurotensin(8-13) in desalting buffer at 5°C taken from the spectra presented in Figure 5.44.

5.3.3 Solution spectra of neurotensin(8-13) in desalting buffer.

The spectra of neurotensin(8-13) in desalting buffer are shown in Figure 5.44A. Expansions of the downfield region containing sidechain and carbonyl resonances are shown in Figure 5.44C. The upfield region containing resonances from the backbone and other aliphatic side chains is expanded in Figure 5.44B.

The chemical shifts, which are clearly resolved are given in Table 5.12, with potential assignments based on resolved splittings, chemical shifts obtained from solution studies (See Chapter 4) and values in the literature.

The data shows sufficient resolution such that the fine structure arising from carbon-carbon and carbon-nitrogen J couplings is clearly visible. Together with the observed chemical shift this data has allowed the assignment of many of the resonances arising from the sidechains present in the neurotensin(8-13) (Table 5.12). Although resolution in the carbonyl and C_α region is apparent, the absence of any sequential assignment strategy limits the assignment of these resonances.

The data is consistent with that obtained from neurotensin(8-13) in water where again a high degree of fine structure is also apparent in the spectrum(P.T.F. Williamson, unpublished results). This indicates that the high glycerol concentration and the

presence of detergents does not affect the mobility of the ligand in solution. This provides support for the hypothesis that the ligand does not interact strongly with detergent micelles present in the sample. Thus subsequent perturbations of spectral features may be attributed solely to the interaction of the neurotensin(8-13) with the detergent solubilised receptor.

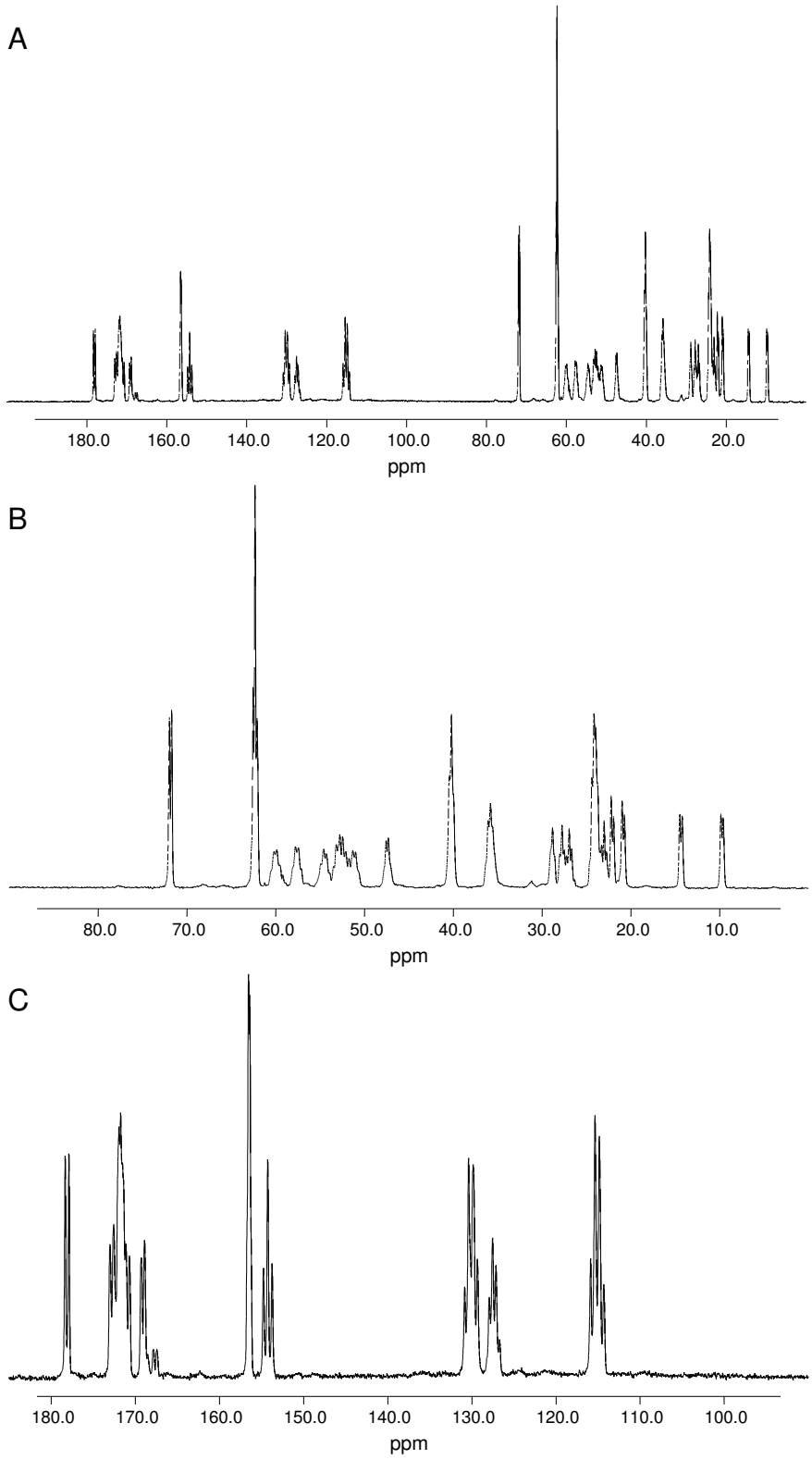

Figure 5.44: ^{1}H decoupled ^{13}C spectrum of uniformly C-13/N-15 labelled neurotensin in desalting buffer. Data was averaged over 1024 acquisitions at 5°C, zero filled to 32768 points and processed with 3Hz linebroadening prior to Fourier Transform.

5.3.4 Nitrogen-15, Carbon-13 Correlation Spectra.

Nitrogen-15, Carbon-13 correlation spectra were acquired with 3, 5 and 8 ms adiabatic mixing pulses, representative spectrum is shown in Figure 5.45. Although the overall signal intensity increases with respect to the mixing time, no new correlations were observed at longer mixing times. In the spectrum presented here the data are dominated by the strong correlations between the amide nitrogen (~120ppm) and the adjacent carbonyl (~170-175ppm) and C_α (~50-60ppm) carbons of the peptide backbone. The resolution being limited by inhomogeneous linebroadening in the lyophilised sample of neurotensin(8-13), but unfortunately it is not possible to resolve the individual labelled sites in the peptide backbone.

The carbon intensity that appears at 150-170ppm, has previously been attributed to the arginine sidechains, however we are now able to assign it to the two magnetically inequivalent nitrogens in the arginine sidechain N_η(25ppm) and N_δ(35ppm) which are both correlated to the C_ζ carbon. The N_δ can then be traced to the C_γ carbon. Such sequential assignment along regions of structures rich in both nitrogen and carbon, would under higher resolution conditions, similar to those found in membrane systems. This should form part of a strategy to allow the sequential assignment both of sidechains and peptide backbone.

At the longest mixing time used (8ms), long range interactions would be expected to become apparent, however none were detected. We attribute this both to the limited spin diffusion that can occur between low gamma nuclei under magic angle spinning and also the effective proton homonuclear decoupling during the mixing time. Even taking these effects into consideration one would still expect the appearance of long range couplings at extended mixing times (~8ms). We attribute the absence of such long range weak couplings to their attenuation in the presence of stronger short range couplings [267].

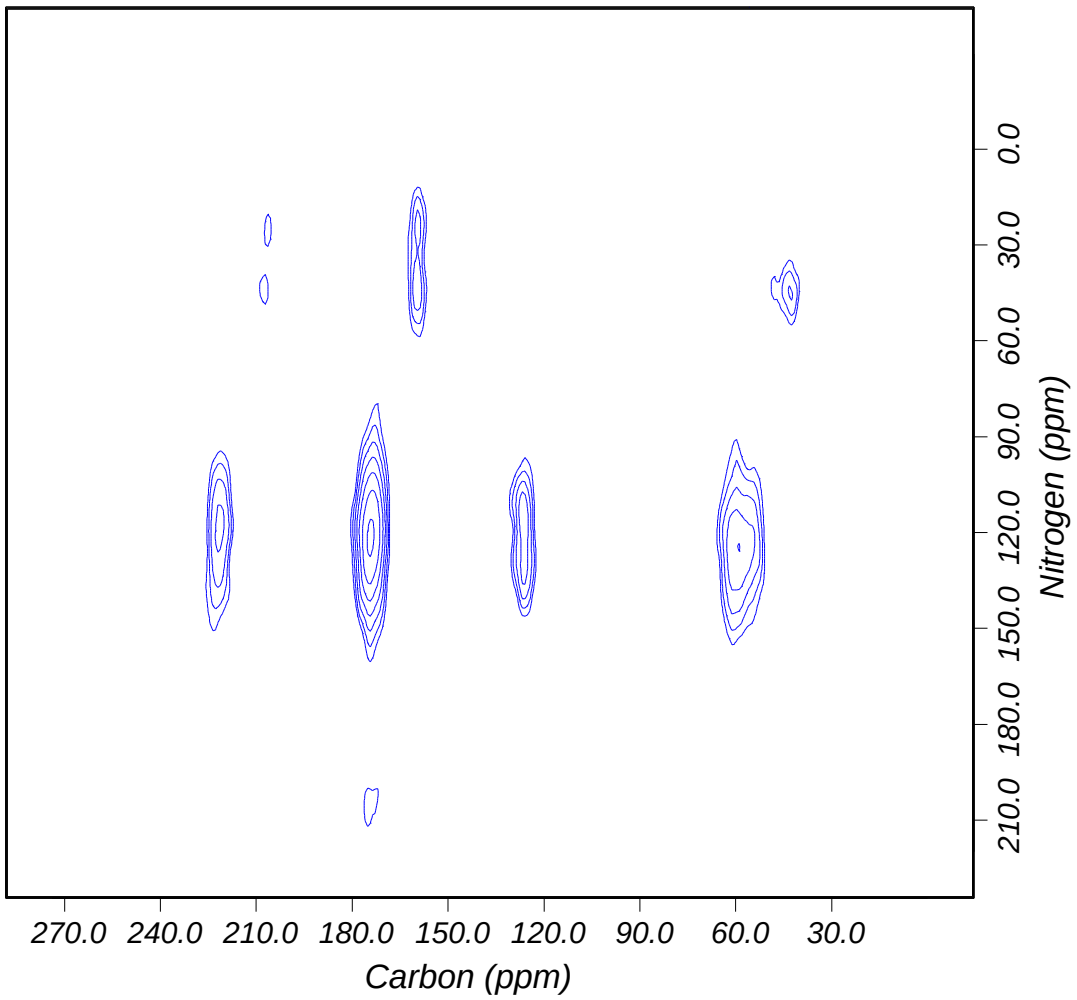

Figure 5.45: Nitrogen-15, Carbon-13 heteronuclear correlation experiment on 10mg of neurotensin(8-13). Data acquired as described in text with 32 t_1 increments, nitrogen-15 sweep width of 20kHz, and carbon-13 sweep width of 50kHz. Data processed with 300 Hz line broadening in t_2 prior to fourier transform. Data in t_1 linear predicted from 32 to 128 points, and 500 Hz linebroadening was applied prior to Fourier transformation.

5.3.5 Broadband dipolar recoupling studies of U-13C/15N neurotensin(8-13) as a lyophilised solid.

TOSSY spectra of uniformly carbon-13 labelled neurotensin(8-13) are shown in Figure 5.46. The data set was acquired at a short mixing time to obtain detailed information regarding the strong couplings between adjacent carbon atoms in the molecule. Longer mixing time experiments were not performed due to the unfavourable relaxation occurring under the RIL-ZQT mixing that arises under the experimental conditions that we were able to create as described in Chapter 2. Figure 5.46 shows data dominated by a strong diagonal ridge, which has a profile similar to that observed in the conventional 1 dimensional carbon-13 CP-MAS spectra of uniformly carbon-13 labelled neurotensin(8-13) with the peaks being largely unresolvable and broad in nature. Auto-correlated sidebands have been largely suppressed by using time reversed acquisition, although some are still present within the carbonyl region possibly due to either molecular rearrangement within the carbonyl region of the peptide, or to incomplete cancellation of the sidebands due to experimental imperfections during the extended acquisition. Off this diagonal, two regions contain a significant spectral intensity mirrored on both sides of the diagonal. The first of these is located in the spectral region ($\sim$58,$\sim$173ppm), which has been attributed to the correlations between the C_α and the carbonyl region. An expansion of this region is shown in the bottom right hand corner of Figure 5.46. Although the signal to noise ratio in these spectra is not so favourable, within this region there are four, possibly five, regions of intensity which are partially resolvable. This suggests the possibility to resolve many of the unique sites along the peptide backbone. The second region containing significant off diagonal spectral intensity is located between 10 and 70ppm. On the basis of the chemical shift in this region we have assigned the resonances to sidechains of many of the amino acids containing aliphatic resonances.

On the basis of the connectivities determined from this dataset it was possible

Residue	CO(ppm)	C_α(ppm)	C_β(ppm)	Others
Arg		55.20	28.89	(26.19) (C_γ)
				(40.56) (C_δ)
				(160.5) (C_ζ)
Pro		(52.38)	(31.96)	(49.62) (C_δ)
Tyr				
Ile	175.43	59.109	38.67	16.27 (C_γ)
				24.85 (C_γ)
				12.81 (C_δ)
Leu	175.05	52.31	41.04	24.89 (C_δ)

Table 5.13: Assignments obtained from the TOSSY spectra given in Figure 5.46. Assignments were made from the complete identification of the coupling pattern given. Values in brackets were assigned on the basis of coupled pairs identified with chemical shifts consistent with those obtained from literature [1].

to propose the partial assignment given in Table 5.13. Data that can be unambiguously assigned on the basis of the connectivities along the sidechains are shown, whilst coupled spin pairs, which possess distinct chemical shifts that suggest a given assignment are given in brackets. Many of the labelled sites in the molecule can be unambiguously assigned in this manner and can act as a suitable reference for further studies in the solid state for ligand bound to receptor. Perhaps the most encouraging observation from this data surrounds the achievable resolution, with clear assignments possible from what in a 1D carbon-13 spectra appears broad and uninterpretable. It is unclear whether the improvement in resolving power is due to the better separation afforded through the dispersion of information across two dimensions or the selection of a particlular population within the sample of the inhomogeneously broadened spectra. This offers the potential to resolve peptides upto 5 residues in size in the solid state. Most of the data that is absent from the assignment of the peptide arises from groups that would be expected to correlate at positions close to the diagonal. The presence of the strong diagonal has hindered our interpretation of this data, although certain areas indicate the presence of such correlation (*e.g.* a broadening of the diagonal at ($\sim$22ppm,$\sim$22ppm)). Methods to

overcome these limitations have been proposed such as suppression of the diagonal by the application of a double quantum filter prior to the recoupling scheme [268]. Although these methodologies offer significant advances, they were not applied due to the poor efficiencies associated with them.

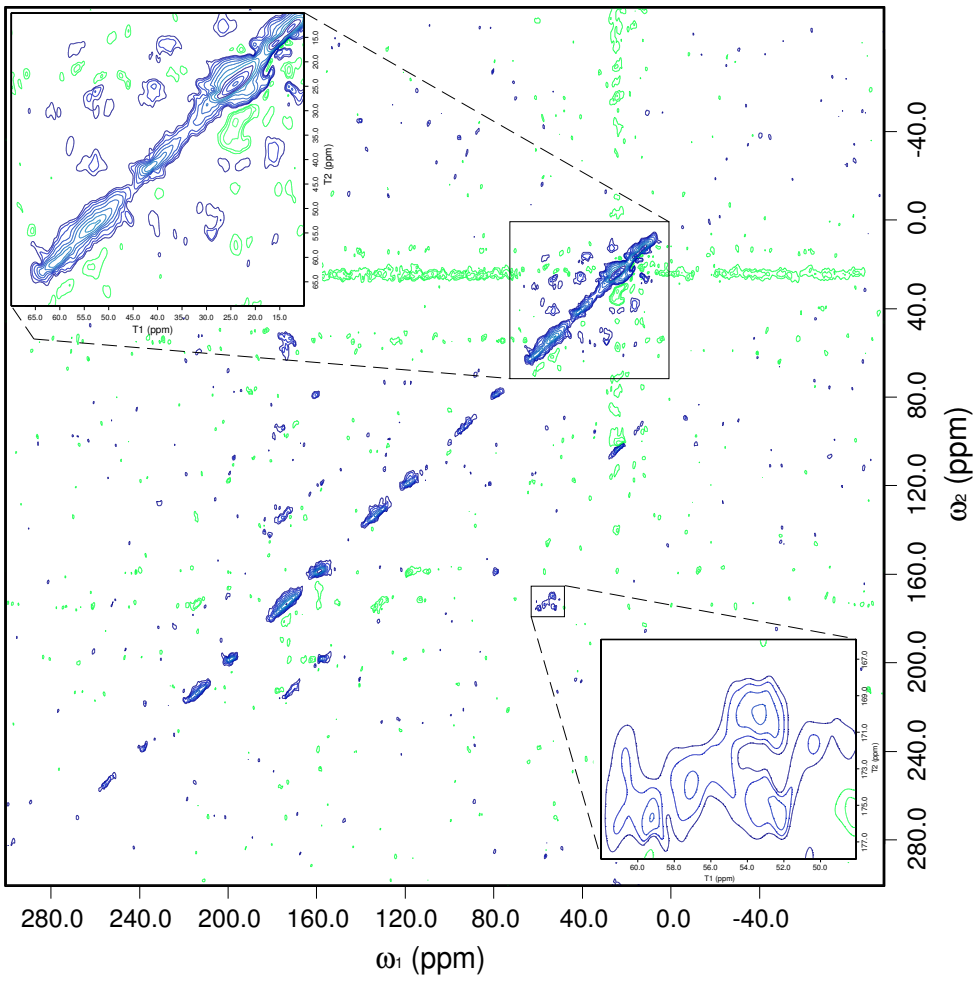

Figure 5.46: TOSSY spectrum of lyophilysed neurotensin(8-13) with a 4ms exchange time, 5 kHz spinning speed at room temperature. Data acquired with 128 t_1 points, of 128 acquisitions each. Data processed with 100 Hz linebroadening in t_2 prior to fourier transform. Data was then linear predicted from 128 to 512 points in t_1 prior to the application of a sinebell apodisation function. Data was then transformed with a real Fourier transform.

5.3.6 Double Quantum filtered CP-MAS studies of uniformly $^{15}N/^{13}C$ labelled neurotensin(8-13).

The C7 double quantum filtered CP-MAS spectrum of uniformly carbon-13 and nitrogen-15 labelled neurotensin(8-13) is shown in Figure 5.47. A CP-MAS spectrum of neurotensin(8-13) is shown in Figure 5.47A whilst the C7 double quantum filtered spectrum is shown in Figure 5.47B. The profile of the CP-MAS spectrum (Figure 5.47A mirrors that described in Section 5.3.2, with the exception of the sidebands arising from the carbonyls and arginine sidechains which are now spaced at intervals of 5 kHz.

With the large number of directly bonded carbon atoms the potential to generate double quantum coherence using sequences such as C7 should be readily obtained. In spite of our inability to resolve unambiguously many of the resonances within this sample, the spectral features observed in Figure 5.47B are largely comparable with those observed in the CP-MAS experiment. This suggests that the C7 recoupling experiment has sucessfully reintroduced dipolar coupling across the entire carbon spectrum, irrespective of frequency offset. This means that the filtering of carbon-13 labelled material against the background of unlabelled detergents should occur with very little bias to the frequency offset.

The major discrepancy between the CP-MAS spectrum and the C7 double quatum filtered CP-MAS spectrum arises from the broad resonance assigned to the C_ζ resonance of the arginines. The absence of significant spectral intensity from this resonance can be attributed to the isolated state of this site, since it is surrounded by nitrogen-15 atoms which are unable to support such homonuclear double quantum coherence. Although the resonance is suppressed, magnetisation is still present arising from the C_ζ of the arginine suggesting that double quantum coherence has been established through longer range, weak dipolar couplings. The relatively weak nature of this resonance might suggest that double quantum coherence between other labelled sites within the neurotensin(8-13) has arisen primarily through interactions

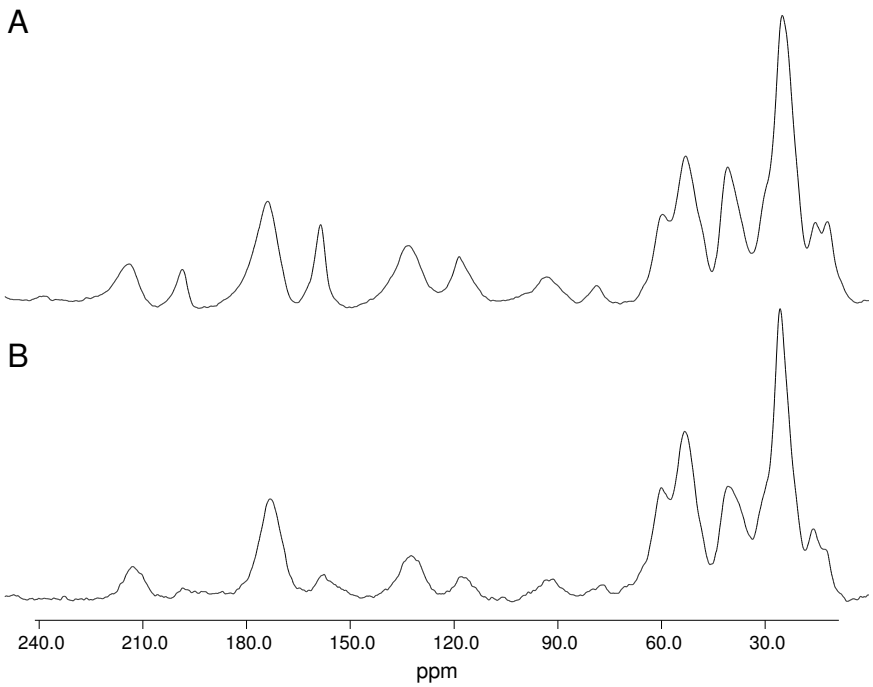

Figure 5.47: C7 double quantum filtered CP-MAS spectrum of uniformly carbon-13/nitrogen-15 labelled neurotensin. Cross polarization spectrum of uniformly C-13/N-15 labelled neurotensin(8-13)(A), C7 double quantum filtered 1ms CP-MAS spectrum of uniformly C-13/N-15 labelled neurotensin(8-13)(B). Data acquired at 5 kHz spinning speed and 1 ms cross polarisation. Double quantum coherence was generated and then selected for using 512 μs of C7 excitation and reconversion. Data averaged over 512 acquisitions, and processed with 100Hz linebroadening. Data was zero filled to 4096 points prior to Fourier Transform.

between neighbouring carbon atoms.

The results obtained here indicate that such sequences might permit the selective observation of carbon-13 labelled neurotensin(8-13) against a background of unlabelled detergent and other solutes across the entire carbon spectrum with reasonable efficiency and minimal bias arising from the frequency offset dependence of such experiments.

5.3.7 INADEQUATE spectra for neurotensin(8-13) in detergent buffer.

A 1D-INADEQUATE spectrum of neurotensin in solution at 5°C under 500Hz MAS is shown in Figure 5.48A with an expansion of the downfield and upfield regions given in Figure 5.48B and 5.48C respectively. The resonance assignments made on the basis of this data are given in Table 5.14. Resonances are apparent from most of the regions assigned to the proton decoupled carbon spectrum. Notable exceptions, include the suppression of signals arising from the glycerol present in the buffer (previously apparent at 62 and 71 ppm). Additionally the C_ζ resonance at 156ppm has been largely suppressed as it is not directly bonded to any carbon atoms and thus does not experience any J couplings in the order of 50Hz (the frequency range for which the experiment was optimized).

In contrast to the natural abundance signals arising from the glycerol the anti-phase doublets arising from the labelled sites within the neurotensin(8-13) are selected with good efficiency and resolution comparable with that observed in the proton decoupled carbon-13 spectra(Figure 5.44). This offers the potential to observe uniformly labelled ligand against a background of strong signals from natural abundance material with high resolution under these solution like conditions. Although this experiment offers the potential to observe the ligands under such conditions, it does not enable the assignment of resonances due to the absence of any correlation data.

Residue	CO(ppm)	C_α(ppm)	C_β(ppm)	Others
Arg	171.96	52.78	30.00-40.00	
Arg	171.96	52.78	30.00-40.00	
Pro	172.82-169.15	60.00-45.00	30.00-40.00	47.46 (C_δ)
Tyr	172.82-169.15	60.00-45.00	30.00-40.00	115.06 (C3,5)
				127.24 (C1)
				130.11 (C2,6)
				154.26 (C4)
Ile	172.82-169.15	60.00-45.00	35.89	14.35 (C_γ)
				9.73 (C_δ)
Leu	178.153	60.00-45.00	40.23	22.06 (C_δ)
				20.83 (C_δ)

Table 5.14: Assignments obtained from an INADEQUATE experiment on uniformly carbon-13/nitrogen-15 labelled neurotensin(8-13).

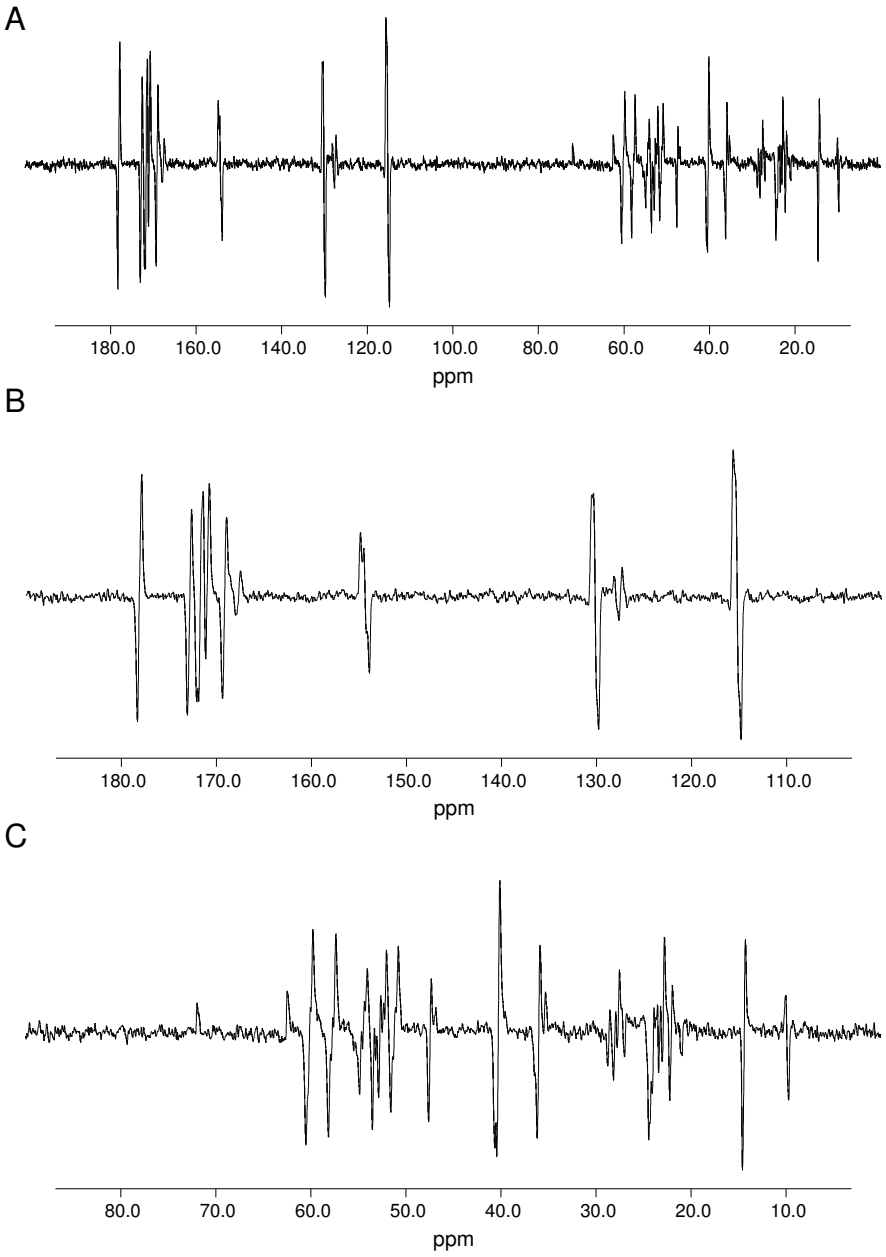

Figure 5.48: INADEQUATE spectrum of uniformly carbon-13 and nitrogen-15 labelled neurotensin(8-13) in desalting buffer. Data acquired with 5ms interpulse delay and 50 kHz proton decoupling. Data averaged over 4096 acquisitions, and processed with 3 Hz linebroadening. Data zerofilled from 8192 points to 32768 point prior to Fourier transform.

5.3.8 NMR studies of U-13C/15N labelled neurotensin(8-13) bound to detergent solubilized neurotensin receptor.

Studies of neurotensin(8-13) bound to the detergent solubilised neurotensin receptor were performed at both 5°C and -120°C. These two temperature regimes allowed high resolution like spectra to be acquired under pseudo solution conditions and solid state NMR techniques to be applied at lower temperatures. The results of these studies are given below.

NMR studies of U-13C/15N labelled neurotensin(8-13) bound to the neurotensin receptor in solution.

The proton decoupled carbon-13 spectrum of U-13C/15N labelled neurotensin(8-13) is shown in Figure 5.49A, with an expansion of the upfield and downfield region shown in Figure 5.49B and 5.49C respectively. The spectra are dominated by two intense resonances at 71 and 62 ppm, that arise from the high glycerol concentration in the sample, which acts as a protein stabilising agent and a cryoprotectant [269]. From studies of the individual components in aqueous solution the region between 10 and 80ppm with significant spectral intensity has been attributed to the carbon-13 natural abundance signals arising from the detergent molecules dodecyl maltoside, CHAPS and cholesterol hemisuccinate within the buffer system. On the basis of the chemical shifts, the downfield resonances at 100 ppm and 110 ppm have been attributed to natural abundance carbon-13 present in the rings of cholesterol hemisuccinate. Resonances arising at 176.5 ppm are assigned to the carbonyl groups present within the detergent molecules with sidebands spaced at intervals of 500Hz from the central isotropic peak.

No resonances appear from the protein in the sample. This is attributed to the relatively low concentration of protein in the sample that contains only natural abundance carbon-13. Additionally, it has been shown that the detection of similar

proteins in lipid bilayers is highly inefficient due to the presence of large amplitude motions that interfere with efficient decoupling of protein resonances within the sample leading to extensive line broadening[1]. It is possible that similar mechanisms may play an important role in the detection of such resonances in detergent micelles.

A proton decoupled spectrum of 1mg of active detergent solubilized neurotensin receptor (as determined by radioligand binding assay) to which 10 nmoles of uniformly U-$^{13}C/^{15}N$ labelled neurotensin(8-13) has been added in shown in Figure 5.50A with upfield and downfield regions displayed in Figures 5.50B and 5.50C respectively. Assuming a disassociation constant for the ligand of 10^{-9}M we would expect that the bulk of the signal observed to arise from ligand bound to the detergent solubilized neurotensin receptor with less than 5% of the ligand remaining free.

Although many of the resonances are masked by the presence of strong signals arising from natural abundance contributions to the spectrum from components of the buffer, many of the sidechain resonances that appear in the region between 100 and 180 ppm are clearly resolved. In addition the upfield region between 0 and 30ppm shows sufficient spectral simplicity to allow the unambiguous assignment of some of the resonances arising from the aliphatic sidechains of the labelled neurotensin(8-13). Upon the addition of U-$^{13}C/^{15}N$ neurotensin intensity appears in the spectral region where one would expect resonances from the C_α, C_β and C_γ resonances. However, the presence of extensive unresolvable J-couplings at these sites causes extensive broadening of these resonances, limiting both spectral intensity and resolution. Thus, we have been unable to identify these sites uniquely against the strong natural abundance background signal.

The resonances which are unambiguously assigned are given in Table 5.15, with the corresponding perturbation in chemical shift in comparison to those obtained for uniformly labelled $^{13}C/^{15}N$ neurotensin(8-13) under identical buffer conditions. Although the observed perturbations are small, extensive efforts were made to ensure

the correct referencing, with many of the resonances arising from components in the buffer system exhibiting shifts that are smaller than both the linewidth (<10Hz) and in the order of the digital resolution with which the spectra were processed, 1.52Hz/point. Together with the data from the radioligand binding assays which were used to monitor the sample preparation, we propose that the perturbations in chemical shift are due to the perturbations in electronic environment upon the binding of the ligand to the receptor binding site. We can rule out the possibility of non specific binding on the basis of the low background binding observed in the radioligand binding assays (typically <5%) and the observation that the perturbation of chemical shifts between and aqueous and the buffered system appears minimal(data not shown). In addition a small increase in linewidth has been observed (See section 5.3.9) consistent with an increase in the rate of transverse relaxation associated with the binding of small molecules to large macromolecular complex [1]. In the absence of a suitable antagonists with which to inhibit the binding of the neurotensin this data is offered to support the conclusion that the ligand observed is that which is bound to the detergent solubilized receptor.

The perturbations in chemical shift observed, indicate the nature of the electronic environment experienced by the nucleus in the binding site. Although the assignment of the backbone resonances of the peptide would have permited limited analysis of the conformation[244], the limited spectral dispersion of both C_α and carbonyl groups and the absence of a suitable assignment scheme has hindered the sequence specific assignments of these groups. However, the perturbation of the carboyl region, with the downfield shift of the carboxy terminus and the reduction in the width of the remaining carbonyl region, perhaps indicates the adoption of some other preferred conformation upon ligand binding. Changes observed in the sidechains, although significant in size are not of sufficient magnitude to determine whether these arise from interactions with the ligand binding pocket or from molecular rearrangement of the sidechains.

Resonance	Assignment	Perturbation
178.89	Carboxy terminus	+0.74
173.09 - 170.31	Carbonyl	+1.00
157.02	Arg C_ζ	+0.56
154.85	Tyr(C4)	+0.59
129.76	Tyr(C2,6)	-0.35
127.15	Tyr(C1)	-0.09
115.06	Tyr(C3,5)	0.00
22.72	Ile C_δ	+0.66
21.53	Ile C_δ	+0.70
14.80	Leu C_γ	+0.45
10.16	Leu C_γ	+0.43

Table 5.15: Observed chemical shifts from labelled carbon-13 labelled ligand bound to detergent solubilised neurotensin receptor. All samples referenced externally to adamantane. No perturbation (<10Hz) in chemical shifts were observed from glycerol and detergent peaks upon the addition of 10 nmoles of neurotensin(8-13).

The results presented have demonstrated the feasibility of detecting neurotensin bound to detergent solubilized receptor under solution like conditions. Through perturbations of spectral features, and biochemical assays we have demonstrated that this binding appears to be physiologically specific, with the uniformly carbon-13/nitrogen-15 labelled neurotensin(8-13) bound at the agonist binding site on the detergent solubilized neurotensin receptor. Further, interpretation of this data has not been possible due to our inability to resolve important resonances against the background of natural abundance signals arising from the buffer system used, and assign those resolved to specific amino acids within the sequence.

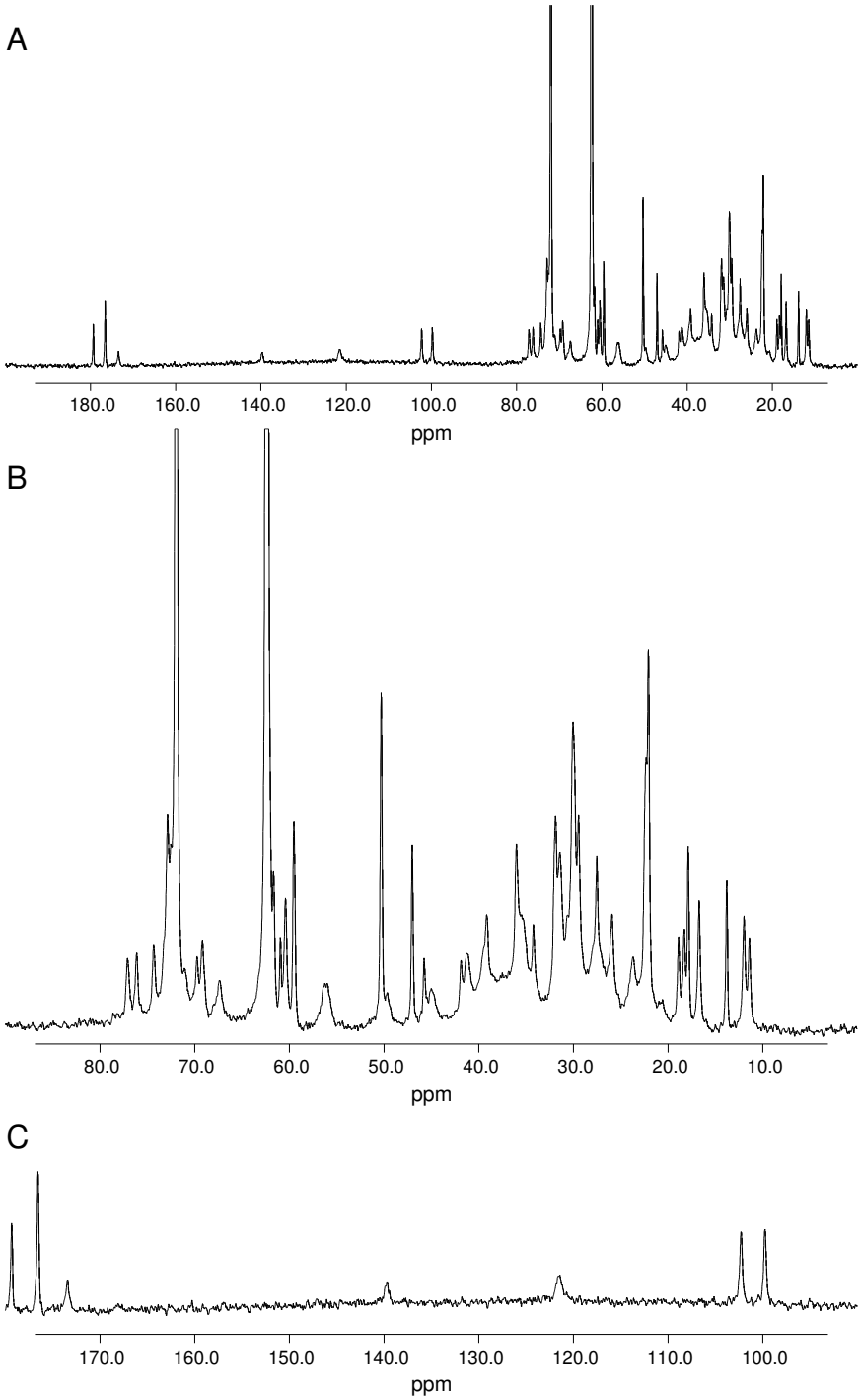

Figure 5.49: Proton decoupled spectra of 1mg of detergent solubilized neurotensin receptor. Data acquired at 500Hz spinning speed and 70 kHz decoupling. Data averaged over 8192 acquisitions, processed with 3Hz linebroadening and zero filled with 32768 points prior to Fourier transform.

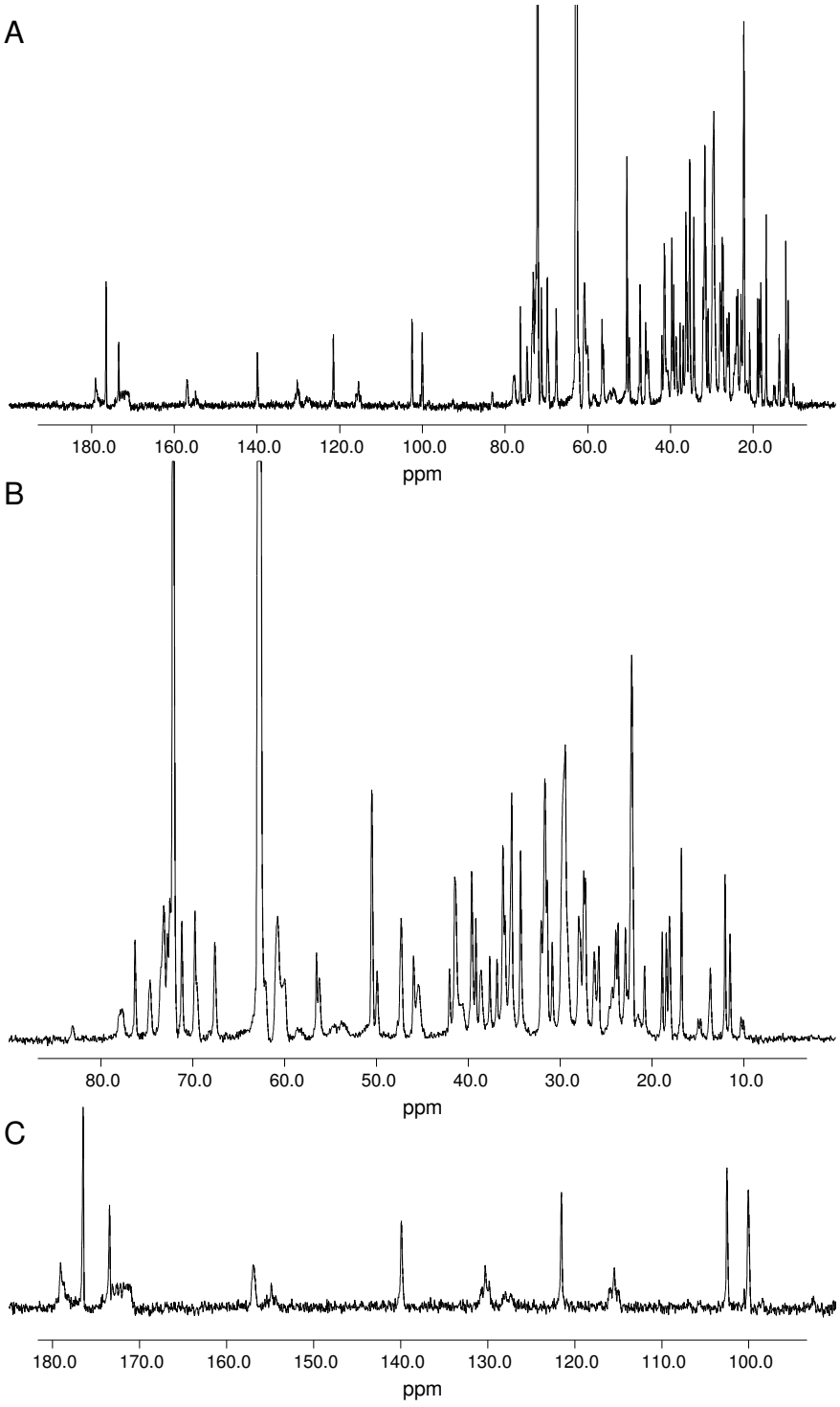

Figure 5.50: Proton decoupled spectra of 1mg of detergent solubilized neurotensin receptor with 10nmoles of N-15/C-13 labelled neurotensin(8-13) added. Data acquired at 500Hz spinning speed and 70 kHz decoupling. Data averaged over 8192 acquisitions, processed with 3Hz linebroadening and zero filled with 32768 points prior to Fourier transformation.

NMR studies in frozen solution of U-^{13}C/^{15}N labelled neurotensin(8-13) bound to the neurotensin receptor.

In an attempt to employ solid state methodology to the detergent solubilised neurotensin receptor, studies comparable to those performed under solution like conditions were performed at -120°C. CP-MAS spectrum of detergent solubilised neurotensin receptor at -120°C is shown in Figure 5.51A. Notably, the spectrum obtained at -120°C is much broader than that observed at 5°C even under MAS conditions and high power proton decoupling. This suggests that significant inhomogeneous broadening of the spectrum has arisen upon freezing, even in the presence of large quantities of cryoprotectants such as glycerol [269]. As in experiments performed at 5°C, the spectrum is dominated by two intense resonances at 62 and 71 ppm arising from the glycerol present at high concentrations within the sample. Similarly, the broad resonance from 10 to 50 ppm has been assigned to natural abundance carbon-13 present in the dodecyl maltoside, CHAPS and cholesterol hemisuccinate on the basis of earlier studies of the buffer systems used (data not shown). Intensity arising between 100 and 110 ppm has been assigned to natural abundance carbon-13 contained within the cholesterol hemisuccinate on the basis of the chemical shift and the extended aromatic systems present within the molecule. Weak intensity occurring between 170 and 180ppm has been assigned to carbonyl groups present in the detergents used, all of which contain such functional groups. The weak intensity present between 130 and 140 ppm has been assigned to the presence of sidebands arising from the carbonyl resonances on spectral differences arising in spectra acquired at various spinning speeds. The presence of such sidebands indicates that there is significant immobilisation of the detergent micelles within the sample. Due to the masking of the spectral regions containing protein resonances (∼5-60ppm) by glycerol and detergent resonances arising from the natural abundance signals assignment of any resonances was impossible.

Upon the addition of 10nmoles of uniform labelled carbon-13 and nitrogen-15

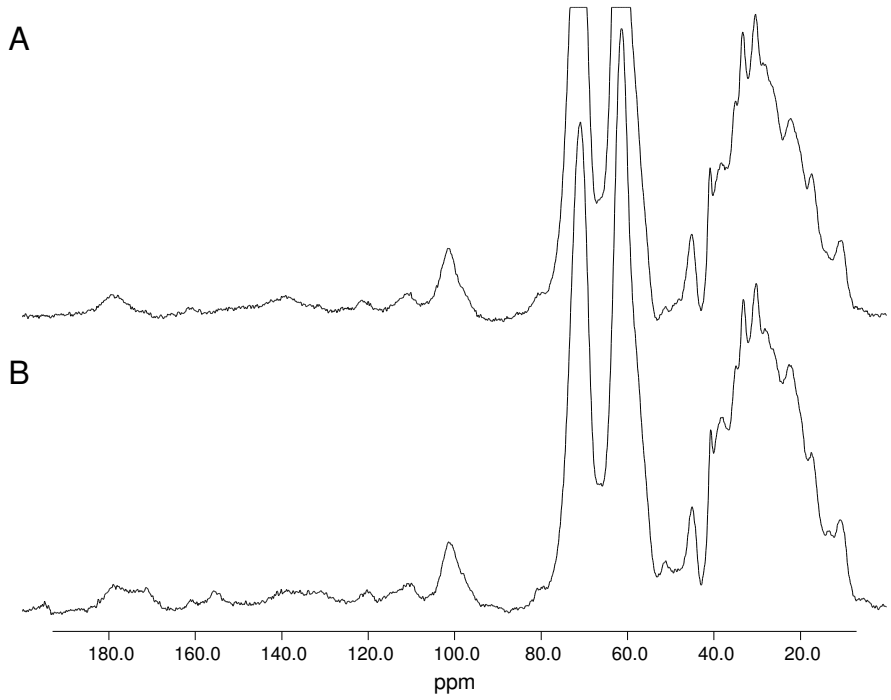

Figure 5.51: Carbon-13 CP-MAS spectra of 1mg of detergent solubilised neurotensin receptor(A) and upon the addition of 10nmoles of uniformly C-13/N-15 labelled neurotensin(8-13) (B). Data acquired with a 1ms contact time, 5000Hz spinning speed and 70 kHz decoupling. Data averaged over 8192 acquisition, processed with 30Hz linebroadening and zero filled to 4096 points prior to Fourier Transform.

neurotensin(8-13) to 1mg of the neurotensin receptor, the major spectral features remain largely constant with larger signal intensities arising from the glycerol and detergents masking any contribution that would be made by the addition of the labelled ligand. In regions that are less complex (180-100ppm) spectral pertubations are apparent with additional peaks arising between 175-169ppm and 157-152ppm. Spectral intensity arising in the region 175-169ppm has been assigned to the carbon-13 labelled carbonyl groups present within the peptide on the basis of the observed chemical shift. The spectral intensity arising between 157 and 152ppm has been assigned to the C_ζ from the arginine sidechains and the C4 of the tyrosine sidechains of the basis of their observed chemical shift. Spectra of 10 nmoles of uniformly labelled neurotensin(8-13) in desalting buffer at these temperatures did not show

these resonances (as in Figure 5.51A) suggesting that the observation of these resonances from the ligand are associated with the additional immobilisation infered on the ligand upon the binding to the detergent solubilised receptor.

In the absence of more favourable observation conditions, assignment of many of neurotensin(8-13) resonances against the background of signals from the buffer system used proved difficult. This coupled with the relatively poor resolution obtainable at these temperatures ($\pm$1.5ppm) has hindered a more detailed analysis of the chemical shifts which may have offered some insights as to the nature of the interaction between the ligand and the receptor.

5.3.9 Double quantum filtered spectra of neurotensin(8-13) bound to detergent solubilized neurotensin receptor.

From the results discussed above it becomes apparent that the correct resolution and assignment of the labelled neurotensin(8-13) bound to detergent solubilized neurotensin receptor is severely hindered by the presence of background signals that arise from carbon-13 natural abundance present in the buffer system. Several types of experiments could be performed that would enable the effective suppression of non correlated background signal through the exploitation of both the homo and heteronuclear coupling present in the ligand but largely absent in the components of the buffer system. Below we have employed double quantum filtration techniques both in solution and solid state through the exploitation of ^{13}C-^{13}C J couplings and ^{13}C-^{13}C dipolar couplings respectively.

INADEQUATE spectra of neurotensin(8-13) bound to detergent solubilzed neurotensin receptor.

An INADEQUATE spectrum of uniformly C-13/N-15 labelled neurotensin(8-13) is shown in Figure 5.52A, with the upfield and downfield regions of the spectrum expanded in Figure 5.52B and 5.52C respectively. Again the spectrum is dominated

by two intense resonances at 71 and 62pppm. These were previously attributed to the glycerol present in the sample. Although the sequence should prevent the detection of resonances arising from material labelled at natural abundance levels, at the high concentrations of glycerol present we are still able to detect the presence of the 0.1% of carbon atoms in the glycerol that contain adjacent carbon-13 atoms. With the exception of these resonances, the others appear to arise exclusively from signals deriving from the adjacent carbon labels within the peptide (the experiment was optimized for adjacent couplings with an interpulse delay of 5ms corresponding to a 50 Hz J coupling), these assignments are given in Table 5.16. The downfield region of the spectrum between 180 and 100ppm is clearly resolved with 4 of the carbonyl groups giving distinct antiphase signals, and resonance appearing from tyrosine side chain. The signal present in the proton decoupled spectra at 156ppm being suppressed due to its inability to support homonuclear J couplings of about 50 Hz. The upfield region again suffers from poor sensitivity due to the presence of multiple couplings which reduce spectral intensity, however peaks are still apparent in the C_α(60-45ppm) and C_β(30-40ppm) region with additional resonances attributable to aliphatic sidechains present in the peptide. The quality of this data is attenutated compared with that obtained from the uniformly labelled ligand in the corresponding buffer, this is in part due to the reduced signal intensity obtained from the broader lines where the antiphase doublets intensity begins to cancel as line broaden. This has been compounded by perturbations of the baseline around the C_α region due to the presence of much stronger signals from the glycerol. Although these studies have demonstrated that it is possible to resolve resonances from bound ligand, they have only facilitated the additional assignment of the C_δ from the proline on the basis of its characteristic chemical shift.

Again further interpretation of the data has been limited by our inability to assign the resonances to specific sites within the peptide. However, the successful

application of this methodology, suggests that the application of similar methodologies exploiting the ^{13}C-^{13}C J coupling should be possible. Many of these should allow the exploitation of these parameters permitting the assignment of many of the resonances within the spectra.

Resonance	Assignment	Perturbation
178.89	Carboxy terminus	+0.74
173.09 - 170.31	Carbonyl	+1.00
157.02	Arg C_ζ	+0.56
154.85	Tyr(C4)	+0.59
129.76	Tyr(C2,6)	-0.35
127.15	Tyr(C1)	-0.09
115.06	Tyr(C3,5)	0.00
47.99	Pro C_δ	+0.5
41.50	Arg C_δ	-0.63
36.10	Ile C_β	+0.21
22.72	Ile C_δ	+0.66
21.53	Ile C_δ	+0.70
14.80	Leu C_γ	+0.45
10.16	Leu C_γ	+0.43

Table 5.16: Observed chemical shifts from carbon-13 labelled ligand bound to detergent solubilised neurotensin receptor as observed by 1D-INADEQUATE spectroscopy. All samples referenced externally to adamantane. No perturbation (<10Hz) in chemical shifts were observed from glycerol and detergent peaks upon the addition of 10 nmoles of neurotensin(8-13).

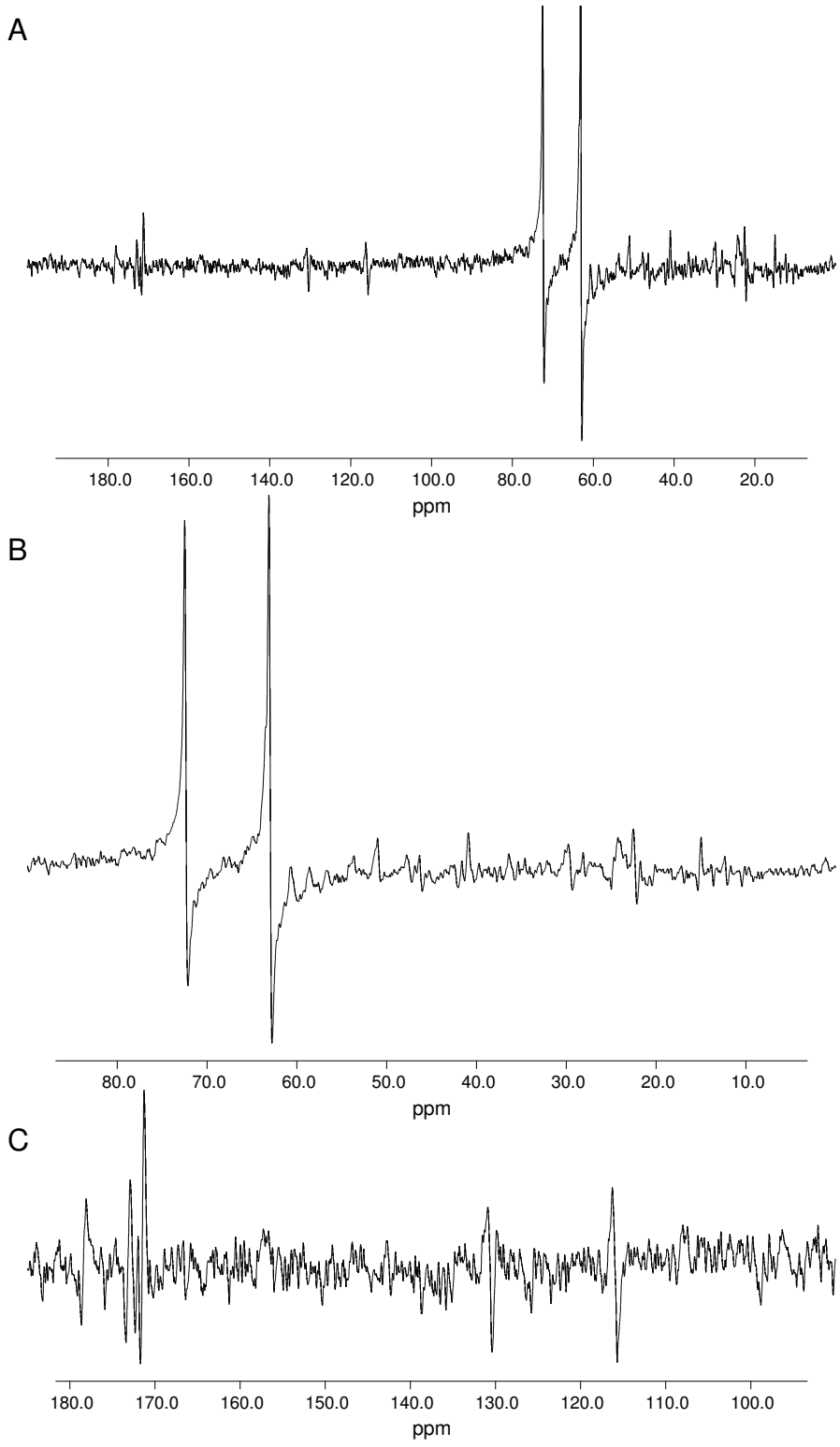

Figure 5.52: INADEQUATE spectrum of uniformly N-15/C-13 labelled neurotensin bound to the detergent solubilised neurotensin. Data averaged over 32768 acquisitions and processed with 10 Hz linebroadening.

C7 Double quantum filtered CP-MAS spectra of neurotensin(8-13) bound to detergent solubilized neurotensin receptor in frozen solution(-120°C).

A C7 double quantum filtered CP-MAS spectrum of uniformly carbon-13/nitrogen-15 labelled neurotensin bound to the detergent solubilised neurotensin receptor is shown in Figure 5.53, with the CP-MAS spectrum shown in A and the double quantum filtered CP-MAS spectrum shown in B. Although the signal to noise observed in the C7 double quantum filtered spectra is low due to the limited acquisition times possible at these temperatures, four major regions can be assigned to groups within the uniformly labelled neurotensin(8-13).

The resonance arising between 167 and 179 ppm has been assigned to the labelled carbonyl groups. Although the signal to noise limits the interpretation of this data, the profile mirrors that observed for the INADEQUATE spectra acquired at 5°C with the free C terminus at 178ppm and other carbonyl groups involved in peptide bonds arising between 167 and 176ppm. In addition to the isotropic lines, a sideband arising from the carbonyl group is apparent between 124 and 133 ppm.

Between 20 and 60ppm significant signal intensity is observed which mirrors the profile observed for the double quantum filtered CP-MAS spectra of the lyophilysed samples of uniformly labelled neurotensin(8-13)(Figure 5.47). This broad resonance can be divided into three distinct regions. The region between 43 and 69 ppm is thought to arise primarily from intensity from C_α carbons within the labelled peptide whilst the region between 30 and 43 ppm has been assigned primarily to C_β carbons within the peptide. The remaining intensity present between 15 and 30 ppm has been assigned to a number of aliphatic carbon present in the sidechains of the residues present in the neurotensin(8-13). Even though many of these are clearly resolved in the 5°C spectra, both the limited signal intensity and the inhomogeneous broadening introduced upon freezing have limited a more detailed assignment of the neurotensin(8-13) bound to the detergent solubilised neurotensin receptor at -120°C.

It was demonstrated here that under solid state conditions similar to those that

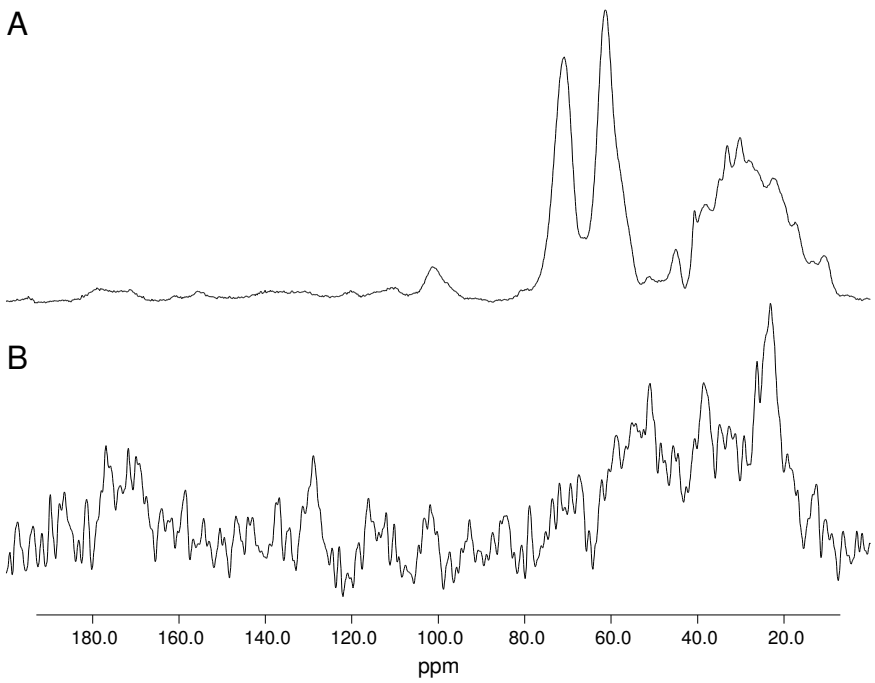

Figure 5.53: C7 double quantum filtered carbon-13 CP-MAS spectra of uniformly carbon-13/nitrogen-15 labelled neurotensin bound to detergent solubilised neurotensin receptor at -120°C. Cross polarization spectra of uniformly C-13/N-15 labelled neurotensin(8-13)bound to detergent solubilised neurotensin receptor(A), C7 double quantum filtered 1ms CP-MAS spectra of uniformly C-13/N-15 labelled neurotensin(8-13) bound to detergent solubilized neurotensin receptor(B). Data acquired at 5kHz spinning speed and 1ms cross polarisation. Double quantum coherence was generated and then selected for using 512 μs of C7 excitation and reconversion sequence. Data averaged over 8192 acquisitions, and processed with 100Hz linebroadening. Data was zero filled to 4096 points prior to Fourier Transform.

would be experienced upon binding of the neurotensin(8-13) to the neurotensin receptor in lipid bilayers, it is possible to selectively observe labelled ligand against the natural abundance background signals present in most carbon-13 spectra of biological systems.

5.4 Conclusion.

5.4.1 Purification and expression of neurotensin receptor.

Using the expression system and purification protocols outlined above we have been able to obtain 3.89mg of pure recombinant neurotensin receptor (as assayed by number of binding sites). In addition 4.3mg of neurotensin receptor was obtained after the initial Ni affinity column purification step, although this sample contains contaminants arising from other proteins present in *E.coli* which bind the Ni affinity resin. The amount of protein is low compared with that used for comparable studies with the nicotinic acetylcholine receptor, however the absolute number of binding sites is comparable and sufficient for solid state NMR studies.

Problems were encountered during the expression of the recombinant neurotensin receptor. These were primarily centred on the reproducibility of both expression levels and subsequent purification. Although many modifications were made to the given protocol, these failed to offer any improvement in either yield or reliability. Our inability to grow large scale fermentations of this system hindered the routine production of suitable quantities of protein for subsequent biophysical studies. Even in the presence of such drawbacks we were still able to culture sufficient material in shaker flasks to permit further biophysical studies.

5.4.2 Assignment of U-13C/15N labelled neurotensin(8-13).

Through the application of a variety of homonuclear and heteronuclear correlation techniques we were able to assign a number of resonances in the neurotensin(8-13) as a lyophilised solid. These are given in Table 5.13. The heteronuclear correlation spectra, although lacking in resolution, allowed the unambiguous assignment of resonances attributed to the arginine side chain, due to the obvious couplings between the carbonyl, amide nitrogen and C_α carbon. The remaining assignments arise from

the partial connectivities obtained from the TOSSY spectra shown. These permitted the tracing of connectivities from the amino acid side chains to the peptide backbone. Certain amino acid residues appear to be absent in the TOSSY spectra, notably the tyrosine residue. This could in part be due to unfavourable cross polarization characteristics of the aromatic group leading to poor initial sensitivity or unfavourable relaxation properties under the RIL mixing scheme, these effects were not further explored. Further assignments were also hindered by the poor resolution obtained for the heteronuclear correlation experiment, which limited our ability to obtain correlation data between adjacent amino acids within the peptide sequence. It is unclear whether the poor resolution offered by the heteronuclear correlation experiments should be attributed to the nature of the magnetisation transfer sequence or the poor resolution attainable in the nitrogen spectra. Experiments utilising alternative magnetisation transfer sequences may clarify this issue, but have not currently been performed. These data indicate that we should be able to undertake a complete assignment of the neurotensin(8-13) in the solid state without the need to crystallize the peptide to reduce inhomogeneous broadening within the sample, which has been used in all assignments of peptide in the solid state to date [79].

Additionally we have demonstrated the application of double quantum filtered experiments to uniformly labelled carbon-13/nitrogen-15 labelled neurotensin(8-13) under both solid state and solution like conditions, under MAS. Both these techniques have proved to be of considerable importance in subsequent studies where the neurotensin(8-13) is bound to the detergent solubilized neurotensin receptor.

5.4.3 Assignment of U-13C/15N labelled neurotensin(8-13) bound to the neurotensin receptor.

It has been demonstrated through both solution and solid state MAS experiments it is possible to detect uniformly labelled neurotensin(8-13) bound to detergent solubilised neurotensin receptor. We have monitored the nature of binding through the

perturbation in chemical shifts upon binding of neurotensin(8-13) to the receptor. The specificity of interaction was further confirmed using a radioligand binding assay which has been used to monitor the activity of the protein at each step of the purification.

Conventional carbon-13 proton decoupled NMR allowed the resolution of many of the side chain resonance appearing in the downfield region of the carbon-13 spectrum at 5°. These results were consistent with carbon-13 CP-MAS spectra of the ligand bound to the receptor at -120°C although the resolution obtained at this temperature was much lower. In contrast to the downfield region many of the resonances arising from the peptide in the upfield region (20 to 100ppm) were masked by the presence of strong signals arising from natural abundance carbon-13 present in the buffer system used. Through the use of double quantum filtered MAS spectra we have been able to largely suppress the natural abundance contributions arising from the buffer system under both solution like and solid state conditions. This has allowed the resolution of many of the resonances arising from the C_α and C_β carbon atoms. However, in absence of correlation data, similar to that obtained in the solid state, we have been unable to assign the bulk of these resonances, although where distinctive chemical shifts are available this information has been used to assign the sites.

We have been able to monitor the perturbations in chemical shift upon binding, however the absence of a suitable assignments of the peptide backbone has prevented any interpretation of the chemical shift data in terms of any prefered structure upon the binding of the ligand to the receptor. Perturbations of the resonances arising from the well resolved and assignable residues, although significant, are not large enough to distinguish between the various processes which may perturb the chemical shift upon binding.

The data presented here suggests that sufficient resolution is possible to allow a complete assignment of the neurotensin(8-13). In the absence of suitable correlation data similar to that obtained for the lyophilised solid, we are unable to assign

these resonances to sites within the ligand. However, the data presented for the lyophilised sample suggests that the NMR methodology employed offers the potential to perform a full assignment of this ligand whilst bound to the receptor. One major improvement to this work would be the reconstitution of the neurotensin receptor into lipid bilayers. Not only will motional characteristics be improved for solid state NMR studies, but higher concentrations of receptor will be attainable improving the signal to noise for NMR studies. This should allow the more efficient use of dipolar recoupling methodologies which will aid in both assignment and structure elucidation of ligand bound to receptor.

Chapter 6

Conclusions.

Results from this thesis can be split into three categories, those which pertain to each of the systems, the nicotinic acetylcholine receptor and the neurotensin receptor. The remaining conclusions concern those drawn from the application of the NMR methodologies to the two systems. These three catergories will be discussed below.

6.1 The nicotinic acetylcholine receptor.

Initial studies on the nicotinic acetylcholine receptor centred on the study of double labelled $N(^{13}CH_3)_3$, $C^{13}CH_3$ acetylcholine bound to the receptor. These studies allowed the resolution of the $N(^{13}CH_3)_3$ group of the acetylcholine against the natural abundance background signal from the receptor membranes. The perturbation in chemical shift observed from this group coupled with the appropriate simulations based on a system proposed to be homologous to the nicotinic acetylcholine receptor allowed us to conclude the environment occupied by the $N(^{13}CH_3)_3$ group in the receptor is in a predominantly aromatic binding pocket. Subsequent structural studies based on rotational resonance methodology which had been shown to work well in the crystalline salt were hindered by our inability to assign the resonance arising from the $C^{13}CH_3$ group in the acetylcholine.

Subsequent studies centred on identifying a methodology that would enable the resolution of these resonances against the natural abundance signal from the receptor membranes. These studies initially centred on broadband dipolar recoupled MAS exchange spectroscopy of uniformly labelled acetylcholine. When applied to the crystalline acetylcholine perchlorate this methodology provided assignment and

qualitative structural information. However, when applied to the nicotinic acetylcholine receptor membranes unfavourable relaxation and experimental constraints limited the effectiveness of the experiments.

An alternative methodology was sought in the form of double quantum filtered CP-MAS NMR spectroscopy. This facilitated the selective observation of molecules able to support higher order coherence. This has enabled an assignment to be made of all carbon sites within the acetylcholine whilst bound to the nicotinic acetylcholine receptor. The low resolution afforded in these spectra limited a detailed interpretation of the chemical shifts.

To complement these MAS studies a deuterium wideline NMR approach was employed. Using powder samples of nicotinic acetylcholine receptor membranes labelled with $N(CD_3)_3$ bromoacetylcholine we have been able to determine that the $N(^{13}CH_3)_3$ of the ligand is relatively constrained in the aromatic agonist binding site, with motions about the C3 and C3' axis of rotation being hindered to a greater extent than those observed in a range of quaternary ammonium crystalline solids.

Through the development of the isopotential centrifugation technique it has been possible to obtain macroscopically aligned samples of nicotinic acetylcholine receptor membranes labelled with $N(CD_3)_3$ bromoacetylcholine bromide. Deuterium wideline NMR spectroscopy of labelled receptor membranes allowed the exploitation of the anisotropy present in the deuterium spectrum to calculate the angle formed between the membrane normal of the $N(CD_3)_3$ rotor to be 42°.

Together the data will enable the positioning of the ligand within the ever improving electron diffraction structures of the nicotinic acetylcholine receptor and assist in our understanding of how the ligand interacts with the agonist binding site of the nicotinic acetylcholine receptor.

Work is currently under development to obtain detailed structural information from acetylcholine whilst bound to the receptor now we have been able to unambiguously assign the ligand against the natural abundance background signal.

6.2 The neurotensin receptor.

The primary goal for the study of neurotensin bound to the neurotensin receptor centred on the application of solid state MAS-NMR to allow both assignment and structural elucidation of the ligand bound to receptor. Due to the complexity and nature of the ligand we adopted a strategy of uniformly labelling of the ligand in analogy with the labelling studies used in studies employed on the nicotinic acetylcholine receptor.

Due to the low natural abundance of the neurotensin receptor an expression system was sought which offered the potential to provide sufficient quantities of recombinant receptor to permit structural studies. Although expression levels in this heterologous expression were low and work undertaken to grow this system on a larger scale in fermenters failed, sufficient protein was produced to allow solid state NMR experiments.

In order to permit NMR studies of neurotensin bound to its receptor, NMR sensitive nuclei had to be incorporated into the ligand. Two ligands were prepared the first neurotensin(8-13), an active N-terminal truncation by solid phase synthesis and the second neurotensin using a novel expression methodology for small peptides developed during the course of this work. Both of these approaches have allowed the production of sufficient quantities of peptide ligand to permit studies of the ligand whilst bound to the receptor. Both of these ligands have been characterised by several biophysical techniques including solution NMR, mass spectroscopy, peptide sequencing and reverse phase HPLC.

Uniformly labelled $^{13}C/^{15}N$ neurotensin(8-13) was studied as a lyophilysed solid to permit an assignment in the solid state. Through the application of both homo- and heteronuclear recoupling experiments we have been able to assign many of the resonances arising from sites within the ligand, although the low resolution obtained in heteronuclear correlation experiments limited the potential for sequential

assignment.

Early studies of neurotensin(8-13) suggested that the results obtained at 5°C under slow MAS would allow the application of solution state experiments, whilst solid state experiments became more favourable at -120°C. Ligand binding events were monitored at 5°C through the perturbation of chemical shift upon binding. Although not as accurate these appeared to be mirrored under solid state conditions at -120°C. The activity of the protein was also monitored using a radioligand binding assay.

Although these early studies allowed the resolution of side chain and carbonyl resonances in the downfield region of the carbon spectrum, resonances assigned to the C_α and C_β sites of each amino acid were largely obscured in the presence of strong natural abundance signals arising from detergents present in the buffer system.

Double quantum filtered NMR spectroscopy was performed in both the solution and solid state using an INADEQUATE experiment with MAS and a C7-CP-MAS NMR methodology to observe selectively labelled ligands able to support high order coherence. This enabled us to resolve resonances previously obscured by the natural abundance signals. However in the absence of a suitable assignment strategy we have been unable to assign many of the resonances arising from the peptide backbone, whose chemical shifts may have indicated a preferred conformation upon binding. Work is currently underway to develop experiments aimed at allowing such an assignment based on both homo- and heteronuclear recoupling techniques, similar to those already decribed in the literature[79].

Although perturbations in chemical shift have been observed for some of the assignable resonances, the small but significant changes do not allow us to determine whether these arise from conformational rearrangement or a change in electrostatic environment upon binding.

Future studies will centre on the incorporation of the neurotensin receptor into

lipid bilayers. This will confer many advantages for solid state NMR as the receptor will experience a restricted range of motions, this will facilitate the application methodologies similar to those employed for the nicotinic acetylcholine receptor. The application of such experiments will perhaps facilitate a more detailed understanding of both the dynamics and structure of the neurotensin at its binding site.

6.3 General Conclusions.

Through the application of recent advances in solid state NMR methodologies we have demonstrated the feasibility of studying uniformly labelled ligands whilst bound to membrane receptors. These studies have enabled us to perform assignments of these bound ligands against a background of natural abundance material present in the sample. Several dipolar recoupling schemes were applied, those presented including C7 and RIL-ZQT used in the double quantum filtered cross polarisation MAS and broadband exchange spectroscopy. Although both these sequences functioned well under solid conditions, when applied to biological membrane systems at 5°C, their sensitivity was severely attenuated. On lowering the temperature, both these sequences showed improved efficiency, suggesting that both had been severely affected by motions present in the system. This suggests retrospectively that assignments based on the exploitation of J-couplings within the system may offer a significant advantage as these are less sensitive to molecular motions. Additionally these sequences showed great sensitivity to the decoupling used. To date optimal results were obtained with frequency offset Lee-Goldburg homonuclear decoupling[47], due to its effectiveness during these mixing sequences and the ease with which it can be implemented. Improvements have been proposed on this sequence which may have offered significant improvements to the results obtained here, however available equipment did not allow its implementation.

To conclude, the work we have demonstrated here has advanced the application of dipolar recoupling experiments to aid in both the resolution and assignment of

uniformly labelled ligands bound to membrane receptors. These will act as a suitable reference on which we can base methodologies which will support the extraction of structural information.

Bibliography

[1] J.N.S. Evans. *Biomolecular NMR Spectroscopy.* Oxford University Press, 1 edition, 1995.

[2] K.E. Van Holde & C.K. Mathews. *Biochemistry.* The Benjamin/Cummings Publishing Company, 1st edition, 1990.

[3] M. Shuster, R.M. Stroud & M.P. McCarthy. Nicotinic acetylcholine receptor superfamily of ligand gated ion channels. *Biochemistry*, 29:11009–11023, 1990.

[4] A.Miyazawa, Y.Fujiyoshi, M.Stowell & N.Unwin. Nicotinic acetylcholine receptor at 4.6 Å resolution: transverse tunnels in the channel wall. *Journal of Molecular Biology*, 288:765–786, 1999.

[5] J.L. Galzi, F. Revah, A. Bessis & J.P. Changeux. Functional architecture of the nicotinic acetylcholine receptor: from electric organ to brain. *Annual Review in Pharmacology*, 31:37–72, 1991.

[6] S. Watson & S. Arkinstall. *The G-protein linked receptor.* Academic Press, 1 edition, 1994.

[7] G. Vriend. WHAT IF: a molecular modelling and drug design program. *Journal of Molecular Graphics*, 8:52–56, 1990.

[8] J.M. Baldwin, G.F.X. Schertler & V.M. Unger. An alpha carbon template from the transmembrane helices in the rhodopsin family of G protein coupled receptors. *Journal of Molecular Biology*, 272:144–164, 1997.

[9] Y.P. Pang. Proposed ligand binding site of the transmembrane receptor for neurotensin(8-13). *The Journal of Biological Chemistry*, 271:15060–15068, 1996.

[10] A.S. Ulrich & A. Watts. ^{2}H NMR linehsapes of immobilized uniaxially orientated membrane proteins. *Solid State Nuclear Magnetic Resonance*, 2:21–36, 1993.

[11] C.F. Valenzula, P. Weign, J. Yguerabide & D.A. Johnson. Transverse distance between the membrane and the agonist binding sites on th Torpedo acetylcholine receptor: a fluoresence study. *Biophysical Journal*, 66:674–682, 1994.

[12] D.A. Johnson, J.G. Voet & P. Taylor. Fluorescence energy transfer between cobra α-toxin molecules bound to the acetylcholine receptor. *The Journal of Biological Chemistry*, 259:5717–5725, 1984.

[13] M.D. Houslay & K.K. Stanley. *Dynamics of Biological Membranes.* John WIley & Sons, 1 edition, 1982.

[14] D.G. Nicholls & S.J. Ferguson. *Bioenergetics 2.* Academic Press, 2nd edition, 1992.

[15] R. Grisshammer & C.G. Tate. Overexpression of integral membrane proteins for structural studies. *Qaurterly Reviews of Biophysics*, 28:315–422, 1995.

[16] A. Watts, I.J. Burnett, C. Glaubitz, G. Groebner, D.A. Middleton, P.J.R. Spooner & P.T.F. Williamson. Structural descriptions of ligands in their binding site of integral membrane proteins at near physiological conditions using solid state NMR. *European Biophysical Journal*, 28:84–90, 1998.

[17] E. PebayPeyroula, G. Rummel, J.P. Rosenbusch & E.M. Landau. X-ray structure of bacteriohodopsin at 3.5 Å from microcrystals grown in lipidic cubic phases. *Science*, 277:1676–1681, 1997.

[18] T.A. Ceska, R. Henderson, J.M. Baldwin, F. Zemlin, E. Beckmann & K. Downing. An atomic model for the structure of bacteriorhodopsin, a 7 helix membrane proetin. *Acta Physiologica Scandinavia*, 146:31–40, 1992.

[19] G.F.X. Schertler, C. Villa & R. Henderson. Projection structure of rhodopsin. *Nature*, 362:347–350, 1993.

[20] S. Iwata, J.W. Lee, K. Okada, J.K. Lee, M. Iwata, B. Raumussen, T.A.Link, S. Ramaswamy & B.K. Jap. Complete structure of the 11 subuni bovine mitochondrial cytochrome bc_1 complex. *Science*, 281:64–71, 1998.

[21] A.R. Crofts & E.A. Berry. Stucture and function of the cytochrome bc_1 complex of mitochondria and photosynthetic bacteria. *Current Opinions in Structural Biology*, 8:501–509, 1998.

[22] D.A. Doyle, J.M. Cabral, R.A. Pfuetzner, A.L. Kuo, J.M. Gulbis, S.L. Cohen, B.T. Chait & R. Mackinnon. The structure of a potassium channel: molecular basis for K^+ conduction and selectivity. *Science*, 280:69–77, 1998.

[23] S.K. Buchanan, B.S. Smith, L. Venkatramani, D. Xia, L. Esser, M. Palnitkar, R. Chakraborty, D. vanderHelm & J. Diesenhofer. Crystal structure of the outer membrane active transporter FepA from E.coli. *Nature Structural Biology*, 6:56–63, 1999.

[24] P. Zhang, C. Toyoshima, K. Yonekura, N.M. Green & D.L. Stokes. Structure of the calcium pump at 8Å resolution. *Science*, 392:835–839, 1998.

[25] W. Kuhlbrandt, M. Auer & G.A. Scarbrough. Structure of the P type ATPase. *Current Opinions in Structural Biology*, 8:510–516, 1998.

[26] M. Auer, G.A. Scarlborough & W. Kuhlbrandt. Three dimensional map of the plasma membrane H^+/K^+ ATPase in the open conformation. *Nature*, 392:840–843, 1998.

[27] W. Kuhlbrandt, D.N. Wang & Y. Fujiyoshi. Atomic model of plant light harvesting complex by electron crystallography. *Nature*, 367:614–621, 1994.

[28] G. McDermott, S.M. Prince, A.A. Freer, A.M. Hawthornewaite-Lawless, M.Z. Papiz, R.J. Cogdell & N.W. Isaacs. Crystal structure of an integral membrane

light harvesting complex from photosynthetic bacteria. *Nature*, 374:517–521, 1995.

[29] K.H. Rhee, E.P. Morris, J. Barber & W.Kuhlbrandt. Three dimensional structure of the plant photosystem II reacton centre at 8 Å resolution. *Nature*, 396:283–286, 1998.

[30] U. Ermler, G. Fritisch, S.K. Buchanan & H. Michel. Structure of the photosynthetic reaction centre from rhodobacter-sphaeroides at 2.65 Å resolution - cofactors and protein cofactor interaction. *Structure*, 2:925–936, 1994.

[31] V.M. Unger, N.M. Kumar, N.B. Gilula & M. Yeager. Three dimensional structure of a recombinant gap junction membrane channel. *Science*, 283:1176–1180, 1999.

[32] T. Schirmer, T.A. Keller, Y.F. Wang & J.P. Rosenbusch. Structural basis for sugar translocation through maltoporin channels at 3.1 Å resolution. *Science*, 267:512–514, 1995.

[33] S.W. Cowan, T. Schirmer, G. Rummel, M. Steiert, R. Ghosh, R.A. Pauptit, J.N. Jansonius & J.P. Rosenbusch. Crystal structures explain functional properties of two E.coli porins. *Nature*, 358:727–733, 1992.

[34] M. Saraste & J.E. Walker. Membrane protein channels, pumps and charge separators - Editorial overview. *Current Opinions in Structural Biology*, 8:477–479, 1998.

[35] A. Watts, I.J. Burnett, C. Glaubitz, G. Groebner, D.A. Middleton, P.J.R. Spooner, J.A. Watts & P.T.F. Williamson. Membrane protein structure determination by solid state NMR. *Natural Product Reports*, 16:419–423, 1999.

[36] S.O. Smith, K. Aschheim & M. Groesbeck. Magic angle spinning NMR spectroscopy of membrane proteins. *Quarterly Reviews in Biophysics*, 29:395–449, 1996.

[37] S.J. Opella. NMR structural studies of membrane proteins. *Nature Structural Biology*, 4:845–850, 1997.

[38] R.R. Ernst, G. Bodenhausen & A. Wokaun. *Principles of nuclear magnetic resonance in one and two dimensions*. Oxford Science Publications, 1st edition, 1989.

[39] E.L. Hahn & S.R. Hartmann. Transfer of magnetisation from protons to low gamma nuclei. *Physics Review*, 128:2042–2046, 1962.

[40] S. Hediger, B.H. Meier, N.D. Kurur, G. Bodenhausen & R.R. Ernst. NMR cross polarization by adiabatic passage through the Hartmann Hahn condition. *Chemical Physics Letters*, 223:283–288, 1994.

[41] S.M. Zhang, B.H. Meier & R.R. Ernst. Mismatched compensated cross polarization - W-MOIST, an improved pulse scheme. *Journal of Magnetic Resoance(A)*, 108:1064–1858, 1994.

[42] G. Metz, M. Ziliox & S.O. Smith. Towards quantitative CP-MAS NMR. *Solid State Nuclear Magnetic Resonance*, 7:155–160, 1996.

[43] G.Metz, X.L. Xu & S.O. Smith. Ramped amplitude cross polarization in magic angle spinning NMR. *Journal of Magnetic Resonance A*, 110:219–227, 1994.

[44] A.J. Shaka, J. Keeler, T. Frenkiel & R. Freeman. An improved sequence for broadband decoupling - WALTZ-16. *Journal of Magnetic Resonance*, 52:335–338, 1983.

[45] Y. Yu & B.M. Fung. An efficient broadband decoupling sequence for liquid crystals. *Journal of Magnetic Resonance*, 130:317–320, 1998.

[46] A.E. Bennett, C.M. Rienstra, M. Auger, K.V. Lakshm & R.G. Griffin. Heteronuclear decoupling in rotating solids. *Journal of Chemical Physics*, 103:6951–6958, 1995.

[47] M. Lee & W. I. Goldburg. Homonuclear proton decoupling at the magic angle. *Physics Review A*, 20:180–190, 1965.

[48] W.K. Rhim, D.D. Elleman, L.B. Schreiber & R.W. Vaughan. Analysis of multiple pulse NMR in solids. *The Journal of Chemical Physics*, 60:4595–4604, 1974.

[49] R.R. Ernst, D.P. Burum & M. Linder. Low power multipulse line narrowing in solid state NMR. *Journal of magnetic resonance*, 44:173–188, 1981.

[50] A.C. Dedious. Predicting C-13 nuclear magnetic resonance chemical shielding tensors in zwitterionic L- threonine and L-tyrosine via quantum chemistry. *Journal of the American Chemical Society*, 116:7784–7786, 1994.

[51] C. Glaubitz & A. Watts. Magic Angle Oriented Sample Spinning (MAOSS): A new approach toward membrane studies. *Journal of Magnetic Resonance*, 130:305–316, 1998.

[52] M.M.Maricq & J.S. Waugh. NMR in rotating solids. *Journal of chemical physics*, 70:3300–3316, 1979.

[53] G. Groebner, A. Taylor, P.T.F. Williamson & A.Watts. Macroscopic orientation of natural and model membranes for structural studies. *Analytical Biochemistry*, 254:132–138, 1997.

[54] R.R. Ketchem, W. Hu & T.A. Cross. High resolution conformation of gramicidin-A in a lipid bilayer by solid state NMR. *Science*, 261:1457–1460, 1993.

[55] A.S. Ulrich, I. Wallat, M.P. Heyn & A. Watts. Re-orientation of retinal in the M-photointermediate of bacteriorhodopsin. *Nature Structural Biology*, 2:190–192, Needs title 1995.

[56] G. Groebner, G. Choi, I.J. Burnett, C. Glaubitz, P.J.E. Verdegem, J. Lugtenburg & A. Watts. Photoreceptor rhodopsin: structural and conformational

study of its chromophore 11-cis retinal in orientated membranes by deuterium solid state NMR. *FEBS Letters*, 422:210–204, 1998.

[57] A. Ramamoorthy, L.M. Gierasch & S.J. Opella. 4-Dimensional solid state NMR experiment that correlates the chemical shift and dipolar coupling frequencies of two nuclei with the exchange of dilute spin magnetization. *Journal of Magnetic Resonance(B)*, 109:112–116, 1995.

[58] Y. Kim, K. Valentine, S.J. Opella, S.L. Schendel & W.A. Cramer. Solid state NMR studies of the membrane bound closed state of the colicin E1 channel domain in lipid bilayers. *Protein Science*, 7:342–348, 1998.

[59] S.J. Opella, F.M. Marassi, J.J. Gesell, A.P. Valente, Y.Kim, M. OblattMontal, & M. Montal. Structures of the M2 channel lining segments from nicotinic acetylcholine and NMDA receptors by NMR spectroscopy. *Nature Structural Biology*, 6:374–379, 1999.

[60] Z.T. Gu & S.J. Opella. Three dimensional C-13 shift/H-1-N-15 coupling/N-15 shift solid state NMR correlation spectroscopy. *Journal of Magnetic Resonance*, 138:193–198, 1999.

[61] W.M. Tan, Z.T. Gu, A.C. Zeri & S.J. Opella. Solid state NMR triple resonance backbone assignments in the solid state. *Journal of Biomolecular NMR*, 13:337–342, 1999.

[62] R.G. Griffin. Dipolar recoupling in MAS spectra of biological solids. *Nature Structural Biology*, 5:508–512, 1998.

[63] R.G. Griffin D.P. Raleigh & M.H. Levitt. Rotational resonance in solid state NMR. *Chemical Physics Letters*, 146:71–76, 1988.

[64] T. Gullion & J. Schaefer. Rotational Echo Double Resonance. *Journal of Magnetic Resonance*, 81:196–200, 1989.

[65] R.G.S. Spencer, K.J. Halverson, M. Auger, A.E. McDermott, R.G. Griffin & P.T. Lansbury. An unusual peptide conformation may precipitate amyloid formation in alzheimers disease - an application of solid state NMR to the determination of protein secondary structure. *Biochemistry*, 30:10382–10387, 1991.

[66] S.O. Smith & B.J. Bormann. Determination of helix-helix interactions in membranes by rotational resonance NMR. *PNAS*, 92:488–491, 1995.

[67] D.J. Hirsh, J. Hammer, W.L. Maloy, J. Blazyk & J. Schaefer. Secondary structure and location of a magainin analogue in synthetic phospholipid bilayers. *Biochemsitry*, 35:12733–12741, 1996.

[68] O.J. Murphy & L.K. Thompson. Local structure and structural changes in membrane proteins by solid state NMR. In *Biophysics Journal*, pages M–PM–G2, 1999.

[69] X. Feng, P.J.E. Verdegen, Y.K. Lee, D. Sandstrom, M. Eden, P. BoveeGeurts, W.J. deGrip, J. Lugtenburd, H.J.M. deGroot & M.H. Levitt. Direct determination of a molecular torsion angle in the membrane protein rhodopsin by solid state NMR. *Journal of the American Chemical Society*, 119:6853–6857, 1997.

[70] M. Hong, J.D. Gross, W. Hu & R.G. Griffin. Determination of the peptide torsion angle phi by N-15 chemical shift and C-13(alpha)-H-1(alpha) dipolar tensor correlation in solid state MAS NMR. *Journal of Magnetic Resonance*, 135:169–177, 1998.

[71] F. Creuzet, A. McDermott, R. Gebhard, K. Vanderhoff, M.B. Spijkerassink, J. Herzfeld, J. Lugtenburg, M.H. Levitt & R.G. Griffin. Determination of membrane protein structure by rotational resonance NMR-bacteriorhodopsin. *Science*, 251:783–786, 1991.

[72] P.J.E. Verdegem, M. Helmle, J. Lugtenburg & H.J.M. de Groot. Internuclear distance measurements up to 0.44nm for retinals in the solid state with 1D rotational resonance C-13 MAS NMR spectroscopy. *Journal of the American Chemical Society*, 119:169–174, 1997.

[73] X. Feng, P.J.E. Verdegem, Y.K. Lee, D. Sandstrom, M. Eden, P. BoveeGeurts, W.J. deGrip, J. Lugtenburg, H.J.M. deGroot & M.H. Levitt. Direct determination of a molecular torsion angle in the membrane protein rhodopsin by solid state NMR. *Journal of the Americal Chemical Socity*, 119:6853–6857, 1997.

[74] P.T.F. Williamson, G. Groebner, K.W. Miller & A. Watts. Probing the agonist binding pocket of the nicotinic acetylcholine receptor a high resolution solid state nuclear magnetic resonance approach. *Biochemistry*, 37:10854–10859, 1998.

[75] P.J.R. Spooner, N.G. Rutherford, A. Watts & P.J.F. Henderson. NMR observation of substrate in the binding site of an active sugar-H^+ symport protein in native membranes. *PNAS*, 91:3877–3881, 1994.

[76] D.A. Middleton, R. Robins, X.L. Feng, M.H. Levitt, I.D. Spiers, C.H. Schwalbe, D.G.Reid & A. Watts. The conformation of an inhibitor bound to the gastric proton pump. *FEBS Letters*, 410:269–274, 1997.

[77] T.S. Balaban, A.R. Holzwarth, K. Schaffner, G.J. Boender & H.J.M. deGroot. CP-MAS C-13-NMR dipolar correlation spectroscopy of C-13 enriched chlorosomes and isolated bacetriochlorophyll-C aggregates of *chlorobiuum tepidium* - the self organization of pigments is the main structural feature of chlorosomes. *Biochemistry*, 34:15259–15266, 1995.

[78] S.K. Strauss, T. Bremi & R.R. Ernst. Experiments and strategies for the assignment of fully C-13/N-15 labelled polypeptides in the solid state. *Journal of Biomolecular NMR*, 12:39–50, 1998.

[79] M. Hong. Secondary structure determination and resonance assignment of extensively labelled solid proteins by high resolution solid state NMR. In *Biophysical Journal*, pages W–AM–F3. Biophysical Society, February 1999.

[80] O.S. Andersen & R.E. Koeppe. Molecular determinants of channel function. *Physiology Review*, 72:S89–S158, 1992.

[81] M.A. Raftery, M.W. Hunkapiller, C.D. Strader & L.E. Hood. Acetylcholine receptor: Complex of homologous subunits. *Science*, 208:1454–1547, 1982.

[82] N. Unwin. Acetylcholine receptor channel imaged in the open state. *Nature*, 373:37–43, 1995.

[83] N. Unwin. Arrangements of the acetylcholine receptor subunits in the resting and desensitized states, determined by cryoelectron microscopy of crystallized Torpedo postsynaptic membranes. *Cell*, 107:1123–1138, 1988.

[84] N. Unwin. Nicotinic acetylcholine receptor at 9Å resolution. *Journal of Molecular Biology*, 229:1101–1124, 1993.

[85] J.L. Sussman, M. Harel, F. Frowlow, C. Oefner, A. Goldman, L. Toker & I. Silman. Atomic structure of acetylcholinesterase from *Torpedo californica*: a prototypic acetylcholine binding protein. *Science*, 253:872–878, 1991.

[86] S.C. Froehner & J.G. Haggerty. Restoration of the ^{125}I-α-bungarotoxin binding activity to the α subunit of Torpedo acetylcholine receptor isolated by gel electrophoresis in SDS. *The Journal of Biological Chemistry*, 256:8294–8297, 1981.

[87] J.P. Changeux & S.J. Tzarto. High affinity binding of α-bungarotoxin to the purified α subunit and to its 27000-dalton proteolytic peptide from Torpedo marmorata acetylcholine receptor. Requirement for the SDS. *EMBOJ*, 2:381–387, 1983.

[88] J.M. Gershoni, E. Hawrot & T.L. Lentz. Binding of α-bungarotoxin to isolated α subunits of the acetylcholine receptor of Torpedo californica: quantitative analysis with protein blots. *PNAS*, 80:4973–4977, 1983.

[89] M.W. Nowak, P.C. Kearney, J.R. Sampson, M.E. Saks, C.G. Labarca, S.K. Silverman, W. Zhong, J. Thornson, J.N. Abelson, N. Davidson, P.G. Schultz, D.A. Dougherty & H.A. Lester. Nicotinic receptor binding site probed with unnatural amino acid incorporation in intact cells. *Science*, 268:439–442, 1995.

[90] D.A. Dougherty. Cation-pi interactions in chemistry and biology: a new view of benzene, phe, tyr and trp. *Science*, 271:163–168, 1996.

[91] I. Tsigelny, N. Sugiyama, S.M. Sine & P. Taylor. A model of the nicotinic receptor extracellular domain based on sequence identity and residue location. *Biophysical Journal*, 73:52–66, 1997.

[92] A. Karlin & P.N. Kao. Acetylcholine receptor binding site contains a disulphide cross link between adjacent half cystinyl residues. *The Journal of Biological Chemistry*, 261:8085–8088, 1986.

[93] P.N. Kao, A.J. Dwork, R.R. Kaldany, M.L. Silver, J. Wideman & A. Karlin. Identification of the half cystine specifically labelled by an affinity reagent for the acetylcholine receptor binding site. *The Journal of Biological Chemistry*, 259:11662–11665, 1984.

[94] R.E. Middleton & J.B. Cohen. Mapping the acetylcholine binding site of the nioctinic acetylcholine receptor [^{3}H]nicotine as a photoaffinity label. *Biochemistry*, 30:6987–6997, 1991.

[95] J.B. Cohen, S.D. Sharp & W.S. Liu. Structure of the agonist binding site of the nioctinic acetylcholine receptor: [^{3}H] acetylcholine mustard identifies residues in the cation binding subsite. *The Journal of Biological Chemistry*, 266:23354–23364, 1991.

[96] M.Dennis, J. Giraudat, F. Kotzyba-Hibert, M. Goeldner, C. Hirth, Y.J. Chang, C. Lazure, M. Chretien & J.P. Changeux. Amino acids in the Torpedo marmorata acetylcholine receptor alpha subsunit labelled by a photoaffinity ligand for the acetylcholine binding site. *Biochemistry*, 27:2346–2357, 1988.

[97] J.L. Galzi, F. Revah, D. Black, M Goeldner, C. Hirth & J.P. Changeux. Identification of a novel amino acid α-tyrosine 93 within the cholinergic ligands binding sites of the acetylcholine receptor by photoaffinity labelling. *The Journal of Biological Chemistry*, 265:10430–10437, 1990.

[98] M.W. Klymkowsky & R.M. Stroud. Immunospecific identification and three dimensional structure of a membrane bound acetylcholine receptor from Torpedo Mamorata. *Journal of Molecular Biology*, 128:319–334, 1979.

[99] T. Barkas, J. Gabriel, A. Mauron, G.J. Hughes, B. Roth, C. Alliod, R.J. Tzartoz & M. Ballivet. Monclonal antibodies to the main immunogenic region of the nioctinic acetylcholine receptor bind to residues 61-78 of the α-subunit. *The Journal of Biological Chemistry*, 263:5916–5920, 1988.

[100] A. Karlin, P.N. Kao & M. Dipaola. Molecular pharmacology of the nicotinic acetylcholine receptor. *Trends in pharmacological sciences*, 7:304–308, 1986.

[101] V.N. Damle & A. Karlin. Affinity labelling of one of two α-neurotoxin binding site in acetylcholine receptor from Torpedo californica. *Biochemistry*, 17:2039–2045, 1978.

[102] J.B. Cohen & S.E. Pedersen d-Tubocurarine, binding sites are located at $\alpha-\gamma$ and $\alpha-\delta$ subunit interfaces of the nioctinic acetylcholine receptor.. *PNAS*, 87:2785–2789, 1990.

[103] P.T. Wilson, T.L. Lentz & E. Hawrot. Determination of the primary amino acid sequence specifying the *alpha*-bungarotoxin binding site on the alpha subunit of the acetylcholine receptor from Torpedo californica. *PNAS*, 82:8790–8794, 1985.

[104] B. Oblas, R.H. Singer & N.D. Boyd. Location of a polypeptide sequence within the α subunit of the acetylcholine receptor containing cholenergic binding site. *Molecular Pharmacology*, 29:649–656, 1986.

[105] M.H. Akabas, C. Kaufmann, P. Archdeacon & A. Karlin. Identification of acetylcholine receptor channel lining residues in the M1 segment of the alpha subunit. *Neuron*, 13:919–927, 1994.

[106] M. Noda, H. Takahashi, T. Tanabe, M. Toyosato, S. Kikyotani, Y. Furutani, T. Hirose, H. Takashima, S. Inayama, T. Miyata & S. Numa. Structural homology of Torpedo californica acetylcholine receptor subunits. *Nature*, 302:528–532, 1983.

[107] A. Deviller-Thiery, J. Giraudet, M. Bentaboulet & J.P. Changeux. Complete mRNA coding sequence of the acetylcholine binding α subunit of Torpedo mamorata acetylcholine receptor: A model for the transmembrane organization of the polypeptide chain. *PNAS*, 80:2067–2071, 1983.

[108] N. Methot & J.E. Baenziger. Secondary structure of the exchange resistant core from nicotinic acetylcholine receptor probed directly by infrared spectroscopy and hydrogen/deuterium exchange. *Biochemistry*, 37:14815–14822, 1998.

[109] N. Methot, M.P. McCarthy & J.E. Baenziger. Secondary structure of the nicotinic acetylcholine receptor: Implications for structural models of a ligand gated ion channel. *Biochemistry*, 33:7709–7717, 1994.

[110] J. Corbin, N. Methot, H.H. Wang, J.E. Baenziger & M.P. Blanton. Secondary structure analysis of individual transmembrane segments of the nicotinic acetylcholine receptor by circular dichroism an Fourier Transform infrared spectroscopy. *The Journal of Biological Chemistry*, 273:771–777, 1998.

[111] R.J. Leonard, C.G. Labarca, P. Charnet, N. Davidson & H.A. Lester. Evidence

that the M2 membrane spanning region lines the ion pore of the nicotinic receptor. *Science*, 242:1578–1581, 1988.

[112] K. Imoto, C. Busch, B. Sakmann, M. Mishina, T. Konno, J. Nakai, H. Bujo, Y. Mori, K. Fukuda & S. Numa. Rings of negatively charged amino acids determine the acetylcholine receptor conductance. *Nature*, 335:645–648, 1988.

[113] J.P. Changeux, J. Giraudet, M. Dennis, T. Heidmann & J. Chang. Structure of the high affinity binding site for noncompetitive blockers of the acetylcholine receptor: Serine 262 of the δ subunit is labelled with [^{3}H]chloroprozamine. *PNAS*, 83:2719–2723, 1986.

[114] J. Guraudet, M. Dennis, T. Heidmann, P. Haumont, F. Lederer & J.P. Changeux. Structure of the high affinity binding site for noncompetitive blockers of the acetylcholine receptor: [^{3}H]chlorpromazine labels homologues residues in the β and δ chains. *Biochemistry*, 26:2410–2418, 1987.

[115] J.B. Cohen & B.J. White. Agonist induced changes in the structure of the acetylcholine receptor M2 regions revealed by photoincorporation of an uncharged nicotinic noncompetitive antagonist. *The Journal of Biological Chemistry*, 267:15770–15783, 1992.

[116] J.B. Cohen & M.P. Blanton. Mapping the lipid exposed regions in the Torpedo californica nicotinic acetylcholine receptor. *Biochemistry*, 31(3738-3750), 1992.

[117] J. Giraudet, C. Montecucco, R. Bisson & J.P. Changuex. Transmembrane topology of the acetylcholine receptor subunits probed with photoreactive lipids. *Biochemistry*, 24:3121–3127, 1985.

[118] J.L. Popot & C.P. Changeux. Nicotinic receptor of acetylcholine: structure of an oligomeric membrane protein. *Physiogical Review*, 64:1162–1239, 1984.

[119] R. Sealock, B.E. Wray & S.C. Froehner. Ultrastructural localization of the Mr 43,000 protein and the acetylcholine receptor in Torpedo post synaptic membranes using monoclonal antibodies. *Journal of Cell Biology*, 98:2239–2244, 1984.

[120] W.J. LaRochelle, B.E. Wray, R. Sealock & S.C. Froehner. Determination of the tissue distribution and relative concentrations of the post-synaptic 43kDa protein and the acetylcholine receptor in *Torpedo*. *The Journal of Biological Chemistry*, 261:5270–5274, 1986.

[121] S.J. Burden, R.L. Depalma & G.S. Gottesman. Cross linking of proteins in acetylcholine receptor rich membranes - association. *Cell*, 35:687–692, 1983.

[122] R. Sealock, B.E. Wray & S.C. Froehner. Identification of regions of high acetylcholine receptor density in tannic acid fixed post synaptic membrane from electric tissue. *Brain Research*, 199:267–281, 1980.

[123] R. Sealock. Cytoplasmic surface structure in postsynaptic membranes from electric tissue visualized by tannic acid mediated negative contrasting. *Journal of Cell Biology*, 92:514–522, 1982.

[124] R.R. Neubig & J.B. Cohen. Permeability control by cholinergic receptors in Torpedo postsynaptic membranes: agonist dose response relations measured at second and millisecond times. *Biochemistry*, 19:2770–2779, 1980.

[125] K.L. Magleby & C.F. Stevens. A quantitative description of end plate currents. *Journal of Physiology*, 223:173–197, 1972.

[126] G. Riquelme, E. Lopez, L.M. Garcia-Segura, J.A. Ferragut & J.M. Gonzalez-Ros. Giant liposomes: a model system in which to obtain patch clamp recordings of ionic channles. *Biochemistry*, 29:11215–11222, 1990.

[127] H. Schindler, F. Spillecke & E. Neumann. Different channel properties of Torpedo acetylcholine receptor monomers and dimers reconstituted in planar

membranes. *PNAS*, 81:6222–6226, 1984.

[128] P. Gardner, D.C. Ogden & D. Colguhoun. Conductance of single ion channels opened by nicotinic agonists are indistinguishable. *Nature*, 209:160–162, 1984.

[129] N.D. Boyd & J.B. Cohen. Kinetics of binding of ^{3}H acetylcholine and ^{3}H carbomylcholine to the Torpedo postsynaptic membranes: Slow conformational transitions of the cholinergic receptor. *Biochemistry*, 19:5344–5353, 1980.

[130] M. Weber, J.L. Popot & H. Grunhagen. Some structural properties of the cholinergic receptor protein in its membrane environmental relevant to its function as a pharmacological receptor. *Experimental Brain Reserach*, 23:215–220, 1975.

[131] S.A. Forman & K.W. Miller. High acetylcholine concentration causes rapid inactivation before fast desensitization in nicotinic acetylcholine receptors. *Biophysical Journal*, 54:149–155, 1988.

[132] J.W. Walker, K. Takeyasu & M.G. McNamee. Activation and inactivation kinetics of *Torpedo californica* acetylcholine receptor in reconstituted membranes. *Biochemistry*, 21:5384–5389, 1982.

[133] J.W. Walker, M.G. McNamee, E. Pasquale, D.J. Cash & G.P. Hess. Acetylcholine inactivation in Torpedo californica electroplax membrane vesicles. Dectection of two processes in the millisecond and second time regeimes. *Biochemical and Biophysical Reseatch Communications*, 100:86–90, 1981.

[134] T. Heidmann & J.P. Changeux. Interaction of fluorescent agonist with the membrane bound acetylcholine receptor from Torpedo marmorata in the millisecond time range: resolution of an intermediate conformational transition and evidence for positive cooperative effects. *Biochemical and Biophysical Research Communications*, 97:889–896, 1980.

[135] G.P. Hess, E.B. Pasquale, J.W. Walker & M.G. McNamee. Comparison of acetylcholine receptor controlled cation flux in membrane vesicles from Torpedo californica and Electrophorus electricus: chemica kinetic measurements in the millisecond region. *PNAS*, 79:963–767, 1982.

[136] S.L. Swope, Z. Qu & R.L. Huganir. Phosphorylation of the nioctinic acetylcholine receptor by protein tyrosine kinases. *Annals of the New York Accademy of Sciences*, 757:197–214, 1995.

[137] R.L. Huganir, A.H. Delcour, P. Greengard & G.P. Hess. Phosphorylation of the nicotinic acetylcholine receptor regulates its rate of desensitization. *Nature*, 321:774–776, 1986.

[138] J.F. Hopfield, D.W. Tank, P. Greengard & R.L. Huganir. Functional modulation of the nicotinic acetylcholine receptor by tyrosine phosphorylation. *Nature*, 366:677–679, 1988.

[139] K. Takeyasu, J.B. Udgaonkar & G.P. Hess. Acetylcholine receptor: evidence for a voltage dependent regulatory sites for acetylcholine. Chemical kinetic measurements in membrane vesicles using a voltage clamp. *Biochemistry*, 22:5973–5978, 1983.

[140] S.A. Forman, L.L. Firestone & K.W. Miller. Is agonist self inhibition at the nioctinic acetylcholine receptor a non specific action. *Biochemistry*, 26:2807–2814, 1987.

[141] E. Neher & J.H. Steinbach. Local anaesthetics transiently block currents through single acetylcholine receptor channels. *Journal of Physiology London*, 277:153–176, 1978.

[142] D.C. Ogden & D. Colquhoun. Ion channel blocked by acetylcholine, carbachol and suberyldicholine at the frog neuromuscular junction. *Proceeds of the Royal Society London B Biological Sciences*, 225:329–355, 1985.

[143] S.A. Forman & K.W. Miller. Procaine rapidly inactivates acetylcholine receptors from Torpedo and competes with agonist for inhibition sites. *Biochemistry*, 28:1678–1685, 1989.

[144] P. Kitabgi. Effects of neurotensin on intestine smooth muscle : application to the study of structure activity relationships. *Annals of the New York Accadamy of Science*, 400:37–55, 1982.

[145] J.F. Kachur, R.J. Miller, M. Field & J. Rivier. Neurohumoral control of ileal electrolyte transport. II. Neurotensin and Substance P. *Journal Pharmacological and Experimental Therapeutics*, 220:456–483, 1982.

[146] A.H. Osbahr, C.B. Nemeroff, P.J. Manberg & A.J. Prange. Centrally administered neurotensin: activity in the Joulou-Courvoisier muscle relaxation test in mice. *European Journal of Pharmacology*, 54:299–302, 1979.

[147] G.N. Ervin, L.S. Birrema, C.B.Nemeroff & A.J. Prange. Neurotensin blocks certain amphetamine behaviour. *Nature*, 291:73–76, 1981.

[148] A.J. Osbahr. Neurotensin induced antinociception in mice; antagonism by thyrotropin releasing hormone. *Journal of Pharmacology and Experimental Therapeutics*, 217:645–651, 1981.

[149] G.R. Uhl, P.J. Whitehouse, D.L. Price, W.W. Tourtelotte & M.J. Kuhar. Parkinsons disease: depletion of substatia nigra neurotensin receptors. *Brain Research*, 308:186–190, 1984.

[150] J.A. Garcia-Sevilla, T. Magnusson, A. Carlsson, J. Leban & K. Folkers. Neurotensin and its aminde analogue Gln^4 - neurotensin: effects of brain monamine turnover. *Archives Pharmacology*, 305:213–218, 1978.

[151] E. Widerlov, C.D. Kilts, R.B. Mailman, C.B. Nemeroff, A.J. Prange & G.R. Breese. Increase in dopamine metabolites in rat brain by neurotensin. *Journal of Pharmacology and Experimental Therapeutics*, 223:1–6, 1982.

[152] A. Reches, R.E. Burke, D. Jiang, H.R. Wagner & S. Fahn. Neurotensin interacts with dopaminergic neurons in rat brain. *Peptides*, 4:43–48, 1983.

[153] P.L. Yeagle, J.L. Alderfer, A.C. Salloum, L. Ali & A.D. Albert. The first and second cytoplasmic loops of the G-protein coupled receptor. rhodopin, independently form β-turns. *Biochemistry*, 36:3864–3869, 1997.

[154] P.L. Yeagle, J.L. Alderfer & A.D. Albert. Three dimensional structure of the cytoplasmic face of the G protein coupled receptor rhodopsin. *Biochemistry*, 36:9649–9654, 1997.

[155] P.L. Yeagle & A.D. Albert. The three dimensional structure of rhodopsin: a domain approach. *Biophysical Journal*, pages Su–Pos549, 1999.

[156] A.D. Albert, A. Watts, P.J.R. Spooner, G. Groebner, J. Young & P.L. Yeagle. A distance measurement between specific sites on the cytoplasmic face of bovine rhodopsin in the rod outer segment. *Biochemica et Biophysica Acta*, 1328:74–82, 1997.

[157] P.L. Yeagle & A.D. Albert. Structure of the G-protein coupled receptor, rhodopsin: a domain approach. *Biochemical Society Transactions*, 26:520–531, 1998.

[158] H.G. Dohlman, J. Thorner, M.C. Caron & R.J. Lefkowitz. Model systems for the study of seven transmembrane segment receptors. *Annual Reviews in Biochemistry*, 60:653–688, 1991.

[159] B.K. Koblika, T.S. Koblika, K. Daniel, J.W. Regan, M.G. Caron & R.J. Lefkowitz. Chimeric α_2-, β_2 adrenergic receptors: delineation of domains involved in effector coupling and ligand specificity. *Science*, 240:1310–1316, 1988.

[160] J. Lechleiter, R. Hellmiss, K. Duerson, D. Ennulat, N. David, D. Clapham & E. Peralta. Diverse functions of muscarinic acetylcholine receptor subtypes.

EMBOJ, 9:4381–4390, 1990.

[161] R.R. Birge. Photophysics of light transduction in rhodopsin and bacteriorhodopsin. *Annul Review of Biophysics and Bioengineering*, 10:315–354, 1981.

[162] D. Donnelly & J.B.C. Findlay. 7-helix receptors - structure and modelling. *Current Opinions in Structural Biology*, 4:582–589, 1994.

[163] S.T. Kallmeyer, J. Hoflack, A. Bruinvels & M. Hibert. Modelling of G-protein coupled receptors: applications to dopamine, adrenaline, serotonin, acetylcholine and mammalian opsin receptors. *Journal of medical chemistry*, 35(3448-3462), 1992.

[164] N.D. Boyd, R. Kage, J.J. Dumas, J.E. Krause & S.E. Leeman. The peptides binding site of the substance P (NK-1) receptor localized by photoreactive analogue of Subsatnce P: presence of a disulphide bond. *PNAS*, 93:433–437, 1996.

[165] M. Boudjelel, A. Sivaorasadarao & J.B.C. Findlay. Membrane receptor for odour binding proteins. *Biochemical Journal*, 317:23–37, 1996.

[166] D.R. Sibley, J.R. Peters, P. Nambi, M.G. Caron & R.J. Lefkowitz. Desensitization of turkey erythrocyte adenylate cyclase - beta-AR phosphorylation is correlated with attenuation of adenylate cyclase activity. *Journal of Biological Chemistry*, 259:9742–9749, 1984.

[167] B. Strrulovici, R.A. Cerione, B.L. Kilpatrick, M.G. Caron & R.J. Lefkowitz. Direct demonstration of impaired functionality of purified desensitized beta-adrenergic receptor in reconstituted systems. *Science*, 225:837–840, 1984.

[168] P. Nambi, J.R. Peters, D.R. Sibley & R.J. Lefkowitz. Desensitization of turkey erythrocyte β-adrenergic receptor in a cell free system - evidence that multiple

protein kinases can phosphorylate and desensitize the receptor. *Journal of Biological Chemistry*, 260:2165–2171, 1985.

[169] J.L. Benovic, L.J. Pike, R. Cireone, C. Staniszweski & T. Yohimasa. β-adrenergic receptor kinase - identification of a novel protein kinase that phosphorylates the agonist occupied form of the receptor. *Journal of Biological Chemistry*, 260:7094–7101, 1985.

[170] J.L. Benovic, R.H. Strasser, M.G. Caron & R.J. Lefkowitz. Phosphorylation of mammalian β-adrenergic receptor by cAMP dependent protein kinase - regulation of the rate of receptor phosphorylation and dephosphorylation by agonist occupancy and effects on coupling of the receptor to the stimulatory guanine nucleotide regulatory protein A. *PNAS*, 83:2797–2801, 1986.

[171] M.J. Lohse, J.F. Benovic, J. Codina, M.C. Caron & R.J. Lefkowitz. β-arrestin: a protein that regulates β-adrenergic receptor function. *Science*, 248:1547–1550, 1990.

[172] T.K. Harden, C.U. Cotton, G.L. Waldo, J.K. Lutton & J.P. Perkins. Catecholamine induced alteration in sedimentation behaviour of membrane bound receptors. *Science*, 210:441–445, 1980.

[173] J. Zhang, L.S. Barak, P.H. Anborgh, S.A. Laporte, M.G. Caron & S.S.G. Ferguson. Cellular trafficking of a G-protein coupled receptor/beta arrestin endocytotic complex. *Journal of Biological Chemistry*, 274:10999–11006, 1999.

[174] B. Cusack, K. Grosham, D.J. McCormick, Y.P. Pang, R. Perry, C.T. Phung, T. Souder & E. Richelson. Chimeric rat/human neurotensin receptors localize a region of the receptor sensitive to binding of novel, species specific, picomolar affinity peptide. *The Journal of Biological Chemistry*, 271:15054–15059, 1996.

[175] C. Labbe-Julie, S. Barroso, D. Nicolas-Eteve, J.L. Reversat, J.M. Botto, J. Mazella, J.M. Bernassau & P.Kitabgi. Mutagenesis and modelling of the

neurotensin receptor. *The Journal of Biological Chemistry*, 273:16351–16357, 1998.

[176] M. Yamada, M. Yamada, M.A. Watson & E. Richelson. Deletion mutation in the putative third intracellular loop of the rat neurotensin receptor abolishes polyphosphoinositide hydrolysis but not cyclic AMP formation in CHO-K1 cells. *Molecular Pharmacology*, 46:470–476, 1994.

[177] H.L. Wang & T.Wu. G($\alpha_{q/11}$) mediates neurotensin excitation of substantia nigra dopaminergic neurons. *Molecular Brain Research*, 36:29–36, 1996.

[178] A.M. Barrocas, D.E. Cochrane, R.E. Carraway & R.S. Feldberg. Neurotensin stimulation of mast cell secretion is receptor-mediated, pertussis-toxin sensitive and requires activation of phospholipase C. *Immunopharmacology*, 41:131–137, 1999.

[179] L. Cathala & D. PaupardinTritsch. Neurotensin inhibition of the hyperpolarization-activated cation current (I-h) in the rat substantia nigra pars compacta implicates the protein kinase C pathway. *Journal of Physiology - London*, 503:87–97, 1997.

[180] M. Najimi, F. Souaze, M. Mendez, E. Hermans, T. Berbar, W. Rostene & P. Forgez. Activation of receptor gene transcription is required to maintain cell sensitization after agonist exposure - study on neurotensin receptor. *Journal of Biological Chemistry*, 273:21634–21641, 1998.

[181] C. Granier, J. VanRietschoten, P. Kitabgi, C. Poustis & P. Freychet. Synthesis and characterization of neurotensin analogues for structure/activity relationship studies. *European Journal of Biochemistry*, 124:117–125, 1982.

[182] P. Kitabgi, R. Carraway, J. VanRietschoten, C. Granier, J.L. Morgat, A. Menez, S.E. Leeman & P.Freychet. Neurotensin specific binding to synaptic membranes from rat brain. *PNAS*, 74:1846–1850, 1977.

[183] A.M. Sefler, J.X. He, T.K. Sawyer, K.E. Holub, D.E. Omecinsky, M.D. Reily, V. Thanabal, H.C. Akunne & A.L. Cody. Design and structure activity relationships of C-terminal cyclic neurotensin fragment analogues. *Journal of Medicinal Chemistry*, 38:249–257, 1995.

[184] C. Labbe-Jullie, J.M. Botto, M.V. Mas, J. Chabry, J. Mazella, J.P. Vincent, D. Gully, J.P. Maffrand & P. Kitabgi. [3H] SR 48692, the first non-peptide neurotensin antagonist radioligand: characterization of binding properties and evidence for distinct agonist and antagonist binding domains on the rat neurotensin receptor. *Molecular Pharmacology*, 47:1050–1056, 1995.

[185] V. Mahajan & R.L. Sass. Crystal structure of acetylcholine perchlorate. *Journal of Crystal Molecular Structure*, 4:15–21, 1974.

[186] M.H. Levitt, D.P. Raleigh, F. Creuzet & R.G. Griffin. Theory and simulations of homonuclear spin pair systems in rotating solids. *Journal of chemical physics*, 92:6347–6364, 1990.

[187] J.M. Griffiths & R.G. Griffin. Nuclear magnetic resonance methods for measuring dipolar couplings in rotating solids. *Analytica Chemica Acta*, 283:1081–1101, 1993.

[188] C. Glaubitz, X. Feng, P.T.F. Williamson, M. Levitt & A. Watts. The simulation of RR magnetization exchange near the resonance condition: An analytical solution. *in preperation*, 1999.

[189] O.B. Peersen, M. Groesbeek, S. Aimoto & S.O. Smith. Analysis of rotational resonance magnetization exchange curves from crystalline peptides. *Journal of the American Chemical Society*, 117:7228–7237, 1995.

[190] M. Baldus, R.J. Iuliucci & B.H. Meier. Probing through bond connectivities and through space distances in solids by magic angle spinning nuclear magnetic resonance. *Journal of the American Chemical Society*, 119:1121–1124, 1997.

[191] M. Baldus & B.H. Meier. Broadband polarization transfer under magic angle spinning: application to total through space correlation NMR spectroscopy. *Journal of Magnetic Resonance*, 128:172–193, 1997.

[192] M. Baldus, M. Tomaselli, B.H. Meier & R.R. Ernst. Broad-band polarization transfer experiments for rotating solids. *Chemical Physics Letters*, 230:329–336, 1994.

[193] T. Fujiwara, A. Ramamoorthy, K. Nagayama, K. Hoika & T. Fujito. Dipolar HOHAHA under MAS condition for solid state NMR. *Chemical Physics Letters*, 212:81–84, 1993.

[194] Z. Luz, H.W. Spiess & J.J. Titman. Rotor syncronized MAS two dimensional exchange NMR in solids. Principles and Applications. *Israel Journal of Chemistry*, 32:145–160, 1992.

[195] A.F. deJong, A.P.M. Kentgens & W.S. Veeman. Two dimensional exchange NMR in rotating solids: a technique to study very slow molecular reorientations. *Chemical Physics Letters*, 109:337–342, 1984.

[196] M.G. Munowitz & R.G. Griffin. Two dimensional nuclear magnetic resonance in rotating solids: time reversal effects in chemical shift dipolar spectra. *Journal of Chemical Physics*, 78:613–617, 1983.

[197] M.G. Hagemeyer, K. Schmidt-Rohr & H.W. Spiess. Two dimensional nuclear magnetic resonance experiments for studying molecular order and dynamics in static and rotating solids. *Advances in Magnetic Resonance*, 85:85–130, 1989.

[198] S. Vega & G.J. Boender. Phase sensitive detection of 2D homonuclear correlation spectra in MAS NMR. *Journal of Magnetic Resonance*, 133:281–285, 1998.

[199] D.M. Gregory, G.M. Wolfe, T.P. Jarvie, J.C. Sheils & G.P. Drobny. Double quantum filtering in magic angle spinning NMR spectroscopy applied to DNA

oligomers. *Molecular Physics*, 89:1835–1849, 1996.

[200] N.C. Nielsen, H. Bildsoe, H.J. Jakobsen & M.H. Levitt. Double quantum homonuclear rotary resonance - efficient dipolar recovery in magic angle spinning nuclear magnetic resonance. *Journal of Chemical Physics*, 101:1805–1812, 1994.

[201] Y.K. Lee, N.D. Kurur, M. Helmle, O.G. Johannessen, N.C. Nielsen & M.H. Levitt. Efficient dipolar recoupling in the NMR of rotating solids - a sevenfold symmetrical radiofrequency pulse sequence. *Chemical Physics Letters*, 242:304–309, 1995.

[202] M. Hohwy, H.J. Jakobsen, M. Eden, M.H. Levitt & N.C. Nielsen. Broadband dipolar recoupling in the nuclear magnetic resonance of rotating solids: A compensated C7 pulse scheme. *Journal of Chemical Physics*, 108:2686–2694, 1998.

[203] R. Verel, M. Baldus, M. Ernst & B.H. Meier. A homonuclear spin pair filter for solid state NMR based on adiabatic passage techniques. *Chemical Physics Letters*, 287:421–428, 1998.

[204] L.M. Brasswell, K.W. Miller & J.F. Sauter. Pressure reversal of the action of octanol on postsynaptic membranes from Torpedo. *British Journal of Pharmacology*, 83:305–311, 1984.

[205] F. James. *MINUIT - Function Minimization and Error Analysis D-506.* CERN Program Library, 1994.

[206] M.P. Williamson. Empirical comparison of models of chemical shift calculations in proteins. *Journal of Magnetic Resonance*, 101:63–71, 1993.

[207] T. Asakura, K. Taoka, M. Demura & M.P. Williamson. The relationship between amide proton chemical shift and secondary structure in proteins. *Journal of Biomolecular NMR*, 6:227–236, 1995.

[208] C.W. Haugh & R.B. Mallion. New tables for ring current shielding in protein magnetic resonance. *Organic Magnetic Resoance*, 4:203–228, 1972.

[209] M.L. Raves, M. Harel, Y.P. Pang, I. Silman, A.P. Kozikowski & J.L. Sussman. Structure of acetylcholinesterase complexed with the nootropic alkaloid (-)-huperzine A. *Nature Structural Biology*, 4:57–63, 1997.

[210] H.J.M. deGroot, S.O. Smith, A.C. Kolbert, J.M.L. Courtin, C. Winkel, J.Lugtenburg, J. Herzfeld & R.G. Griffin. Iterative fitting of magic angle spinning NMR spectra. *Journal of magetic resonance*, 91:30–38, 1991.

[211] H. Zhang & R.G. Bryant. Bound ligand motion in crystalline carboxypeptidase A. *Biophysics Journal*, 68:363–372, 1997.

[212] H. Zhang & R.G. Bryant. Characterization of enzyme bound ligand dynamics by solid state NMR in the presence of ligand exchange: L-Phenylalanine on CarboxypeptidaseA. *Biophysics Journal*, 68:303–311, 1995.

[213] V. Copie, A.E. McDermott, K. Bashah, J.C. Williams, M. Spijker-Assink, R. Gebhard, J. Lugtenburg, J. Herzfeld & R.G. Griffin. Deuterium solid state NMR studies of methyl group dynamics in bacteriorhospsin and retinal model compounds: Evidence for a 6-s-trans chromophore in the protein. *Biochemistry*, 33:3280–3286, 1994.

[214] E. Oldfield, R.A. Kinsey & A.Kintanar. Recent advances in the study of bacteriorhodospin dynamic structure using high field solid state NMR spectroscopy. *Methods in Enzymology*, 88:310–325, 1982.

[215] M.A. Kinery, A. Kintanar, R.L. Smith, H.S. Gutowsky & E. Oldfield. NMR studies of amino acids and proteins. Deuterium NMR relaxation of deuteriomethyl labelled amino acids in crystals and in Halobacterium halobium ad E.coli membranes. *Biochemistry*, 23:288–298, 1984.

[216] D.A. Torchia. Solid State NMR studies of protein internal dynamics. *Annual Review of Biophysics and Bioengineering*, 13:125–144, 1984.

[217] G.H. Penner, J.M. Polson, S.I. Daleman & K. Reid. A deuterium NMR study of molecular dynamics and geometry in two classes of onium salts. *Canadian Journal of Chemistry*, 71:417–426, 1992.

[218] G.H. Penner, B. Zhao & K.R. Jeffrey. Molecular dynamics in the solid trimethylamine-borane complex: a deuterium NMR study. *Z. Naturforsch*, 50a:81–89, 1994.

[219] C.I. Ratclffe & J.A. Ripmeester. 2H nuclear magnetic resonance studies of motions in tetramethylammonium salts: the question of methyl reorientation. *Canadian Journal of Chemistry*, 64:1348–1354, 1986.

[220] C. Morrison & M. Bloom. Orientation dependence of 2H nuclear magnetic resonance spin lattice relaxation on phospholipid and phosphoplipid cholesterol systems. *Journal of Chemical Physics*, 101:749–763, 1994.

[221] M. Ge, D.E. Budil & J.H. Freed. ESR studies of ED spin labelled membranes aligned by isopotential spin dry ultracentrifugation - lipid protein interactions. *Biophysics Journal*, 67:2326–2344, 1994.

[222] H.C. Jarrell, P.A. Jovall, J.B. Giziewicz, L.A. Turner & I.C.P. Smith. Determination of conformational properties of glycolipid headgroups by ^2H NMR of oriented multilayers. *Biochemistry*, 26:1805–1811, 1987.

[223] S. Auge, H. Mararguil, M. Tropis & A. Milon. Preparation of oriented lipid bilayers on ultrathin polymers for solid state NMR analysis of peptide membrane interactions. *Journal of Magnetic Resonance Ser A*, 124:455–458, 1997.

[224] C.R. Sanders & C.G. Landis. Reconstitution of membrane proteins in lipid bilayered mixed micelles for NMR studies. *Biochemistry*, 34:4030–4040, 1995.

[225] K.P. Howard & S.J. Opella. High resolution solid state NMR spectra of integral membrane proteins reconstituted into magnetically oriented phospholipid bilayers. *Journal of Magnetic Resonance Series B*, 112:91–94, 1996.

[226] L.C.P.J. Molevanger, E.A. Dratz, B. DeKruiff, C.W. Hilbers & W.J. de Grip. P-31 NMR investigations of magnetically oriented rod outer segments - spectral analysis and identification of individual phospholipids. *European Journal of Biochemistry*, 156:383–390, 1986.

[227] N.A. Clark, K.J. Rothschild, D.A. Luippold & B.A. Simon. Surface induced lamellar orientation of multilayer membrane arrays - theoretical analysis and a new method with application to purple membrane patches. *Biophysical Journal*, 31:65–96, 1980.

[228] K.J. Rothschild, K.M. Rosen & N.A. Clark. Incorporation of photoreceptor membranes into multilamellar films. *Biophysics Journal*, 25:45–52, 1980.

[229] J. Seelig. Deuterium magnetic resonance: theory and applications to membranes. *Quarterly review in biohysics*, 10:353–418, 1977.

[230] M.S. Greenfield, A.D. Ronemus, R.L. Vold, R.R. Vold, P.D. Ellis & T.E. Raidy. Deuterium quadrupolar echo NMR spectroscopy. III. Practical aspects of lineshape calculations for multiaxis rotational processes. *Journal of Magnetic Resonance*, 72:89–107, 1987.

[231] J. Seelig. 31P Nuclear Magnetic Resonance and the head group structure of phospholipids in membranes. *Biochimica et Biophysica Acta*, 515:105–140, 1978.

[232] B.V. Rama Sastry & C. Chiou. Acetylcholinesterase hydrolysis of halogen substituted acetylcholine. *Biochemical Pharmacology*, 17:805–815, 1968.

[233] A.M. Delegeane & M.G. McNammee. Independent activation of the AChR for *Torpedo californica* at two sites. *Biochemistry*, 19:890–895, 1980.

[234] M. Ratnam, W. Gullick, J. Spiess, K. Wan, M. Criado & J. Linstrom. Structural heterogeneity of the alpha subunits of the nicotinic acetylcholine receptor in relation to the agonist affinity alkylation and antagonist binding. *Biochemistry*, 25:4268–4275, 1986.

[235] S.A. Smith, T.O. Levante, B.H. Meier & R.R. Ernst. Computer simulations in magnetic resonance - an object oriented programming approach. *Journal of Magnetic Resonance(A)*, 100:75–105, 1994.

[236] J.K. Herdklotz & R.L. Sass. The crystal structure of acetycholine chloride: a new conformation for acetylcholine. *Biochemical and Biophysical Research Communications*, 40:583–588, 1970.

[237] H.R. Ing, P. Kordick & D.P.H.T. Williams. Structure activity studies of acetylcholine. *British Journal of Pharmacology*, 7:103–117, 1952.

[238] D.B. Smith & K.S. Johnson. Single step purification of polypeptides expressed in *E. coli* as fusion with glutathione S transferase. *Gene*, 67:31–40, 1988.

[239] F.W. Studier & B.A. Moffat. Use of bacteriophage T7 RNA polymerase to direct selective high level expression of cloned genes. *Journal of Molecular Biology*, 189:113–120, 1986.

[240] J. Grodberg & J.J. Dunn. ompT encodes *E.coli* outer membrane protein that cleaves T7 polymerase during purification. *Journal of Bacteriology*, 170:255–260, 1988.

[241] P.C. Simons & D.L. VanderJagt. Purification of Glutathione S- transferase by glutathione affinity chromatography. *Methods in Enzymology*, 77:235–237, 1981.

[242] M. Uhlen & T. Moks. Gene fusions for purpose expression: an introduction. *Methods in Enzymology*, 185:129–143, 1990.

[243] M.P. Williamson. Empirical comparisons of models for chemical shift calculation in proteins. *Journal of Magnetic Resonance*, 101B:63–71, 1993.

[244] D.J. Wishart & A.M. Nip. Protein chemical shift analysis: a practical guide. *Biochemistry and Cell Biology*, 76:153–163, 1998.

[245] J. Jones. *Amino acid and peptide synthesis.* Oxford Chemistry Primers. Oxford University Press, 1st edition, 1997.

[246] J. Sambrook, E.F. Fritsh, T. Maniatis. *Molecular Cloning.* Cold Spring Harbor Laboratory Press, 2nd edition, 1992.

[247] B.J. Smith. Chemical cleavage of polypeptides. *Methods in Molecular Biology*, 64:57–72, 1997.

[248] J.L. Nieto, M.Rico, J.Santoro, J.Herranz & F.J.Bermejo. Assignment and conformation of neurotensin in solution. *International Journal of Peptide Science*, 28:315–323, 1986.

[249] A. Kuliopulos & J. Walsh. Production, purification and cleavage of tandem repeats of recombinant protein. *Journal of the American Chemical Society*, 116:4599–4607, 1994.

[250] Y. Miyamotolee, S. Shiosaka & M. Tohyama. Purification and characterisation of neurotensin receptor from rat brain with special reference to comparison between newborn and adult age rats. *Peptides*, 12:1001–1006, 1991.

[251] J. Tucker & R. Grisshammer. Purification of a rat neurotensin receptor expressed in *Eschericha coli. Biochemical Journal*, 317:891–899, 1996.

[252] R. Grisshammer & J. Tucker. Quantitative evaluation of neurotensin receptor purification by immobilized metal affinity chromatography. *Protein Expression and Purification*, 11:53–60, 1997.

[253] A.J.S. MacPherson, M.C. Jonesmortimer, P.Horne & P.J.F. Henderson. Identification of the GalP galactose transport protein of E.coli. *Journal of Biological Chemistry*, 258:4390–4396, 1983.

[254] A.F.L. Creemers, C.H.W. Klaassen, P.H.M. BoveeGeurts, R. Kelle, U. Kragl, J. Raap, W.J. DeGrip, J. Lugtenburg & H.J.M. deGroot. Solid state N-15 NMR evidence for a complex Schiff base counterion in the visual G-protein coupled receptor rhodopsin. *Biochemistry*, 38:7195–7199, 1999.

[255] P.J. Reeves, J. Klien-Seetharaman, E.V. Getmanova, M. Eilers, M.C. Loewen, S.O. Smith & H.G. Khorana. Expression and purification of rhodopsin and its mutants from stable mammalian cell lines for NMR studies. In *Biochemical Society Transactions*, page D15. Biochemical Society, 1999.

[256] R. Langen, K.W. Cai, C. Altenback, H.G. Khorana & W.L. Hubbell. Structural features of the C-terminal domain of bovine rhodopsin: A site-directed spin-labelling study. *Biochemistry*, 38:7918–7924, 1999.

[257] M. Eilers, P.J. Reeves, W.W. Ying, H.G. Khorana & S.O. Smith. Magic angle spinning NMR of the protonated retinylidene Schiff base nitrogen in rhodopsin: Expression of N-15-lysine- and C-13-glycine-labeled opsin in a stable cell line. *PNAS*, 96:487–492, 1999.

[258] A.F.L. Creemers, C.H.W. Klaassen, P.H.M. BoveeGeurts, R. Kelle, U. Kragl, J. Raap, W.J. deGrip, J. Lugtenburg & H.J.M. deGroot. Solid state N-15 NMR evidence for a complex Schiff base counterion in the visual G-protein-coupled receptor rhodopsin. *Biochemistry*, 38:7195–7199, 1999.

[259] K. Tanaka, M. Masu & S. Nakanishi. Structure and function of the cloned rat neurotensin receptor. *Neuron*, 4:847–854, 1990.

[260] A.Hing, S. Vega & J. Schaefer. Measurement of heteronuclear dipolar coupling by transferred-echo double-resonance NMR. *Journal of Magnetic Resonance*, 103:151–162, 1993.

[261] M. Baldus, D.G. Geurts, S. Hediger & B.H. Meier. Efficient N-15-C-13 polarization transfer by adiabatic-passage Hartmann-Hahn cross polarization. *Journal of Magnetic Resonance*, 118:140–144, 1996.

[262] M. Baldus & B.H. Meier. Total correlation spectroscopy in the solid state. The use of scalar couplings to determine the through-bond connectivity. *Journal of Magnetic Resonance*, 121:65–69, 1996.

[263] A. Bax & R. Freeman. Investigation of ^{13}C-^{13}C couplings in natural abundance samples: The strong coupling case. *Journal of Magnetic Resonance*, 41:507–511, 1980.

[264] T. Thiested, A.K. Nielsen & K. Gerdes. Mechanism of post segregational killing: translation of Hok, SrnB, Pnd mRNAs of plasmid R1, F and R483 is activated by 3'-end processing. *EMBOJ*, 13:1960–1968, 1994.

[265] T. Thisted, N.S. Sorensen, E.G.H. Wagner & K. Gerdes. Mechanism of post segregational killing: Sok antisense RNA interacts with Hok mRNA via its 5' end single stranded leader and competes with the 3' end of Hok mRNA for binding to the mok translational initiation region. *EMBOJ*, 13:1960–1968, 1994.

[266] T. Thisted, N.S. Sorensen & K. Gerdes. Mechanism of post segregational killing: secondary structure analysis of the entire Hok mRNA from plasmid R1 suggests a fold back structure that prevents translation and antisense RNA binding. *Journal of Molecular Biology*, 247:859–873, 1995.

[267] B.J. vanRossum, H. Forster & H.J.M. deGroot. High-field and high-speed CP-MAS C-13 NMR heteronuclear dipolar-correlation spectroscopy of solids with frequency-switched Lee- Goldburg homonuclear decoupling. *Journal of Magnetic Resonance*, 124:516–519, 1997.

[268] H.E. Hatcher, J.G. Hu, B.Q. Sun, C.M. Rienstra, J.C. Lansing & R.G. Griffin. Two dimensional solid-state NMR correlation spectroscopy applied to

multiply-labeled bacteriorhodopsin. *Biophysical Journal*, 74:A297, 1998.

[269] D.L. Jakeman, D.J. Mitchell, W.A. Shuttleworth & J.N.S. Evans. Effects of sample preparation conditions on biomolecular solid-state NMR lineshapes. *Journal of Biomolecular NMR*, 12:417–421, 1998.